A Study of the Progressive Degradation of Masonry Shear Walls Subjected to Harmonic Loading

by
John Nichols, Bachelor of Engineering (Civil, Honours I.)

A Thesis submitted to the University of Newcastle in partial fulfilment of the requirements for the degree of Doctor of Philosophy.

October 2000.

I hereby certify that that the work embodied in this thesis is the result of original research and has not been submitted for a higher degree at any other University or Institution.

John Nichols

ACKNOWLEDGEMENTS

I would like to thank all those who have contributed to this research work or persevered during this period. I dedicate this work to Ken Jarrett who died as I was finishing this Dissertation. God created a few good Men and he still is one of the few.

And to remember the words of a better author than I, those words appear particularly relevant when one considers the quantity of poorly constructed masonry and the prevalence of seismic activity in the world.

> Any man's death diminishes me because I am involved in Mankind;
> And therefore, never send to know for whom the bell tolls;
> It tolls for thee.
>
> **John Donne**

Date of printing: Monday, 21 April 2003
Revision number: 276
Total pages: 297

TABLE OF CONTENTS

LIST OF TABLES

LIST OF FIGURES

NOTATION

Notation is in accordance with standard mathematics symbolism (Kaplan and Lewis, 1971; Borowski and Borwein, 1989). The notation is defined in the order it is presented in the chapters. No redefinition is provided in subsequent chapters, except when there is a change in definition of a variable.

Chapter 1:

D	Damage parameter, defined as a tensor to encapsulate the effective stiffness as an internal state variable

Chapter 2:

f'_m	Characteristic strength of the masonry unit (MPa)
$E_{Ø}$	Composite Young's modulus (measured by experiment) (GPa)
E_1	Volume fraction 1 - Young's modulus (measured by experiment)
E_2	Volume fraction 2 - Young's modulus calculated using equation (1)
V_1	Volume fraction 1
V_2	Volume fraction 2
Q	FEMA 273 Applied Load
$Q_{\exp}$	FEMA 273 Expected Strength from backbone curve analysis
c	FEMA 273 Force ratio
d	FEMA 273 Drift (%)
e	FEMA 273 Drift (%)
D_{eff}	FEMA 273 Height
h_{eff}	FEMA 273 Height to force resultant
X	Component of a vector
H_{SM}	The maximum static shear strength (kN)
H_{DM}	The maximum dynamic shear strength (kN)
u	Frequency range (Hz)
s	Stress (MPa)
ζ	Damping (%)
$f(x_i, v_i)$	Forcing function definition from Benedetti and Pezzoli (1996) (N)
v_i	Velocity (m/s)

k_{eff}	Effective stiffness[1] defined by Benedetti and Pezzoli (1996) (GPa)
x_i	Displacement definition from Benedetti and Pezzoli (1996) (m)
k^2	Normalized spring stiffness to provide an equivalence relation to the material stiffness. (GPa)
A_{spring}	The unit area of a spring used to provide equivalence between the k^2 spring stiffness that is normally expressed as N/m and the k_{eff} material stiffness expressed as GPa (m^2)
L_{spring}	The unit length of a spring used to provide equivalence between the spring stiffness measured as Newtons/metre and the material stiffness measured as GPa (m)
K_{eff}	Effective stiffness from Benedetti and Pezzoli (1996) Figure 5 (GPa)
K_1	Point stiffness from Benedetti and Pezzoli (1996) Figure 5 (GPa)
K_4	Point stiffness from Benedetti and Pezzoli (1996) Figure 5 (GPa)
$\overline{K}$	Mean stiffness from Benedetti and Pezzoli (1996) Figure 5 (GPa)
f	Force/unit mass (kN/kg) Benedetti and Pezzoli (1996) Figure 5 (GPa)
x	Displacement (m) from Benedetti and Pezzoli (1996) Figure 5 (GPa)
D_c	Critical damage parameter at which the manifold breaks
E	Young's modulus (GPa)
$\overline{E}$	Effective stiffness (GPa)
D_p	Damage parameter for a pristine sample nominally assumed zero
e	Strain from Krajcinovic Figure 6
S	Force ratio from Krajcinovic Figure 6

Chapter 3:

l^2	Measured stiffness defined as normalized spring stiffness (GPa)
m	Mass of the object (kg)
a	Acceleration (m^2/s)
v	Velocity (m/s)
t	Time (s)

[1] The physical sciences use the symbol, k^2, as spring stiffness, which implies an area and a length term. The term in this dissertation has the engineering sciences concept of a unit area and unit length term assumed in the definition and so the stiffness is measured in GPa, rather than Newtons/metre. This method is for mathematical convenience only to maintain the simplicity of the mathematics and the usual engineering meaning.

h	Damping variable ($kgm^{-1}s^{-1}$ or Pa/s or PaHz)
$p(t)$	Forcing function, usually a time dependent harmonic (N)
$F(x,v)$	Function used by Benedetti and Pezzoli (1996) to represent the effective stiffness (N)
$\ddot{z}(t)$	Vertical acceleration function used by Benedetti and Pezzoli (1996), (m^2/s)
$g(x)$	Stiffness function used by Benedetti and Pezzoli (1996)
$f_a(E,e,\dot{e},f)$	Defining function for the effective stiffness (GPa)
e	Strain
$f_b(E,e,\dot{e},f)$	Defining function for the measured stiffness (GPa)
$\dot{e}$	Derivative of the strain ($\mu\varepsilon$/s)
f	Frequency (Hz)
h	Spring stiffness (N/m)
U	Potential energy (Nm)
K	Kinetic energy (Nm)
E_t	Total energy (Nm)
A	Wave amplitude (m)
e_{yield}	Strain at yield point
$k^2(t)$	Time dependent effective stiffness using assumptions of unit area and length (nominally a material stiffness GPa)
$l^2(t)$	Time dependent measured stiffness using assumptions of unit area and length (nominally a frequency dependent pseudo-material stiffness GPa)

Chapter 4:

t_{ii}	Diagonal element of a stress tensor (Pa)
V	Measured voltage (V)
A_t	Cross-sectional area in tension or compression field (m^2)
t_{ij}	Non-diagonal element of a stress tensor (Pa)
A_s	Shear area (m^2)
e_{ij}	Element of a strain tensor
L	Length (m)
K_{LVDT}	Calibration constant for a linear velocity displacement transducer (m/V)
$\dot{D}$	Derivative of the damage parameter ($\mu\varepsilon^{-1}$)

Chapter 5:

q	Angle (deg.)
t_{xy}	Stress on x face at y normal (Pa)
t_{11}	First principal stress (Pa)
t_{xx}	Stress on x face at x normal (Pa)
t_{yy}	Stress on y face at y normal (Pa)
t_{22}	Second principal stress (Pa)
t_{yx}	Stress on y face at x normal (Pa)
$t_{\max}$	Maximum shear stress (Pa)
$t_{\min}$	Minimum shear stress (Pa)
Y	Effective frequency limit for quasi-static loading rates (Hz)
w	Circular frequency (rad/s)
D	Strain gauge length (m)
g_1	Constant of proportionality
g_2	Constant of proportionality
g_3	Constant of proportionality

Chapter 6:

F_0	Applied force (N)
$x(t)$	Time dependent displacement (m)
$\frac{dx(t)}{dt}$	Time dependent velocity (m/s)
$\frac{d^2x(t)}{dt^2}$	Time dependent acceleration (m/s^2)
$F_i(t)$	Harmonic applied force (N)
G	Shear modulus (GPa)
u	Poisson's ratio
D_{ci}	Damage parameter defining the onset of the cracking in the manifold

Appendix A:

Â	Set of real numbers
I	Is an element of:
x	Dependent variable used in a differential equation an element of the set of real numbers (typically defined as a displacement m)

$\ddot{x}$	Second derivative of x or acceleration using the dotted derivative (m^2/s)
$f(x)$	Function of x (m/s^2)
u	Transformed displacement
e^{-kt}	Transformation variable
k	Transformation number
a^2	Transformed stiffness
$\ddot{u}$	Transformed acceleration

Appendix B:

M	Compact orientated k dimensional manifold with boundary
f	(k-1) form on M
dM	Differential of M
df	Differential of f
e_{xx}	Strain on x face at x normal
e_{xy}	Strain on x face at y normal
e_{yy}	Strain on y face at y normal
E_{xx}	First orthotropic Young's modulus (GPa)
E_{yy}	Second orthotropic Young's modulus (GPa)
u_{yx}	First orthotropic Poisson's ratio
u_{xy}	Second orthotropic Poisson's ratio
G_{xy}	Orthotropic shear modulus (GPa)
$G(t)$	Time dependent variable defining the effective shear stiffness for a set of reinforced concrete experiments (GPa)
K_0	A definition of elastic stiffness constants as an upper bound (GPa)
g	Lag angle (rad)
$F(t)$	Time dependent applied force (N)
$a(t)$	Variable (m)
$b(t)$	Variable (m)
$W(t)$	Time dependent function
$\dot{a}(t)$	Derivative of $a(t)$
$\dot{b}(t)$	Derivative of $b(t)$

$\dot{x}(t)$	Derivative of $x(t)$
$\ddot{x}(t)$	Derivative of $\dot{x}(t)$
e	Error limit (%)
$err(t)$	Time dependent function (Nominal GPa)
d	Error limit (%)

Appendix C:

T	The period between data collection points (s)
T_0	Period (s)
A	Fast Fourier transform scale factor
N	Number of samples in a period
f_o	Base frequency (Hz)

Appendix D:

g	Gravitational acceleration 9.81 (m/s^2)

ABSTRACT

This masonry research investigated the differences in the static and dynamic stiffness for the seismic range of loads and frequencies for a pressed clay masonry wythe. The effective stiffness has been defined in Newtonian physics and Damage Mechanics. This research used the concept of measured stiffness defined as the measured stress field divided by the measured strain field. A two-part test rig was constructed to apply the loading to the wythe. The first loading mechanism was a compression frame that supplied in plane bi-axial nonproportional compression stress to reflect the loading on a shear wall from the dead load of a structure. The second loading mechanism was a shear yoke designed to apply a harmonic shear stress to the edge of the panels. A finite element analysis of two masonry structures concluded that the forcing function applied to the shear yoke could be represented as a harmonic function of single frequencies. The experimental study was based on a systematically varied harmonic loading pattern. The measured stiffness was shown to approach the effective stiffness as the frequency of the loading function approaches zero. A relationship has been established between the static or effective stiffness and dynamic or measured stiffness based on Newton's second law and shown to be experimentally valid. The damage parameter was encapsulated from the effective stiffness data and tri-linear curve recommended for engineering design purposes. The degrading stiffness can now be used in the further development of codes such as FEMA 273.

Chapter 1 Introduction

Masonry is an age-old material that represents a permanence of feature which human beings find attractive. The rock art of earlier peoples and the masonry developed since the time of farming provide continuity in human history and habitation. Their voice literally in the fine arts sense speaks across the generations. It is the voice of silence and reason; it is the voice of beauty; it is the voice of war. Powerful additions to this voice have been made in every generation of man from the Mecca of Stonehenge to the memorial of the Vietnam era in Washington. Man in his meinie Companies[2] has moved stone, clay, lime, and other elements to create this historical strand, this evolution of form. These structures can last for millennia or they can be destroyed in an eye blink. The destruction of masonry can come from many sources: from the passing of time, from the carelessness of construction or maintenance, and from the many acts of God. This current research was undertaken to understand part of that process. We do not have the time to spend waiting on the vagaries of Mother Nature to explore the properties of masonry. Therefore, we work to prematurely strain our masonry samples. We work masonry at the types of limits that one prays will never occur in reality, but all too often does with tragic consequences. This current research seeks to understand the change in the material as it is loaded. In a sense, we design our experimental work to parallel the real destructive forces that dominate the design limits of masonry. These are the impulsive forces, the force of an earthquake, wind, or waves. These environmental loads are a random pattern often striking without discernible reason. They overwhelm entire communities creating cries of anguish as eloquently expressed by Hadjian (1992) when writing on the tragic events in Spitak.

A love of the material was brought forth in the works of Heyman (1995) and Grimm (1996) whose work bears testament to the development of the guild rules and the economic forces that shape the use of a primary construction material. Economic forces will always shape the destiny of masonry. The fundamental principle of engineering states that: one seeks to make use of any material to create structures that are sound and yet with no superfluous elements save those deemed by the designer. The requirement of soundness must be one for the lifetime of the masonry, not merely for a warrant period, yet may be one that often leads to failure when an earthquake such as the Northridge earthquake tests new methods and previously untested buildings.

[2] A Middle English expression.

Baker (1912) noted that the tensile strength of masonry was strain rate dependent when he reported on tests on mortar. Subsequent experimental research supports the known degradation of masonry shear walls that occurs in an earthquake or windstorm, and showed that the measured stiffness of masonry had a frequency effect (Tercelj, Sheppard, and Turnsek, 1969; Paulson and Abrams, 1990; Klopp, 1996). The first observation from this previous research was of a difference in the measured stiffness resulting from the frequency of loading. These experimental observations have been attributed to a distinct static stiffness and a distinct dynamic stiffness (Freund, 1990). The second observation was of the subsequent degradation of the material with time of loading and increasing strain in a dynamic experiment (Paulson and Abrams, 1990; Krajcinovic, 1996).

This thesis established a formal relationship between the stiffness definitions. The primary definitions are for a measured stiffness and an effective stiffness. The measured stiffness was deemed the experimentally determined stiffness that can be obtained by dividing the stress field results by the strain field results that includes acceleration, velocity, and displacement components directly implying frequency dependence. The effective stiffness was deemed the mathematical functional representation of the stiffness defined explicitly by the displacement term of the differential equation of motion for a harmonic function. This functional representation has no frequency dependence in a strict static test (Kaplan and Lewis, 1971, 554[3]). The generalized static Hooke's law sets out the standard relationship where the effective stiffness and the measured stiffness are identical functions (Lekhnitskii, 1963, 8).

The principal objectives of this research were to:

Experimental investigation

I. Investigate the dynamic stiffness properties of shear walls constructed from a single wythe of masonry
II. Experimentally observe the change in stiffness properties of shear walls subjected to specific loading and boundary conditions
III. Determine the form of a loading pattern to be used in the experimental work
IV. Design and construct a test rig that will support the experimental work
V. Determine the measured stiffness for shear walls subjected to the loading pattern presented in objective III

[3] This is a standard method to provide a page number reference.

Numerical analysis

I. Use fast Fourier transform methods to investigate the measured stiffness of the shear walls, and identify the conditions of loading in terms of amplitude and frequency that yield the experimentally observed static stiffness and the dynamic stiffness
II. Determine the time domain degradation of the effective stiffness from the measured stiffness
III. Encapsulate the damage parameter and determine the critical damage level

Research Outcomes

I. Determine the relationship between the peak strain data and the damage parameter data
II. Explain in a systematic manner the results of the experimental investigation, the numerical data from the assessment of the damage parameterization, and the opportunities and constraints in the use of this research
III. Provide a practical set of guidelines for application and use of this study in the development of new buildings and in the assessment of old buildings
IV. Relate the results to the recently introduced FEMA 273 guidelines (1997) on assessment of buildings subjected to earthquake loading. These guidelines extend the concept of building design to include the controlled failure of a building in an extreme environmental loading situation

The thesis structure is presented as follows:

I. A literature review is presented for the fields of masonry and masonry buildings in Chapter 2. The review also looks at the development of the field of seismology in the last 150 years. The purpose of this review is to establish the framework for the development of a loading pattern for the experiments, investigate the field of continuum and damage mechanics to establish the principles for the evaluation of the effective stiffness, the measured stiffness and the encapsulation of the damage parameter, D. The experimental studies, which support the observation of a static failure and dynamic failure mechanism, are presented and the results related to a strict mathematical formalism in Appendix B. This work includes the recent observational data related to the static stiffness and dynamic stiffness measurements for masonry.

II. An outline is provided in Chapter 3 of the background to the problem, the problem definition, and the solution method.

III. The details of the experimental study are outlined in Chapter 4. A number of photographs and plans of the test rig, the hydraulic system and electronic system are provided to assist with the explanation of the research method. Details are provided of the data acquisition system and the equipment settings, which were used in these experiments. A loading pattern is established for the experimental work based on separate numerical finite element analysis of two masonry structures. The loading pattern is presented in Appendix D.

IV. The collection and analysis of data is presented in Chapter 5 for the shear wall elements, the masonry prisms, and masonry units. The analysis includes the determination of the change in the effective stiffness in the time domain and the encapsulation of the damage parameter. Appendix A presents the complete set of experimental panels results.

V. The analysis of the results for the stiffness degradation of the shear walls is explained in Chapter 6. This chapter outlines the use of the graph of the stiffness against the total strain. This graph formed an essential portion of the original research work related to the change in the effective stiffness of masonry shear walls. This information provides a tool for the design, analysis, and reengineering of masonry shear walls designed for seismic loads.

VI. Conclusions are provided in Chapter 7.

Chapter 2 Literature Review

2.1 INTRODUCTION

This literature study reviews the historical strands that have influenced the engineering of masonry under in plane seismic loading. The strands that are reviewed commence with the historical perspective that looks briefly at the classifications of masonry, methods of analysis, the two types of failure mechanisms, the difference between static unforced and forced harmonic motions, and the postulate for the research work.

The review discusses masonry providing a brief background to the material, a review of the intrinsic and extrinsic properties of masonry, and the constituents that it is made from in the modern construction world. Masonry buildings are examined in some detail particularly considering the development of masonry analysis and design in the last five centuries. The review of the FEMA 273[4] document presents the currently accepted methods of analysis of structures for extreme environmental loads. Seismology is presented with a detailed review of the seismicity of the world to place the problem in context and to provide sufficient data for the development of a rational loading pattern. This review looks in detail at the development of seismology during the last 150 years from the perspective that seismic loads are a harsh environmental test for any masonry structure.

An overview of structural and damage mechanics provides the mathematical fragments that are used to explain the proposed problem and the method used to present the solution. This mathematical fragment covers from the well-established fields of elasticity[5] to the more recent research on damage mechanics.[6] It provides the framework for investigating the mathematics of the change in effective stiffness of masonry subjected to harmonic steady state loads. The dynamic fracture mechanics section has a review of the observations about two failure mechanisms.

The Canadian reinforced concrete shear panel tests[7] are reviewed to determine whether any properties can be established for the definition of the effective stiffness.

---

[4] *Op. cit.*, FEMA 273 , (1997), 1-4.
[5] Lekhnitskii, S.G., (1963), *Theory of Elasticity of an anisotropic elastic body*, (San Francisco: Holden-Day Inc., trans: P Fern), *passim*.
[6] Krajcinovic, D., (1996), *Damage Mechanics*, (New York: Elsevier), 446.
[7] Stevens, N.J., Uzumeri, S.M., and Collins, M.P., (1991), Reinforced Concrete subjected to Reversed Cyclic Shear-Experiments and Constitutive Model, *ACI Structural Journal*, 88, 2, 135.

2.2 HISTORICAL PERSPECTIVE

2.2.1 INTRODUCTION

The term masonry derives from the Old French word *maçonerie*[8] that was introduced into the English language about the middle of this millennium, although the Latin root had probably been used in England during the Roman occupation. Clarke and Engelbach[9] detail the materials, methods, and construction techniques for ancient Egyptian masonry. Cowan[10] presents a history of masonry and concrete dome construction from the Roman to the modern era and the history of the development of pozzalonic materials from the use of *pulvis puteolanus* to Portland cement.

Heyman[11] summarizes the development of the field of modern structural analysis. The field of experimental stress analysis was presented in detail by Hetenyi.[12] Hetenyi covers the measurement issues using precomputerized data acquisition systems. The basic equations and methods from this text were used in the analysis of the experimental work. Baker[13] provides a text on masonry construction practice at the end of the nineteenth century. Baker's treatise provides both a theoretical review of the relevant results for masonry testing undertaken from the 1860s to the early 1910s, and a course in masonry construction practice. The text has sufficient examples to provide a comparison with modern practice at the end of the twentieth century. The issues that were relevant to Baker are still relevant in modern research.

Masonry analysis has developed into a mature analytical field in the last half century as the guild rules[14] are replaced by modern standards that are based on a mixture of proven empirical rules, extensive numerical and experimental research, and finite element based analysis.[15] One of the three elements missing from current sets of design rules is the reality that masonry moves with time[16] and that each structure should be capable of accommodating slow movement without significant distress. The second missing element is the acceptance by the community that some structures will last a millennium, and

[8]Little, W., *et al.*, (1973), *Shorter Oxford English Dictionary on Historical Principles*, (Oxford: Oxford University Press), 1285.
[9]Clarke, S., and Engelbach, R., (1930), *Ancient Egyptian Masonry- the building craft, (*Oxford: Oxford University Press), *passim.*
[10]Cowan, H.J., (1977), A history of masonry and concrete domes in building construction, *Building and Environment*, 12, 2, *passim*.
[11] Heyman, J., (1998), *Structural Analysis – A Historical Approach*, (Cambridge: Cambridge UP), *passim.*
[12] Hetenyi, M., (1950), *Handbook of experimental stress analysis*, (NY: Wiley), *passim.*
[13] Baker, I.O., (1912), *A Treatise on Masonry*, (New York: Wiley and Son), Chaps 5, 12.
[14] Heyman, J., (1995), *The Stone Skeleton*, (Cambridge: Cambridge UP), 1-9.
[15] Page, A.W., (1979), The inplane deformation and failure of brickwork, diss. 636, U of Newcastle, 1-7.
[16] *Op. cit.*, Heyman, J., (1995), 24.

should be engineered considering both the gravitational and the infrequent horizontal loads.[17]

The development of FEMA 273[18] focussing on the design of engineering structures for four possible loading stages has shifted the design methods for structures in the direction earlier suggested by Heyman.[19] The FEMA document will undoubtedly form the foundations for further revisions to the modern structural codes. The third element missing from current design standards is that buildings should fail in a controlled manner without exposing the occupants to undue risk. Modern codes of practice tacitly recognize these elements, but they still fail to address adequately the points covered by Heyman's work or the FEMA document. It must be recognized that these comments will be controversial in some settings because of the change in paradigm, but they begin to address the issue of both the design and retrofitting stages for building work. The FEMA and similar documents place a significant responsibility on the building owner and designer to select an appropriate design standard in place of proscribed standards.

The development of mathematical models and the gathering of experimental data are progressing to a stage that will soon provide a formal unified approach to the design of masonry from conception of the idea to failure of the masonry. Alternatively, for the analysis and design required for the retrofitting of existing buildings there is Epperson and Abrams'[20] comment *'that most masonry buildings are old.'* Their statement implies that there exists a need for methods to assess existing buildings particularly for dynamic design loads that were not available for the analysis stage at the time of the original analysis and design. The comments of Heyman[21] are based on English and northern European practice for an intraplate zone. Page[22] published a literature review on structural brickwork and completed a test program on proportional bi-axial loading of masonry elements. Ali[23] and Dhanasekar[24] researched on further aspects of the static analysis of masonry. Their work has been instrumental in the development of the current code provisions related to the design of masonry structures for bi-axial loading, concentrated loads, and in plane loading of masonry. Extensive research programs have investigated

[17] Epperson, G.S., and Abrams, D.P., (1989), *Non destructive evaluation of masonry buildings*, (Urbana, IL: UIUC), 1-2.
[18] FEMA (1997), *NEHRP Guidelines for the Seismic Rehabilitation of Buildings*, (Washington: FEMA), Manual 273, chap 1.
[19] *Op. cit.*, Heyman, J., (1995), 1-9, 24.
[20] *Loc. cit.*, Epperson, G.S., and Abrams, D.P., (1989), 1-2.
[21] *Op. cit.*, Heyman, J., (1995), 1-9, 24.
[22] Page, A.W., (1973), *Masonry - Literature Review*, (Newcastle: University of Newcastle), 1.
[23] Ali, S., (1987), Concentrated Loads on solid masonry, diss. 1143, University of Newcastle, *passim*.
[24] Dhanasekar, M., (1985), The performance of brick masonry subjected to in-plane loading, diss. 990, University of Newcastle, *passim*.

the properties of mortars and the further development of the bond wrench and the flexural strength of masonry. [25]

2.2.2 CLASSIFICATIONS OF MASONRY

Masonry is now generally classified into six categories, historic (or load) bearing, unreinforced structural masonry, confined masonry, retrofitted masonry, reinforced masonry and prestressed masonry. Heyman[26] presented the definitive text on historic and load bearing masonry and comments[27] that "masonry is supposed to crack and any cracks visible in a structure indicate merely that the building has at some time been subjected to imposed movements from the external environment. If there is no evidence of recent movement then the proper course of action is to point the cracks with mortar to prevent ingress of water but otherwise to leave well enough alone". Heyman's observation is consistent with the author's experience after the Newcastle 1989 earthquake, provided of course, that the structure is still structurally sound.

An older building has a greater probability that it will encounter a major environmental event and most of these events are lateral loadings.[28] Unreinforced masonry has been widely used as a construction material for housing, flats, and commercial premises across large areas of the world and has been common in those parts of the world identified as intraplate zones. The designation of intraplate covers the interior of the tectonic plates. The definition of the intraplate boundary has now generally been accepted as being 2 degrees from the plate boundary[29] established from work on intraplate earthquakes in the Atlantic region. Page[30] identifies the acceptance of the structural action of the shear wall as the principal element in the progression from historic to structural masonry. A shear walls capacity derives from a high moment of inertia about one axis, high compressive strength brickwork, and some tensile capacity, preferably augmented with a compressive stress generated by dead load from higher storeys. Shear walls have the problem of slenderness about the other principal axis that requires careful design to avoid out of plane failure even if reserve strength exists in plane. These structures rely on shear walls or connected elements on all three orthonormal planes to tie the shell together. The shear walls design method meets the requirements of sound building practice if it has been

[25] Sugo, H.O., *et al.,* (1998), Influence of Age on the bond strength in clay brickwork, *5ANMS,* 365.
[26] *Op. cit.*, Heyman, J., (1995), 14.
[27] *Ibid.* Sec. 2.3, 22.
[28] *Loc. cit.*, Epperson, G.S., and Abrams, D.P., (1989), 1.
[29] Wysession, M.E., Wilson, J., Bartkó, L., and Sakata, R., (1995), Intraplate seismicity in the Atlantic Ocean Basin: A teleseismic catalog, *Bulletin of the Seismological Society of America,* 85, 3, 755.
[30] *Op. cit.*, Page, A.W., (1973), 57.

coupled with the assumption of some tensile capacity[31] in the masonry walls that provides capacity to resist some transient dynamic loads. Hughes and Zsembery's[32] development of the bond wrench test provided a systematic method of comparing the results of a tensile test between different prisms of mortar. Its simple and effective use as a site quality test overcomes the usual objections of stress distribution anomalies in the test rig and the difference between a bending test and a true tensile test. Lourenço and Rots[33] have identified the need to establish micro mechanical models and obtain experimental data for masonry that are accurate beyond the structural prepeak regime. Part of their work was to obtain a mathematical model for masonry and to undertake the necessary numerical modelling. Their model should allow for the damage accumulation in the material and the change in effective stiffness properties with time.

Whilst there has been a plethora of research on confined masonry much of the earlier research appears to lack focus and a consistency in the definitions and approach. Angel *et al.*[34] demonstrated the current methodologies and indirectly identified the clear lack of definitions for studying the theoretical aspects of in fill shear wall elements. Angel *et al.* provide a harsh judgment, but the field is still in the empirical data collection stage of structural methods. The study of infill panels would appear to be attractive for further research using the proposed test rig. The use of shaking tables and racking tests are not likely to cast further light on the infill problem until there exists a degree of standardization to the problems faced throughout the world. Further fundamental research is required on the behaviour of infill panels.

Reinforced masonry has generally used in interplate regions such as California, New Zealand, and Japan. Reinforced masonry provides increased strength and ductility during seismic events compared to unreinforced structural masonry. The use of reinforced masonry can improve the structural capacity of a building. This increased resistance of reinforced masonry has been shown to be critical for areas that are subjected to large and frequent environmental loads. Lizzi[35] presents the history of Italian churches being

[31] AS 3700, *Masonry Structures*, (Sydney: Standards Australia), Section 3.3.3.
The flexural tensile strength is deemed to be 0.2 MPa, which is 10 PSI from an older British Standard. This can only be applied in the structural analysis to resist transient loads.

[32] Hughes, D.M., and Zsembery, S., (1980), A method of determining the flexural bond strength of brickwork at right angles to the bed joint, *2CMS*, Ottawa, *passim.*

[33] Lourenço, P.B., and Rots, J.G., (1997), *On the use of homogenization techniques for the analysis of masonry structures*, (Delft: n. Pub.), 3.

[34] Angel, R., Abrams, D.P., Shapiro, D., Uzarski, J., and Webster, M., (1994), *Behavior of reinforced concrete frames with masonry infills*, (Urbana, IL: UIUC) ISSN 0069-4274, *passim.*

[35] Lizzi, F., (1981), *The restoration of static monuments*, (Genoa: Sagep), *passim.*
*(*Active areas where this type of repair has been undertaken would include Southern Italy, although similar methods were used on a number of buildings in Newcastle after the 1989 earthquake- specifically St John Cathedral (minor repairs) and the Christ Church Cathedral (major repairs)).

retrofitted with reinforcement and subjected to further seismic activity during the construction period. Lizzi's method developed since the Second World War has become a commonly accepted repair method for major church structures in active seismic areas, although one can wonder at the long-term impact on the fabric of the structure. Prestressed masonry has generally been used in interplate regions such as California, New Zealand, and Japan. Prestressed masonry provides increased strength and ductility compared to unreinforced masonry during seismic events by imparting a permanent compressive stress to the masonry elements. Post tensioning rods were used to retrofit two church towers in Newcastle after the 1989 earthquake.[36] The impetus for this current research on the dynamic loading of clay masonry wythes was to establish an understanding of the causes of the degradation of the stiffness of masonry when it is subjected to environmental loads. The areas of direct interest in this shear wall research are in historic, load bearing, and structural masonry. The other categories were not studied as part of this work. Current practice has been to construct buildings that can meet the requirements of the Heyman[37] rules for gravitational structures with the addition of a substantive environmental load as defined by Epperson and Abrams.[38]

2.2.3 TWO FAILURE MECHANISMS

Freund[39] notes that there are two failure mechanisms for a brittle ceramic material. The first mechanism has been termed a static mechanism where the weakest plane is activated and the material fails. The second mechanism has been termed a dynamic mechanism where, in Freund's words, failure occurs "during impulsive loading where multiple fractures on different planes can be nucleated and they grow to a significant size without arresting each other". Baker[40] first reported an observation about the dynamic mechanism. Bolotin[41] in dealing with the dynamic stability of elastic systems outlines an experiment on a rod that was subjected to harmonic steady state loads of varying frequency. He noted that the force developed in the vibrating rod increases in proportion to the square of the frequency. These researchers have identified a frequency effect governing the failure of ceramic materials that are subjected to a harmonic loading pattern. A masonry shear wall that is subjected to a seismic load is a ceramic being

[36] Nichols, J.M., (1999), The assessment and repair of certain structures after the Newcastle Earthquake, *Masonry International*, 13, 1, 11-12.
[37] *Op. cit.*, Heyman, J., (1996), 14.
[38] *Loc. cit.*, Epperson, G.S., and Abrams, D.P., (1989), 1.
[39] Freund, L.B., (1990), *Dynamic Fracture Mechanics*, (Cambridge: Cambridge University Press), 13.
[40] *Loc. cit.*, Baker, I.O., (1912), 77.
[41] Bolotin, V.V., (1964), *The dynamic stability of elastic systems*, (San Francisco: Holden-Day Inc), translated by V.I. Weingarten, L.B. Greszczuk, K.N. Trirogoff and K.D. Gallegos, 31.

subjected to a randomly varying dynamic load. Klopp[42] has investigated shear walls using a shaking table. He could not get a direct relationship between frequency and in plane stiffness. Klopp concluded that workmanship and material variability were the primary causes of the wide scatter of results. He calculated a value of 1.065 GPa for the Young's modulus of masonry, concluding that the dynamic value was reduced in comparison to the static value. Klopp and Griffith[43] have studied the dynamic characteristics of masonry buildings using a vibrating machine. Their work demonstrates one of the key elements for the development of any building loading pattern that must be related to the specific response frequencies of masonry buildings. Klopp and Griffith's results form part of the experimental evidence for the use of the finite element model buildings in the development of the loading pattern. The conclusion reached by Paulson and Abrams[44] was that the specimen responded with higher initial strength and stiffness with dynamic loading than the statically loaded specimen. The difference in response for these reinforced specimens the researchers attributed to the rate of cracking. The set of experimental observations were based on the interpretation of each researcher in terms of the experimental data being considered and the background of the research. Paulson and Abrams' experimental work clearly points to a difference between the responses of a specimen loaded statically and one loaded dynamically. The points that can be summarized from the existing research findings are presented in Table 1.

TABLE 1 PUBLISHED RESEARCH FINDINGS

Number	Findings from Published Research	Source of Finding
1	There are two failure mechanisms for a brittle ceramic material.	Observations of Freund
2	The dynamic failure mechanism has a frequency component that on first reading of the research has an impact as the square of the frequency.	This point is postulated from the observations of Bolotin
3	The use of poor quality control on the mortar and masonry may mask the nature of the failure mechanism. The static stiffness is greater than the dynamic stiffness.	Klopp makes both of these points
4	The use of a seismic load may make the interpretation of the results difficult.	This was concluded from the work of Paulson and Abrams.

[42] Klopp, G.M., (1996), Seismic design of unreinforced masonry structures, diss. , U of Adeilade, *passim*.
[43] Klopp, G.M., and Griffith, M.C., (1993). Dynamic characteristics of unreinforced masonry buildings. *Australian Civil Engineering Transactions*, 35, 1, 59.
[44] Paulson, T.J., and Abrams, D.P., (1990), Correlation between static and dynamic response of model masonry structures, *Earthquake Spectra*, 6, 3, 573.
' When one specimen was free to shake when excited dynamically with simulated earthquake motions it responded with significantly higher initial stiffness and strength than another specimen which was subjected to the same history of lateral deflections at a static rate. Differences in behavior were attributed to the rate of crack propagation in the reinforced masonry structures'.

2.3 MASONRY

2.3.1 INTRODUCTION

Architecture begins when two bricks are placed together – carefully Mies van der Rohe.

Masonry has been constructed from a variety of materials since the first πλιυο οπτη[45] emerged from the fire. This section of the literature review briefly examines the constituents of the mortar, reviews a number of recent tests on the intrinsic properties of masonry, and points to details on the extrinsic properties. The intrinsic properties are those that are not dependent on the size of the sample, such as Poisson's ratio and Young's modulus. The extrinsic properties that are size and shape dependent include the characteristic strengths.

2.3.2 EXTRINSIC PROPERTIES

The extrinsic properties were discussed in Lourenço's dissertation[46] and Page's literature review.[47] Standard extrinsic property tests in Australia are based on the requirements of AS 3700.[48]

2.3.3 INTRINSIC PROPERTIES

Krajcinovic[49] notes in the field of damage mechanics that the intrinsic properties including the Young's modulus and the Poisson's ratio are assumed invariant constants that statement represents an upper bound limit on the Young's modulus and the shear modulus. Krajcinovic notes further that the effective stiffness properties are experimentally determined from time dependent strain properties. There are a multitude of papers on masonry units and masonry with typical work being Knutsson & Nielson[50] on the modulus of elasticity of masonry and Knutsson[51] on the stress strain curve for masonry. Nichols and Totoev[52] experimentally determined the dynamic modulus of elasticity for masonry units using two non-destructive techniques. Vermeltfoort[53] and Wolde-Tinsae, *et al.*[54] looked at the mathematical relationship between the characteristic

[45] Grimm, C.T., (1996), Masonry throughout History, *TMSJ*, 14, 5. (Greek for baked brick.)
[46] Lourenço, P.B., (1996), *Computational Strategies for Masonry Structures*, (The Netherlands: Delft University Press), 15-26.
[47] *Op. cit.*, Page, A.W., (1973), 24-56.
[48] *Op. cit.*, AS 3700 *Masonry Structures*, Appendices B, C and D.
[49] *Op. cit.*, Krajcinovic, D., (1996), *passim.*
[50] Knutsson, H.H., & Nielson, J., (1995), On the modulus of elasticity for masonry, *MI*, 9, 2, 57.
[51] Knutsson, H.H., (1993), The stress strain relationship for masonry, *MI*, 7, 1, 33.
[52] Nichols, J.M., and Totoev, Y.Z., (1997a), A comparative experimental study of the Modulus of Elasticity of Bricks and Masonry, *11thIB^{2}MC*, Shanghai, *passim.*
[53] Vermeltfoort, A. Th., (1997), Properties of Some Clay Bricks under varying load conditions, *MI*, 10, 3, 85.
[54] Wolde-Tinsae, *et al.*, (1993), State of the Art: Modulus of Elasticity of Masonry, *Proceedings of the Sixth North American Masonry Conference*, Phil. PA, 6-9 June 1993, 1211.

strength of the masonry unit, f'_m, and the modulus of elasticity and established a numerical factor of 400 to 550. A direct measurement of the modulus of elasticity of the mortar was not practically feasible with the test protocol. Davidge[55] states "if an assumption of isotropicity is made for the two phases and the stress is applied normally to the slabs, then the stress in each slab is constant and the corresponding composite Young's modulus" is:

$$E_{\emptyset} = \frac{E_1 E_2}{E_2 V_1 + E_1 V_2} \quad (1)$$

The subsequent research by Totoev and Nichols[56] on the properties of masonry prisms was based on a single river sand and mortar type. Mortar cubes of size 70 ± 1 mm had a mean compressive stress of 2.2 ± 0.2 MPa. The Poisson's ratio results for the several types of masonry units used in the manufacture of the prisms ranged from 0.1 to 0.4. The results for the elastic constants for two typical brick types are presented in Table 2.

TABLE 2 MASONRY ELASTICITY RESULTS

Description	Young's Modulus of the Masonry (quasi-static Protocol) (GPa)	Nominal Poisson's Ratio for central brick in the Prisms	Calculated Young's Modulus of the Mortar (GPa)	Peak Stress (MPa)	Ratio of the Young's Modulus of Masonry to the Mean Compressive Stress
Pressed Red Brooklyn	15 ± 3	0.25	-	19 ± 4	780
Calcium Silicate	5 ± 4	-	2	8 ± 1	610

Young's modulus for the mortar within the joints has been calculated to be within a range of 1 to 2 GPa using the method presented in equation (1). These results are static properties usually determined using a compressive test protocol. The compressive test protocol encounters the problem of crack closure that can result in changes in the stiffness of bricks or prism samples during testing. Krajcinovic[57] presents a method for the measurement of the modulus of elasticity using a tensile test with the results determined between the 15 % and 85 % of the yield stress.

[55] Davidge, R.W., (1979), *Mechanical Behaviour of Ceramics*, (Cambridge: Cambridge UP), 1st paperback ed. 163, *passim.*

[56] Totoev, Y.Z., and Nichols, J.M., (1998), Dynamic Testing of Masonry by the Longitudinal Vibration and Ultrasonic Pulse Method, *8th CMC*, Jasper, *passim.*

[57] *Op. cit.*, Krajcinovic, D., (1996), *passim.*

2.3.4 HISTORIC MORTAR

Baker[58] revised his 1888 *Treatise on Masonry Construction* and discussed the problems encountered when working with masonry and mortars. Test results for masonry samples from Baker's text are presented in Table 3.

TABLE 3 TEST RESULTS (AFTER BAKER, 1912)

Test Number	Test Description	Test Result Imperial Units (PSI)	Test Results SI Units (MPa)
A	Tensile Test of Cement manufactured with three parts standard sand.	165 - 328	1.1 - 2.2
B	Crushing Strength of Illinois Bricks	3996 - 12280	27 - 89
C	Compressive Strength of Stiff Mud Face Brick	Mean 12766 Range 8930 - 15330	Mean 87 range 61 - 104
D	Transverse Shear Strength Tests 11 bricks and 37 tests total	308 - 2589	2 - 18
E	Crushing Strength of Piers made from Stiff Mud Face Brick	Portland - 4021 1:C 3:S - 2410 1:L 3:S - 1420	27 16 10

These tests were performed at the US testing machine at Watertown Arsenal. The stiff mud face bricks (Tests numbered C and E) were manufactured in one kiln, no history was provided for the other bricks (Tests numbered B and D). Baker[59] observed a considerable variation in the results even to noting that six-month results might be lower than a one-month result. The interesting point from Baker's work was the effect of the standard test on the tensile strength of mortar. Baker's testing was sophisticated enough to observe and document the strain rate effect on the ultimate strength. It would be worth repeating these tests with current materials. Baker has presented the first known documented experimental results for masonry that demonstrate the increased strength result of dynamic testing. The applied energy in the testing divides between the mass and the spring terms of the equation of motion resulting in a higher apparent strength, whilst causing an apparent drop in spring stiffness due to the frequency impact on the measured force and the use of static measurement techniques being applied to a dynamic problem. These observations are not contradictory. Baker discusses the problems of workability, compressive and tensile strength currently being investigated by Sugo.[60] The basic result found by both the two research groups was that sand to pozzalonic volume ratio of three

[58] *Op. cit.*, Baker, I.O., (1912), 76-77, 105-131.
[59] *Loc. cit.*, Baker, I.O., (1912), 316.
[60] Sugo, H.O., (2000), Strength and Microstructural Characteristics of Brick/Mortar Bond, Diss. (unnumbered), UN, *passim.*

provides consistently good results for the tensile and compressive properties. The delivery and use of lime as the workability agent in mortar remains as much an area of future research as it was in 1888.

2.3.5 LIME

The types of lime that are available or that can be manufactured are hydrated lime,[61] lime slurry, and lime putty.[62] Lime manufactured in Australia is governed by the standard AS 1672.1.[63] Lime[64] as an ingredient can improve the workability and strength of the mortar. The use of hydrated lime without sufficient mixing time does not provide the benefit of workability, but does meet the requirements for strength. The use of lime slurry or putty can meet both requirements if care is taken in the batching. A mortar overdosed with lime results in a statistically significant loss of strength. The forms of lime delivery for mortar are presented in Table 4.

TABLE 4 FORMS OF LIME DELIVERY

Form	Description
Lime	Hydrated lime in bag form
Lime slurry	Equal parts by weight of water and hydrated lime are left to stand and age for at least 24 hours. (This author seals the containers although there is a school of thought that suggests that sealing is contra indicated.[65] The age and consistency of the lime slurry affects the mixing time.)
Calcium oxide	Quick lime in the form of powder after the firing but before hydration. (This material is not normally available to produce lime putty, however a batch was made available for this current research work from the limekiln at Tamworth.)
Lime putty	Equal parts by weight of water and calcium oxide were left to stand and age for at least 24 hours.

The use of lime requires a period of standing to allow the apparent chemical reaction between the lime and sand to provide the workability improvement that represents an area of potential research.

[61] Tsimas, S., and Raikos, K., (1995), Lime , an irreplaceable mortar constituent, *Zement-Kalk-Gips International*, 48, 6, 350 – 6.
[62] Kateiva, G., (1969), Structural brickwork design: Practice, *Symposium on the Australian Standard CA 47 1969 SAA Brickwork Code*, Institution of Engineers (Australia), Perth, Paper 3, 1-5.
[63] 1672.1-1997, *Limes and limestones - Limes for building*, Standards Australia, Sydney, *passim.*
[64] Sugo, H.O., Page, A.W., and Lawrence, S.J., (1998), The influence of lime and methylcellulose on the microstructure and bond strength of mortars in combination with calcium silicate units, 8*CMS*, Jasper, AL, May 29-June 1, 1998, *passim.*
[65] Sugo, H.O., (personal comm., November 1998).

2.3.6 WATER

The use of clean water free from organic and dissolved chemicals is preferred for the manufacture of mortar.

2.3.7 SAND

A typical grading limit for sands for use in concrete has been presented in AS 2578.1.[66] This grading limit was developed in the 1940s from research on concrete mixes. It has limited applicability to mortar. The types of sand that are available for the production of mortars are beach and river sands. Beach sand has a problem of mono sized grains due to the long period of wind and water action that the sand has been subjected to since its separation from the parent rock. These sands were often dosed with additives[67] to provide the workability required for a construction mortar. River sand generally has a better grading with a higher fine fraction that provides an improved workability compared to beach sand mortars. Ground Test Pty Ltd.[68] graded several of the available sands within the Hunter and Newcastle regions (Figure 1). The graduation results show two distinct groups of sand. The Rosebank (fine) river sands show a coarser grading and the Fern Bay beach sands are mono sized. Staley[69] commented that poorly graded sands make a harsh mortar and that such sands were harmful in high cement mortars. He concluded that the graduation of the sand, shape of the sand particles in the samples, and the ratio of sand to the other constituents were important in achieving a workable strong and watertight mortar.

2.3.8 PORTLAND CEMENT

Pozzalonic cements are manufactured in accordance with AS 3972.[70] Cement type A was used in this current research work.

2.3.9 ADDITIVES

No additives were used in this current research work. Sugo, Page, and Lawrence[71] discuss in detail the results of the use and abuse of common additives such as air entraining agents. The difficulty was not the use of these additives, but the misuse by overdosing.

---

[66] AS 2578.1-1998, *Aggregates and rock for engineering purposes - Concrete aggregates*, (Standards Australia: Sydney).
[67] Sugo, H.O., Page, A.W., and Lawrence, S.J., (1996), Influence of the Macro and Micro constituents of air entrained mortars on Masonry Bond Strength, 7*NAMC*, Notre Dame, Indiana 1, 230 – 241.
[68] Ground Test Pty Ltd, (1990), *Sand Samples – Grading Results*, 1.
[69] Staley, H.R., (1940), A petrographic study of the Bond between Bricks and Mortar, *Transactions of the British Ceramic Society*, 39, 100.
[70] AS 3972-1991 *Portland and blended cements*, (Sydney: Standards Australia), *passim.*

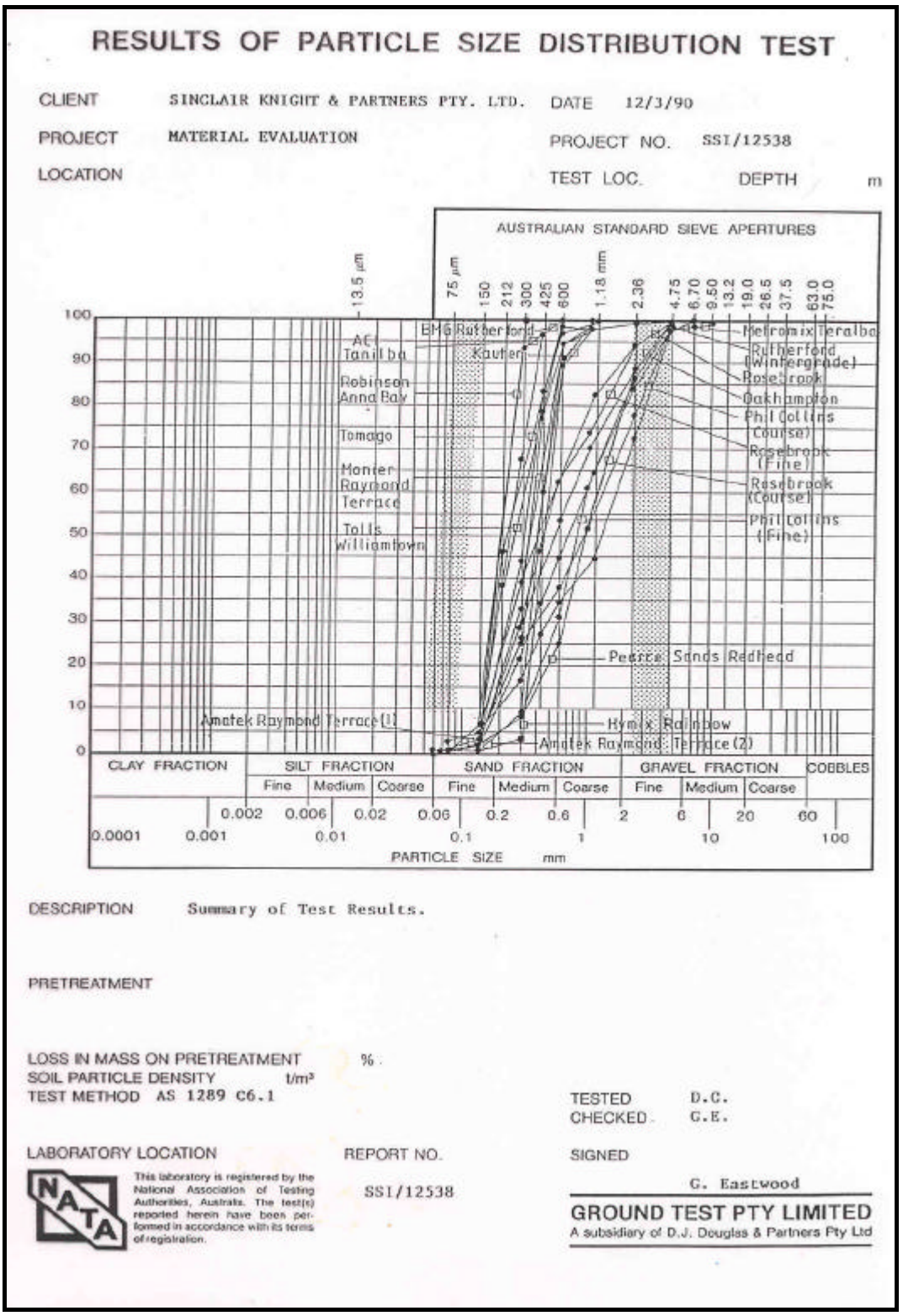

FIGURE 1 RESULTS OF PARTICLE SIZE DISTRIBUTION TEST - HUNTER REGION

[71] *Op. cit.*, Sugo., *et al*, (1996), 230.

2.3.10 BRICKS

Bricks are manufactured in accordance with AS/NZS 4455.[72] Typical dimensions for Australian bricks are 225 by 110 by 75 millimetres.

2.3.11 BOND

Staley's[73] petrographic study of the mortar to brick bond reviewed masonry construction and problems related to the leaky wall problem. The conclusions from Staley's first class research were that a tight bond was required with the interstitial spaces filled and interfacial bonds that are intimate continuous and permanent. High lime mortar has proved better at meeting these requirements.

Sugo, Page and Lawrence[74] have completed a study into the mortar to brick bond. Their study established a systematic quantification of a number of factors that detract from bond such as air entraining agents and completed a scanning electron microscopy study that explains the characteristics of good and poor bond. The conclusions, reached by Sugo, Page and Lawrence, are consistent with and offer a systematic study of the earlier results from Staley.[75] These results are consistent with the earliest discussion provided by Baker.[76]

2.4 SEISMICITY

2.4.1 INTRODUCTION

> *And it shall come to pass, that when they make a long blast with the Ram's Horns and when ye hear the sound of the trumpet, all the people shall shout with a great shout; and the wall of the city shall fall down flat, and the people shall ascend upon every man straight before him.*[77]

Earthquakes have been documented from before the time of Christ yet earthquakes continue to plague man. Seismicity the study of earthquake phenomena has become an integral part of estimating the dynamic loads that may be applied to masonry structures during the design lifetime of the building irrespective of whether one is interested in intraplate or interplate regions.[78] Earthquakes[79] can take a devastating[80] toll on urban

[72] AS/NZS 4455:1997, *Masonry Units and Segmental Pavers,* (Sydney: Standards Australia), *passim.*
[73] *Loc. cit.,* Staley, H.R., (1940), 85.
[74] *Op. cit.,* Sugo., *et al,* (1996), 230.
[75] *Op. cit.,* Staley, H.R., (1940), *passim.*
[76] *Loc cit.,* Baker, I.O., (1912), Chapter 12.
[77] *The Holy Bible* (*King James Version*), (1940), (Cambridge: Cambridge University Press), Joshua, 6:5.
[78] The major earthquakes in New Madrid, Mo., USA in 1811-12, in Lisbon in 1755 and Tangshan in 1976 would provide the evidence to support this opinion.
[79] Rosenblueth, E., (1960),The earthquake of 28 July 1957 in Mexico City, 2*ICEE,* 1, 359.
[80] Hadjian, A.H.,(1992), The Spitak, Armenia Earthquake - Why so much damage?, 10*WCEE*, 1, 6.

areas.[81] Some of the wealthy communities in interplate regions have moved away from unreinforced masonry to reinforced and prestressed masonry. This change arises because of the improved ductility of reinforced masonry and prestressed masonry under seismic loading. It has been stated so often in the literature to be monotonous that well designed and built masonry can withstand substantial earthquakes whilst poor masonry can be damaged at the first whisper.[82] Major earthquakes are considered rare[83] in intraplate zones.[84]

Masonry research particularly for unreinforced masonry has typically been focused on a reasonably limited range of earthquake magnitudes. The earthquake risk in intraplate zones is considered low except in some specific locations.[85] This current research work does not start with predefined limits on the earthquake intensity or on a set pattern. Interplate events have now been defined as occurring within two degrees of the plate boundary,[86] thus the intraplate region of interest for masonry covers about 95 percent of the earth's land surface. Interplate earthquakes typically occur at boundaries that have one plate being subsumed beneath or sliding past a second plate. The boundary area becomes highly stressed and deformed because of the subduction or movement. The effect of such significant land mass deformation provides an attenuation of the amplitude of the earthquake waves across the various damaged boundaries in the interplate region. The same level of attenuation does not occur in intraplate regions as the land mass has not been as damaged.[87]

The assumption of limited earthquake loading has been set aside in this detailed literature review. The primary interest of this current research centres on the rate of change of the stiffness tensor as it crosses a defined failure surface for any shear wall and implicitly taking the environmental load from the normal to the abnormal level.

Each of the continental plates that make up the land surface has unique and interesting features. It is of more than passing interest in this current research work to consider the

[81] Steinbrugge, K.V., and Moran, D.F., (1954), An engineering study of the southern California earthquake of July 21, 1952 and its aftershocks, *BSSA*, 44, 2B, 210. are probably three of the seminal post earthquake report papers of the last 50 years that support this view.
[82] Melchers, R.E., and Page, A.W., *(*1992), The Newcastle Earthquake, *Building and Structures*, 94, 143.
[83] Richter, C.F., (1958), *Elementary Seismology*, (San Francisco: Freeman), 359, provides evidence of swarms in areas considered seismically quiet.
[84] Bent, A.L., *(*1994), The 1989 (M_s 6.3) Ungava, Quebec, Earthquake: A complex Intraplate event, *BSSA*, 84, (4), 1075, notes the surprise this type of event caused in the local community. A similar tale can be recounted for the Newcastle and many other earthquakes.
[85] Frankel, A., *et al.*, (1997), USGS Seismic Hazard Map.
[86] *Loc. cit.*, Wysession *et al.*, (1995), 755.
[87] Abrams, D.P., (1997), LAMB Project Memphis Keynote Speech. *Earthquakes In Australian Cities*, Brisbane, *passim.*

similarities between interplate or intraplate areas that are separated by great distance. This interest focuses not only narrow areas of regional or state interest, but also the world. This focus properly occurs with the design of a single building using now traditional statistical methods to estimate the design-loading pattern.[88] The current research should be viewed within a relevant worldwide statistical framework. It is not the probability that a single building at a known location will be struck by an earthquake. But that a piece of unreinforced masonry shear wall from any age in any building will be affected by an earthquake event that presents a different probability problem to that problem solved using the Cornell method.

The development of seismology can be placed in four age contexts. The first was the period to the start of this century. There was considerable interest in earthquakes and written records of the felt effects during that time but limited other scientific data. The second stage covers the period up to the 1930s ending with the start of the seminal work of Gutenberg and Richter[89] in the early 1930s. The third stage continues until 1956 and the first world conference[90] where we see a wide application of the techniques developed by Richter, Gutenberg, Housner, and others. There is a wide interest in the development of numerical models and the predication of earthquakes. The development of modern codes of practice can be traced from these four early decades of research.[91] The current period from 1956 to 2001 involves application of such diverse fields as numerical techniques and paleoseismology to broaden the understanding of earthquake patterns and behaviour over time. This seismic review considers the four identified periods and points to the research relevant to the development of the loading pattern that is to be used in the experimental study.

2.4.2 SEISMOLOGY TO THE MODERN ERA

The recent work on the Chinese catalogue of Lee *et al.*[92] covers the documented history of the Chinese earthquake felt records along with a nominal epicentre location for these earthquakes. Mallet[93] believed that earthquakes were fundamentally volcanic in nature.

[88] Cornell, C.A., (1968), Engineering seismic risk analysis, *BSSA*, 58, 5, 1583-1606.
[89] Gutenberg, B., and Richter, C.F., (1954), *Seismicity of the earth and related phenomena*, (Boston: Princeton UP, 2nd ed.), *passim.*
[90] World Conference on Earthquake Engineering, (1956), *Proceedings of the World Conference on Earthquake Engineering*, (Berkeley: EERI), 1 volume.
[91] Heidebrecht, A.C., (1995), Insights and challenges associated with determining seismic design forces in a loading code, *Bulletin of the New Zealand Society for Earthquake Engineering, 28*, 3, 224.
[92] Lee *et, al.*, (1976), Catalogue of Historical Earthquakes in China compiled from recent Chinese publications, *BSSA*, 66, 6, 2003.
[93] *Op. cit.*, Richter, C.F., (1958), 33.

Milne[94] provided one of the earliest useable texts on seismology. Imamura[95] stated that 'While admitting the futility of any attempt to deduce comprehensive seismic zones from a catalogue of earthquakes covering no more than 330 years it may be pointed out that statistics of older dates have also been drawn upon.' This mirrors the later comment of Richter[96] on the use of short base records. Kotò[97] has been quoted as stating 'that the alluvial plain in the area showed the peak meizoseismal area'. He further observed 'that the effects fall off in the surrounding hilly area.' As Richter noted 'one assumes because of the more competent rock although this is not explicitly stated.' These earliest comments represent the beginning of the realization by seismic researchers that the ground conditions affect building response to the earthquake forces.

Umemura[98] details the work of Sano (1916) presenting the concepts of seismic coefficients for lateral force design in aseismic design and then states that 'Naito subsequently used this material in designing buildings in the Kanto of Japan. These buildings withstood the great Kanto 1923 earthquake'. There exists anecdotal evidence that the use of lateral force provisions were developed by several researchers in the early 1900s.

Of minor interest and within the Australian context, Cotton[99] described the Kurrajong earthquake of August 15, 1919 and Clarke[100] detailed felt events up until that time in New South Wales. Clarke's article was interesting within the context of this current research work as it provides some ideas as to the type of data that is available for early events, whilst the first article provides insight into the rapid advances made in the intervening time. Richter's[101] definitive text on elementary seismology and Gutenberg and Richter's[102] monograph effectively summarized the state of the art until the mid fifties.

---

[94] Milne, J., (1898), *Seismology*, (London: Kegan) *passim.*
[95] Imamura, A.,(1937), *Theoretical and Applied Seismology,* (Tokyo: Maruzen), (reference from Richter, C.F., (1958)), 209.
[96] *Op. cit.*, Richter, C.F., (1958), 389.
[97] Kotò, B., (1893), On the causes of the great earthquake in Central Japan, 1891, *J. Coll. Science. Imp. Univ. Japan, 5*, part 4, 296-353, pls. XXVIII-XXXV. Professor of Geology : Imperial University: (reference from Richter, C.F., (1958), 563-566, discussing the Mino-Owari Earthquake of 1891).
[98] Umemura, H., (1975), The development of dynamic design of buildings in Japan, *Fifth European Conference on Earthquake Engineering*, 2, 122, 1.
[99] Cotton, L.A, (1921), The Kurrajong Earthquake of August 15, 1919, *Proceedings and Journal of the Royal Society of New South Wales.* 55, 83.
[100] Clarke, W., (1869) On the causes and phenomena of earthquakes, especially in relation to shocks felt in New South Wales and in other provinces of New South Wales, *Proceedings and Journal of the Royal Society of New South Wales*, 2, 51.
[101] *Op. cit.*, Richter, C.F., (1958), *passim.*
[102] *Op. cit.*, Gutenberg, B., and Richter, C.F., (1954), *passim.*

The work of Gutenberg and Richter provides a starting point to describe modern seismology and set out the orders of accuracy of measurements. Gutenberg and Richter pointed out there were no effective seismographs until the 1880s, and the use of reports from non trained staff could not be considered an accurate method to assign any type of realistic magnitude value to an earthquake. Timing of the events was a problem until the 1910s. Non-standard seismographs were a problem until the development of the world network in the late 1950s through the early 1960s. Richter and Gutenberg[103] established the methodology for the statistical analysis of earthquake events. The Gutenberg Richter law provides a power relationship between earthquake intensity and the number of events in an area over a given period. This can be viewed in a linear plot as a two-part equation with a break point about M7. Housner[104] established the properties and characteristics of strong ground motion generated by seismic events. Richter[105] details the estimated amplitudes of the expected surface movement in a moderately strong earthquake (Table 5).

TABLE 5 HARMONIC OSCILLATION FREQUENCIES (HZ)

Acceleration a (g)	Amplitude of Surface Movement (cm)						
	0.0001	0.001	0.01	0.1	1	10	100
1	500	160	50	16	5	1.4	0.5
0.1	160	50	16	5	1.6	0.5	0.16
0.01	50	16	5	1.6	0.5	0.16	0.05

He stated that 'in this table the shaded numerals indicate the combinations of amplitude and acceleration, the corresponding frequencies, most common in the analysis of moderately strong ground motion; the data of a locally more violent earthquake should cover a larger area of the table. In that case it would probably remain true that the highest accelerations are associated with small amplitude and the large amplitudes with low frequency and acceleration.' These estimated surface movements are a direct result of the form of an equation for a harmonic oscillator with low damping. The design range for the test regime for the experimental work should account for the shaded combinations identified in Table 5. Richter[106] provides an interesting summary of the types of damage that can occur in an earthquake for four classification of masonry (Table 6).

[103] Gutenberg and Richter: A body of work from 1933 to the 1960s predominately published in the *BSSA.*
[104] Housner, G.W., (1947a,1955b), Characteristics of Strong Ground Motion, *BSSA, a.* 37, 19-31, b. 45, 197-218.
[105] *Op. cit.,* Richter, C.F., (1958), 25.
[106] *Op. cit.,* Richter, C.F., (1958), 136.

TABLE 6 CLASSIFICATIONS OF MASONRY FOR THE MM SCALE

Definition	Richter's Classifications 1956	Masonry Terms
Good workmanship mortar and design; reinforced especially laterally and bound together by using steel, concrete etc designed to withstand lateral forces	Masonry A	Reinforced Masonry or Confined Masonry
Good workmanship and mortar; reinforced but not designed in detail to resist lateral forces	B	Reinforced Masonry, Structural Masonry (possibly)
Ordinary workmanship and mortar; no extreme weaknesses like failing to tie in at the corners but neither reinforced or designed against horizontal forces	C	Masonry
Weak materials such as adobe; poor mortars; low standards of workmanship and weak horizontally	D	Adobe Masonry and brickwork using fireclays or other plasticizers

Housner[107] considered the characteristics of strong motion earthquakes, albeit with subsequent revisions in 1955 of the response spectra curve due to a seismograph flaw. The understanding of plate tectonics provides an explanation as to the geophysical limits that control the depth of intraplate earthquakes and the depth and location of the interplate regions. The limit of 100 km is for intraplate earthquakes and about 700 km for interplate earthquakes[108]. This first limit has been attributed to the cool brittle nature of the crust. The limit of 700 km has been attributed to the rate of heating of the crust being subsumed at the interplate boundary. The geophysical estimate for the 700 km appears to match the seismicity data. The modern era of seismology realistically dates from 1964[109] with the establishment of a world network for arms control purposes. Heidebrecht[110] using the Canadian and New Zealand codes as examples illustrates the development of seismic code provisions in this period. Denham, *et al.*[111] determined experimentally the principal direction of the stress in eastern Australia noting that the compression is east to west. These authors have shown that the northern part of the plate for Australia exhibits a high level of intraplate activity. The deformation of this plate is analogous to the buckling of an elastic plate with a wavelength of the order of 160 km. They note that the earthquakes are associated with brittle fracture close to the surface. Dick[112] looked at extreme value theory and earthquakes, and made the point that one should consider human life in the determination of the return period.

[107] *Loc. cit.*, Housner, G.W., (1955), *passim*.
[108] Gubbins, D., (1992), *Seismology and Plate Tectonics*, (Cambridge: Cambridge UP), 2nd ed, 276.
[109] *Ibid.*, 57.
[110] *Loc. cit.*, Heidebrecht, A.C., (1995), 224.
[111] Denham, D., *et al.*, (1981), Earthquake evidence for compressive stress in the southeast Australian crust, *Journal of the Geological Society of Australia*, 28, 323.
[112] Dick, I.D., (1964), Extreme value theory and earthquakes, *Third International Conference on Earthquake Engineering*, III, 45.

In considering the Cornell McGuirre method and its probabilistic surface, there are limitations of the temporally short database and the peaks identified so far may at best be illusionary within the timeframe of a reasonable statistical analysis temporal period. Richter[113] indicated the relative magnitude of displacements and accelerations on the surface and underground. Gaull, *et al.*[114] have revised the probabilistic earthquake risk maps of Australia using the Cornell McGuire method. Their work was a direct result of the Newcastle earthquake and contributed to the revised Australian standard for earthquake loading.[115]

Abe and Yoshida[116] demonstrate the well-documented alluvial response to earthquake waves. By the start of 1995 there were a multitude of papers on site response estimation techniques,[117] probabilistic seismic hazard assessment,[118] and testing models for earthquake nucleation,[119] to cover just a few of the areas. Hutchinson *et al.*[120] discussed the development of a common Australian New Zealand code to cover a range from intraplate to interplate regions for the four main islands[121] of the two nations.

Potentially productive areas of research include paleoseismology (Johnston and Kantor[122]), seismic geology (McCue *et al.*[123] and Nakamura[124]), and the mathematics of historically recorded earthquakes (Atkinson and Boore,[125] and Sykes[126]). One of the currently productive research areas has been the development of Fourier transforms to examine the power of the earthquake in the frequency domain.

---

[113] *Op. cit.*, Richter, C.F., (1958), 147.
[114] Gaull, *et al.*, (1990), Probabilistic earthquake risk maps of Australia, *Australian Journal of Earth Sciences*, 37, 169-87.
[115] AS 1170.4 *Minimum design loads on structures Part 4: Earthquake Loads*, (Sydney: Standards Australia), 8.
[116] Abe, K., and Yoshida, Y., (1992), Seismic response analysis of alluvial valley with dipping layers by a boundary element - finite element coupling method, *International Journal for Numerical Methods in Engineering*, 35, 1753.
[117] Field, E.H., and Jacob, K.H., (1995), A comparison and test of various site response estimation techniques, including three that are not reference site dependent, *BSSA*, 85, 4, 1127.
[118] McGuire, R.K., (1995), Probabilistic seismic hazard analysis and design earthquakes: Closing the loop, *BSSA*, 85, 5, 1275.
[119] Abercrombie, R.E., Agnew, D.C., and Wyatt, F.K., (1995), Testing a model of earthquake nucleation, *BSSA*, 85, 6, 1873.
[120] Hutchinson, G., *et al.*, (1995), Developing a common Australasian earthquake loading standard, *Bulletin of the New Zealand Society for Earthquake Engineering*, 28, 4, 288-93.
[121] The four islands are the North and Osuth Island of New Zealand, Tasmania and the Australian mainland.
[122] Johnston, A.C., and Kantor, L.R., (1990), Earthquakes in stable continental crusts, *Scientific American*, 262, 3, 42.
[123] McCue, K., and Love, D., (1997), Microtremor survey of Adelaide, *Earthquakes in Australian Cities*, 19, 1-3.
[124] Nakamura, Y., (1989), A method for dynamic characteristics estimation of subsurface using microtremor on the ground surface, *Quarterly report of the Railway Technical Research Institute*, 30, 1, 25-32.
[125] Atkinson, G.M., and Boore, D.M., (1995), Ground motion relations for Eastern North America, *BSSA*, 85, 1, 17-30.
[126] Sykes, L.R., (1996), Intermediate and long term earthquake prediction, *Proceedings of the National Academy of Sciences of the USA*, 93, April, 3732.

2.4.3 THE INFORMATION AGE

The current level of knowledge should be considered before embarking on a study of the characteristics of particular earthquakes. As a minimum, an engineer generally has access to a set of acceleration levels and spectra for a particular location on the earth's surface for one of two recurrence intervals that are approximately 500 and 2500 years. A design spectra in the frequency domain allowing for varying damping levels will be provided and there may be access to finite element or boundary element code sets to model the particular earthquake or loading pattern. The rules for the design of buildings are now often being harmonized in a region. Examples of this work include the Eurocode provisions, the PacRim conferences on loadings, and the work of such groups as typified by the Californian groups in the series of EERI[127] monographs.

Horton, Barstow, and Jacobs [128] have generated synthetic earthquakes of varying M r combinations and stress drops for the LAMB project in Memphis (Abrams and Shinozuka).[129] Jacobs[130] noted that in the production of these records that 'natural records are always 'holey' or peaked and troughed, but to various degrees. This spectral roughness is pronounced when you make Fourier spectra or undamped response spectra, but diminishes of course with increasing damping of the SDoF resonator for response spectra. The latter is what happens really in damped structures.

Occurrence of spectral roughness is a strong function of the site conditions: i.e. of the impedance (shear wave velocity times density) profile with depth for the site. The Nahanni and El Centro records have less contrast rich soil/rock profiles, while the sites for Memphis we modelled have very soft soils overlying denser sands, and eventually hard rock, therefore being very ringie and full of holes and peaks. We start out in the synthetics with a smooth Brune spectrum, which becomes a bit more ringie after the crustal wave propagation scattering function is applied (and the Earth does that also, that's why we mimic it); but once we add in the soil response we really get site specific 'holiness'. That is the reason why you sometimes get surprising damage for certain structures at certain sites: double resonance between site peak and fundamental period of the structure. The most famous case for this is of course the Mexico City effect in 1985

[127] *Earthquake Engineering Research Institute Monographs,* (Berkeley, California: EERI).
[128] Horton, S.P., Barstow, N., and Jacobs, K., (1997), Simulation of earthquake ground motion in Memphis, Tennessee, *Proceedings of the Eleventh World Conference on Earthquake Engineering,* June 23-28, 1997, Acapulco, Mexico, Elsevier Science, Paper 1302, *passim.*
[129] Abrams, D.P., and Shinozuka, M., (1997), *Final Report Loss Assessment of Memphis Buildings,* Technical Report NCEER-97-00, (Urbana, Illinois: UIUC), *passim.*
[130] Jacobs, K., Lamont Doherty Observatory, Columbia University, in personal communication in November 1997.

(?): 1- 2 second 10-20 story high rise buildings located on the clayey Old Lake bed (site resonance's peaked near 1 - 2 seconds) collapsed, while people in adjacent old colonial masonry buildings 2 or 3 stories high did not even realize there was an earthquake (totally detuned).

If you are interested in a generic study, then you must use several of the records from different site conditions, and average the effects, so that you never have structural performance for a given building height or fundamental period influenced by the peaks or troughs of just one site condition. I do not think that the use of artificially smoothed spectra is a valid substitute. Rather the smoothing of performances over real site conditions seems to me a more valid approach, at least if you are not only interested in the mean response, but also want to get a measure for the variability of response, which highly depends on whether double resonance's of sites and structures do or do not occur under region-specific site conditions and their respective variability.'

2.4.4 TIME SERIES ANALYSIS

The recent seminal paper by Ebel and Kafka[131] on the time series analysis for the earthquake data for the New England region represents a definitive step in the analysis and understanding of earthquakes as far as they affect the human population in intraplate zones. Their method may ultimately change the existing mapping hazard programs and the methods for dealing with insurance work.

The paper of Kafka and Levin[132] on the spatial distribution of smaller earthquakes supports this method. The mathematics that underlies the Gutenberg distribution points strongly to a driving mechanism based on an area function. A simple analysis of the 43,000 earthquakes in the USGS[133] database from 1973 to the present suggests a logarithm linear plot, with the slope of the count versus the magnitude plotting as a straight line (Figure 2).

[131] Ebel, J.E., and Kafka, A.L., (1999), A Monte Carlo Approach to Seismic Hazard Analysis, *BSSA*, 89, 4, 854.
[132] Kafka, A.L., and Levin, S.Z., (1999), Does the spatial distribution of smaller earthquakes delineate the areas where larger earthquakes are likely to occur?, *BSSA (submitted)*.
[133] USGS (1999), Earthquake bulletins, (owner-qedpost@NEIS.CR.USGS.GOV, now bigquake@gldmutt.cr.usgs.gov and qedpost@gldmutt.cr.usgs.gov), (Colorado, NEIS).

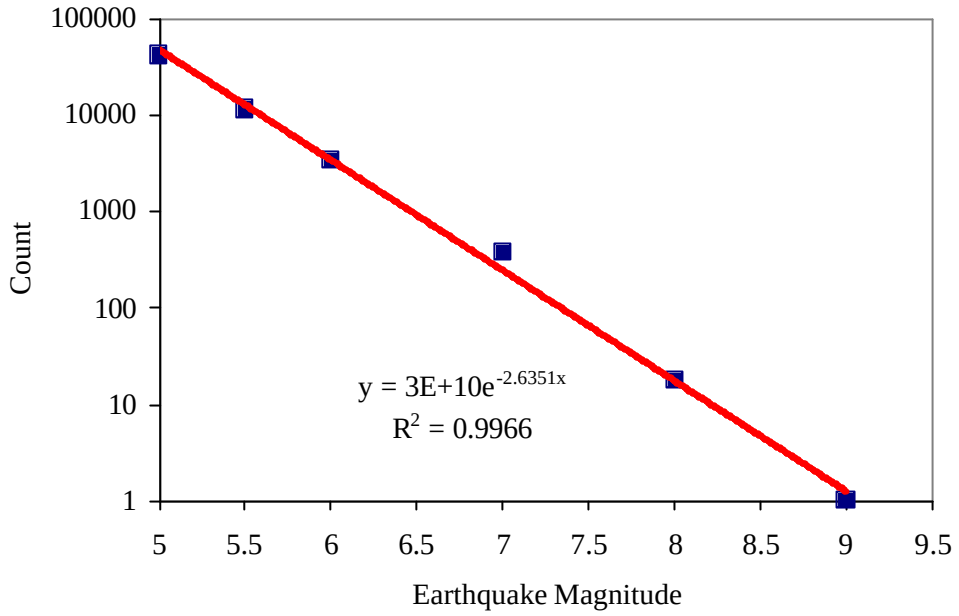

FIGURE 2 USGS DATABASE 43,000 EARTHQUAKES FROM 1973

The analysis of the earthquake shown on Figure 2 supports the conclusions reached by Ebel and Kafka. A century period of earthquake data now exists that permits further regional development and use of the time series analysis method developed for the New England. One such region extends from New Madrid to Maine and the side spur area to Charleston with the logical extension to this work being the development of the fault model.[134]

2.4.5 REVIEW OF EARTHQUAKE LIMITS

The United States Geological Service[135] publishes a number of reports on earthquakes. These reports generally meet a set of criteria that place the earthquakes in a range that will damage urban infrastructure including unreinforced masonry (Table 7).

TABLE 7 USGS RECORDS

Bulletin Type	QED Bulletin	Earthquake Bulletin
Start Date	22/8/1997	22/8/1997
End Date	5/3/1998	5/3/1998
Number of records	3169	120

[134] Marshak, S., and Paulsen, T., (1997), Structural Style, Regional Distribution, and Seismic implications of Mid-continent Fault-and Fold Zones, United States, *Seismological Research Letters*, 68, 4, 511.
[135] USGS (1999), Earthquake bulletins, (owner-qedpost@NEIS.CR.USGS.GOV, now bigquake@gldmutt.cr.usgs.gov and qedpost@gldmutt.cr.usgs.gov), (Colorado, NEIS).

A review of the earthquake data suggests that this information shown on Figure 2 and presented in Table 7 is count accurate to about magnitude 5.5. There is a fall in recording of events for the usual seismological reasons of interest, number, and available resources below that magnitude. The critical lower bound in these data sets is the M5.5 event. The USGS collect data on a limited number of events below this threshold, and from a fatality rate viewpoint, it seems a reasonable lower bound, although the current research on the time series analysis will require an improved collection for low magnitude events in the range of M2 to 5. There has been an average of one M8 per annum. Thirty six earthquakes have caused more than 5000 deaths in the last century. The Tangshan earthquake (M8) caused 242,000 deaths.[136] A death count becomes appreciable in some events of M5.5 or greater and this is particularly significant in untested urban areas.[137] In all probability, these events now number 38 with the May 1998 Afghan earthquake, the recent Turkish swarm, the Athens, and the Taiwan earthquakes. An earthquake kills more than 5000 people with a mean period between such occurrences of 900 days.

2.4.6 TANGSHAN EARTHQUAKE

The Tangshan earthquake was the most devastating this century. Shiono[138] provided a summary of the fatality statistics of the event (Table 8).

TABLE 8 TANGSHAN EARTHQUAKE STATISTICS

Seismic Intensity	Collapse Rate %	Area (km^2)	Fatality Rate %
5	0	216,000	0
6	1		
7	7	33,300	
8	16	7,270	3
9	30	1,800	
10	60	370	15
11	90	47	
11.2+	100		30

The dominant wall material in Tangshan was noted as stone or brick. The adobe damage was not counted in the analysis because of its limited use in the Tangshan area. Shiono[139] also provide a comparison of fatality rates to earthquakes in eastern Turkey, China (average), Europe (average), and two Italian earthquakes in 1930 and 1982.

[136] Shiono, K., (1995), Interpretation of published data of the 1976 Tangshan, China Earthquake for the determination of a fatality rate function, *Japan Society of Civil Engineers Structural Engineering/ Earthquake Engineering*, 11, 4, 155s.
[137] *Op. cit.*, Richter, C.F., (1958), *passim.*
[138] *Loc. cit.*, Shiono, K., (1995), 155s.
[139] *Loc. cit.*, Shiono, K., (1995), 155s.

2.4.7 GROUND EFFECTS

The development of boundary element techniques has allowed a number of interesting side issues such as the wave amplification from alluvial valleys and the dynamics of stratified layers to be studied in some detail. Nakamura[140] developed a method based on the Fast Fourier transform of the acceleration traces to estimate the natural frequency of a site and the vertical amplification due to the ground geology. It is no longer acceptable for major design to ignore the site-specific response to the loading from an earthquake. McCue and Love [141] have looked at the micro tremor results and plotted the response contours for Adelaide. There are, of course, questions as to the validity of the use of micro tremors in terms of the energy source and relation to earthquake sources. However, the response gives some assistance in assessing buildings against known frequency patterns.

2.4.8 DISCUSSION

The use of masonry in the interplate areas has some uses when well constructed, but otherwise is too brittle for major use. The main issue with these areas was identified as the retrofit of the existing stock of unreinforced masonry buildings. This retrofitting represents a significant cost to these communities.

Three seismological strands are relevant to this research and future masonry research for intraplate regions of the world. The first strand is continued data collection. Secondly, further refinement and development of numerical models for earthquake generation where each brings a continually evolving knowledge will permit the development of buildings better able to withstand earthquakes. The final strand is the use of paleoseismology, geology, and other disciplines to investigate historic earthquakes. In studying the work of early researchers on masonry subjected to inplane loads such as Tercelj *et al,*[142] there was urgency to their work. This urgency came from the increasing realization that the development of the major housing tracts in the last few hundred years from stone and masonry potentially posed a significant seismic risk. In looking to the research, there is a realization that these types of experiments provide new data that will eventually be incorporated into more sophisticated computer models.

[140] *Loc. cit.,* Nakamura, Y., (1989), 25.
[141] McCue, K., and Love, D., (1997), Microtremor survey of Adelaide, *Earthquakes in Aust. Cities*, 19, 1.
[142] *Loc. cit.,* Tercelj, *et al.,* (1969), *passim.*

2.5 MASONRY BUILDINGS

2.5.1 INTRODUCTION

The Heyman rules[143] demonstrated the fundamental concepts for the design of historic or load-bearing masonry subjected to gravitational loads and normal environmental loads. These rules can be extended for unreinforced structural masonry using the work of Epperson and Abrams[144] with the inclusion of an infrequent environmental load[145] to augment the development of the loading pattern. The reason for adopting this type of design loading relates to a philosophical view of the design and construction of a building. This philosophy is irrespective of the time, place, or mores of the period in which a particular building is conceived and developed. The entity that conceives the building has a certain expectation for the building. For instance, a Pharaoh of Egypt expected a building that would last forever. In much the same manner, the Federal Emergency Management Agency is concerned to protect life.[146]

This literature review explores the expectation that life will be protected in building design and construction. This evolution in the design framework stems from the Heyman rules as the community looks to establish a theoretical framework or model for masonry design and construction. The proposed model incorporates the changes in the development of the loading patterns, the analysis methods, the design methods, and construction in the last four centuries. The review covers the development of guild rules during the Middle Ages to modern theories of elasticity and analysis, controlled building failure, and structural reliability. The design and construction of buildings has progressed from the period when adobe was common. The use of baked bricks from the Roman to the Industrial era required as a minimum design and construction methodology; a loading pattern that in this case should include a seismic loading pattern,[147] a method of analysis, a method of design, and a construction capability to develop a building product that meets the design requirements. Each step provided the data required for the subsequent step

[143] *Loc. cit.*, Heyman, J., (1995), *passim*.
[144] *Op. cit.*, Epperson, G.S., and Abrams, D.P., (1989), 1-2.
[145] Suggeted Definition for an environmental load:
* the daily or normal environmental loads will be deemed to be normal loads, these loads will have a notional return period of less than 475 years.
* the abnormal environmental loads are loads which are greater than the elastic resistance of the structure but less than the failure loads. These will have a notional return period of 475 – 2475 years.
*the extreme environmental load is the failure load for a competently designed structure. The extreme load will not have a return period less than 2475 years.
[146] FEMA, (1997), *passim.*
[147] This decision to use a seismic loading pattern is based on the author's experiences in the Newcastle 1989 earthquake.

allowing for the normal iterations of design. The four methods have developed at different rates and times.

2.5.2 LOADING PATTERNS

The Scottish broach of the first century AD was designed for an unusual environmental load that of Roman slaving parties or northern invaders.[148] These structures have withstood two millennia of use and weathering to remain essentially intact. The Comrie swarm in Scotland[149] represents the starting point to the field of seismology. This development continued through the work of Sano, Richter, Housner, and Gutenberg[150] who were at the forefront in the development of the field of seismology.

The development of a design loading standard in the last four centuries has reached a stage where the argument is not the addition of an environmental load to the analysis stage, but merely its representation. The representation of an applied load in the analysis procedure needs to consider the terms in a statistical sense as to the probability of occurrence and a physical sense as to the magnitude, direction, and period of the loads. This subject has discussed in detail in the literature review and the following conclusions have been reached from the findings of the literature review. The development of the loading pattern for the experimental work must be a realistic representation of a seismic load applied to a building element. The results need to be analyzed so that they can be used with current and future building loading patterns.

2.5.3 STRUCTURAL ANALYSIS OF MASONRY

A modest dwelling can be constructed from masonry using a common sense approach without resorting to analysis and design or being aware of the environmental loads. This development from modest dwellings to the development of Gothic structures with flying buttresses necessitated the development of the guild rules. These rules were used extensively up until the development of the mathematical theory of structural mechanics. Deemed to comply provisions and the minimum provisions are now usually provided for robustness reasons. Timber flooring is an example of an area where the floor is designed to be stiff to avoid excessive deflection underfoot. This is a normal and logical extension to a guild rule although the interesting exception is the dance floor that needs flexibility to protect the dancers feet from high stress concentration and damage.

---

[148] Cruden, S., (1960), *The Scottish Castle*, (Edinburgh: Nelson), *passim.*
[149] Musson, R.M.W., (1993), Comrie, a historical Scottish earthquake swarm and its place in the history of seismology, *Terra Nova*, 5,5, 477
[150] *Loc. cit.*, Richter, C.F., (1958), *passim.*

Traditional structural analysis that has evolved from the work of Hooke was based on analytical solutions and elastic analysis.[151] This class of analysis has been augmented in the last half of this century, primarily due to the limited range of analytical solutions; firstly, with plastic analysis,[152] then with finite difference methods,[153] and then principally with finite element methods.[154] There has been a wider use of the boundary element method[155] for some types of analysis. The boundary element technique has a number of advantages from the use of Green's function and boundary elements rather than a forced discretization of the total volume of the problem. The boundary element method was initially coupled with finite element methods[156] for thin problems, although techniques now exist to solve some thin body problems.[157] The stage has been reached where a competent designer can use a finite element model to analyse a masonry structure.

The design has to be predicated on the assumption that the designer can make the transition to a reasonable design from the limited analysis tools currently available whether using the theory of elasticity or other means. The simple classic masonry arch has been well researched both from an analytical viewpoint and experimentally. It is known to form a number of 'pins'. In the analysis stage, the modelling of the 'pins' can be an interesting problem in determining the appropriate representation of the mechanism. The main point is that the analysis results are still only a mathematical model and require a sound interpretive design skill.

The development of the FEMA 273 manual provides a direction for considering the post elastic behaviour of the masonry elements using the example of the force displacement curve[158] (Figure 3).

[151] Filonenko-Borodich, M., (1958), *The Theory of Elasticity,* (Moscow: n. Pub.), *passim.*
[152] Hill, R., (1949), *The Mathematical Theory of Plasticity,*(Oxford: Clarendon), *passim.*
[153] Timoshenko, S.P., and Goodier, J.N., (1970), *The Theory of Elasticity* (NY: McGraw, 3rd ed.), *passim.*
[154] Segerlind, L., (1993), *Applied Finite Element Analysis*, (New York: Wiley), *passim.*
[155] Banerjee, P.K., and Butterfield, R., (1981), *Boundary Element Methods in Engineering Science*, (London: McGraw), *passim.*
[156] *Loc. cit.*, Abe, K., and Yoshida, Y., (1992), 1753.
[157] Krishnsamy, G., Rizzo, R.J., and Liu, Y., (1994), Boundary Integral Equations for thin bodies, *Int. J. Num. Meth. in Eng.*, 37, 107.
[158] *Op. cit.*, FEMA, (1997), *Chapter 7, Figure 7.1.*

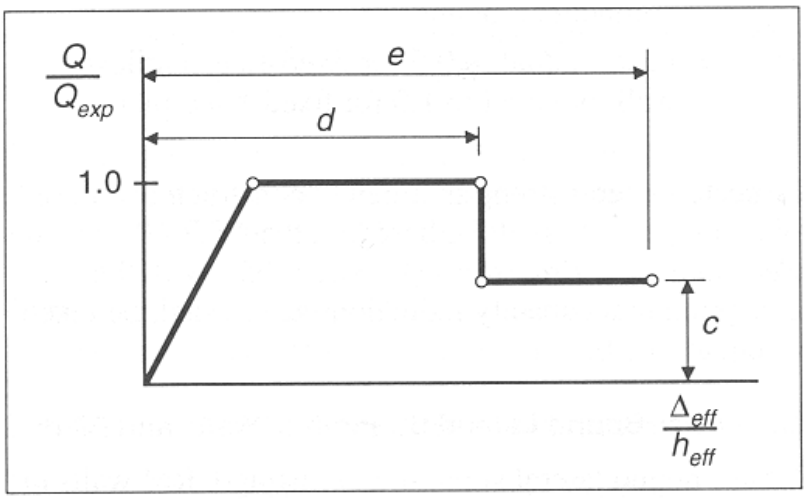

Figure 7-1 Idealized Force-Deflection Relation for Walls, Pier Components, and Infill Panels

FIGURE 3 FEMA 273 FORCE DISPLACEMENT DESIGN CURVE

2.5.4 THE DESIGN STAGE AND THE DEVELOPMENT OF MODERN CODES

The guild rules from the Middle Ages have evolved into the modern standards. These standards proscribe the methods to be used for the analysis stage[159] and the specific design methods.[160] Modern codes are pragmatic devices for ensuring a consistency of approach by designers. Since the Second World War, the development of the major masonry standards in Britain, Switzerland, the US, Yugoslavia, and Australia has progressed from static analysis techniques to the start of the inclusion of modern dynamic analysis tools.

McNeilly [161] noted that the British Code of Practice for Load Bearing Walls CP 111-1948 was the leader in the development of modern load bearing practice, but commented that the subsequent Swiss Code overshadowed this code. Francis[162] dealt with the development of the structural provisions of the SAA Brickwork Code AS CA47 – 1969 and enumerated the research areas of interest to code committees in 196 and in the next two decades several researchers investigated material models identified at that time as a significant research need.

[159] *Op. cit.*, AS 3700 (1988), Section 2 Performance Requirements for Design.
[160] *Op. cit.*, AS 3700 (1988), Section 3 Design Properties.
[161] McNeilly, T.H., (1969), Architects and the Code, *Symposium on the Australian Standard CA 47 1969 SAA Brickwork Code* Institution of Engineers, Perth, Paper 4, 1-15.
[162] Francis, A.J., (1969), Structural brickwork design: basis of the code provisions, *Symposium on the Australian Standard CA 47 1969 SAA Brickwork Code*, Institution of Engineers (Australia), Perth Paper 2, 1 -29.

Page's[163] work was on the static properties of solid clay masonry tested at the limits of failure. Ganz and Thurlimann[164] who extended this research to include extruded masonry confirmed the static properties research. They established the failure surfaces for masonry under inplane quasi-static loading along with Page. This type of analysis has been included in the modern codes of practice to provide a sound rational approach to static analysis methods. The work since the mid sixties of the Slovenian team[165] on the dynamic analysis of masonry provides the foundation for the current research work. Several studies of shear walls have provided data for the development of the empirical rules that are now included in the major masonry codes of practice.

2.5.5 THE CONSTRUCTION PHASE

Site control of masonry has been a problem for the industry that is slowly being addressed.[166]

2.5.6 DISCUSSION

Humans have used masonry as an empirically designed material for millennia. It is only in recent times that a proper formalization of the theory of masonry design has developed, firstly with the development of the modern Swiss, British, American, Yugoslavian, and Australian codes. These codes applied the principles of the mechanics of structures to the analysis and design tools. The theoretical work can then be traced through the work of Heyman on the stone skeleton that provides the starting point to define the building theory for a gravitational structure. Then to the research of Epperson and Abrams who comment on the large environmental loads that need to be added to the design procedures, and to the rules developed from the work of Page, and Ganz and Thurlimann on the static failure surfaces for masonry subjected to a static loading. The modern code has evolved to rational set of design rules developed from sound research and using the proven empirical rules from the previous millennia. Like all such documents, they will continue to evolve as new ideas are tried and proven or discarded. The next stage in the development of the theory of masonry design must be to gain an understanding of the failure of masonry that is subjected to a dynamic loading. FEMA has initiated this research and development work on new codes of practice.

---

[163] *Op. cit.*, Page, A.W., (1979), *passim*.
[164] Ganz, H.R., and Thurlimann, B., (1982), *Tests on the strength of masonry walls under bi-axial loads*, (Zurich: Federal Technical University), Y/OLS-93/7, *passim*.
[165] *Loc. cit.*, Tercelj, S., Sheppard, P., and Turnsek, V., (1969), 2292.
[166] Sutherland, R.T., (1989), How much did workmanship affect the robustness and load bearing capacity of old masonry walls, *Proceedings of the British Masonry Society*, 3, 51.

2.6 DYNAMIC TESTING PROCEDURE

2.6.1 INTRODUCTION

The experimental rig was designed to vibrate the masonry element about a fixed base point. The method used by the Canadian experimenters[167] of vibrating about a fixed centre point was not available at this university. The two methods provide an equivalent set of results, but have varying solutions for the differential equation of motion. The use of different methods provides a reliable means for cross checking the results with planned future experimental work.

Macchi outlined the four alternative test procedures[168] that can be used in masonry shear wall testing are shown on Figure 4 and discussed the benefits and disbenefits of the alternative test rigs including shear and racking tests. The paper presented the principles of a diamond shaped rig that was capable of measuring the constitutive properties of a material. He explained why the diamond shaped shear test provides the only method able to arrive at an estimate of the constitutive properties. The interest of this masonry wythe research lies in the calculation of the effective stiffness of the shear wall using the fourth test method shown in Figure 4.

2.6.2 EQUATIONS OF MOTION OF THE TEST RIG

Hooke's law dominates the differential equation of motion at low velocities and accelerations. In the limit of zero frequency, the equation of motion reduces to Hooke's law. This law describes the relationship between the stress field and the strain field for a monotonically increasing quasi-static load. [169] Halliday and Resnick[170] explain for an unforced vibration and Kaplan and Lewis[171] explain for the forced vibration case the equation of motion for a harmonic steady state system.

[167] Vecchio, F.J., and Collins, M.P., (1986), The modified compression-field theory for reinforced concrete elements subjected to shear, *ACI Structural Journal*, 83, 2, 219.

[168] Macchi, G., (1982), Behaviour of masonry under cyclic actions and Seismic design, *Proceedings of the Sixth Brick Masonry Conference*, (Rome, ANDIL), LI – LXXV.

[169] At this stage, we do not worry about the definition of a quasi-static load and simply note that we can load slowly enough to reach an acceptable quasi-static state.

[170] Halliday, D., and Resnick, R., (1974), *Fundamentals of Physics*, (NY: John Wiley and Sons, Inc.), 231, Figure 13-7. This figure shows the relationship between displacement, velocity, and acceleration in simple harmonic motion. The acceleration and velocity components are absent in the quasi-static system because of the assumption that the sample is loaded slowly.

[171] Kaplan, W., and Lewis, D.J., (1971), *Calculus and Linear Algebra*, (NY: John Wiley and Sons, Inc.), 554.

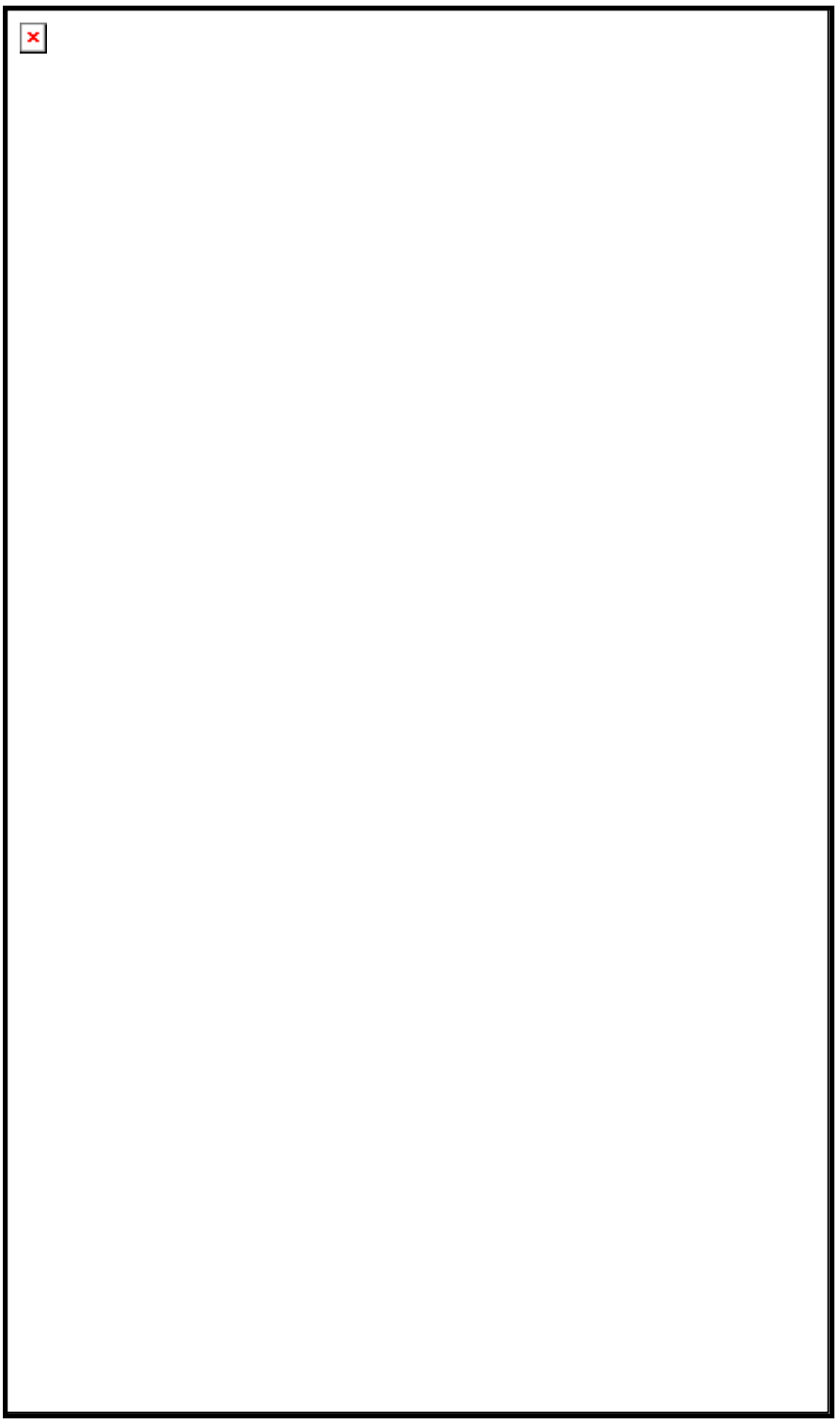

FIGURE 4 MASONRY SHEAR WALL TEST ALTERNATIVES (AFTER MACCHI, 1982)

The extension to a forced vibration with damping was a non trivial, but straightforward exercise that has been shown by McLachlan.[172] A solution to the differential equation of

[172] McLachlan, N.W., (1951), *Theory of Vibrations*, (NY: Dover), 18.

motion requires a feasible solution space. The solution vector has three component independent terms (1, X, X^2). The harmonic loading function adds the complication of the sine and co-sine terms that are linearly dependent between the first and third terms with a phase angle of 90 degrees between the first and second term. The velocity component typically is a defined as linear viscous damping term. This can be visualized conceptually from the data in Table 5.[173]

2.7 CONTINUUM DAMAGE MECHANICS

2.7.1 INTRODUCTION

The theory of linear elasticity assumes that Hooke's law is valid and that the material returns to its starting condition when the applied loads are removed. This assumption works for many design cases but not for masonry buildings subjected to extreme environmental loads. These types of buildings degrade, the shear walls fail, and the buildings collapse under some seismic loads.[174]

Freund[175] commented on the probable cause of the observed dynamic failure mechanism in his recent text. He states that it is due to the dynamic failure occurring across multiple planes rather than the weakest plane as theorized for the static failure mechanism. Bolotin[176] observes from experimental work that the force absorbed by a vibratory rod increases with increasing frequency. These experimental observations provide a plausible physical explanation for the observation of a dynamic failure mechanism but fail to outline the mathematical fragment that explains the observations. This section of the literature review outlines the development of the understanding of the failure of brittle ceramic materials subjected to cyclic dynamic loading.

The strands of the study of the failure mechanisms are based on:

I. Previous dynamic experiments that provide the experimental evidence of the existence of the dynamic failure mechanism as a distinct entity to the static failure mechanism
II. Shaking table tests that outline the relevant information on shaking table tests of masonry structures

[173] Refer pg. 44.
[174] *Loc. cit.,* Shiono, K., (1995), *passim.*
[175] Freund, L.B., (1990), *Dynamic Fracture Mechanics,* (Cambridge: Cambridge University Press), 508.
[176] *Op. cit.,* Bolotin, V.V., (1964), 13.

III. A brief review of the continuum mechanics field to explore the current foundations for investigating the dynamic failure mechanism.

IV. Damage mechanics considering the standard definitions and methods taken from this field

V. Dynamic fracture mechanics: - the dynamic failure and static failure mechanisms are examined against the results from recent Canadian experiments on reinforced concrete shear walls

2.7.2 PREVIOUS DYNAMIC EXPERIMENTS

Mott[177] has investigated the statistical nature of the fragmentation of a ductile material. Grady and Kipp[178] investigated brittle fragmentation. These two sets of research work provide the first documented observation of the dynamic failure mechanism. Kingery *et al.*[179] discuss the elastic, anelastic, and strength properties of ceramics. He makes the point that these materials have limited use because of *'their relatively poor mechanical properties*.' Lemaitre [180] provided an outline of the methods of damage mechanics including sections on brittle damage of ceramics.

There have been several sets of experiments on the dynamic in plane properties of masonry walls. None replicate the material model work of Page,[181] and Ganz and Thurlimann[182] for static loading of masonry, or Lourenço's[183] work on the numerical modelling of the failure surface. Tercelj, Sheppard, and Turnsek[184] after an earthquake in Skopje, Yugoslavia, in 1963 investigated the influence of frequency of the loading on the shear strength of masonry walls. A set of dynamic experiments on walls and model masonry buildings commenced in Yugoslavia before 1969. The seismic loads applied by these researchers were incrementally increasing block loads. These loads were in the range of 0.02 Hz to represent quasi-static loading (being a ~50 second cycle), to 1 to 5 Hz, to represent typical earthquake loads. They established horizontal load deflection diagrams and hysteresis loops for the wall elements. These researchers defined the static shear strength, H_{SM}, and the maximum dynamic shear strength, H_{DM}, with the frequency range, u, Hz. The relationship derived from the research work is:

---

[177] Mott,N.F., (1947), Fragmentation of Shell Cases, *Proceedings of the Royal Society, (London)* A300, 300.
[178] Grady, D.E., and Kipp, M.E., (1985), Geometric statistics and dynamic fragmentation, *Journal of Applied Physics*, 58, 1210.
[179] Kingery, W.D., Bowen, H.K., and Uhlmann, D.R., (1976), *Introduction to Ceramics, 2nd Edition*,(New York: John Wiley and Sons), 768.
[180] Lemaitre, J., (1992), *A course on Damage Mechanics*, (Berlin: Springer-Verlag), 112.
[181] *Op. cit.*, Page, A.W., (1979), *passim.*
[182] *Op. cit.*, Ganz, H.R., and Thurlimann, B., (1982), *passim.*
[183] *Op. cit.*, Lourenço, P.B., (1995), *passim.*
[184] *Loc. cit.*, Tercelj, S., Sheppard, M.S., and Turnsek, V., (1969), 2292.

(2) $$H_{DM} = H_{SM}(1.0 + [0.03n])$$

Paulson and Abrams'[185] conclusion was that with dynamic loading the specimen responded with higher initial strength and stiffness than the statically loaded specimen. The researchers attribute the difference for these reinforced specimens to the rate of cracking. Mann, König, and Ötes[186] using a shaking table illustrated that the static load case replicates with some qualifications the results for seismic loadings. These qualifications were that particular combinations of brick and mortar worked better and reinforcement slowed the degree of cracking. Their conclusion for solid units with low axial loads was that 'the wall exhibited large deformations with constant strength. The vertical load, s, transfers through the horizontal joints even when the crack widths became excessive. Failure occurred after numerous runs, caused by excessive opening of the cracks and local failure of the units in the lower corners'. The noted failure is as expected for a brittle material. Mann, König, and Ötes appeared to be looking for confirmation that the static case can be used for analysis. The hope is that the earthquake is short enough or the earthquakes are temporally distributed so that a cumulative failure does not occur during the building's lifetime. The problem is the danger presented by major aftershocks, such as occurred in Spitak (1989), Assisi (1997), Turkey (1999), Taiwan (1999), and the Kermadec Islands (1999).[187]

The work of Tomazevic and Lutman[188] looked at reinforcement in masonry. The work was completed because of their earlier conclusion that 'when failing in shear, unreinforced masonry walls behave as brittle structural elements with almost no energy absorption capacity, especially if subject to high level of compression.' These reinforced walls reduced the propensity for the cracks to open in the mid height of the wall, as expected from this type of reinforcement if properly designed. These walls appeared to fail in flexure, as noted by the authors (and from the published pictures), in the lower corners from compression (appearing to be brittle more like the confined compression test) and yielding of the reinforcement. These results demonstrate the change in failure mode and capacity from reinforcement in a masonry walls. The hysteresis curves show clearly the ability of reinforcement to carry the load and resist the opening of the masonry resulting in the increased capacity. Data from the analysis is presented in Table 9.

[185] Paulson, T.J., and Abrams, D.P., (1990), Correlation between static and dynamic response of model masonry structures, *Earthquake Spectra*, 6, 3, 573.
[186] Mann, W., König, G., and Ötes, A., (1988), Tests on masonry walls subjected to seismic forces, 8IB^{2}MC, 2, 764.
[187] USGS, (1999), Earthquake database, (owner-qedpost@NEIS.CR.USGS.GOV, now bigquake@gldmutt.cr.usgs.gov and qedpost@gldmutt.cr.usgs.gov), NEIS, Colorado.
[188] Tomazevic, M., and Lutman, M., (1988), Seismic resistance of reinforced masonry walls, *9WCEE*, 6, 97.

TABLE 9 LOAD DEFLECTION DIAGRAMS (AFTER TOMAZEVIC AND LUTMAN, 1988)

Description	Squat Wall	Tall Wall
Height (mm)	760	1405
Depth (mm)	68	68
Width (mm)	610	610
Maximum horizontal load For the unreinforced walls (kN)[189]	30	30
Maximum horizontal deflection (mm) for the unreinforced walls	5	9 before a major jump to 15 and failure
Maximum horizontal load for the reinforced walls (kN)[190]	38	42
Maximum horizontal deflection for the reinforced walls (mm)	5 prior to the onset of rapidly increasing deflections for each load cycle maximum 13	28 with a reasonably uniform distribution maximum 33

This data indicates the relative strength increase with reinforcement and the relative deflections for walls of differing height to width with all else held relatively constant. Their conclusion was that the horizontal reinforcement was critical. It appears to stop the cracks from spreading causing early failure, so that the vertical reinforcement can then act. The paper by Tomazevic and Modena[191] has some interesting concepts on earthquake simulation, but this work is detailed for reinforced masonry and concrete models. One feature of the work was the measurement of the natural frequencies of the two models. This data is presented in Table 10.

TABLE 10 MODEL BUILDING PROPERTIES (AFTER TOMAZEVIC AND MODENA, 1988)

	Frequency (Hz)	Frequency (Hz)	Damping %	Damping %
	Model 1	Model 2	Model 1	Model 2
Virgin Model	9.58	13.06	6.6	4.8
Virgin model after prestressing	11.90	13.29	5.6	3.8
First Damage	9.52	11.09	5.6	6.6
Maximum resistance	9.15	7.38	4.5	6.1
Before Collapse	4.77	5.54	7.0	6.5

The model buildings were 1800, 1400, 1400 mm, each with three storeys having the height of 533 mm. Mortar was 1C: 2L: 9S. The measured modulus of elasticity of model

[189] Tomazevic, M., and Modena, C., (1988), Design of reinforced masonry walls for seismic actions, *8IB²MC*, 2, 805. This data is scaled from the graphs in this paper.
[190] *Ibid.*, 805.
[191] *Loc. cit.*, Tomazevic, M., and Modena, C., (1988), *passim.*

1 was 6.450 GPa, the tensile strength of the masonry was 0.4 MPa, and the compressive strength was 6.33 MPa. They concluded that the horizontal reinforcement arrested the shear failure leading to compressive failure and failure of the reinforcement. The buildings were noted as remaining elastic up to a loading of 0.25g. These results were expected for this type of building model.

Shing, Manivannan, and Carter[192] developed what they called the pseudo dynamic testing of masonry. An equivalent earthquake loading was supplied through actuators. In this case, the El Centro earthquake was used and scaled to three different damage levels. The hysteresis curve development was dominated in the end by the reinforcement. Paulson and Abrams[193] used a shaking table and the models were based on reinforced masonry. The quasi-static loading was applied using an equivalent force method to match the dynamic loading. The equivalent quasi-static loading was applied over a 6 to 8 hour period. These results demonstrated that static tests provide greater damage for the same theoretical applied loading level. The difference results from the application of Newton's second law as opposed Hooke's law that has been commonly used in static analysis.

Klopp[194] looked at the use of building period formula and concluded that the fit to the measured values for the buildings was not high. The best R^2 of 0.67 was for concrete floors. This result matched the Tena-Colunga and Abrams' observation[195] of building periods being shorter and closer to code values with the use of more rigid roof diaphragms. It is interesting to note that Klopp could not get a relationship between frequency and in plane stiffness, blaming workmanship and material variability. Klopp calibrated a value of 1.065 GPa for the E modulus of masonry but considered that the dynamic value was reduced in comparison to the static value that is the correct conclusion for the definitions used in the analysis. Papa and Nappi[196] undertook a comprehensive study of the effect of bi-axial dynamic loading using a square test rig on a shaking table. They demonstrated the anelastic properties of masonry.

[192] Shing, P.B., Manivannan, T., and Carter, E., (1990), Evaluation of reinforced masonry shear wall components by pseudodynamic testing, *Fourth National Conference On Earthquake Engineering*, Palm Springs, California, 2, 835.
[193] *Loc. cit.*, Paulson, T.J., and Abrams, D.P., (1990), 573.
[194] Klopp, G.M., (1996), *Seismic design of unreinforced masonry structures*, diss. UA. *passim.*
[195] Tena-Colunga, A., and Abrams, D.P., (1996), Seismic behaviour of structures with flexible diaphragms, *ASCE Journal of Structural Engineering*, 122, (4), 440.
[196] Papa, E., and Nappi, A., (1995), A test rig for the application of biaxial cyclic loads to structural models, *Building and Structures*, 28, 299.

Lam, Wilson, and Hutchinson[197] modelled a cantilever wall with out of plane action. Their experimental set up was interesting, as they appeared to have measured from the shaking table and achieved an elastic modulus of 0.410 GPa but failed to explain its derivation. It was simply noted that this value was less than the 1.0 GPa measured in quasi-static tests. A 1.25 Hz natural frequency has been identified as a suitable design frequency for this type of wall.

Tena-Colunga and Abrams' work[198] was a response study of a number of buildings in California to the Loma Prieta earthquake. This work demonstrates that a well built masonry building can survive some interplate earthquakes. The data gathered was useful for comparison to the recent Australian research. The interesting building was the Gilroy two storey firehouse. This building has a height for the first storey of 3.76m, height for the second storey of 4.34m, width of 12.25m and depth from front to rear wall of 19.03m with the central wall 6.1m from the rear wall. The typical large doors at the front of the building for the fire trucks would affect the response of the structure. This impact seems to be diminished with a more rigid roof. Acceleration levels were measured up to 0.29 g in the east west direction, 0.79 at the mid span of the roof diaphragm, and 0.41 at the top of the central walls at the rear of the garage area. The conclusion of the study was 'that consideration of ground flexibility was essential for good correlation with the measured dynamic response of the firehouse.' The period of the building varied from 1.11 seconds for flexible roof diaphragms to 0.97 seconds for rigid diaphragms when calculated with a finite element package. They concluded that 'the current code provisions for fundamental period are consistently shorter for a flexible roof building and that the peak tensile stresses normal to the head joints were determined to be only slightly larger than allowable working stresses prescribed by 1994 UBC (Uniform Building Code)'.

Tomazevic and Lutman,[199] and Tomazevic, Lutman and Petkovic[200] investigated reinforced masonry. This research was an extension of the work of Tercelj's et al.[201] work in 1969 and onwards at Ljubljana in Slovenia. This group looked at developing hysteretic rules and experimental simulation of seismic behaviour and loads. They noted that 'by imposing the same displacement pattern dynamically rather than statically that higher

[197] Lam, N.T.K., Wilson, J.L., and Hutchinson, G.L., (1995), The seismic resistance of unreinforced masonry cantilever walls in low seismicity areas, *Bulletin of The New Zealand Society for Earthquake Engineering*, 28, (3), 180.
[198] *Loc. cit.*, Tena-Colunga, A., and Abrams, D.P., (1992), 79.
[199] Tomazevic, M., and Lutman, M., (1996), Seismic behaviour of masonry walls: modelling of Hysteretic rules, *ASCE Journal of Structural Engineering*, 122, (9), 1048.
[200] Tomazevic, M., Lutman, M., and Petkovic, L., (1996), Seismic behaviour of masonry walls: experimental simulation, *ASCE Journal of Structural Engineering*, 122, (9), 1040.
[201] *Loc. cit.*, Tercelj, S., Sheppard, M.S., and Turnsek, V., (1969), 2290.

values of lateral resistance for reinforced walls and more apparently rigid initial behaviour of the walls occurs.' Differences have been observed from monotonic, cyclic, and earthquake loading patterns. The paper went on to ignore the differences and to group the results under the categories of applied vertical load. The difference in the monotonic to cyclic pattern has been used productively to estimate the hysteretic response of the walls to cyclic loading. This is a definitive extension of earlier Slovenian work. They went onto look at stiffness and strength degradation. The final note was that additional experimental research was needed to validate the idea. The second paper deals with the test methods.

Tomazevic *et al.*,[202] and Tomazevic and Klemenc[203] as a Slovenian group, looked at confined masonry buildings. This research was part of their ongoing work in the field of masonry and was coordinated with a Chilean team at the Universdad de Chile. The experimental work was based on the north south component of the Petrovac record from the Montenegro earthquake of April 15, 1979. The use of a single earthquake masks the causes of the damage unless there is access to the time series data and the Fast Fourier transform data. Magnes and Calvi[204] provided a thorough review of the seismic analysis of masonry walls in existing dwellings. Their work on the damage mechanic and the effective stiffness is interesting and provides confirmation of the starting points for this research work.

Lafuente, Casatilla, and Genatios[205] looked at a series of tests on confined masonry using the procedures outlined philosophically in Macchi.[206] The main conclusion from this recent research was that 'It is not recommended to take advantage of the inelastic behaviour of masonry for the seismic resistant design of confined masonry wall structures. The studies performed show that it is possible to guarantee the safety of masonry wall bearing structures under seismic actions if an adequate structural configuration as well as a thoroughly detailed and strict control of the building procedures

[202] Tomazevic *et. al.*, (1996), *Seismic Behaviour of confined masonry buildings: Part One : Shaking Table Tests of Model Buildings M1 and M2 Test Results'* (Ljubljana: National Building and Civil Engineering Institute ZAG : A report to the Ministry of Science and Technology Republic of Slovenia) , 1996 ZAG/PI-95/04, *passim.*

[203] Tomazevic, M., and Klemenc, I.,(1997), *Seismic Behaviour of confined masonry buildings Part Two Shaking Table Tests of Model Builidngs M1 and M2 Analysis of Test Results.* (Ljubljana: National Building and Civil Engineering Institute ZAG : A report to the Ministry of Science and Technology Republic of Slovenia), 1997 ZAG/PI-95/06, *passim.*

[204] Magnes, G., and Calvi, G.M., (1997), In-plane seismic response of brick masonry walls, *Earthquake Engineering and Structural Dynamics*, 26, 1091.

[205] Lafuente, M., Casatilla, E., and Genatios, C., (1996), Experiences on the seismic resistant behaviour of masonry wall structures, *Proceedings of the Seventh North American Masonry Conference*, Notre Dame, Indiana. 2-5 June 1996, 2, 1121-9.

[206] *Loc. cit.*, Macchi, G., (1982), LI - LXXV.

are guaranteed.' It could be considered that the last conclusion was well meaning, but that it needs to be seen in light of the standard it was measured against and not necessarily for all earthquakes.

FEMA[207] has published guidelines to assist in the rehabilitation of buildings. This document places the concepts of building performance levels and ranges into a model that provides guidance for the standards to be considered at the design stage. The performance levels range from immediate occupancy to the collapse prevention. These guidelines are a natural extension to the concepts outlined by Heyman[208] and Epperson and Abrams.[209] Three problems of this method relate to the existing building stock that fails to meet minimum standards, the economic cost of upgrading the buildings, and the general apathy in intraplate areas to earthquake hazard.

2.7.3 SHAKING TABLE TESTS OF MASONRY STRUCTURES

Tomazevic *et al.*[210] provided a summary of several of the recent shaking table tests on both plain and confined masonry buildings. The tests of interest to this research work are the ISMES buildings tested in Milan by Benedetti and Pezzoli.[211] The researchers undertook a series of shaking table tests on masonry buildings of a historical Italian style and size. These buildings represent an approximation to a two-storey building constructed of 'poor quality' masonry. The objectives of the research were to validate existing repair techniques for old masonry buildings and to test new repair techniques. The series of experiments are broad and documented in detail in the reports. The buildings were constructed and then tested using the Irpinia earthquake. This earthquake was a 90 second event. One of the stone buildings collapsed at the start of the tests. The remaining buildings were retrofitted and the buildings then re tested on the shaking table. They noted from the results for the building tests that the damping coefficient, ζ, increased with damage, which suggests there is more internal work being done on damaged cracks and by the mechanisms that cause damping in structures. The first building designated A1 was repaired and was redesignated A2. The natural frequencies were higher than the original A1 structural values, the impact of the damage. They measured degradation in this building after the seismic loads were applied. The damping values rose from 16 to 35 percent for the first mode across the five tests. The conclusions from the tests on building

[207] *Op. cit.*, FEMA (1997), *passim.*
[208] *Op. cit.*, Heyman, J., (1995), 24.
[209] *Loc. cit.*, Epperson, G.S., and Abrams, D.P., (1989), 1-2.
[210] *Op. cit.*, Tomazevic, M., *et al.*, (1996), *passim.*
[211] Benedetti, D., and Pezzoli, P., (1996), *Shaking table tests on masonry buildings - results and comments*, (Milano: Politecnico di Milano), *passim.*

A were that strengthening of the building increased the stiffness and ability to resist seismic loading with a reduced rate of damage accumulation. It is interesting that the local sealing of major cracks was not sufficient to modify the damping values, which suggests that crack sealing probably keeps out the moisture, but has little other than aesthetic appeal. This test provides a suitable data set for establishing a model of a two storey building under seismic loading. The issues raised in the shaking table work relate to the use of free field earthquake traces that leads to a difficulty interpretating the results (Benedetti and Pezzoli).[212] These authors have handled the interpretation well and identified the modal issues, problems, and failure methods in an entirely consistent and understandable manner. However, the use of particular traces raises analysis issues that are best avoided in the types of constitutive experiments proposed for this research work. The definition of the effective stiffness in their report was:

(3) $$k_{eff} = \frac{f(x_i, v_i = 0)}{x_i}$$

This definition represents a model with zero damping. The secondary issue was the relationship between the physical sciences spring stiffness, k^2, and the stiffness of a structural member that is usually described by the elastic constants and the extrinsic shape dependent properties. The type of function that relates the two entities is presented in equation (4).

(4) $$k_{eff} = \frac{k^2 L_{spring}}{A_{spring}}$$

A copy of Figure 7 from Benedetti and Pezzoli's report[213] is presented in Figure 5. This figure shows the change of the measured stiffness for the different test regimes. The elliptical portion of the curve represents the acceleration component. The mean stiffness is shown in the figure in view (a).

[212] *Ibid.* 15.

[213] The three effective stiffness – displacement curves on the right hand side of the exhibit implicitly include an x axis. The graph has not been changed from the original to include the three x's.

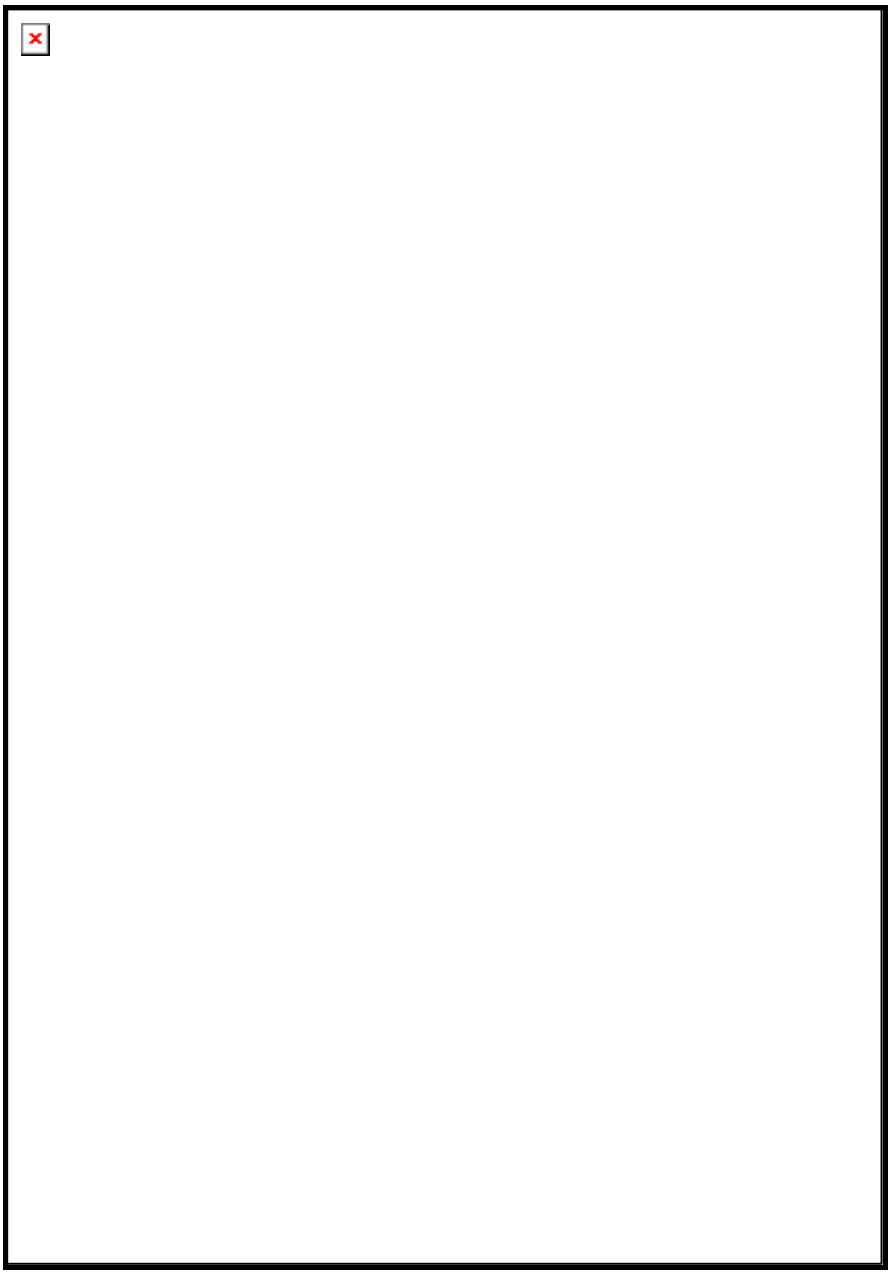

FIGURE 5 STIFFNESS DIAGRAMS (AFTER BENEDETTI AND PEZZOLI, 1996, FIG. 7)

The assumptions for this thesis were that A_{spring} and L_{spring} are equal to unity and so the equivalence shown in equation (5) holds allowing for the difference in the variance in the two results. A similar reasoning could be offered for the moment of inertia properties.

(5) $$k_{eff} \approx k^2$$

2.7.4 CONTINUUM MECHANICS

This section of the literature review focuses on the mathematics of the masonry assemblages. The interest lies in determining an acceptable representation of the masonry

and investigating the various models that can be used to capture the time variant properties of the effective stiffness. This review will examine the theory of a continuum, considering the alternative models studied for masonry. Then consider the computational costs of the models to determine a suitable elemental model representation of masonry and finally, review the basics of damage mechanics, which in this study is of the pattern of the effective stiffness of the masonry as it degrades under a harmonic loading. The stiffness drops from the initial value to a critical value usually termed D_c at which point the material fractures.

Elastic theory is built on the mathematics of a continuum or interacting continuums. Each separate continuum is described in mathematical terms as a manifold.[214] A manifold is simply a discrete volume or area. Each manifold is assumed to have some form of quantifiable elastic or anelastic properties, whether it is considered as an isotropic or anisotropic material. Finite or boundary element methods are useful to model the continuum. It can be modelled as a manifold with a boundary element(s). Alternatively, it can be modelled as a discrete series of elements using finite element method (FEM). Page's[215] continuum model was based on a finite element representation. The material properties for his model were determined from standard masonry tests. He concluded that the model: 'Reproduced the non-linear characteristics of brickwork caused by material non-linearity and progressive joint failure' [and] 'is considered as an assemblage of elastic brick continuum elements acting in conjunction with linkage elements simulating the mortar joints. The joint elements are assumed to have high compressive strength (with non linear deformation characteristics), low tensile strength and limited shear capacity depending upon the bond strength and degree of compression present.' In the figure developed from the RC wall experiments, the slope of the tangent stiffness modulus is smoothly decreasing with time. The results do not show significant jumps, which would suggest that the first order derivative at least exists. This mathematical constraint on the effective stiffness is consistent with the findings for other materials presented in Krajcinovic's[216] seminal text. It simply means that the effective stiffness does degrade, but that up until the point of failure it does so in a slow continuous degradation of the material. It is not a series of large jumps in the stiffness, but a slow change in damage to the shear wall elements. This slow rate of change of the stiffness with time directly implies that the degrading material can still be considered as a first approximation to be a

[214] Masiani, S., and Trovalusci, P., (1996), Cosserat and Cauchy Materials a continuum model of brick masonry, *Meccanica*, 31, 422.
[215] *Op. cit.*, Page (1979), Abstract and Chapter 1.
[216] *Op. cit.*, Krajcinovic, D., (1996), 460.

macroscopically homogeneous body of brittle material. This statement is valid up until the point of failure and the breaking of the specimen.

The definitive work of Lourenço[217] provides a starting point for considering the development of masonry models. Masonry is not a continuum; it is continuous, but not a true continuum. It is composed of a series of discrete blocks separated by mortar elements. Page[218] in his original work on the failure surface for solid clay masonry has modelled these mortar elements separately.

Masiani, Rizzi, and Trovalusci[219] treated masonry as a structured continuum. Masiani and Trovalusci [220] further considered Cosserat and Cauchy materials with continuum models of brick masonry. These authors' concluded 'In general, the Cauchy continuum does not provide a proper description of the brick masonry behaviour while the structured continuum model, accounting for the mutual blocks rotation, gives satisfactory results.' The use of the structured continuum from the work of Page[221] to that of Masiani, Rizzi, and Trovalusci[222] demonstrates that a discrete structured continuum is an acceptable representation of masonry. The difficulty with discrete models has always been the computational expense of these types of models. This generally requires some form of homogenization of the model. Nichols and Totoev[223] used an elastic analysis of a structured continuum for two buildings with one degree of homogenization eliminating the header joints for the reason of computational efficiency. In a sense, Nichols and Totoev are attempting to represent a countable finite system of blocks using continuum methods with the minimum level of discretization within the model whilst providing satisfactory results.

Gebara and Pan[224] used masonry arch examples to demonstrate a contact variant on the FEM that they termed the finite block analysis. The reason for their research appears to be related to the failure of large reinforced concrete structures after an explosion. Totoev and Kleeman[225] developed a ground swell shrink model that would subsequently be used

[217] Lourenço, P.B., (1995), *Computational Strategies for Masonry Structures*, (Delft, Delft UP, diss.), *passim.*
[218] *Op. cit.*, Page (1979), Abstract and Chapter 1.
[219] Masiani, R., Rizzi, S., and Trovalusci, P., (1995), Masonry as structured continuum, *Meccanica*,30, 674.
[220] Masiani, S., and Trovalusci, P., (1996), Cosserat and Cauchy Materials a continuum model of brick masonry, *Meccanica*, 31, 421.
[221] *Op. cit.*, Page (1979), Abstract and Chapter 1.
[222] *Loc. cit.*, Masiani, R., Rizzi, N., and Trovalusci, P., (1995), 674.
[223] Nichols, J.M., and Totoev, Y.Z., (1998), Criteria for establishing a dynamic test loading pattern for masonry, *Proceedings of the ASEC*, Auckland, NZ, *passim.*
[224] Gebara, J.M., and Pan, A.D., (1994), Finite Block Analysis of masonry arches, *TMS Journal*,13, 1, 55.
[225] Totoev, Y. Z., and Kleeman, P.W., (1998), An infiltration model to predict suction changes in the soil profile, *WRR*, 34, 7, 1617.

by Muniruzzam and Totoev [226] to model failure in a masonry wall assemblage. They used Strand6[227] to model the cracking failure of walls for a serviceability study. Moroni, Astroza, and Tavonatti[228] discussed non-linear models for shear failure in confined masonry walls. From this body of research work it can be concluded that the finite element method used as a discrete continuum provides an acceptable modelling tool for clay masonry that is generally isotropic in each discrete unit as Page[229] assumes. However, as noted by Davidge[230] mild orthotropicity is introduced by the variations between the properties of the layers and the differences in the structured continuum.

2.7.5 THE CONCEPTS FROM CONTINUUM DAMAGE MECHANICS

Kachanov[231] discussed the development of continuum damage mechanics from his pioneering work in the 1950s. Lemaitre[232] uses the example of an apple to illustrate the application progression from the micro scale work of the material scientist to the continuum mechanics of the design engineer. This linkage is becoming increasingly important in understanding the size effect, which carries on from earlier work on fracture mechanics, the damage mechanic, the principles of strain equivalence, and the effective stress concept. Tensor analysis provides a tool for the development of damage mechanics. Goodbody [233] provides a summary of the Cartesian tensor methods. Kachanov *et al.*[234] suggested that 'the second order tensor representation of damage satisfies all rational criteria of accuracy for the approximation of the effective properties.' The second order tensor is a matrix representation. The theory of damage mechanics is predicated on the assumption that the intrinsic elastic constants are invariant properties, measured using tensile rather than compression tests. The effective stiffness then is noted to change as the material fails or degrades. This degradation is quantified using the damage parameter, D.

---

[226] Muniruzzaman, A.R.M., and Totoev, Y.Z., (1998), Generation of 3D mound shapes for the analytical study of masonry on reactive soils., *ACSE Transactions*, Canberra (to appear).
[227] G+D Computing (1993), *Strand 6 Reference Manual and User Guide (*Ultimo: G+D Computing), 427.
[228] Moroni, M. O., Astroza, M., and Tavonatti, S., (1994), Non linear models for shear failure in confined masonry walls, *The Masonry Society Journal*, 13, 1, 72.
[229] *Op. cit.*, Page, A.W., (1979), Abstract and Chapter 1.
[230] *Op. cit.*, Davidge, R.W., (1979), *passim.*
[231] Kachanov, M., (1996), On the relationship between fracturing of brittle microcracking solid and its effective elastic properties, *ASME-AMD*, 109, 11-5, Dallas Texas, The Winter Annual Meeting DB 3, *passim.*
[232] Lemaitre, J., (1992), *A course on Damage Mechanics*, (Berlin: Springer-Verlag), Chapter 1.
[233] Goodbody, A.M., (1982), *Cartesian Tensors with applications to mechanics, fluid mechanics and elasticity*, (Chicester: Ellis Horwood Limited Publishers), *passim.*
[234] Kachanov, M., Tsukrov, I. And Shafiro, B., (1994), Effective Moduli of Solids with cavities of various shapes, *Micro-mechanics of Random Media*, M. Ostojap-Starzewski and I. Jasiuk Editors, ASME Book No AMR139, s151.

The scalar representation of the damage parameter is:

(6) $$D = \frac{E - \overline{E}}{E}$$

Or alternatively,

(7) $$D = 1 - \frac{\overline{E}}{E}, \quad 0 \leq D \leq 1$$

Equation (6) is a simplistic representation of the reality of any material; nevertheless, it demonstrates the normalization procedure implicit in the concept of a damage tensor. Krajcinovic[235] presented Kachanov's concept for an integrity tensor. It can be viewed as mathematically simpler, but conceptually not as satisfying as the currently accepted definition for the damage parameter. The damage parameter, D_p, was zero at the commencement of the experiment and its value was given by the change in the effective stiffness, $\overline{E}$, relative to the Young's modulus, E. This representation was simply a method for comparing two materials with different Young's modulus. The theoretical maximum value for D was one; however, a critical value of 0.5 was generally reached at the point of fracture of the manifold or the sample.[236]

Krajcinovic[237] outlined the development of stress strain curves for a number of alternative materials including those that are perfectly brittle materials[238], those that are ductile materials, and those that are general brittle ductile materials. He went on to illustrate the normalized stress strain curves for materials with a plastic to elastic modulus of 0.25. The results are plotted in Figure 6.

[235] Krajcinovic, D., (1996), Damage *Mechanics*, (New York: Elsevier), *passim.*
[236] The point of view as to a manifold implies a mathematical model of the failure and the view of a sample implies the engineering view of a failure of a sample.
[237] *Ibid.,* Chapter 4: Continuum Models.
[238] The original graph contains a misprint in labelling the first graph (a) instead of a (1). This has not been corrected from the original.

FIGURE 6 STRESS STRAIN CURVES (AFTER KRAJCINOVIC, 1996)

Krajcinovic noted that 'for the perfectly brittle material the stress strain curve for the material returns to the origin along a straight line with reduced slope'. This is possibly true in the tensile mode, but in a compressive test, the stress strain curve does not return to the origin. Krajcinovic noted the temptation to treat the general brittle ductile material as a ductile material with the resultant application of the theory of plasticity to non-linear structures manufactured from rock, concrete, and ceramics. He stated that 'the temptation is more understandable than justifiable.'

A typical elastic or current modulus for Salem limestone [239] is presented in Figure 7.

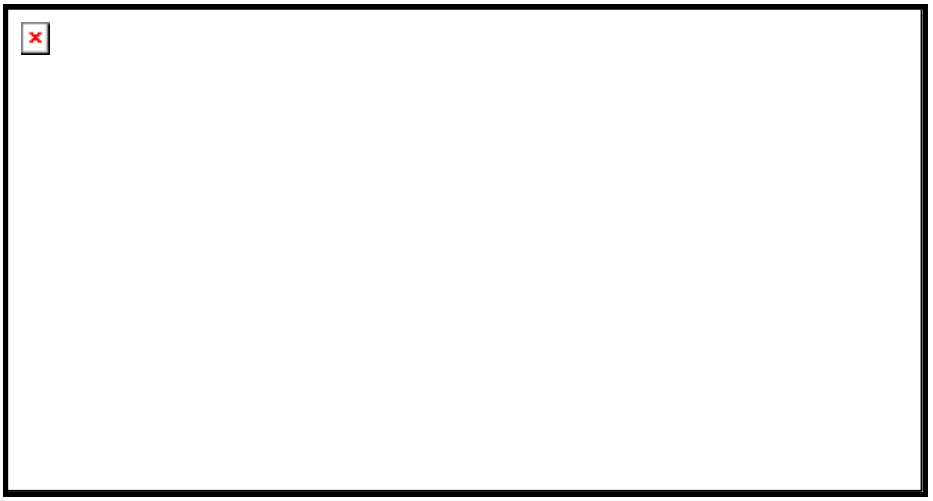

FIGURE 7 CHANGE OF ELASTIC MODULUS (AFTER KRAJCINOVIC, 1996)

[239] *Ibid.,* 509.

The material was tested in a uni-axial compression test. It had a modulus of elasticity of 37.5 GPa, and degraded to a critical damage parameter, D_c, of about 0.75 or 10 GPa. This is a simple illustration of one of the methods used to present the damage parameter.

2.8 FRACTURE MECHANICS - THE STATIC AND DYNAMIC FAILURE MECHANISMS

2.8.1 INTRODUCTION

The experimental observations presented in section 2.7.2 presents a summary of the masonry experiments completed since the late 1960s that provide evidence of the existence of two failure mechanisms. The two failure mechanisms have variously been termed static and a dynamic mechanism. The common observation is that masonry is initially stiffer when subjected to a dynamic loading as compared to an equivalent static loading. There are two essential features to these observations from the experimental work:

Observation 1: The specimen is initially stiffer.[240] This observation implies that there is a degradation of the stiffness with time.

Observation 2: Given a dynamic loading that is considered equivalent to a static loading, as in the experiments of Paulson and Abrams[241] as these two loading patterns are applied to the specimens, they result in an experimentally measured higher initial stiffness for the dynamic loading in comparison to the static loading. This observation implies that equivalent force loadings may not generate equivalent energy and momentum solutions related to the differential equation that governs the motion and strains of the specimens.

This section reviews the background of these two features observed in the experimental work. The procedure required to investigate these two features is outlined and compared to the previous experimental procedures on reinforced concrete shear walls.

2.8.2 THE DEFINITIONS OF TWO FAILURE MECHANISMS

Freund[242] noted the two distinct failure mechanisms for a 'macroscopically homogeneous body of brittle material'. The static failure mechanism is defined as a 'quasi-static or stress wave loading of low intensity' when a single failure plane predominates activated

[240] *Op. cit.*, Page, A.W., (1979), Abstract and Chapter 1. As Page noted the effective stiffness is dependent upon the loading history.
[241] *Loc. cit.*, Paulson T.J., and Abrams, D.P., (1990), *passim.*
[242] *Op. cit.*, Freund, L.B., (1990), 508.

by a 'flaw in the material being stressed to a critical condition'. The dynamic failure mechanism for masonry occurs 'during impulsive loading where multiple fractures on different planes can be nucleated and they grow to a significant size without arresting each other.' Ceramics and other brittle materials have been shown to have a greater fracture resistance to loading causing the dynamic failure mechanism. He provides a detailed explanation of the effect and notes the difficulties of providing a model for this failure mechanism. The definition of a macroscopically homogeneous body of brittle material implies some form of continuum. This review illustrates that a structured continuum is required to provide a reasonable representation of shear wall element. This statement is based on the work of Page and the highly mathematical treatment of the problem of representing masonry as a manifold in the work of Masiani, Rizzi, and Trovalusci.[243]

2.8.3 REINFORCED CONCRETE SHEAR WALL TESTING

Vecchio and Collins[244] used a shear rig to measure properties of reinforced concrete shear walls that were subjected to both static and dynamic loads. Their principal work looked to establish the properties that are necessary for design purposes. Their rig shares the features of the test rig used by Stevens *et al.,*[245] who investigated *'Reinforced Concrete subjected to reversed cyclic shear'*. Stevens *et al.*[246] appear to have solved the problem of a moving mass of concrete by placing the reinforcement at an angle and using rams to load on all four faces of the edge of the shear wall element. This holds the mass steady as the static and dynamic loading vibrates these concrete shear wall elements about their centre point. These experiments provide a useful guide to the mathematical characteristics of a stiffness function that evolves with time under a static and dynamic loading pattern.

The Canadian tests did not need to look at a wide range of frequencies and provided an excellent representation of a continuous experimental method. This experimental procedure, from start of the tests to a tensile failure mode of the reinforced concrete, would be as expected for this type of material. This continuity in the data collection and the method of fixing the shear wall element about a centre point provides excellent experimental data for reviewing the changes in the stiffness of the reinforced concrete shear wall elements with time of loading.

---

[243] *Loc. cit.*, Masiani, M., Rizzi, N., and Trovalusci, P., (1996), 674.
[244] Vecchio, F.J., and Collins, M.P., (1986), The modified compression-field theory for reinforced concrete elements subjected to shear, *ACI Structural Journal*, 83, 2, 219.
[245] Stevens, N.J., Uzumeri, S.M., and Collins, M.P., (1991), Reinforced Concrete subjected to Reversed Cyclic Shear-Experiments and Constitutive Model, *ACI Structural Journal*, 88, 2, 135.
[246] *Ibid.* 138.

The functional form of Figure 4(a) [247] from Stevens *et al.* demonstrated that the stiffness is a smooth function as it degrades (Figure 8). In the figure developed from the RC wall experiments, the slope of the tangent stiffness modulus smoothly decreases with time. The results do not show significant jumps that point suggests that the first order derivative at least exists. This mathematical constraint on the effective stiffness is consistent with the findings for other materials presented in Krajcinovic's[248] seminal text. It simply means that the effective stiffness does degrade, but that up until the point of failure it does so in a slow continuous degradation of the material. It is not a series of large jumps in the stiffness, but a slow change in damage to the shear wall elements. This slow rate of change of the stiffness with time directly implies that the degrading material can still be considered at first approximation to be a macroscopically homogeneous body of brittle material. This statement is valid up until the point of failure and breaking of the specimen.

FIGURE 8 CYCLIC SHEAR RESPONSE OF RC WALLS (AFTER STEVENS, *ET AL.*, 1991)

These results are much more significant than this simple set of comments would suggest at first reading. This result directly points to Observation 2 in section 2.8.1 about an initial higher dynamic stiffness. This stiffness was a result of the test methods and the assumptions made in those experiments, rather than a true and measurable change in the effective stiffness. This observation of a slow degrading function for the effective stiffness provides the expected mathematical constraints on the solution to the differential equation of motion.

[247] *Ibid.*
[248] *Op. cit.*, Krajcinovic, D., (1996), 460.

2.8.4 SUMMARY

A hypothesis can be formed that an alternative method of absorbing energy was producing the observations that have been termed, for the want of a better name, the dynamic stiffness. This hypothesis leads directly to the acceptance of the view that if there was a change in the quantity termed the dynamic stiffness there was not necessarily a change in the true effective stiffness. Of course, this does not preclude the view that the effective stiffness was changing, but its rate of change does not have to be at the same rate of change as the dynamic measurements. The experimental work has to be structured to identify these mechanisms and to quantify the separate results so that a satisfactory and mathematically sound explanation is provided for the experimental observations. This conclusion now permits the development of a theory to explain the observations within the constraints of the mathematics of the differential equation of motion and the measurement of the true effective stiffness.

The first proposition is that the term defined as the dynamic or measured stiffness[249] for brittle ceramics is a distinct mechanism and that it has a frequency component and a stiffness component. This quantity is not constrained by the requirements of being a continuous smooth function and may be piecewise smooth with distinct jumps. The term has linearly independent components $\{1, X, X^2\}$. The second proposition is that the effective stiffness is a static concept that has no frequency component and that it is a slowly evolving quantity as is implied by the theories of damage mechanics and observed in the reinforced concrete shear wall experiments. It is concluded that the experimental work requires strict quality control of the masonry. A detailed review of the loading patterns is required to identify the critical aspects of shear wall loadings in a real building. A final point is that the use of a free field acceleration trace for the experimental work may be an inappropriate loading condition.

The use of a static concept of stiffness from Hooke's law in a dynamic setting introduces the interesting problem of interpreting the results. The problem becomes one of establishing a simple mathematical representation of the change in the stiffness function with time. The work of Stevens *et al.*[250] was consistent with the findings for other

[249] The use of the word stiffness is contradictory to a dynamic property. However, this is the set of terms that have developed in the body of literature that pertain to the dynamic properties of ceramics. The word is retained to maintain the link and express the concept in a manner that is understandable by the practicing engineers. In reality, the quantity is a mathematical operator, which has three orthonormal components, these being the acceleration, velocity, and stiffness. In the limit as the acceleration and velocity tend to zero, then the dynamic stiffness approximates the static stiffness. One would have to conclude that the term dynamic strength or stiffness has arisen because of this limiting feature.

[250] *Loc. cit.,* Stevens, N.J., *et al.,* (1991*),* 138.

materials that the effective stiffness was a slowly degrading continuous function. This finding means that any experimental work that observes a stepped change from a nominal static to a nominal dynamic stiffness is not observing the actual stiffness of the material. Instead, the observation indicates that the result is dependent upon the experimental set up and the mathematical assumptions made for the analysis of the results. This does not negate the experimental observations; there is no doubt as to the observed difference in the response of ceramics to static and dynamic loads.

2.9 DISCUSSION

Page,[251] whilst acknowledging the time dependent effects on the effective stiffness, completed his initial work assuming a static loading regime. His work demonstrated that a structured continuum provided a reasonable representation of masonry. This work has been confirmed with numerical analysis and modelling.[252] Experimental observation supports the known degradation of the masonry under cyclic loading such as occurs in an earthquake or windstorm. This research work has shown that the measured stiffness of masonry has a frequency effect.[253] This observation has been confirmed in a number of shear wall[254] and shaking table experiments[255] undertaken in the last three decades. The observation of the initial difference in the measured stiffness that is due to frequency of loading is coupled with experimental observation of the subsequent degradation of the material with time of dynamic loading. The standard relationship in which the effective stiffness and the measured stiffness are identical functions is the generalized Hooke's law.[256] This functional relationship is achieved with the types of experimental method used by Page.[257] The types of experiments conducted on shear walls or oscillators[258] at seismic frequencies yield measured stiffness values that have been shown to have frequency dependence. Krajcinovic[259] presented a seminal text on the quantification of the change in the effective stiffness of materials termed the field of damage mechanics. The change in the effective stiffness was encapsulated using a damage parameter. The damage parameter, D, is a strict functional normalization. The theory assumes that the elastic stiffness constants are intrinsic invariant properties of a material forming an upper bound to an effective stiffness.

[251] *Op. cit.*, Page, A.W., (1979), Abstract and Chapter 1.
[252] *Loc. cit.*, Masiani, M., Rizzi, N., and Trovalusci, P., (1996), 674.
[253] *Loc. cit.*, Tercelj, S., Sheppard, M.S., and Turnsek, V., (1969), 2292.
[254] *Loc. cit.*, Paulson, T.J., and Abrams, D.P., (1990), 573.
[255] *Op. cit.*, Klopp, G.M., (1996), *passim.*
[256] *Op. cit.*, Lekhnitskii, S.G., (1963), 8.
[257] *Op. cit.*, Page, A.W., (1979), Abstract and Chapter 1.
[258] *Op. cit.*, Bolotin, V.V., (1964), 31.
[259] *Op. cit.*, Krajcinovic, D., (1996), *passim.*

The issues that arise in the preparation of this literature survey are:

I. There are a plethora of definitions and statements in the engineering masonry and ceramic literature as to the meanings of the observations and the notation. However, the fields of damage mechanics, masonry, and seismology have matured to a stage where a consistent level of definition can be provided to tie together the disparate threads.

II. The frequency effect on the dynamic response of structures was observed in both building and shear wall test results. This effect was presented in the works of Benedetti and Pezzoli,[260] although their definition of effective stiffness is different to the standard definition provided for damage mechanics by Krajcinovic. Attempts to quantify and compare the static and dynamic stiffness fail if using a comparison of forces as explained by Bolotin. The frequency effect exists, but it is related to the differential equation of motion not the stiffness as understood from a pure formulation of Hooke's law. This is one of the tasks of this research work. The work focuses part of its attention on the dynamic stiffness to explain the various measurements offers a plausible explanation in a strict mathematical formalism, and provides a consistent level of definition, so that all results can be compared and understood against this constitutive experimental work. This formalism requires that the various stiffness terms are defined and the strict mathematical relationships established. The field of masonry has reached a level that will support this formalism.

III. Macchi[261] outlined the alternative forms of test rigs that can be developed to experiment on masonry shear walls. He offered comment on the uses of each of the four rig types. This work will be based on the diamond shaped shear rig presented in his paper. The reinforced concrete shear wall experiments undertaken by Vecchio and Collins[262] provide a continuous data set. The loading patterns used in experimental masonry work are summarized in the work of Tomazevic and Lutman[263]. The interesting points that require discussion are the use of earthquake traces, the definition of static loading rate, and the advantages of the various types of synthetic harmonic patterns.

[260] *Op. cit.,* Benedetti, D., and Pezzoli, P., (1996), *passim.*
[261] *Loc. cit.,* Macchi, G., (1982), LI – LXXV.
[262] *Loc. cit.,* Vecchio, F.J., and Collins, M.P., (1986), 219.
[263] *Loc. cit.,* Tomazevic, M., and Lutman, M., (1996), 1048.

IV. The use of earthquake traces presupposes that the trace will be repeated. That is highly unlikely. The use presupposes that the trace has properties that are relevant in both the time and frequency domain that needs to be proven with each trace used in research work. The provision of Fast Fourier transforms of the time traces was rare in the literature and interpretation of time traces alone was unproductive.

V. The definition of a static loading rate is an interesting limit concept in pure mathematics. Every quasi-static loading rate implies a period. It is reasonable to assign this to a quarter wave and determine an equivalent frequency from this simplistic analysis. There is a need to investigate what is a reasonable approximation to static loading rate and what is an unreasonable approximation. The systematic error introduced with the non-static loading rate can be determined analytically using standard procedures. An acceptance limit needs to be established where the systematic error is not affecting the static measurement beyond an acceptable limit. The limit of a 1 % error in the measurements being tolerable from the dynamic loading effects seems a reasonable standard. This method leads to the definition of a quasi-static loading rate.

VI. The use of a synthetic loading pattern requires that the pattern be shown to have relevance to a seismic loading on a masonry shear wall. This research work requires an investigation of the modal properties of masonry buildings in the range of two to seven stories. The use of elastic finite element analysis, whilst plagued with the obvious and usual problems, permits interpretation of the initial response of the shear wall to inplane loads. A sensible decision can then be reached on the frequency steps for the harmonic loading pattern. The traditional engineering block pattern for the amplitude steps was consistent with the observations of Richter (1956).

Chapter 3 The Degradation of Masonry

3.1 INTRODUCTION

A study of the degradation of masonry shear walls was required by the community to gain an understanding of the levels of damage in brick buildings after a seismic event. This data provides an input to the structural reliability assessment of a building required after an earthquake and for design purposes. This research study extends the work of Benedetti and Pezzoli (1996) to the constitutive material level. This chapter presents the theoretical basis for the problem, the definition of the problem, the research aims and the solution method.

3.2 THEORETICAL BASIS FOR THE PROBLEM

3.2.1 INTRODUCTION

The concept of stiffness was introduced into engineering mathematics with the work of Hooke. Baker (1912) showed that there were two different stiffness entities or measurable quantities with experiments on masonry elements. The difference in the stiffness entities related to the rate of application of the strain field. These two entities were termed by subsequent researchers as static stiffness and dynamic stiffness. Damage mechanics studies the degradation of the static stiffness with applied strain using the concept of effective stiffness.

This masonry research investigated the changes in the measured stiffness, l^2, of a pressed clay masonry panel subjected to harmonic loading. This section presents a summary of the development of the theoretical basis for the relationship between the measured stiffness entities and the effective static stiffness, with the detailed mathematical derivation presented in Appendix B.

3.2.2 MATHEMATICAL BASIS

The differential equation of motion in the usual structural sense is a linear equation with constant coefficients. The form of the linear equation in a traditional engineering form is:

(8) $$ma + hv + k^2 x = p(t)$$

from the derivation in Chopra (1995, 25), although Chopra's use of the dotted derivative is changed to the traditional symbolism of acceleration and velocity. A number of alternative solutions are presented in Chopra (1995) for varying initial conditions and the

forcing function, $p(t)$. The implicit definition of the stiffness coefficient, k^2, was a primitive of the differential equation of motion shown in equation (8) (Kaplan and Lewis, 1971). The stiffness coefficient, k^2, in traditional terms was a constant. Three previous experimental investigations related to the dynamic analysis of structures provided clear documentation of the problem and the issues relevant to the definition of the effective stiffness and the measurement of its change with strain loading. These experiments included the Italian shaking table tests where as part of their shaking table work Benedetti and Pezzoli (1996) provided a definition of the effective stiffness that includes a frequency component. This definition was used consistently in their analysis. This formulation was useful for the analysis of degrading structures on a shaking table. Benedetti and Pezzoli (1996, 15 - 17) presented the differential equation in terms of an earthquake excitation for a single degree of freedom system. The defining equation was:

(9) $$ma + F(x,v) = m\ddot{z}(t)$$

Their comment was that the function $F(x,v)$ was 'the restoring force, which depends on the mechanical characteristics of the system. If it is linear elastic then'*:*

(10) $$F(x,v) = hv + k^2x$$

Benedetti and Pezzoli (1996) made the comment that the damping was assumed to remain constant.[264] These researchers introduced a functional representation of the stiffness term defined as $g(x)$, and outlined a series of alternative forms of this function.

The next investigation was the equivalent force experiments. This experimental method used a technically equivalent force experimental procedure to compare a static and dynamic force regime. This work from Paulson and Abrams (1990) established an alternative method of considering what these researchers termed the dynamic stiffness. These researchers reached the conclusion that the masonry responded to the dynamic force with a higher stiffness when compared to the static force.

A set of rod experiments looked at the force in a vibrating rod as the frequency was changed and increased (Bolotin, 1964, 31). He reported that at increased frequency the force developed in the vibrating rod increased as the square of the frequency.

[264] The damping component can be investigated with this rig using non-linear analysis techniques.

The measured stiffness is defined in this thesis as l^2, which is the measured stress field divided by the measured strain field. Two functions are postulated to represent the degrading effective stiffness and the degrading measured stiffness with increasing strain for all loading conditions:

(11) $$k^2 = f_a(E, e, \dot{e}, f)$$

(12) $$l^2 = f_b(E, e, \dot{e}, f)$$

The two functions f_a and f_b are postulated to be dependent on the Young's modulus, the strain, the strain rate and the frequency of loading. The problem reduces to establishing the data that supports the determination of the relationship between f_a and f_b. They represent a fundamental extension of the stiffness primitive (Kaplan and Lewis, 1971), whilst maintaining the static symbolism, which represents the limits of these functions.

Krajcinovic (1996) explained the original concept of an integrity scalar to represent the damage condition of a structural element. The current definition of the scalar damage parameter has the form:

(13) $$D = \frac{E - \overline{E}}{E}$$

Thermodynamics requires that $\dot{D} > 0$. The second requirement is the first derivative of the function is continuous. A piecewise jump in the damage parameter, D, implies a break in the manifold. The use of a critical damage parameter, D_c, implies that at a critical test stage the manifold had fractured. Halliday and Resnick (1971, 228 - 238) presented the theory for a simple harmonic oscillator. The two key figures from this text are shown on Figure 9 and Figure 10. The energy within the oscillator is simply the sum of the potential and kinetic energy. This is shown in the following equations where:

(14) $$U = \frac{1}{2} h x^2$$

(15) $$K = \frac{1}{2} m v^2$$

In addition, the total energy is:

(16) $$E_t = K + U$$

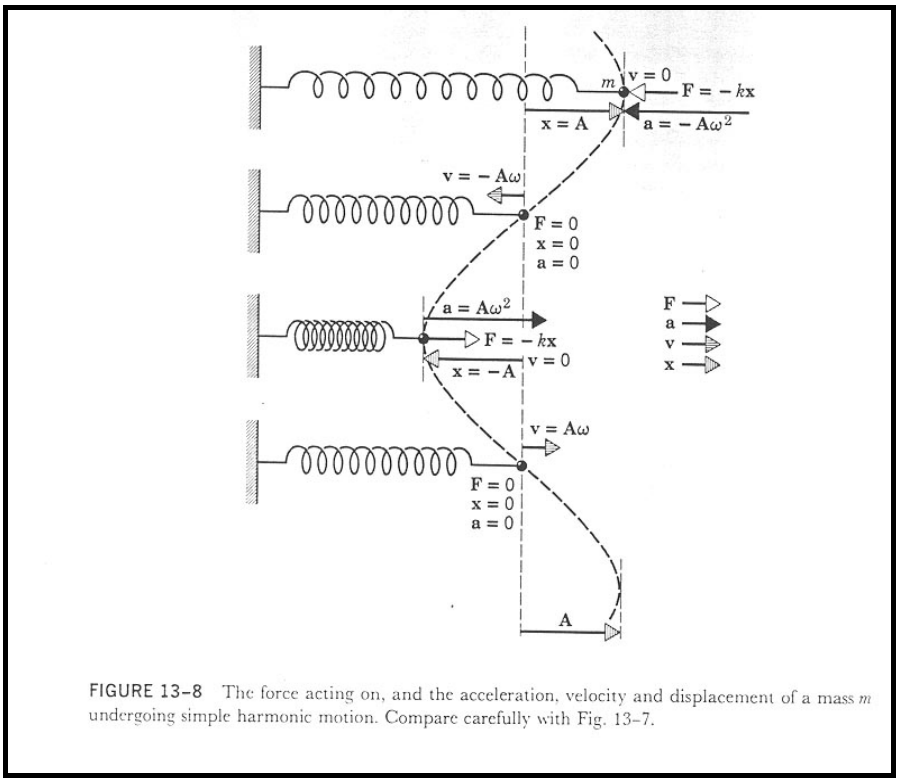

FIGURE 13–8 The force acting on, and the acceleration, velocity and displacement of a mass m undergoing simple harmonic motion. Compare carefully with Fig. 13–7.

FIGURE 9 SIMPLE HARMONIC MOTION (AFTER HALLIDAY AND RESNICK, 1971)

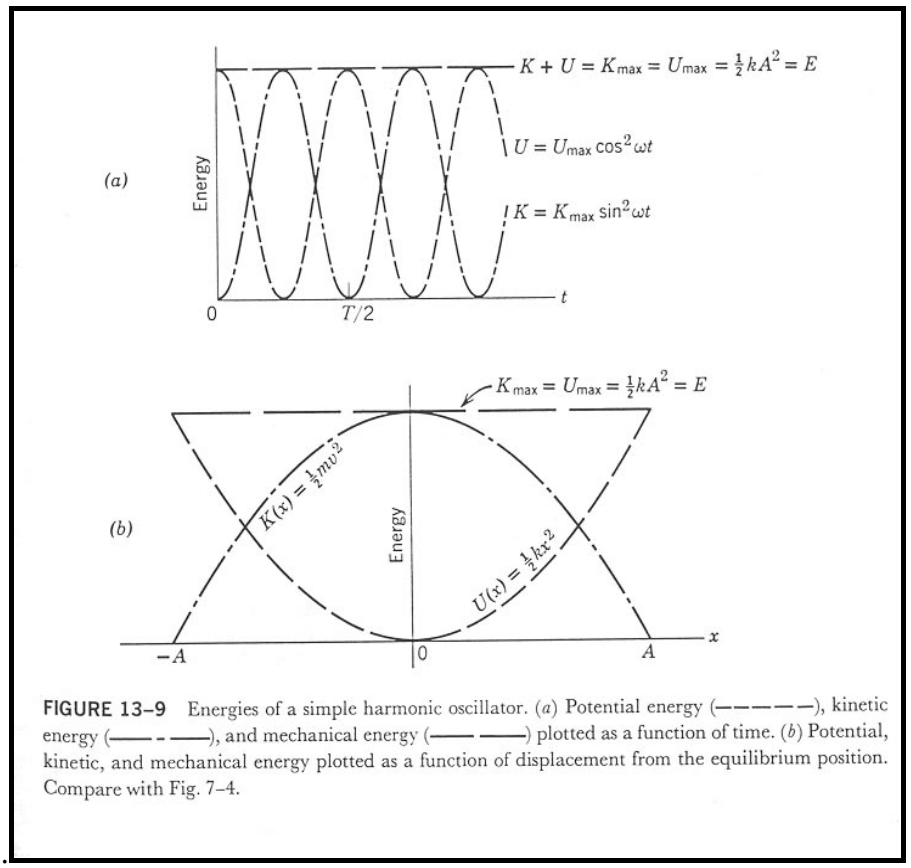

FIGURE 13–9 Energies of a simple harmonic oscillator. (*a*) Potential energy (– – – –), kinetic energy (— - —), and mechanical energy (——) plotted as a function of time. (*b*) Potential, kinetic, and mechanical energy plotted as a function of displacement from the equilibrium position. Compare with Fig. 7–4.

FIGURE 10 HARMONIC OSCILLATOR ENERGY (AFTER HALLIDAY AND RESNICK, 1971)

In a simple harmonic oscillator, the two energies are second order polynomials. The problem with seismic loading is that the building is subjected to a forcing function, but fundamentally, energy is conserved in the elastic displacement and acceleration and dissipated in the nonelastic displacement and the damping. The final observation by these authors was:

$$v = \pm\sqrt{\frac{h}{m}(A^2 - x^2)} \tag{17}$$

The displacement, x, can be obtained for the oscillator from equations (16) and (17). The energy balance within the perspective of this simple harmonic oscillator theory suggests that the mass and the stiffness terms dominate the damping term that depends directly on the velocity. This forms the basis for the derivation of the stiffness theory in Appendix B.

3.3 DEFINITION OF THE PROBLEM

The section provides the critical definitions for the problem formulation. The problem is outlined in detail, and the aims of the experimental work are established. The study used a representative volume element to model the progressive degradation and failure of pressed clay masonry panels subjected to harmonic shear loads.

Hooke's law represented the stiffness, k^2, of a material as a constant determined from the linear function of force and displacement. This law when related to the stress field and the strain field provided the standard elastic constants. These are Láme's constants alternatively, as the familiar elastic moduli. The relationship between the frequency, acceleration and displacement for seismic events are presented in Table 5.[265] The critical assumption with Hooke's experimental work was a very slow loading rate so that the frequency of loading and strain rate approach zero and the stress to strain has been shown to be a linear relationship[266] defined by:

$$k^2 = f_a([E = const.],[e < e_{yield}],[\dot{e} \to 0],[f \to 0]) \tag{18}$$

which reduces to $k^2 = E$. The elastic constants are not defined for $[e \to e(yield)]$.

[265] Refer pg. 44.

[266] This relationship reduces to the trivial $k^2 = E$ for a static linear analysis. The power of the mathematical formalism $k^2 = f_a()$ is in deducing the relationship between the measured stiffness and the effective stiffness functions and then establishing the conditions for understanding the static and dynamic stiffness entities.

The postulated relationship in Appendix B between the effective[267] stiffness, $k^2(t)$, and the measured stiffness, $l^2(t)$, for dynamic stress loading was:

(19) $$k^2(t) \;^3\; l^2(t)$$

The two stiffness functions have been related to an arbitrary time function[268] defined with a loading pattern set by the strain, strain rate and the frequency. The fundamental problem for the research is to establish the properties of the effective stiffness $f_a(E,e,\dot{e},f)$ and the measured stiffness $f_b(E,e,\dot{e},f)$ functions within the theoretical constraints imposed by equation (19) and to confirm the applicability of this equation to define the measured stiffness for engineering purposes. The properties of the damage parameter, D, were estimated from the results for $f_b(E,e,\dot{e},f)$ determined from the experimental work.

This study will establish an estimate of the damage parameter for a masonry shear wall subjected to harmonic loads. The research aims are as follows:

I. To explain and confirm the various experimental observations of the effective and measured stiffness.
II. To investigate the mathematics of the differential equation of motion of the system to satisfactorily explain the various observed stiffness operators.
III. To provide numerical values for the damage parameterization to establish $l^2 : f_b(E,e,\dot{e},f)$ and the properties of the damage parameter, D.

3.4 THE SOLUTION METHOD

3.4.1 INTRODUCTION

The research study will investigate the degradation of the shear wall of an unreinforced masonry structure subjected to a seismic type of loading. There are a number of steps to arrive at the encapsulation of the damage parameter, D, in a form that is useful to the design world. The mathematical analysis stage includes the proposed mathematical work to conceptually relate the current experimental results to the results from previous test programs. The design stage outlines the alternatives for the loading pattern and develops a pattern that permits a systematic statistical analysis of the experimental results. The

[267] The shorthand notation of $k^2(t)$ represents the time dependent forcing function pattern. This pattern ultimately applies a monotonically increased strain that is measured in the time domain.
[268] This method provided a shorthand mathematical technique to manipulate the two stiffness entities in the time domain.

experimental work stage defines the methodology. The methods stage outlines the analytical and statistical procedures used for the analysis of the results and the form of the results for the encapsulation of the damage parameter. The penultimate stage formulates the types of design recommendations. The final stage provides a set of conclusions on the study of the degradation of masonry shear walls.

3.4.2 MATHEMATICAL ANALYSIS

The differential equation of motion of a simple harmonic oscillator subjected to a forced harmonic wave with an increasing strain field provides the data to encapsulate the changes in the effective stiffness of a masonry element of a shear wall (equations (12), (18) and (19)). The objectives of the mathematical analysis are:

I. To define the stiffness terms in an approach that considers the degrading system. This formal approach will explain the relationships between the various mathematically defined stiffness entities.
II. To establish the two stiffness operators used to report the experimental results that have been termed the effective stiffness and the measured stiffness.
III. To establish a function that identifies and quantifies the measured stiffness strictly in terms of the differential equation of motion.
IV. To investigate the concept of a static loading to determine the point in the frequency domain where the measured stiffness may be an acceptable representation of the effective stiffness.
V. To provide a finite element model of the system to check the observations against analysis.

3.4.3 BACKGROUND TO THE DEVELOPMENT OF THE LOADING PATTERN

The loading pattern provides the systematic changes in the dependent variables for the function $l^2 : f_b(E, e, \dot{e}, f)$. The engineering constraints for real world buildings will require:

I. A ground block in the FEM development to minimize the problems of edge restraint on buildings in simpler finite element modelling systems.
II. A pattern that accounts for the following earthquake parameters and data:
    a. Develop a function based on a reasonable data set that reflects not parochial issues, but the likelihood that a real shear wall in a real masonry building will be demolished in one of these events.

b. Look at a range of earthquakes that have time and frequency components that reflect real earthquakes and not non-debunked myths and hopes.

III. No use of spectral accelerations, which are useful in design.

IV. Allow for the acceleration and frequency data presented in Table 5.[269]

The pattern will be used to understand the likely loading on a shear wall element and will not be a pattern that is based on free field acceleration.

3.4.4 LOADING PATTERN DESIGN

The section on the development of the loading pattern will:

I. Provide a review of existing patterns and comment on their applicability.

II. Consider the range of seismic events and available traces to provide for a statistically valid pattern.

III. Develop a number of finite element models to establish the loads that are applied to an element of a shear wall, by a free field acceleration record. These models will include a ground block to provide realistic base conditions.

IV. Establish the criteria for a set of loading patterns that provides a satisfactory statistical foundation for the numerical analysis.

3.4.5 EXPERIMENTAL WORK

The experimental work will entail:

I. Investigation into the properties of a number of masonry units and prisms to gain an understanding of the elastic moduli at static loading rates and ultrasonic frequencies.

II. Design development of the test rig and its construction.

III. Initial experimental work to calibrate the rig and the measurement devices.

IV. Standard experimental procedures to measure the properties of the masonry units and prisms used in the experimental work.

V. Calibration of the various electronic measuring devices.

VI. Final experimental work on the shear wall elements to measure the response of the panels to harmonic loading from the quasi-static range to the seismic frequency range.

[269] Refer pg. 44.

3.4.6 ANALYTICAL AND STATISTICAL METHODS

This work will involve:

I. Development of a Fast Fourier transform program based on standard modules for use in the earthquake loading pattern development and the statistical analysis of the results.
II. Use of a nonlinear program based on a broad search procedure to estimate the best fit for the orthotropic properties of the masonry as it degrades in the test rig.
III. Statistical analysis of the shear stiffness results to establish the variables that control the effective and measured stiffness for the given loading pattern.
IV. Estimating the damage parameter for the selected masonry shear wall. The damage parameter will be investigated against amplitude, frequency, and total strain.

3.4.7 DESIGN RECOMMENDATIONS

This section outlines the design recommendations on:

I. The use of the parameterization of the degradation of the effective stiffness. This is presented as the damage parameter. A normalization procedure will provide a guide as to the likely drop in effective stiffness with the damage to the shear wall element. The critical damage parameter that provides the numerical value at which cracking is likely to occur in masonry will be estimated.
II. Interpreting the mathematics that relates the effective stiffness to the measured stiffness.
III. Applications of the study results.

3.4.8 CONCLUSIONS

The conclusion section summarizes the experimental and analytical work. The key findings related to the critical aspects, uses of the research will be presented, and the future research direction will be suggested.

Chapter 4 Experimental Study

4.1 INTRODUCTION

This chapter outlines the development of the test rig and the methodology used for the experimental work. The development of the loading pattern is outlined and related to existing loading patterns. The data, which was obtained from the various tests, is detailed and explained in relation to the effective and measured stiffness. Details are provided for the selection of the materials and the design of the masonry panels.

The study of masonry shear walls in a dynamic setting required the development of a test rig that can apply a nonproportional bi-axial compressive stress and a harmonic shear stress to a panel of masonry. The harmonic strain field was used to provide numerical values for the degrading stiffness properties that can be used for design purposes such as the shear stiffness. This form of data provides numerical values for the damage parameter, D, for analysis techniques such as finite element or boundary element models.

A schematic representation of the test rig is presented in Figure 11.

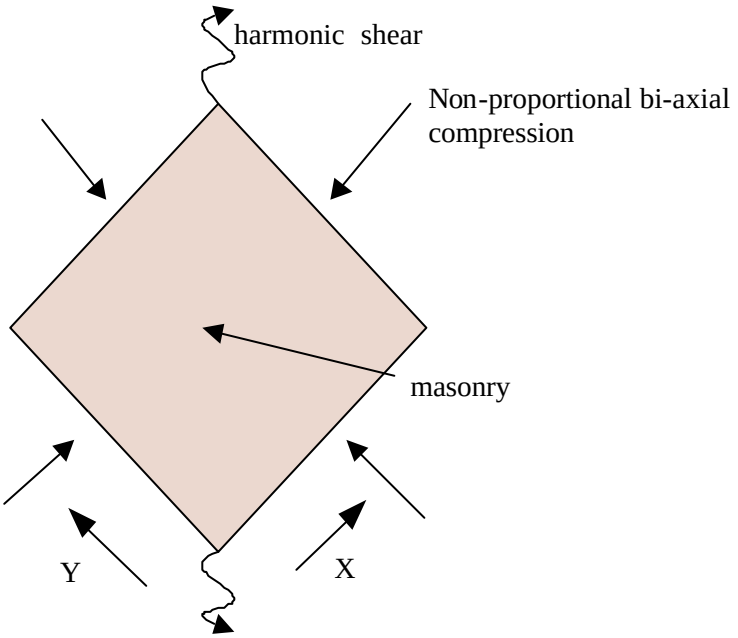

FIGURE 11 TEST RIG CONCEPT (AFTER MACCHI, 1982)

This test rig was designed to fit within the existing uni-axial reaction frame at the University of Newcastle civil engineering laboratory (Figure 12).

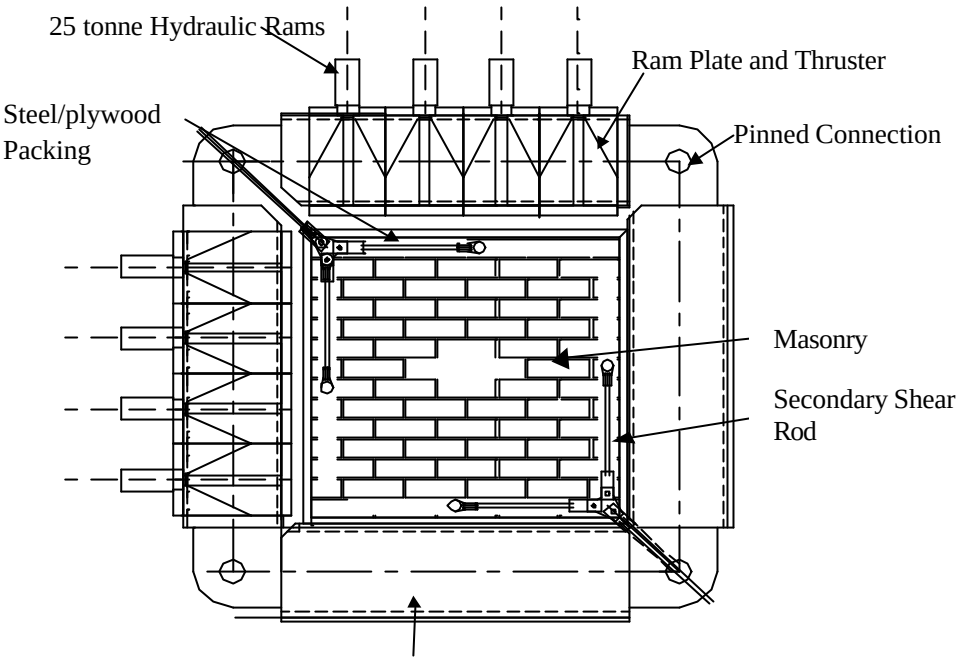

FIGURE 12 THE TEST RIG

4.2 DETAILS FOR THE MASONRY PANELS

4.2.1 PANEL CONSTRUCTION

The panels were designed to be realistic elements[270] of a shear wall. This section discusses the selected brick and its properties, the sand, the mortar, and the prism test results. The number of panels constructed on each day and the applicable construction dates are presented in Table 11. Further details are provided in Appendix F for the development of the masonry panels, and in Appendix G for the results for the standard tests completed on the masonry.

The laboratory number represents the Julian day of the year for the panel's construction. The alpha designation was the number of the panel constructed on that day. Panel 210 and 226 were constructed from an extruded brick and used for calibration purposes.

[270] The Y direction is retained as being normal to the bed joint irrespective of the orientation of the panels when they are placed in the test rig. This nomenclature conforms to standard practice.

TABLE 11 MASONRY PANEL CONSTRUCTION DATES AND DESIGNATIONS

Construction Date	Julian Date	Number Constructed (Tested)	Laboratory Designations
29 July 1998	210	1 (1)	210
14 August 1998	226	1 (1)	226
2 September 1998	245	4 (4)	245A to 245D
3 September 1998	246[271]	3 (1)	246A to 246C
25 November 1998	329	4 (1)	329A to 329D
27 November 1998	331	3 (2)	331A to 331C
19 March 1999	77	4 (0)	77A to 77D

4.2.2 PANEL EXPERIMENTAL NUMBERING

Details of the masonry panels tested for this research are presented in Table 12. Each panel was given a designation Panel AP: xx. The xx represents the integer order of the testing of the panels. Ten panels were tested from the twenty constructed for the experiments.

TABLE 12 MASONRY PANELS DETAILS

Laboratory Designation	Thesis Number	Manufacture Date	Test Date	Last Test Date
210	AP: 1	210/98	August 98	
226	AP: 2	226/98	August 98	
246A	AP: 3	246/98	4 November 98	
245A	AP: 4	245/98	22 December 98	12 January 99
331A	AP: 5	331/98	23 February 99	1 March 99
245B	AP: 6	245/98	4 March 99	11 March 99
245D/E	AP: 7	245/98	18 March 99	25 March 99
245C	AP: 8	245/98	8 April 99	
331C	AP: 9	331/98	28 April 99	
329D	AP: 10	329/98	4 May 99	7 May 99
329D	Further tested	Files numbered as	329E	30 July 99

4.2.3 SELECTED BRICK

The bricks selected for the detailed experiments were an Austral pressed brick of Sydney, Australia origin (Figure 13). The photograph shows brick units in the lower left quadrant, a fully completed panel, and a partially completed panel to demonstrate the method of construction of the panels.

[271] A number of 246 and 329 panels were accidentally destroyed before use.

FIGURE 13 AUSTRAL MOTTLED CHOCOLATE BROWN BRICKS

Sugo (2000) has extensively tested these bricks and documented a range of their properties. The measured properties for these bricks are presented in Table 13.

TABLE 13 BRICK DETAILS

Property	Unit	Detail
Manufacturer		Austral
Name		Chocolate Mottled Brown
Type		Pressed
Frog		Shallow Prismoidal
Length Range	mm	225 - 230
Breadth Range	mm	108 - 111
Depth Range	mm	74 - 76
Initial Rate of Absorption	$kg/m^2/min$	5.6
Weight	kg	3.8

A set of measurements of the brick units undertaken in accordance with AS/NZS4455: 1997 are presented in Appendix G. The results were within a normal range for pressed bricks of Australian origin, except for the IRA, which was higher than normal. This IRA did affect the construction of the panels. The weaker panels generally failed in handling with a bed joint failure. Broken panels were discarded.

4.2.4 SAND

Grading of aggregates for mortar was based on the AS 1141.[272] Beach sand was used for the construction of the masonry panels. Details of the grading of the sand are provided in Table 14.

TABLE 14 GRADING OF THE NEWCASTLE BEACH SAND

Sieve Size	Sieve Mass (g)	Sieve Fraction (g)	Retained Mass (g)	% Retained	Cumulative % Retained	% Passing
1.18mm	438.0	438.2	0.2	0.2	0.2	99.8
600µm	404.1	407.7	3.6	3.5	3.7	96.3
300µm	330.1	403.1	73.0	70.9	74.6	25.4
150µm	363.0	388.2	25.2	24.5	99.1	0.9
75µm	350.0	350.8	0.8	0.8	99.9	0.1
Pan	339.6	339.7	0.1	0.1	100.0	0.0

The sand was considered sharp with a distinct mono sized fraction between the 300 to 600 micron sizes. The lack of fines was a problem in creating a workable mix. Mortars constructed from this sand were hard to use without the use of additives. This issue was beyond that covered in this research. It has been the subject of extensive research at Newcastle University (Sugo, 2000). The method to overcome this problem was the use of lime. The delivery method for the lime required that sufficient time be provided for the apparent chemical reaction to occur between the sand and the lime.

4.2.5 MORTAR

The mortar used in the construction of the shear wall element was a Portland cement: lime: sand mix of 1:1:6 by volume. No additives were used in the mix. No variations in the basic mix were made except for slight adjustments to the lime (less than 1 percent by weight of lime) to allow for different delivery methods that included lime slurry and putty. The panel dimensions for design purposes were set at 1200 millimetres in both of the principal axes. This size required 70 bricks per panel, allowing for a 10 mm joint thickness. The joints were not tooled, but simply finished flush. This finish provided a uniform cross sectional area to the panels, important for the analysis stage.

The details of the mortar compressive strength results are presented in Appendix G. The mortar had a mean compressive stress of 2.2 ± 0.2 MPa.

[272] AS 1141.11-1996/Amdt 1-1999, *Methods for sampling and testing aggregates - Particle size distribution by sieving*, (Sydney: Standards Australia), *passim.*

4.2.6 PRISM TEST RESULTS

The prism test results for the flexural strength are presented in Table 15.

TABLE 15 PRISM FLEXURAL STRENGTH RESULTS

Description (Day)	245	246	329	331	77	Units
Mean Flexural Strength:	0.85	0.29	0.37	0.62	0.42	MPa
Standard Deviation:	0.16	0.06	0.11	0.11	0.07	MPa
Coefficient of Variation:	19	20	29	18	16	%
Characteristic Strength Factor K:	0.83	0.82	0.75	0.84	0.85	
Characteristic Flexural Strength:	0.51	0.16	0.17	0.44	0.20	MPa

The results highlight the range of values that can be obtained even under strict quality control for masonry construction. The difference between Series 245 and 246 was explained by the prewetting of bricks before laying the Series 246. The weaker walls proved extremely difficult to move and test, particularly those that tested in the range of 0.16 to 0.2 MPa flexural strength in the prism test results.

4.3 DESIGN OF THE TEST RIG

4.3.1 INTRODUCTION

The load application system consists of two separate and distinct mechanisms. The first mechanism is a compression frame designed to supply uniform pressure to the masonry panel. The mechanism supplied in plane bi-axial nonproportional compression stress to reflect the loading on a shear wall from the dead load of a structure. The second mechanism was a shear yoke that was designed to apply a harmonic shear stress to the edge of the panels. The shear yoke fitted between a 50 mm base plate to anchor the shear yoke to the strong floor and the 250 kN Instron Testing Machine (ITM) hydraulic ram. This ram provided the harmonic shear stress applied to the masonry panel. This loading replicated the seismic loading applied to a building by a ground movement, which in turn loaded the shear wall element within the overall structural mechanism. This section summarizes the design of the compression frame and the design of the shear yoke. Specific details of the equipment and the set up of the experiments are presented in Appendix E, Appendix H, and Appendix I.

4.3.2 COMPRESSION FRAME

The mechanism that applied nonproportional bi-axial compression to the masonry is shown in Figure 14.

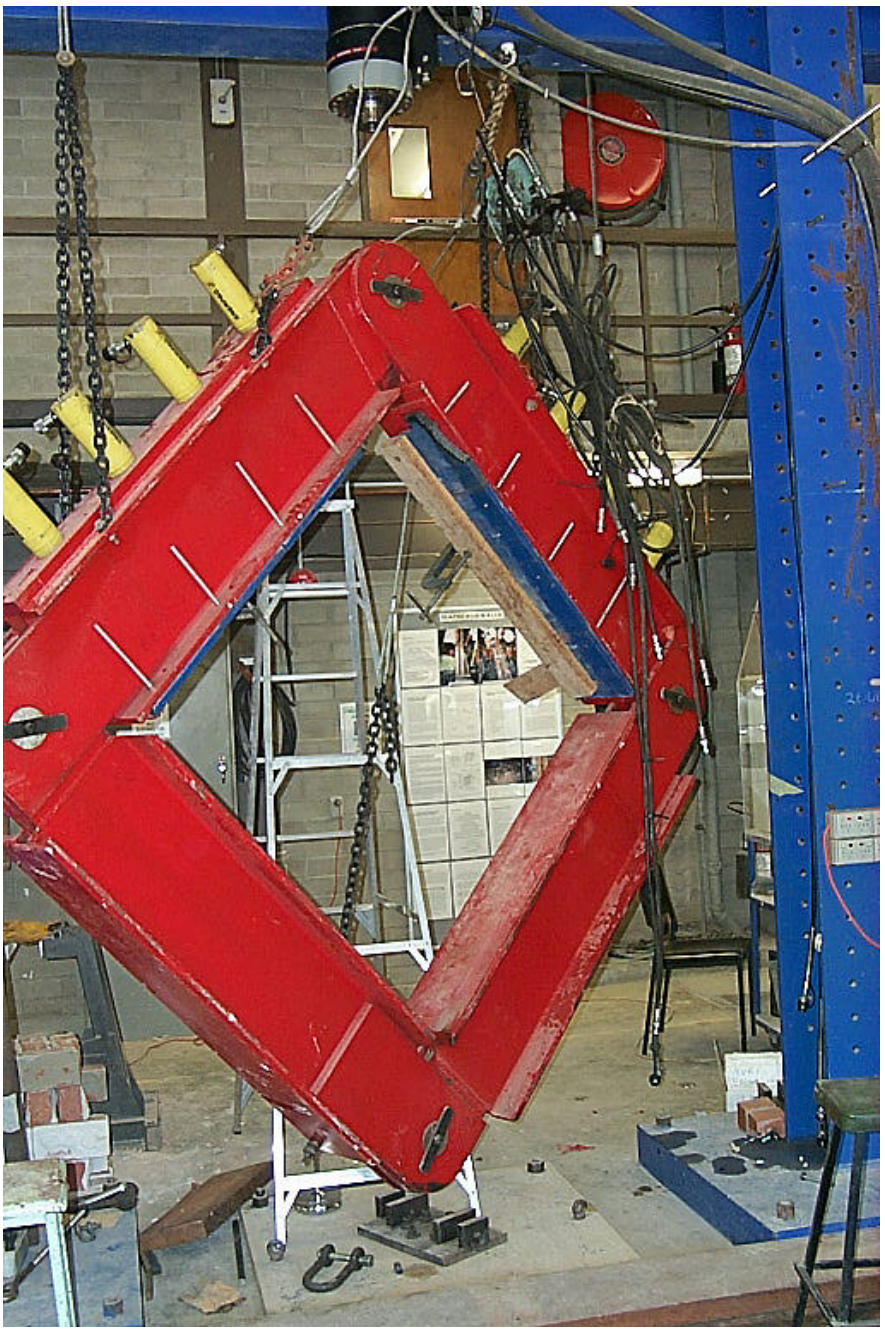

FIGURE 14 COMPRESSION FRAME HANGING ON CHAINS IN THE REACTION FRAME

It shows the compression mechanism in place ready to receive a masonry panel. A sketch through one of the arms is shown in Figure 99.[273] The compression frame hung on chains in the reaction frame. These chains placed the compression frame and the panel assemblage coincident with the centre line of the ITM. The two upper arms of the compression frame were constructed from back to back channels. Two 12 mm guides and a socket in the ram stopped sway in the thrust block. Four 25 tonne rams loaded thrust

[273] Refer pg. 294.

blocks to apply uniform stress to the edge of the panel. The design ensured that the deflection of the arm of the compression frame had minimal impact on the compressive stress on the face of the masonry panel. The pressure in the static hydraulic system was recorded for each arm. The bottom arms were reaction beams. Plywood packing was used between the steel elements and the masonry element.

4.3.3 DESIGN OF THE SHEAR YOKE

A photograph of the shear yoke installed on panel AP: 6 ready for testing is shown in Figure 15. The shear yoke was designed to apply harmonic shear on to the 4 edge faces of the panel. The shear yoke design was the most interesting element of the whole mechanism because of the use of a set of bolted plates to apply the harmonic shear force with a uniform harmonic stress level. Plywood packing pieces and tension bolts supplied the friction required to develop the shearing stresses. The shear yoke consists of a thin rod and bar system designed to hold the masonry panel and the compression frame in axial tension. The shear yoke was axi-symmetric about the middle of the diamond shaped panel. It was mirror imaged on the two sides of the shear wall element. The measured wave patterns from the orthonormal rings confirmed that the design objective of providing uniform stress regime had been achieved with the rig set up.

This force application system was the critical elements of the design. The shear yoke system maintains a prestress of about 150 kN in each panel through the test program. The shear yoke does not have the stiffness to apply a compression load. The displacement was measured about the mean prestress displacement level to eliminate the prestress force from the differential equation of motion. The design of the system with the applied compression stress in the masonry means that the system has the first principal stress in compression at the start point of each test run. The applied harmonic shear drove the first principal stress into the tensile region that created the stress regime that allowed the damage to occur in the panel.

4.4 DESIGN OF THE LOADING PATTERN

4.4.1 INTRODUCTION

The study of buildings and shear walls subjected to dynamic loads such as seismic loads required the selection of a forcing function. The appropriate type of the forcing function was investigated using finite element techniques, a simple building model set, and the use of Fast Fourier transforms. This section defines the underlying principles, methods and results in the development of the loading pattern used to characterize the forcing function.

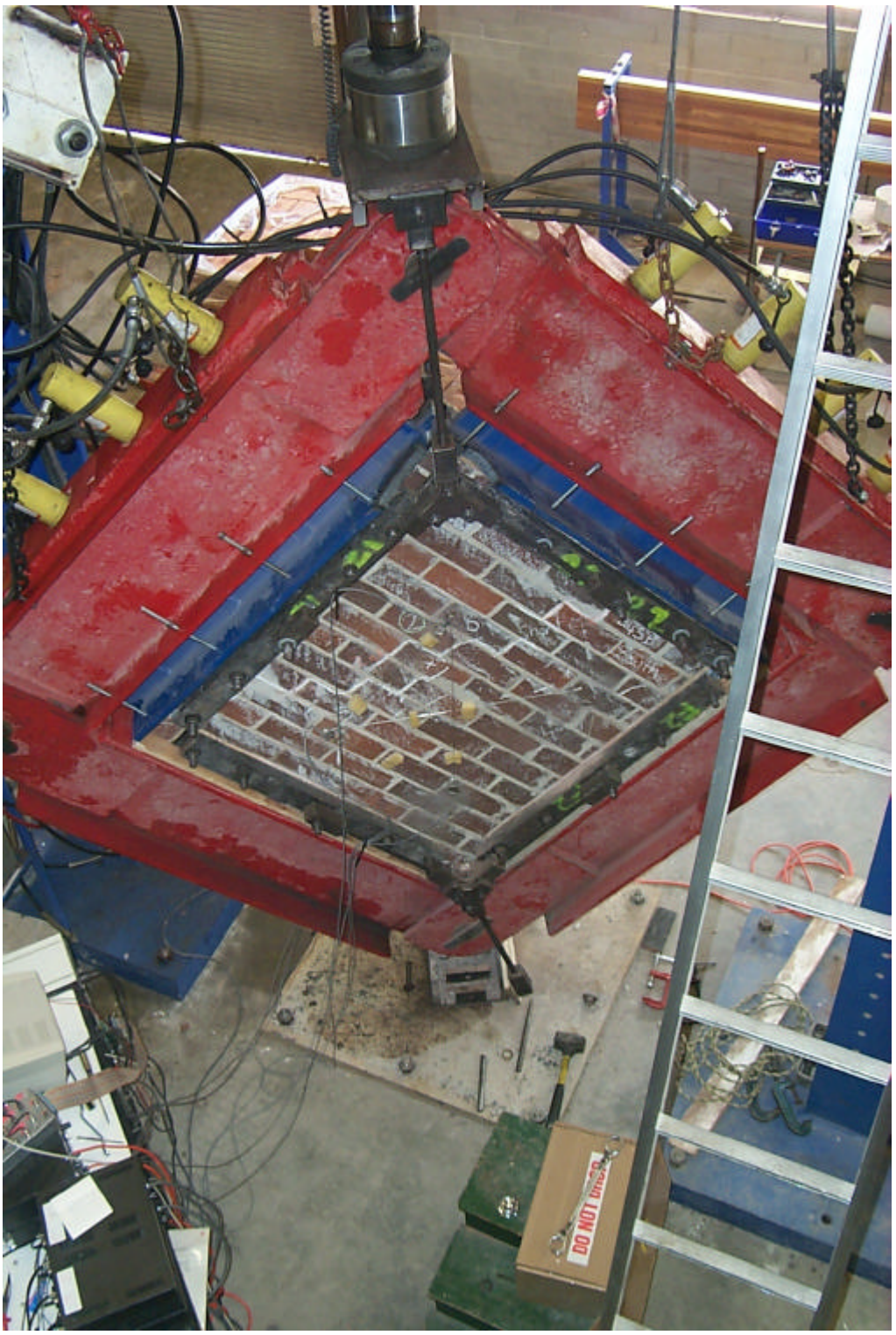

FIGURE 15 SHEAR YOKE

The purpose of the development of the bading pattern for the forcing function was to provide a systematically controlled method for determining the statistical properties of the measured stiffness, l^2, given the postulated dependent variables and then to deduce the

form of the effective stiffness, k^2. Complete details of the development of the loading pattern are presented in Appendix D.

4.4.2 PATTERN DEVELOPMENT

The development of the loading pattern commenced with a review of patterns that had been used in previous experimental work. Alternative patterns that have been used in recent experimental work are shown on Figure 16.

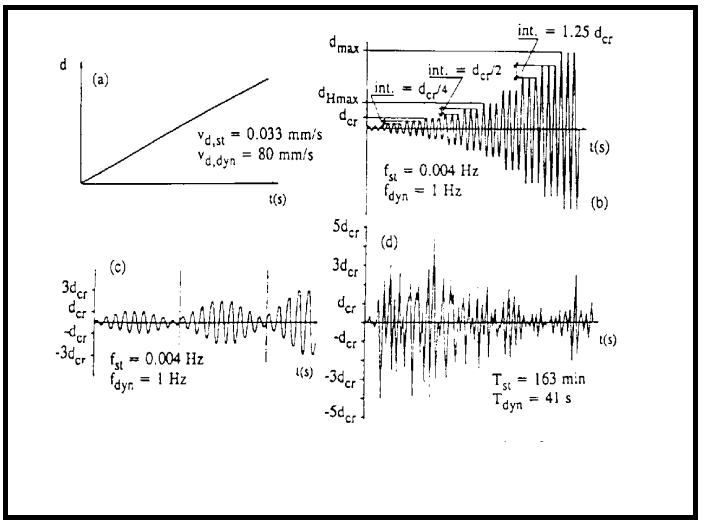

FIGURE 16 LOADING PATTERNS (AFTER TOMAZEVIC AND LUTMAN, 1996.)

These patterns represent the range of patterns in use in the seismic field. Pattern (a) is a monotonically increasing load, which can represent either static or a dynamic load depending upon the rate of stress wave loading. This pattern provides insufficient time at a dynamic loading rate to record the change in the effective stiffness. Pattern (b) shows the basics of sound pattern design. This pattern shows a single frequency that matches the results of shaking table tests on masonry structures that have been subjected to free field accelerations. The pattern also shows the increase in amplitude that provides the increasing strain rate in the analysis. Pattern (c), as a beat pattern, provides results that require a Fast Fourier transform to separate out the results for the two frequencies and will need further interpretation. Pattern (d) represents an earthquake loading with a free field acceleration trace. This represents a particular Fourier series, and that this Fourier series was preferred to another Fourier series represents a moot point in a circular argument.

A damaged masonry shear wall was subjected to the stresses generated by the buildings response to the free field acceleration, but this was not the same as a free field

acceleration trace. A FEM analysis was completed on two representative masonry buildings to investigate the transformation from free field acceleration to the functional form of the stress-loading pattern on the masonry shear wall.

The first building was a 2 storey scale model of a typical Italian stone or masonry home. Benedetti and Pezzoli (1996) tested this building on a shaking table. The second building was a 7 storey Perth apartment documented by Page (1973). A set of typical values for the material properties was obtained for the buildings. Each building was modelled on a ground block to improve the foundation boundary conditions.

The observations from Benedetti and Pezzoli (1996) that there was a carryover of energy to the second fundamental mode were confirmed with the finite element analysis of the two buildings. The finite element analysis demonstrated the difference in circular frequency for short squat buildings to tall slender structures. This investigation concluded that the forcing function could be represented as a harmonic function of single frequencies. This function represents the sway at the fundamental mode of the building.[274]

The specific earthquake traces used in the analysis of the structures for the development of the loading pattern are presented in Appendix C. The constraints to the development of the pattern determined in the investigation are presented in Table 16.

TABLE 16 CONSTRAINTS TO THE DEVELOPMENT OF THE FORCING FUNCTION LOADING PATTERN

Number	Constraint
1	Range of frequencies should span from the static to the dynamic range including the seismic frequency range. This provides the observational data to determine the effect that frequency has on the effective stiffness of the masonry sample.
2	Amplitude should increase as a regular stepped pattern. This provides the observational data to determine the effect that an increase in strain rate has on the effective stiffness of the masonry sample.
3	Number of replicates at each amplitude frequency point should be sufficient to allow point trends to be estimated.

[274] This analysis ignores the issue of serviceability with the cracking and degradation of the structure. This can be viewed firstly as theoretical research of use to the finite and boundary element modellers, who are able to model cracking and rocking directly, and secondly in the post earthquake assessment of buildings in accordance with the FEMA 273 guidelines. Simply, the research is interested in the intact behaviour of a compact manifold as it degrades.

4.4.3 THE PATTERN AND THE REVISIONS TO THE PATTERN

The initial pattern used for panel AP: 3 was a test set essentially at a single frequency for the purpose of demonstrating the existence of the degradation of the effective stiffness. The pattern developed after this panel AP: 3 in accordance with the principles established from results outlined in Appendix D. The changes in the pattern's development after Panel AP: 3 testing are shown in Figure 17.

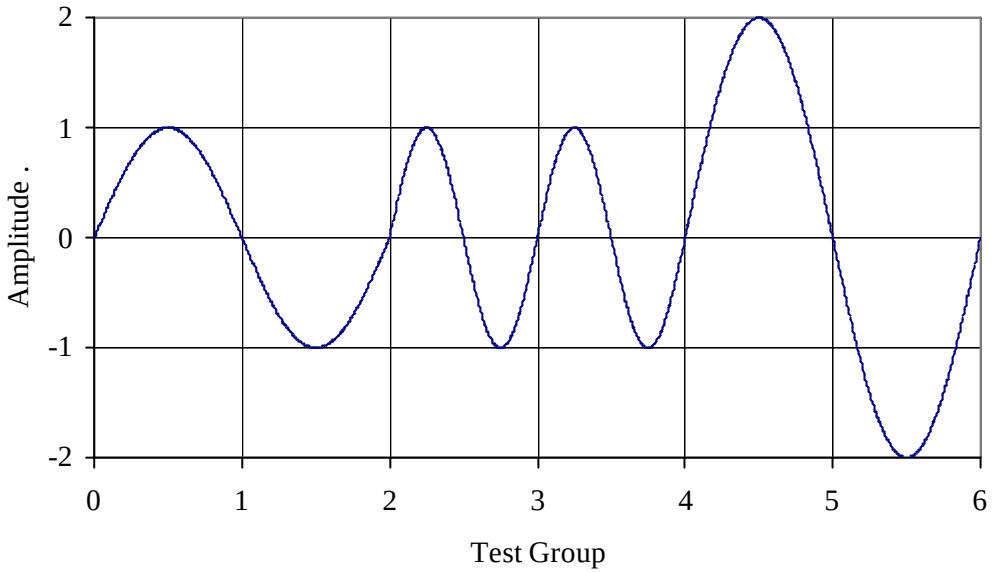

FIGURE 17 CHANGES IN THE PATTERNS DEVELOPMENT AND STRUCTURE

This graph shows the principal schematic features of the pattern. The specific pattern structure used for AP: 6 is presented in Table 17.

TABLE 17 PANEL AP: 6 SPECIFIC PATTERN DETAILS

Amplitude (mm) [275]	Frequency (Hz)	Replicates	Count
2.54	0.06: 0.1: 0.3: 1.0: 5.0: 10.0	15	90
3.81	0.06: 0.1: 0.3: 1.0: 5.0: 10.0		180
5.08	0.06: 0.1: 0.3: 1.0: 5.0: 10.0		270
6.35	0.06: 0.1: 0.3: 1.0: 5.0: 10.0		360
7.62	0.06: 0.1: 0.3: 1.0: 5.0: 10.0		450
8.89	0.06: 0.1: 0.3: 1.0: 5.0: 10.0		540
10.16+	Varies		640

[275] The amplitudes are nominal values. The ITM was calibrated in 1/10 of an inch and the dial gauge had a systematic error of +10 percent.

The frequency was increased systematically as the amplitude was held constant. Then the amplitude was increased and the frequency was returned to the starting frequency. The evolution of the pattern for Panel AP: 9 involved a repeat of the frequencies at constant amplitude. The revised pattern is presented in Table 18.

TABLE 18 PANEL AP: 9 PATTERN DEVELOPMENTS

Amplitude (mm)	Frequency (Hz)	Replicates	Comment
1.25	0.1: 0.2: 0.32: 0.65: 1.0: 2.0: 3.2: 6.5: 10	5	Energy spacing is even.
1.25			
2.54			
2.54			
3.75			

The purpose of this revision was to investigate the effect of frequency changes at constant amplitude where the frequencies were repeated as two blocks. This test used five replicates per amplitude frequency point. This pattern evolution is shown schematically in Figure 18. The loading pattern details for each panel are presented in Appendix A

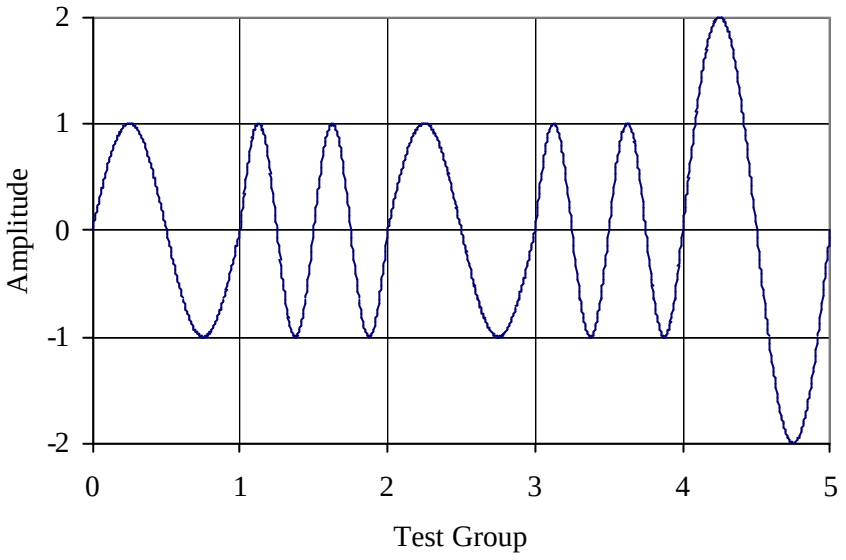

FIGURE 18 EVOLUTION OF THE PATTERN STRUCTURE

The original spread of frequencies used in the tests on panel AP: 6 provided a poor spacing for the measurement of the energy levels that are dependent on the square of the frequency. The original and the revised frequency sets are illustrated in Figure 19. This graph clearly shows the piecewise nature of the energy levels for the first set of frequency distributions compared to the revised set of distributions.

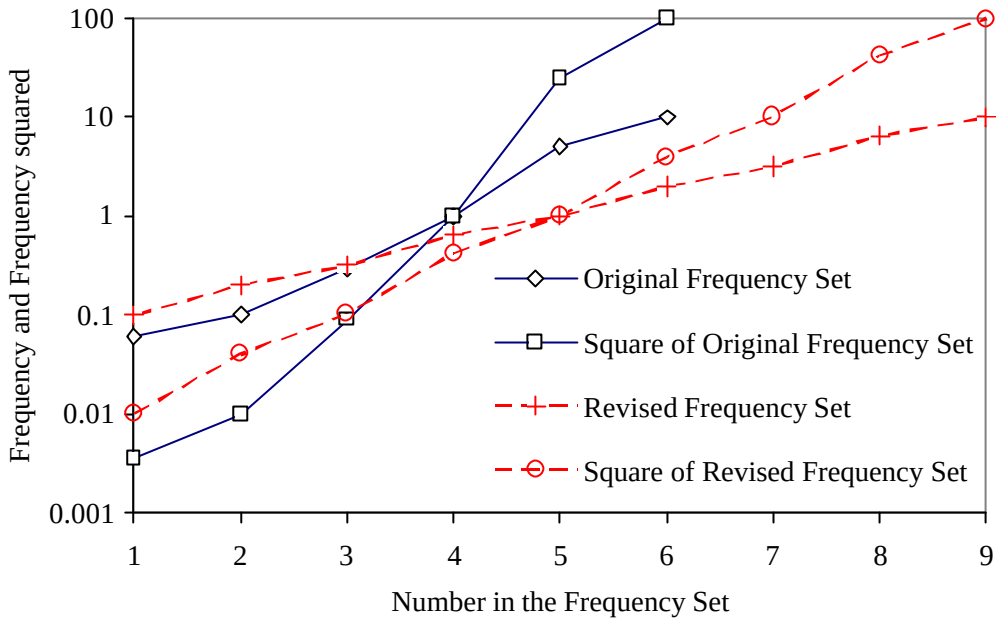

FIGURE 19 REVISED FREQUENCY DISTRIBUTION

4.4.4 THE OVERALL PATTERN STRUCTURE

The fundamental purpose of the test program was to identify and explain the differences between the static and the dynamic strength of the ceramic masonry. The knowledge that was gained in the test program and the analysis of results was used systematically through the subsequent experimental work to further refine the hypothesis or to confirm aspects of the fundamental research. These minor, nevertheless systematically applied, revisions to the loading pattern had one purpose to investigate the differences between the effective stiffness and the measured stiffness, and to confirm the hypotheses in Appendix B within the limits of this investigation.

4.5 HYDRAULIC SYSTEM SETTING AND CONTROLS

4.5.1 INTRODUCTION

Two hydraulic systems were used in the operation of the test rig. The first system was a static pressure system used to supply the hydraulic fluid to the rams on the compression frame. This system used manifolds and pressure gauges to maintain a different pressure in each of the arms of the compression frame.

The second system was a 45 kW electric motor driving a hydraulic pump set to supply the ITM. This system limited the slew rate on the ITM ram.

4.5.2 STATIC PRESSURE SYSTEM

The Raripress static hydraulic system details are presented in Appendix E.7. The definitions of the vertical and horizontal directions are shown on Figure 11.[276] The mean values of the static pressures for the different test elements are presented in Table 19.

TABLE 19 APPLIED STATIC PRESSURES TO PANELS

Shear Wall Element	Vertical Pressure MPa	Horizontal Pressure MPa	Ratio of the Pressures
AP: 3	2.8	1.5	1.9
AP: 4	2	1.1	1.8
AP: 5	1.8	0.9	2
AP: 6	1.8	1.2	1.5
AP: 7	1.8 (1.9)[277]	1.2	1.5
AP: 8	1.9	1.3	1.5
AP: 9	1.9	1.3	1.5
AP: 10	2.7	1.2	2.25

4.5.3 INSTRON TESTING MACHINE - HYDRAULICS

The pumping unit details are presented in Appendix E.5. The maximum pumping rate on the hydraulic pump set was 80 l/s. The ITM has a dynamic ram that was controlled with an internal linear velocity displacement transducer. The system was operated under displacement control to ensure that the post peak region of the stress strain curve was investigated as part of this experimental study.

The ITM displacement dial was calibrated to an increment of $1/10^{th}$ of an inch. This unit was adopted for the base unit of displacement and was increased by $1/20^{th}$ or $1/10^{th}$ of an inch in each block increase in amplitude. This was equivalent to 2.54 mm and 1.27 mm respectively and whilst the use of Imperial measurements was not necessarily appropriate, this was the reason for the oddly selected equivalent metric increments.

The slew rate for the pumping set limited the response of the machine at higher frequencies. A typical response displacement list as achieved with panel AP: 6 is presented in Table 20.

[276] Refer pg. 90.
[277] The E series of tests had a ratio of 1.9.

TABLE 20 INSTRON TESTING MACHINE - DISPLACEMENT CONSTRAINTS

Frequency Hz	Requested Displacement (mm)	Actual to Requested Displacement (%)
0.06	5.08	100
0.1	5.08	100
0.3	5.08	100
1	5.08	100
5	5.08	80
10	5.08	50

This test displacement of 0.2 inches or 5.08 millimetres was mid range for the displacements. The results were clearly limited by the hydraulic oil delivery rate available from the pumping unit. The other problems encountered during the experimental work were a cooling problem and the motor response to feedback from the ITM's LVDT causing a shudder at higher frequencies and amplitudes. The nominal force levels used in the control of the experiments are presented in Table 21.

TABLE 21 INSTRON TESTING MACHINE - FORCE LEVELS

Description	Force (kN)
Design limit	250
Maximum force achieved	320
Self weight of the rig	20
Applied prestress level	150

A few experiments on panel AP: 3 were completed at a prestress level of 175 kN. The value of 150 kN was adopted after testing on panel AP: 3 as it was mid range in the nominal force limits of the ITM. The peak force of 250 kN when resolved and translated to a shear was equivalent to about 1.3 MPa. This limited the maximum compressive stress, so that the first principal stress was driven slowly into tension during the incremental stepping of the harmonic loading. It should be noted that the reaction frame was not equivalent to a fixed point and the force and displacement at the ITM rams were the forcing function values, but these do not relate directly to the force associated with the effective stiffness values of Hooke's law. This point is discussed in detail in Appendix B. The ITM electronic system details are presented in Appendix E.6.

4.6 INSTRUMENTATION

4.6.1 INTRODUCTION

The purpose of the instrumentation was to obtain and record the data from the hydraulic and electronic equipment used in the experimental work. The limitations on the data

acquisition system were a nominal maximum voltage range of ± 5 V.[278] The data acquisition software was able to internally amplify the signal by units of 1, 10, and 100. The last limitation on the system was the general error level in the readings that applied to all the recorded readings. This general error level was ± 2.4 mV. This was an absolute constraint on the accuracy of the measurements.

4.6.2 DATA ACQUISITION SYSTEM

The data acquisition board was a sequential read board that had a maximum through put of 330 kHz. The maximum number of channels for the board was 16 that were numbered 0 to 15 in the usual binary fashion. The boards' limitations provided a constraint on the total channels that could be recorded, and on the duration of the record. A record for a test with a forcing function frequency of 10 Hz required a read rate approaching the 2000 Hz. A 30 second record at 2000 readings per second usually caused a computer reset. This rate was required to obtain sufficient readings on each wave for the analysis. The problem of a sequential sweep limited the analysis of the derivatives of the readings, particularly any attempt to calculate accelerations on the wall elements. A direct determination of the acceleration and velocity was not possible from the results. Details of the data acquisition board are presented in Appendix H.4.

4.6.3 DATA ACQUISITION SOFTWARE

The data software generated a time domain printout of the data and a frequency domain analysis of the data files. The frequency domain output was used to calibrate the ITM's dial gauge for frequency. There was a systematic error in the frequency of ten[279] percent, allowed for in the test protocol. Software output data was created in the form of text files that were saved after each 30 second test. The software FFT feature was used after panel AP: 4. This data was stored with the text file that holds the time domain data. Details of the data acquisition software and the common operating protocols are presented in Appendix H.5.

4.6.4 FILTER AMPLIFIERS AND SIGNAL FILTERS

The filter amplifiers were used as calibration tools for the signals from the displacement measurement devices the ring displacement transducers (RDT). The amplifiers were calibrated to 0.2 mm/V for the RDTs and recalibrated after half of the test program. The

[278] The system can be switched to ± 10 V as the displacement increases.
[279] A requested frequency of 1 Hz was measured at 1.1 Hz.

recalibrated values were used for subsequent analysis and were hard coded into the Fortran programs. Details of the filter amplifiers are presented in Appendix H.6.

The signal filters were used to condition the signal from the pressure transducers and the ITM. The signal filtering was to reduce the high frequency noise. Details of the signal filters are provided in Appendix H.7.

4.6.5 LINEAR VELOCITY DISPLACEMENT TRANSDUCERS

Linear Velocity Displacement Transducers (LVDTs) are standard instruments that are commonly used in laboratories. Details of the LVDTs used in the experiments are provided in Appendix H.8.2.

4.6.6 RING DISPLACEMENT TRANSDUCERS

The ring displacement transducers (RDT) were designed to measure displacement over a distance of approximately 0.5 metres to 0.7 metres. The assumption was that the average strains could be recovered from the data. The RDTs were initially checked for accuracy against the 0.5 mm LVDTs using panel AP: 4. The 0.5 mm LVDTs, whilst theoretically having similar accuracy to the RDTs, had a problem of mass and distance from the wall. This problem manifested as a difficulty in holding the LVDTs steady during the harmonic motion. The low mass of the rings and the low centre of gravity provided a stable platform for the measurements. The rings were used exclusively for the strain measurements after panel AP: 4.

4.6.7 PRESSURE GAUGES

The pressure gauges were capable of reading to 68.9 MPa.[280] The results are in the range of zero to + five V.

4.7 EXPERIMENTAL METHOD

4.7.1 INTRODUCTION

The experimental methodology was based on a systematic study of a number of masonry panels tested to destruction in the 2 part test rig. This section provides details of the test set up procedure, the methods of measurement of the average stress and strain fields, and the definition of a standard test point for each point in the amplitude frequency space of the harmonic forcing function.

[280] These pressure gauges were 10,000 psi units.

4.7.2 EXPERIMENT SET UP PROCEDURE

This section provides a summary of the procedure used for the test set up for a typical masonry panel. The equipment was calibrated using standard procedures. The constructed panels were laid flat and precompressed using a frame. The panels were drilled using a magnetic drill and a 25 mm diamond tipped corer. The frame was used to stand the panels, to allow them to be lifted and placed in the compression frame with a forklift and lifting frame. The panel was squared in the precompression frame and the thrust blocks were driven onto the masonry panel. The panel and precompression frame were then hanging in chains from the reaction frame. The safety strap was removed from the precompression frame to allow the masonry to provide the stiffness to the precompression frame. The upper and lower shear plates and plywood packing were placed on the panel and bolted together with the friction grip bolts. The shear yoke mechanisms were placed and the bolts tightened after the precompression frame and panel were located on the centreline of the ITM. This mechanism consisted of a primary rod, two secondary rods, and six clevises for each of the four quadrants of the test rig.

The balancing of the test rig was achieved by measurement of the shear yoke rods. These were set to lengths that provided a square fit to the shear yoke when it was centrally located. The nominal lengths of the rods were 600 ± 5 mm. The essential point was that all were the same length on both sides of the top and the bottom. The vertical bars were set to length to suit the panel size. The instrumentation was installed on the test panel. The instrumentation consisted of the displacement transducers in a standard rosette pattern placed on the two sides of the panel. The pressure transducers measured the pressure in each of the two manifolds, which supplied the hydraulic pressure to the precompression frame. The standard test procedure is presented in Table 22. Data logging used a standard board and program.

TABLE 22 STANDARD TEST PROCEDURES

Stage	Description
1	The precompression was set in each arm using the data logger.
2	The shear yoke was loaded to a mean point typically of 150 kN. This provided a static estimate of the effective stiffness.
3	The frequency and amplitude points required for the test were selected on the ITM Controller.
4	A standard 30 second test was applied and the FFT of the results obtained and recorded. This step was repeated for the number of replicates typically 5 or 10 depending on the block pattern.
5	Stage 3 was repeated for the new set of points with an amended typically higher frequency.
6	Stage 4 was repeated until a full block of tests at one amplitude and varying frequency was obtained. This stage was typically 90 tests.
7	Stage 7 increased the amplitude by a pre set amount and repeating Stages 3 to 6.

Two photographs provide a basic outline of the method used to drill the holes in the panel. The panel was set normal to the drill press using a right triangle and a jig was used to locate the holes before drilling. The equipment and a panel ready for drilling are shown in Figure 20.

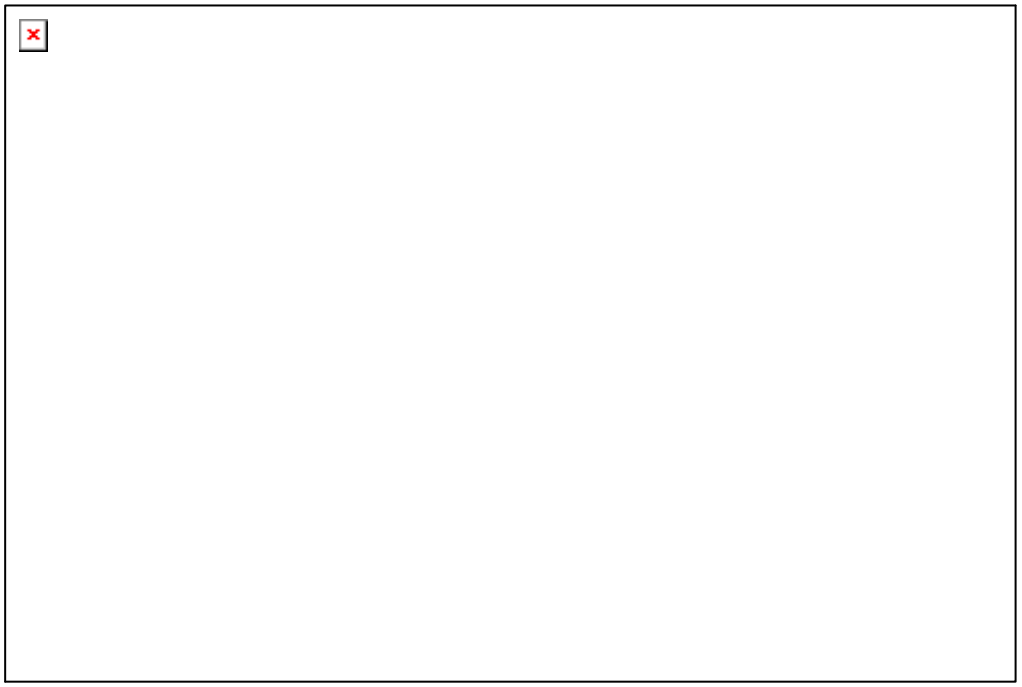

FIGURE 20 PANEL, MAGNETIC DRILL WITH DIAMOND TIPPED CORER, AND FRAME

Table 23 shows the logging frequencies used in the data acquisition software.

TABLE 23 NOMINAL LOGGING FREQUENCIES

Frequency	Nominal Logging Frequency (Hz)	Comment
0.06	200	This test period of 30 seconds provided a lower limit to the frequency that could be recorded. This frequency was considered as a reasonable limit.
0.1, 0.3, 0.6	200	
1.0	200 - 400	
2.0	200 - 800	
5.0	200 - 1350	
10.0	1200 - 2000	The computer memory was the limit in the save operation.

4.7.3 BI-AXIAL COMPRESSIVE FORCE APPLICATION AND MEASUREMENTS

The pressures in the two hydraulic manifolds applied by the Raripress pump set were used to calculate the stress applied to the face of the masonry panel. The stress calculations were based on the methods presented in Table 24.

TABLE 24 COMPRESSION STRESS CALCULATION METHODS

Method	Description
Force application	Using the Enerpac rams, a pressure of 68.9MPa applied a load of 23.6 kN to the thrust plate.
Voltages	0 to +5 V represent 23.6 kN.
Stress calculations	The voltage represents the stress directly using equation (20).
Error calculations	The error in the stress given an error in the voltage of ±2.4 millivolts for 1 V was five percent.
Data logging	Each of the pressure voltage reading was recorded with the data for each time point. The actual voltages were used in the calculations of the stress at each time step.
Filtering	The data was filtered to remove a high frequency component.

$$t_{ii} = \left(\frac{V \times 23600}{5}\right) \times \frac{1}{A_t} \tag{20}$$

4.7.4 SHEAR FORCE APPLICATION AND MEASUREMENTS

The application of the shear force was assumed to provide a stress field within the masonry panel that could be used to calculate the measured stiffness given the measured strain fields. The shear force was measured using the analog data from the ITM. The force was measured at the ITM ram. This force application does not imply that the nominated displacement was reached. The displacement selected may be infeasible within the limitations of Newtonian physics for the achievable slew rate of the hydraulically driven ram. The stress calculations were based on the methods noted in Table 25.

TABLE 25 SHEAR STRESS CALCULATION METHODS

Method	Description
Force application	Using the ITM a load of 250 kN could be applied dynamically.
Voltage	±1 V represents 100 kN.
Stress calculations	The voltage represents the stress directly using equation (21) with the angel in degrees.
Error calculations	The error in the stress given an error in the voltage of ±2.4 mV for 1 V was five percent.
Data logging	Each of the ram force voltage readings were recorded with the data for each time point. The actual voltages were used in the calculations of the stress at each time step.
Filtering	The data were filtered to remove a high frequency component.
Displacement	The relative displacement data were recorded at the hydraulic ram.

$$t_{ij} = \left(\frac{V \times 100000}{1}\right) \times \frac{1}{A_s} \times \cos(45) \tag{21}$$

4.7.5 STRAIN FIELD MEASUREMENTS TESTS

The 10 mm LVDTs were placed on one side of the panel and the 0.5 mm LVDTs were placed on the other to provide a minimal strain rosette. The standard equations for these strain rosettes are presented in Hetenyi (1950). These strain calculations for the LVDTs are based on the methods set out in Table 26.

TABLE 26 LVDT STRAIN CALCULATION METHODS

Method	Description
Voltage	±5 V represents the nominal full scale deflection. Each LVDT was calibrated. The calibration constants were coded into the Fortran programs.
Strain Calculations	The voltage represents the strain directly using the equation (22).
Error calculations	The error in the strain given an error in the voltage of ± 2.4 mV for 1 V was six percent.
Data logging	Each of the LVDTs voltage readings was recorded with the data for each time point. The actual voltages were used in the calculations of the strain at each time step.
Problems	1. The high inertia of the LVDTs and the moment arm required on the fixing points made securing these in place and then holding them steady a difficult task. 2. The systematic difference observed in results between the two sides was due to the initial method of placement of the rosette points.

(22) $$e_{ij} = \frac{V \cdot K_{LVDT}}{L}$$

The first problem shown in Table 25 was resolved using the ring displacement transducers. These were held with 6 mm masonry anchors. Damping foam rubber pieces were provided. The second problem was resolved by drilling boltholes through the masonry to ensure that the placement of the rosettes on the two sides was identical. Final testing used the ring displacement transducer.

4.7.6 STRAIN FIELD CALCULATIONS

Detailed methodologies for the equations used in the computer programs were provided in Hetenyi (1950) and Megson (1991). These were based on the standard definitions presented in Solkinoff and Sprecht (1946). A sketch and the associated angles that form the standard linearly independent components for calculation of the shear strains from Solkinoff and Sprecht (1946) are presented in Figure 21. A standard rosette pattern was used for the experimental work. The Y direction was assumed normal to the bed joints and the X direction was parallel to the bed joints. It was assumed for the analysis that the XY direction is vertical and the YX is horizontal. This is a simple convention to assist in the analysis of the results.

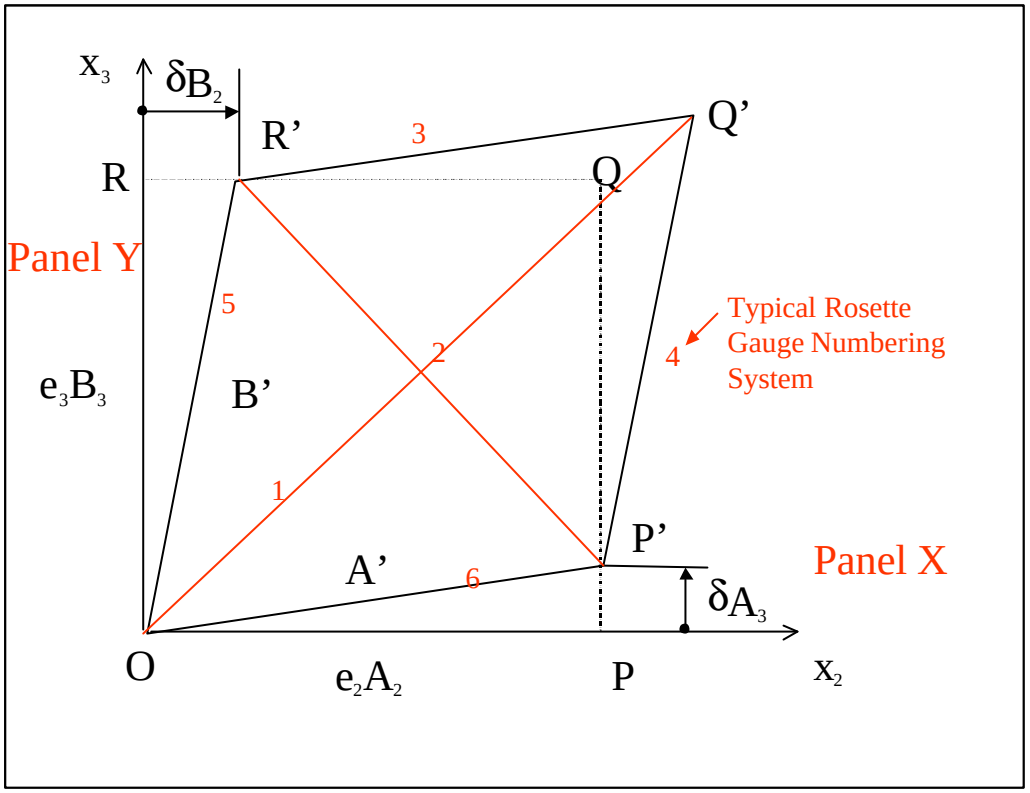

FIGURE 21 SHEAR STRAIN DEFINITION SKETCH (AFTER SOLKINOFF AND SPRECHT, 1946.)

4.7.7 STRAIN FIELD SET OUT MEASUREMENTS - STANDARD

The rosette details used in the analysis of the results are shown on Figure 22.

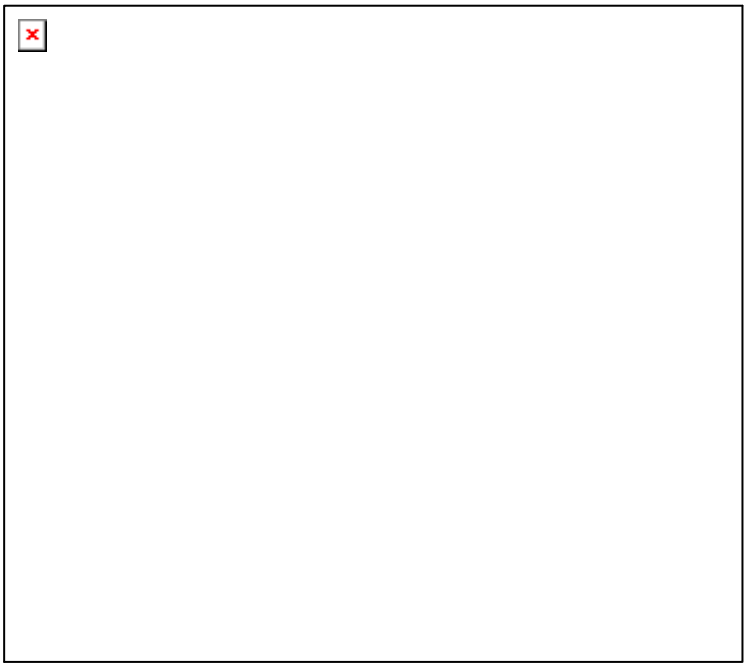

FIGURE 22 STRAIN ROSETTE DETAILS

The correspondence between the points of the rosette shown in Figure 21 and Figure 22 and the coordinate points used in the analysis of the strain results is presented in Table 27.

TABLE 27 CONFIGURATION DETAILS

Coordinate Direction	Side of Plane
XX	AD
YY	AB
XY	AC
YX	BD

This configuration permits the calculation of the shear stiffness in two orthonormal directions. The relationship between the data logger channels and the sides of the rosette were hard coded into the Fortran programs. These programs are included on the CD.

4.7.8 TEST RIG SET UP

The test rig with a panel mounted and the equipment in place is shown in Figure 23.

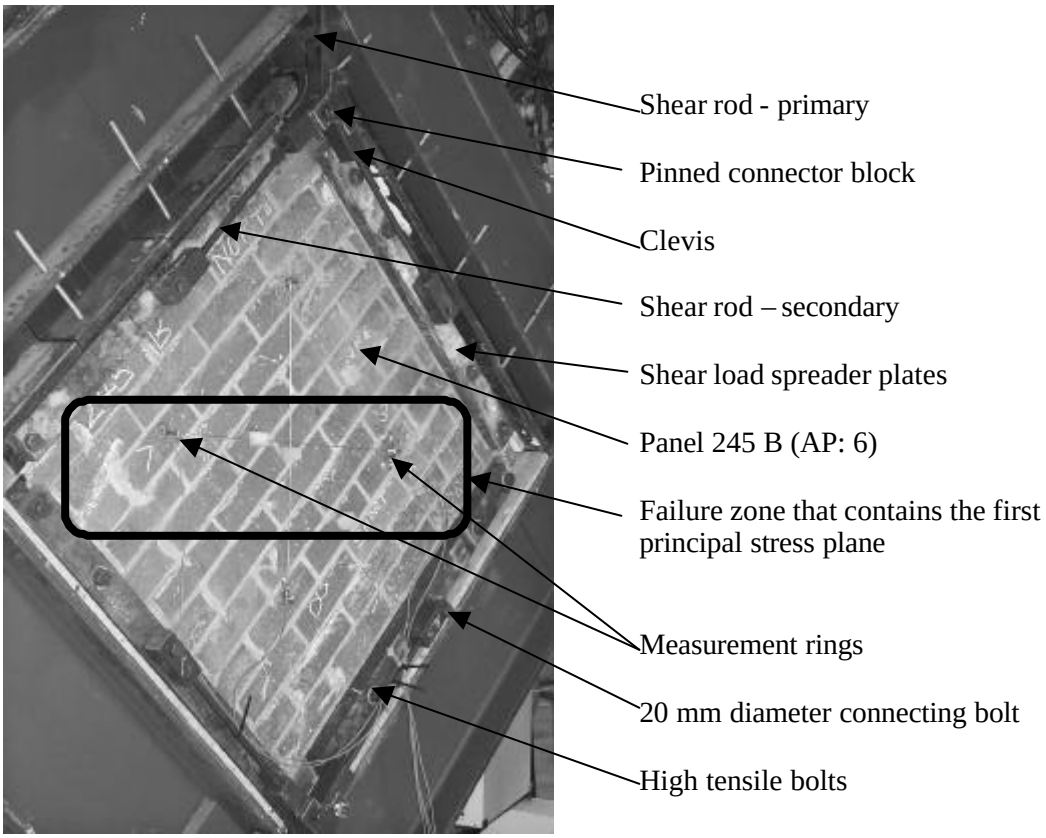

FIGURE 23 PANEL AP:6 TEST SET UP

4.7.9 WAVEVIEW SET UP

The program WaveView was used to capture the data in analog format. Details of the operation of the program WaveView are published in the board manual (Tinker, 1997). The details provided in this section relate to options available within the program. An issue with the data was that it represented not a point in time, but a slice in time. This meant that calculation of the derivatives and second derivatives of the data was difficult because of the time spread of the data.

The channel configuration was designed to minimize the impact of this problem on the analysis of the results. The typical WaveView program settings used in the experimental work are presented in Table 28. Specific settings for each panel are listed in Appendix A

TABLE 28 WAVEVIEW PROGRAM SETTINGS

Description	Unit	Value
Rings Type 1	Channels	4 - 6 and 12
Rings Type 2	Channels	0 - 3
Rings Type 1	Gain	10
Rings Type 2	Gain	10
ITM Load	Channel	8
ITM Load	Gain	1
ITM Displacement	Channel	9
ITM Displacement	Gain	1
Pressure A and B	Channel	10 and 11
Pressure A and B	Gain	1
Typical Test Period	Seconds	30 - 50
Typical Test Frequency at 0.6 Hz Ram Frequency	Hz	200
Test Frequency Adjustment	Rate	Ratio of the frequencies with a limit of 2000 at 10 Hz Ram Speed.

4.8 PANEL TEST PURPOSES AND METHODS

The testing of the masonry panels used a standard statistical technique. The procedure held some variables constant and used a systematic change in the domain of a single variable to produce a corresponding change in the range of the results. The purpose of each experiment for all of the test panels is summarized in Table 29. This table outlines the basic purpose of the test, within the systematic statistical study.

TABLE 29 SUMMARY OF PANEL TEST PURPOSES AND METHODS

Laboratory Designation	Thesis Number	Test Description
210	AP: 1	This panel was used to confirm the operation of the LVDT units and the test rig in compression. The panel used an extruded brick.
226	AP: 2	This panel was used to confirm the operation of the shear yoke and to gain further data on the use of the LVDTs and the data acquisition software. The panel used an extruded brick.
246A	AP: 3	This panel was tested at a constant frequency of 1 Hz with increasing amplitude in a classic block pattern.
245A	AP: 4	This panel was tested frequencies of 1 and 5 Hz with increasing amplitude.
331A	AP: 5	This panel broke on the ramp up test. It provided an estimate of the Young's modulus and shear modulus, and confirmation of the static damage parameter.
245B	AP: 6	This panel was tested with a full range of frequencies from quasi-static to 10 Hz in a 90 block stage. After each 90 block of tests the amplitude was increased by 1.25 mm starting at 1.25 mm and increasing to 12.5 mm.
245D/E	AP: 7	Similar to AP: 6.
245C	AP: 8	Similar to AP: 6.
331C	AP: 9	This panel was tested as a variant on the method for AP: 6 to determine the change while the amplitude was held constant through two sets of frequency.
329D	AP: 10	Similar to AP: 9, and this panel was tested in the final test series at frequencies of 1 and 10 Hz.

4.9 STORAGE AND ACCESSING EXPERIMENTAL RESULTS FILES

4.9.1 INTRODUCTION

This section presents the organization and method to retrieve data and the analysis results. The file naming convention follows a consecutive and logical order based on the Julian data and the number of the test. Special tests are designated within the files.

4.9.2 RAW DATA FILE STRUCTURE

This program output has the structure presented in Table 30. The Fast Fourier transform data is contained in the files. This FFT data has a standard structure. The raw data files were named to provide a logical and systematic numbering of the files for the analysis stage.

TABLE 30 DATA FILE STRUCTURE AND SAMPLE

Line Number	Description	Example of the data stored on each line of the file
1	Title	Wave View for DOS 1.24 Multi board (3) text output
2	Sample rate	8000 samples at 200 Hz in normal mode on PC30F
3	Input Range	Input range: -5 to +5 volts
4	Channels	12 channels sampled: 0 1 2 3 4 5 6 8 9 10 11 12
5	Start Time	First sample taken at 08/04/99 11:44:33
6		Blank
7	Data Format	Data is in float (volts) format
8		Blank
9	Count, Time Channels	Number, time(s), 0, 1, 2, 3, 4, 5, 6, 7, 8, 9, 10, 11, 12
10	Data	0, 0.000, -0.194, 0.101, -0.087,

The file name standard is presented in Table 31.

TABLE 31 FILE NAMING CONVENTION

Component	Description
245B	Laboratory Panel Designation
001	File Number
A, B, C	Used for specials such as ramp up.
*. txt	Standard Text File

4.9.3 ANALYSIS FILE STRUCTURES

Each data file was placed in a separate directory of the CD. A database of the files was created for each panel using Fortran. This database provided a method to reanalyse the data files.

4.9.4 COMPUTER PROGRAMS

The computer programs that were developed for the analysis of the data files and the Fast Fourier transform analysis are outlined in this section. The programs were a raw data file analyser, a summary program and a FFT conversion program. A copy of the code for these programs in Fortran 90 format is contained in the program directory of the CD. A database file in Microsoft PowerStation format is presented with each program.

The Fast Fourier transform programs were checked using standard data files. The analysis programs were checked with a manual check of the results.

The first program named *Hugh* provided the analysis of the raw data files for each of the 30 second tests. This data was stored in a database file, which was accessed by the

program Neal. The various material and test constants were encoded in to the program. Two procedures were used for the linear regression. The first was least squares fit and the second a robust fit. The least square fit was the standard routine, with the robust fit provided as a check on outlying points. Both methods generated an error estimate on the linear regression using standard statistical techniques (Press, *et. al.*, 1992). The orthotropic moduli were determined using a hill search procedure that grided the probability space and sought the objective function as the greatest regression co efficient in the least squares data. The method was checked against NLFIT (Kuczera, 1994) using a number of data files. The difficulty in using a traditional hill climb procedure was the relative short domains of the Poisson's ratios that provided slow convergence. The analysis was significantly faster computationally by coding the method into the analysis routines and running multiple regression using fixed values for the Poisson's ratios. These fixed values were then systematically incremented as the solution space was investigated for an optimal answer.

The program named *Neal* summarized the data files into a single set of data suitable for analysis using EXCEL.

The program named *Convert* was developed to provide a Fast Fourier transform routine for the earthquake traces and then for the statistical analysis of the measured stiffness.

Chapter 5 Analysis of the Results

5.1 INTRODUCTION

This experimental study investigated the degradation of masonry shear walls that were subjected to a stress regime of nonproportional compression and a harmonic shear. This chapter presents the analysis of the results for the experimental data from the panel tests. This chapter is based on the experimental data collection phase summarized in Chapter 4. The study of the properties of the effective stiffness based on the results derived in this chapter is one of the areas of investigation presented in Chapter 6.

This chapter provides a summary of the results, a typical failure mechanism, and the critical results for the measured shear stiffness for the eight panels specifically panels AP:3, AP: 6 and AP: 10. The establishment of the effective stiffness for each panel was related to the particular loading pattern and the measured shear stiffness results. The features of the damage parameter, D, were determined from the measurements of the effective stiffness and were related to the change in peak strain in the panels.

5.2 LOADING PATTERN AND THE FAILURE PATTERN FOR THE PANELS

5.2.1 INTRODUCTION

The analysis of the results for the ten panels was completed using the procedures outlined in section 4.7 and Appendix B. The detailed results for the ten panels are presented in Appendix A. This section provides a summary of the results for the experiments. The summary uses critical examples from the ten panels to illustrate the systematic investigation of the measured shear stiffness, determination of the effective shear stiffness, and the encapsulation of the damage parameter. Ten panels were tested to failure. The first two were used to confirm the operation of the test rig and the remaining were used to determine the properties of the measured shear stiffness for a systemic variation of the loading pattern.

5.2.2 LOADING PATTERN

The loading pattern was established from a finite element analysis of two masonry structures. The first structure was a typical 7 storey apartment block (Page, 1973) from Perth, Australia and the second structure was a 2 storey ISMES test building of Italian construction (Benedetti and Pezzoli, 1996). The development of the loading pattern is

presented in Appendix D. It conforms to the general comments on earthquake amplitudes and frequencies offered by Richter (1956) that are summarized in Table 5.[281] The specific variations in the loading pattern for each panel are presented with the detailed results in Appendix A.

The results from the panels are used in this chapter to illustrate the systematic variation in the development of the loading pattern and the development of the understanding in the relationship between the loading pattern and the measured shear stiffness. Three panels represent critical points in understanding the degradation of the damage parameter with strain. The first critical panel was Panel AP: 3 which was essentially loaded at a single frequency. The second critical panel was Panel AP: 6 where the results were analysed using a theory of the functions and a standard statistical technique using Fast Fourier transforms. The third critical panel was Panel AP: 10 where the initial testing was based on the standard loading pattern and with a final sequence of tests at frequencies of 1 and 10 Hz.

5.2.3 THE FAILURE PATTERN

The loading pattern was designed to provide a failure on the first principal plane. In this case, the harmonic shear stress causes the first principal plane to rotate from the initial static principal plane to the final dynamic principal plane. This final dynamic plane is approximately 15 to 30 degrees from the horizontal plane. Macchi (1982) elegantly presents the uses and limitations of the various tests that can be undertaken on masonry shear wall elements. This experimental study used the simplest failure model (Macchi's fourth plan). The model assumes that failure will occur on the first principal strain plane.

The common assumption from the work of Vecchio and Collins (1986) was that the principal stress planes and strain planes are coincident. This was a reasonable approximation for their method of testing which combined the shear and direct stress elements into one loading system. The procedure, which was developed for this experimental work, uses separate direct stress and shear stress systems. The assumption that the principal stress planes and principal strain planes are coincident is also consistent with these methods and results. The application of a bi-axial compression on both faces of the masonry panel provided both first and second principal stresses that are in compression. The bi-axial compression was nonproportional ensuring that the first principal stress was always greater than and never equal to the second principal stress

[281] Refer pg. 44.

under all loading conditions.[282] The principal planes rotate within the masonry panel with the application of the harmonic shear stress. The typical loading values used in the experimental work result in a peak 15 to 30 degree rotation of the principal planes. This is shown conceptually in Figure 24.

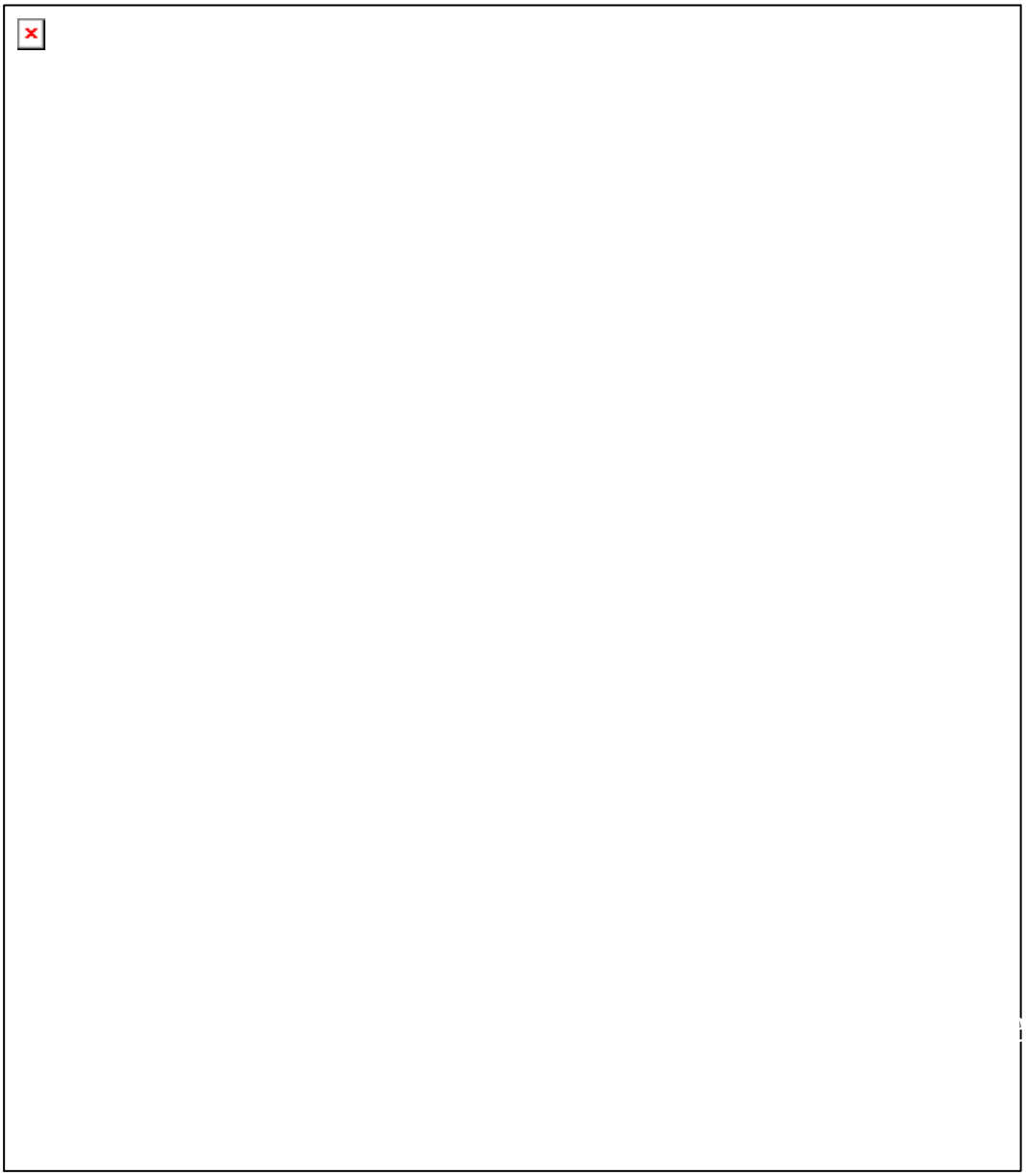

FIGURE 24 PANEL AP:6 FAILURE PLANE

The masonry had adequate stiffness and strength to remain elastic when subjected to the compressive loads. The harmonic shear force applied by the ITM ram provided shear stress onto the masonry panel. This shear stress affects the principal stresses and strains

[282] This loading pattern avoids a point load in the Mohr's circle.

with the first principal stress and principal strain being driven by the ITM's shear force towards a tensile stress. This was the main mechanism that causes the degradation of the masonry panel under a tensile stress field as has commonly used in the study of the damage of materials (Krajcinovic, 1996). The value of θ will be 105 to 120 degrees. The principal plane shown was drawn parallel and offset to the chalked failure line for clarity. A typical failure pattern is shown in Figure 24. This panel cracked starting at the point A and progressing over about 10 tests to the point circled x. At this point, the cracking was arrested and the testing continued for about twenty tests before the crack extended further. The crack, in this panel, was initiated in the mortar joint near point A. There was no systematic evidence that the boltholes initiated the cracking. However, the drilling on a mortar joint may have contributed to the crack initiation. A similar pattern of cracking failure was observed in all tests.

The approximate angle of the first principal plane and the Cartesian co ordinate system is shown on Figure 24. This plane angle represents the peak of the harmonic shear stress function. The line is drawn parallel to the cracking plane that is evident in the photograph. The features of the structured continuum constructed from masonry, the inherent variability of masonry within a panel, and the edge conditions provide a typical scatter to the location of the failure plane. However, the plane was within the expected region from the theory and there was no evidence to support an alternative failure mode. The only panel that did not follow the typical results was Panel AP: 9. This panel cracked in the lower third of the panel on a line that was parallel and offset to the typical failure plane in the remaining panels. The result occurred at low amplitude of loading (2.2 mm) and at a low frequency of 0.1 Hz.

5.2.4 MOHR'S CIRCLE

The failure pattern observed in the masonry panels was the pattern expected from a simple Mohr's circle analysis. The failure plane always initiated at a point and progressed across the panel element.

A stress regime comprising a constant nonproportional compression stress, and a harmonic shear stress was applied to each panel. The application of the shear force was designed to slowly increase the shear stress, t_{xy}, until the first principal stress, t_{11}, became tensile. The strains in the masonry are measured as the first principal stress was systematically increased. A summary of the Mohr's circle for the test stress conditions is shown in Figure 25.

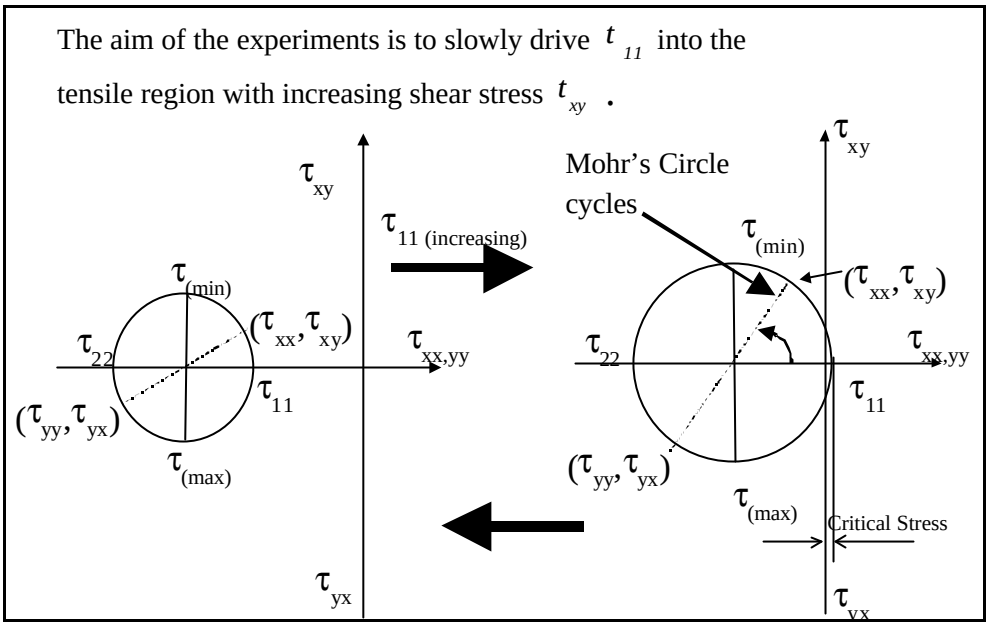

FIGURE 25 MOHR'S CIRCLE OF THE TENSILE LOADING REGIME WITH TIME

This figure shows a simplification of the algebra of the harmonic functions. The symbols are based on the tensor analysis using the standard τ notation. The practical problem is that the angle of the principal plane follows the applied harmonic shear stress. The problem of soft mortar joints introduces the orthotropicity that compounds this issue by providing planes of weakness that preferentially attract the opening cracks. Here the principal stress tensor and strain tensor have been assumed to remain co incident, which is a reasonable assumption given the loading rates.

5.3 ANALYSIS OF THE CRITICAL PANEL RESULTS

5.3.1 INTRODUCTION

Ten panels were tested in the rig. The first two panels were used to test the operation of the rig. No measurements were made with these panels. The results for the ten panels are presented in detail in Appendix A. Three critical panels Panel AP:3, AP:6, and AP: 10 confirmed the basic hypotheses being tested in this experimental work.

5.3.2 PANEL AP: 3 MEASURED SHEAR STIFFNESS RESULTS

Panel AP: 3 was tested at an age of 129 days. It has a prism flexural strength of 0.85 ± 0.16 MPa. The mean prestress force was 175 kN and the number of tests to failure was 129. The test set up and the detailed results are presented in Appendix A.5.[283] The loading

[283] Refer pg. 181.

pattern was based on a single frequency of 1 Hz and cyclic amplitude with a maximum displacement of 8 mm. A small number of tests at the end of the pattern were performed at 5 Hz and with a maximum displacement of 10 mm. The results for the measured shear stiffness for the two sides of panel AP: 3 are shown in Figure 26.

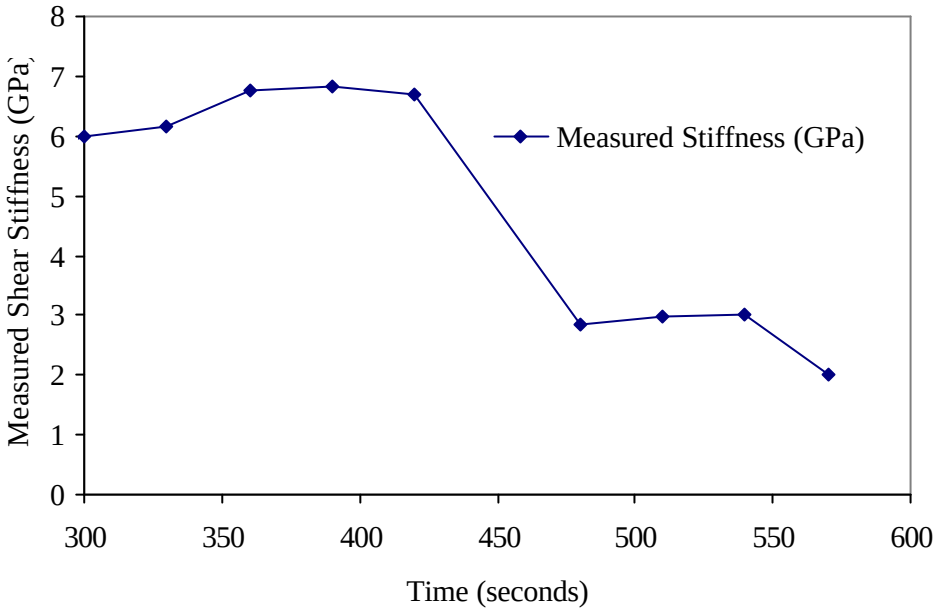

FIGURE 26 PANEL AP: 3 MEASURED SHEAR STIFFNESS RESULTS WITH TIME

The results show a clear degrading of the effective stiffness with time of loading. The peak stiffness was approximately 7 GPa. This panel demonstrated the existence of the degrading effective stiffness in masonry shear walls.

5.3.3 PANEL AP: 6 MEASURED SHEAR STIFFNESS RESULTS

Panel AP: 6 was tested at an age of 183 days. It had a prism flexural strength of 0.85 ± 0.16 MPa. The mean prestress force[284] was 150 kN and the number of tests to failure was 640. The test set up and the detailed results are presented in Appendix A.8.[285] The loading pattern was based on a sweep of frequencies from 0.06 to 10 Hz, in which each sweep was performed with constant amplitude on the ITM's ram. The ram displacement was incremented in 1.27 mm increments from 2.54 mm. The results for the measured shear stiffness for the two sides of panel are shown on Figure 27.

[284] This force is half of the static failure load on Panel AP: 5.
[285] Refer pg. 197.

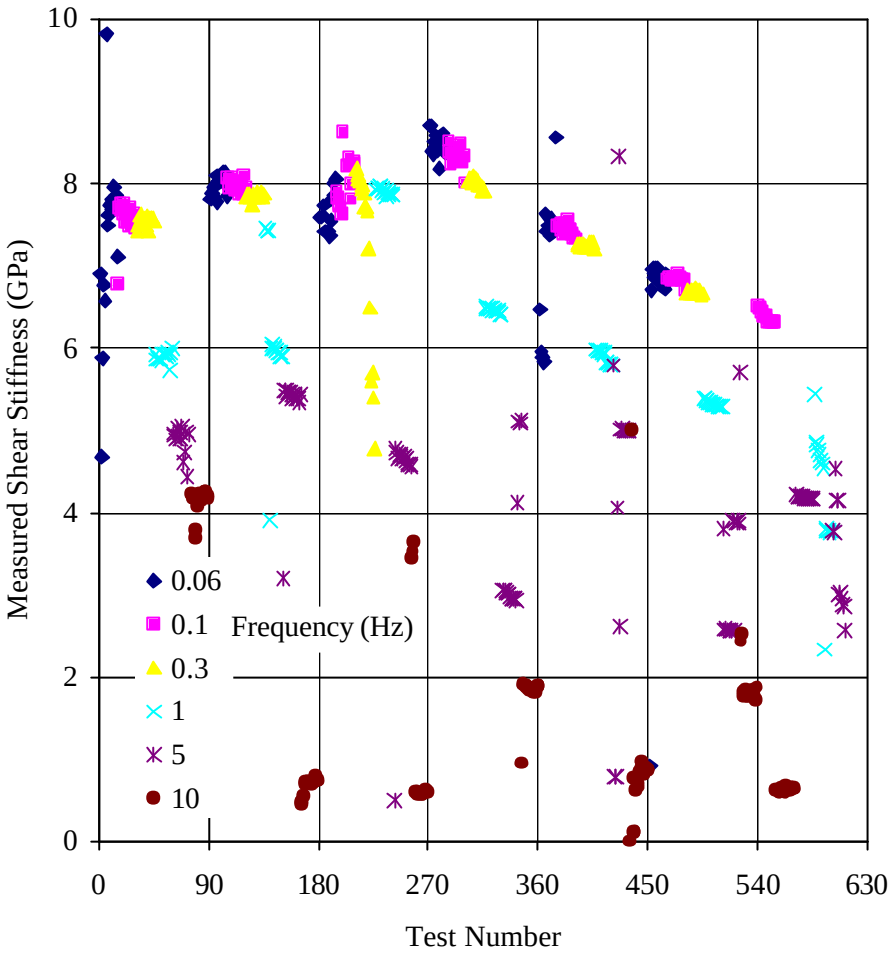

FIGURE 27 PANEL AP:6 MEASURED SHEAR STIFFNESS RESULTS

There are three features to observe with this graph of the measured shear stiffness. There was a slight rise in the peak measured shear stiffness for each block of 90 tests to the maximum at the 270th test. This feature was observed to decrease with increasing stiffness of the test rig. The first change was welding additional stiffeners on the base plate and then changing the shear rods from 16 mm HT bolts to 20 mm HT all threaded rod. This feature of the slight initial rise in the initial measured stiffness was not considered significant and was attributed to the characteristics of the rig.

The second feature was the bounding curve that was distinct at the low frequencies. The results for the 0.06 Hz tests document this curve.

The third feature was the parabolic function that was shown in each of the constant amplitude tests.

5.3.4 STATISTICAL STUDY OF THE PANEL AP: 6 RESULTS

To ensure that these results did not contain any other features the results were investigated using standard statistical methods. The purpose of this work was to confirm that the relationship, $k^2(t) \ ^3 \ l^2(t)$, could be statistically recovered from the analysed data. This section presents the statistical study of the stiffness results initially in terms of the measured stiffness. The properties of the measured shear stiffness were established using linear regression and Fast Fourier transform methods. The shear modulus was estimated from the measured shear stiffness and compared to the quasi-static estimates from the compression testing of prisms. The effective shear stiffness was confirmed to exist as a conceptually separate entity, which could be recovered as a fitted line using some of the measured stiffness data points.

5.3.5 ANALYSIS OF THE MEASURED STIFFNESS

A linear regression procedure was suitable for the graphical form of the measured shear stiffness shown in Figure 27 and from the postulated relationships in Appendix B. The steps in the analysis procedure were:

I. Application of a linear regression procedure to the measured shear stiffness data.
II. Calculation of the residuals for the linear regression and graphing of the normal probability plot.
III. Determination of the Fast Fourier transforms of the residuals of the linear regression.
IV. Comparison of the FFT results to the loading pattern to determine whether the dominant frequencies matched any of the components in the loading pattern.
V. If the dominant loading pattern frequencies matched the FFT frequencies, then the reasonable statistical conclusion reached was that the results for the residuals plot were caused by the loading pattern and were not related to the change in the effective shear stiffness.

The regression result for the measured stiffness for panel AP: 6 is shown in Figure 28.

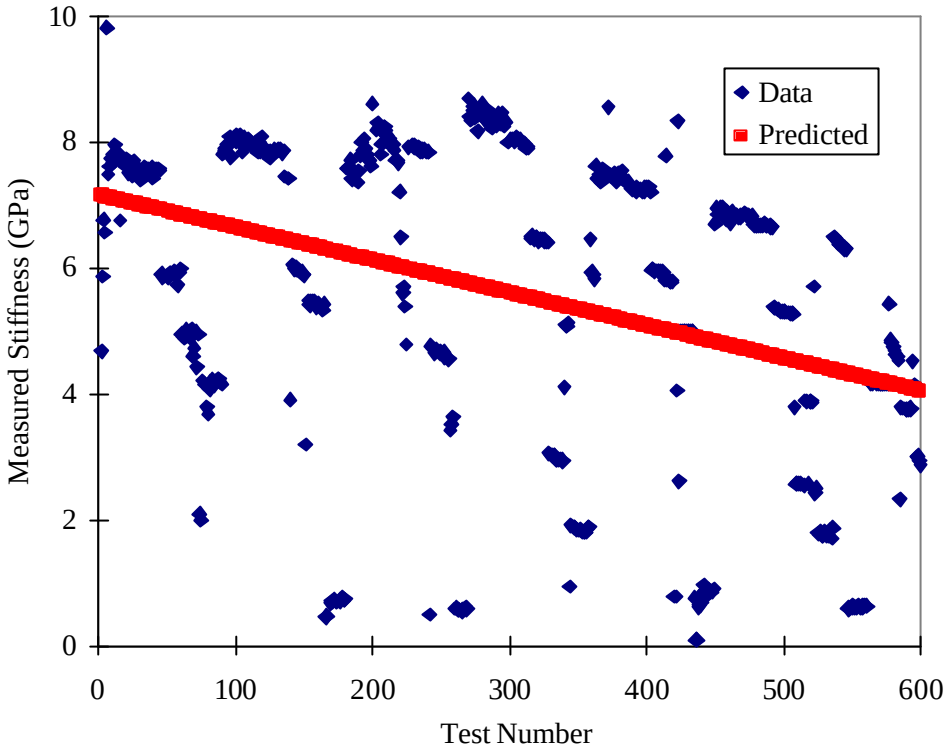

FIGURE 28 PANEL AP:6 MEASURED SHEAR STIFFNESS - LINEAR REGRESSION

These results for the linear regression of panel AP: 6 are summarized in Table 32.

TABLE 32 PANEL AP:6 MEASURED SHEAR STIFFNESS LINEAR REGRESSION RESULTS

	Coefficients	Standard Error	t Stat
Intercept	7.16	0.19	38
Slope	-0.0052	0.00053	-9.7

The residual values from the linear regression model for Panel AP: 6 are shown on Figure 29. The residual values shown in Figure 29 have a clear cyclic pattern. However, the curve is not a simple sine wave and has a distortion in the upper half of the residuals. This is due to the asymmetry of the acceleration and damping terms. These terms approach zero as the frequency decreases whereas the effective stiffness is constant over a short time period. The FFT results include a set of waveforms that account for this limit as the frequency approaches zero, and the procedure attempts to match the shape of the original data set.

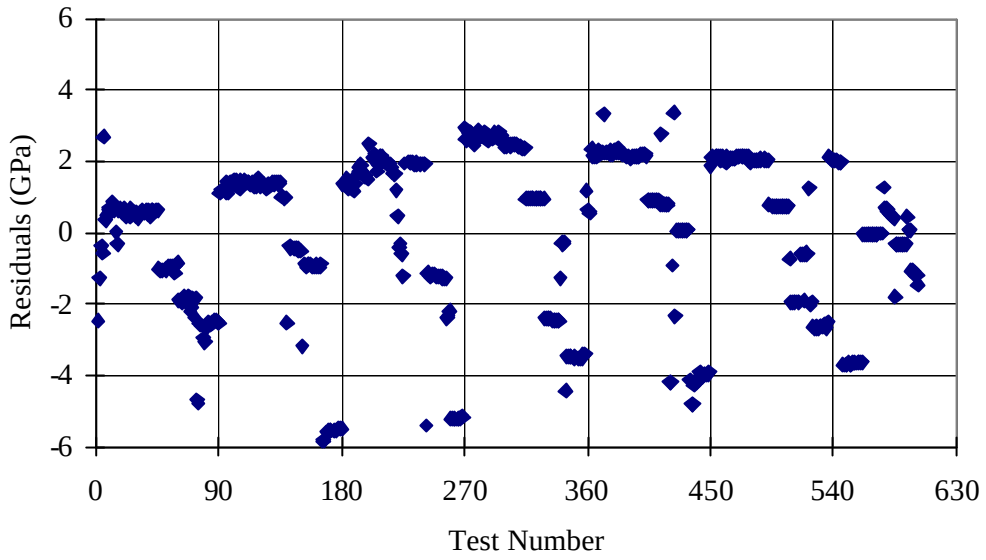

FIGURE 29 PANEL AP:6 LINEAR REGRESSION - RESIDUAL VALUES

Figure 29 was plotted symmetrically about the zero y axis for presentation purposes. This plot shows residuals in each of the 90 block patterns. If the results were random or Gaussian, the points would be scattered across the plot. There is a clear pattern to the results. This pattern can be analysed using Fast Fourier transforms. The purpose of this type of analysis is to identify the waves or series of waves that make up the changing pattern.

The experimental procedure of systematically controlling the input variables of the amplitude and frequency provides a tight constraint on the meaning of the results. The implicit operators that translate the input variables to the output data are the components of the differential equation of motion and the energy balance. Where there is a cyclic pattern in the input, a cyclic pattern in the output, and a simple transformation mathematical procedure, then the FFT of the residual data provides the data to establish the relationships and controlling features for the transformation and the operators. This is a standard statistical method. The distortion in the data points shown in Figure 29 results in a pattern in the FFT results. The features of the pattern provide the information to establish the relationship.[286] The Fast Fourier transforms results for panel AP: 6 are shown in Figure 30.

[286] An analogous concept of a simple operator is the operation 1___1 = 2. The trivial solution is +. This one to one operator is unique. The FFT exercise is a little more jumbled, but essentially this is the procedure followed. The FFT transform is one to one and invertible. The solutions are unique like the + operator and in this case are based on the circular frequency of the applied load.

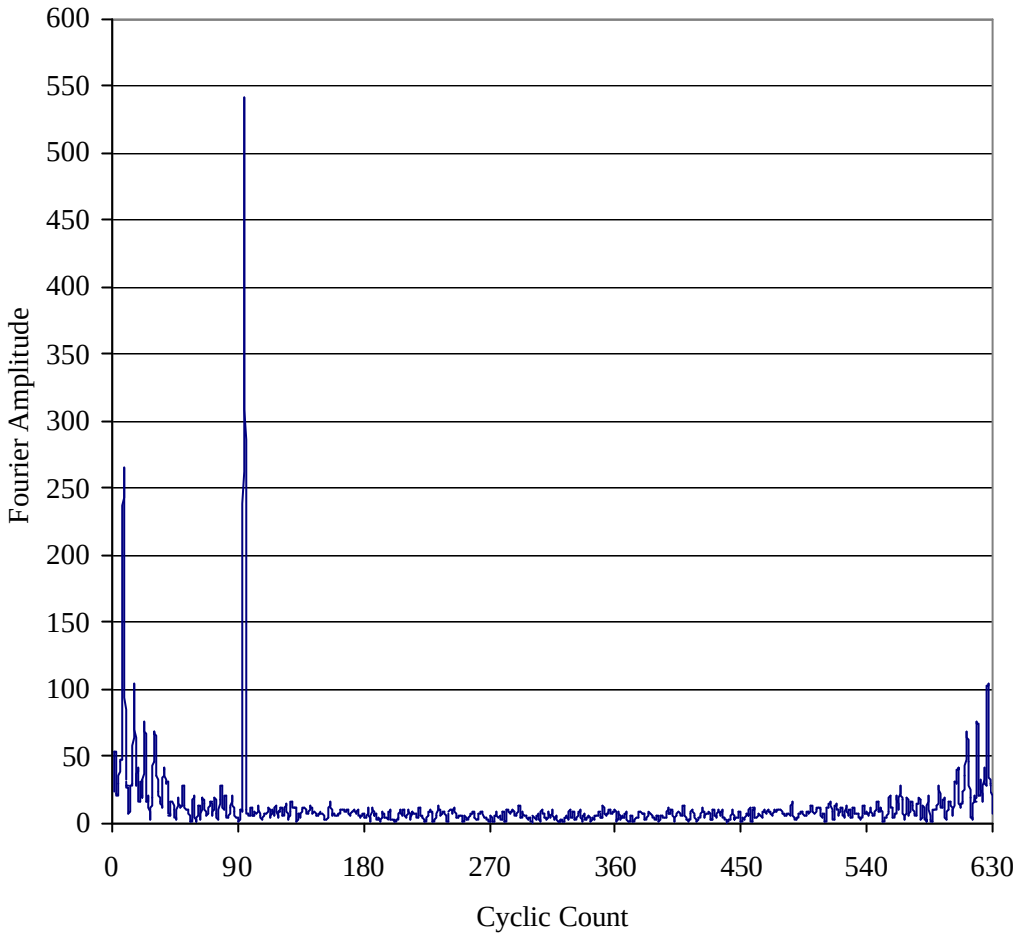

FIGURE 30 PANEL AP:6 RESIDUALS FFT RESULTS

The FFT plot is based on a binary array that is a direct result of the mathematics of a DFFT process. The results from the transformation shown in Figure 30 provide clear peaks in the FFT plot. The background noise level is consistent with the typical background noise level observed in this procedure. The peak values for the equivalent Fourier cyclic count and the frequency at which they occur are presented in Table 33.

TABLE 33 PANEL AP:6 FFT RESULTS FOR THE EQUIVALENT FOURIER TEST COUNT

Description	Equivalent Fourier Test Count	FFT Maximum Value
Single Test	1	23
First Peak	8	265
Second Peak	15	104
Third Peak	90	541
Final Peak	630	265

The meaning of each of the peak points in the FFT analysis was determined using the data from the loading pattern and considering the mathematics of the differential equation of motion presented in Appendix B. The meaning of each peak is:

I. The single test indicates the discrete frequency system of the FFT. This represents the noise level of the system. There were 640 thirty-second tests. The values below 23 in the Fourier spectra are not directly relevant to the analysis. This is an inherent part in signal processing.

II. The first set of peak points is an interesting feature. The shape of the residual value points in Figure 29 has a squashed or changing sinusoidal waveform particularly for the data points that represent the low frequencies of less than 1 Hz. This is the first half of the block of 90 tests. The first significant peak is considered a part of the waveform generated by the second peak at 15 tests, the minor array of peaks to 45 tests, and the third peak at 90 tests to give the squashed shape of the residuals curve. The signal in the region of 45 to 90 tests is clearly noise and is not considered a separate entity with a specific physical meaning, but a shape constraint to the FFT analysis. This shape effect is caused by the non-sine shape in the waves evident in Figure 29. It is directly attributed to the form of the input data in the frequency pattern and specifically related to the changes in the circular frequency.

III. The second peak point indicates the change in frequency at each of the 15 replicate points. The two points represent a series of Fourier waves that when combined using the principals of linear superposition yield the original residuals series of data. The small wave in the peaks of the FFT around the two peaks is a normal feature of the FFT analysis and is not considered to represent any physical meaning in the original data other than a set of data smoothing waves typical of the discrete Fast Fourier transform. This conclusion is reinforced by the spacing of the waves and the steady decrease in the amplitude for this small series that clearly represent smoothing waves of multiple equally spaced frequencies.

IV. The third peak point represents the change in the amplitude of loading. The numerical value for the FFT indicates that this is the significant change feature in the pattern. This is the statistically significant feature in the change to the residuals for the measured shear stiffness.

V. The final peak point confirms the break in the manifold at about 600 tests and the overall presence of a degrading effective stiffness due solely to the increase in the amplitude of testing. This incremental increase in the amplitude results directly in increased strains in the masonry panel.

In summary, the FFT results clearly point to a cyclic pattern in the residuals for the measured stiffness data points. The normal features of the discrete Fourier transforms are seen in the FFT results graph and do not obviate the meaning of the peak points. The FFT results explain the shape of the residuals curve and confirm the effect of the frequency on the measured stiffness. They confirm that the changes in the measured stiffness are due to the frequency effect and that the overall change in the effective stiffness is due to the testing at increased amplitudes. No other interpretation having an accepted physical meaning would fit this FFT input and output data.

It is concluded from these results that the following observations apply:

Observation A: The measured stiffness has a frequency component.

Observation B: This frequency component is dominant as the frequency increases.

Observation C: The strain of the object is increasing even for constant amplitude and frequency points.

Observation D: Given a constant stress field, there is an identifiable change in the strain field.

Observation E: The increase in amplitude of the loading is the only identified feature of the FFT analysis that has a physically admissible meaning in relation to the effective stiffness.

Observation F: These observations prove the existence of the measured shear stiffness and the applicability of the fundamental concept of $k^2(t) \neq l^2(t)$.

An analysis method for estimating the effective stiffness is presented in Appendix B. This method is based on the definition of a quasi-static frequency limit. This limit has been established from a numerical error approach and a pragmatic review of the results of an upper limit of 0.3 to 0.4 Hz. The lower the upper limit, the lower the systematic error in the results due to the frequency component in the measured stiffness.

The effective stiffness with this FFT analysis has been shown for Panel AP: 6 to be the upper bound to the measured stiffness, which is consistent with the classical theory of

mechanics. The effective shear stiffness does not have a frequency component and is dependent on the level of the applied stress and the applied strain. The conclusion that is drawn for this third feature is that the measured shear stiffness has a frequency dependent component.

The graph clearly demonstrates the three features present in the determination of the measured shear stiffness, and required to determine the effective shear stiffness with this test rig.

5.3.6 PANEL AP: 10 MEASURED SHEAR STIFFNESS RESULTS

Panel AP: 10 was tested at an age of 218 days. It has a prism flexural strength of 0.37 ± 0.11 MPa. The mean prestress force was 150 kN and the number of tests to failure was approximately 800. The test set up and the detailed results are presented in Appendix A.12.[287] The frequency pattern was the same as for Panel AP: 9 up until test number 640. A set of tests at frequencies of 1 and 10 Hz was used after test number 640 until the panel failed. The results for the peak strain at each test are shown in Figure 31.

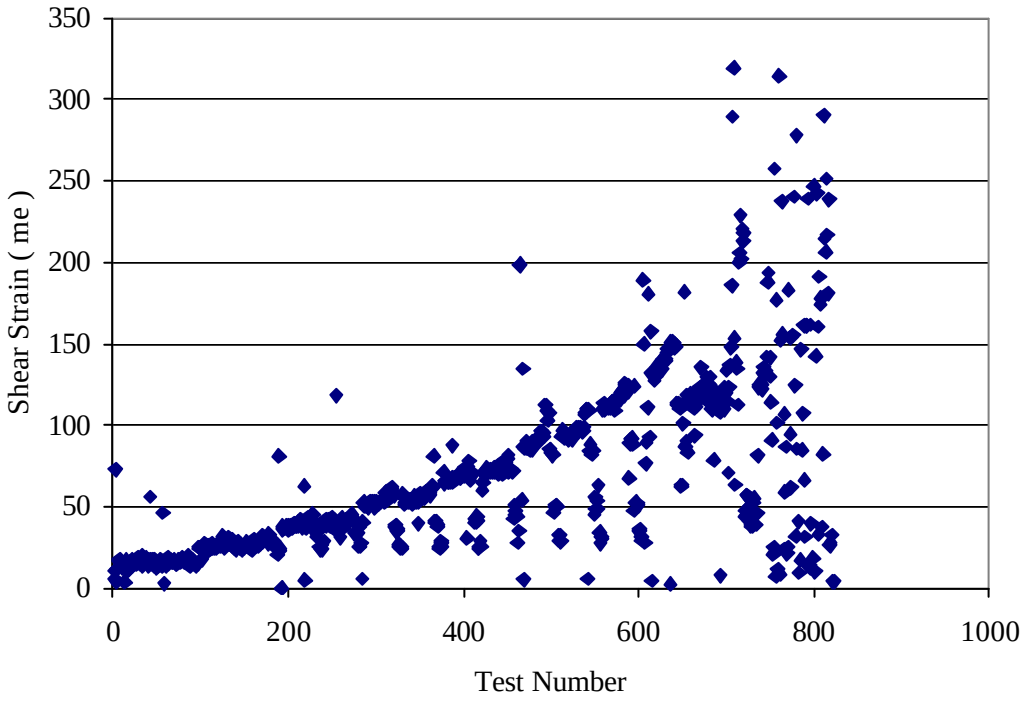

Figure 31 Panel AP: 10 Peak Shear Strains for each Test

[287] Refer pg. 217.

The interesting feature is the increase in the strain level at low amplitudes for all frequencies that is evident up until test 200 - 250. The graph of the measured shear stiffness is shown in Figure 32.

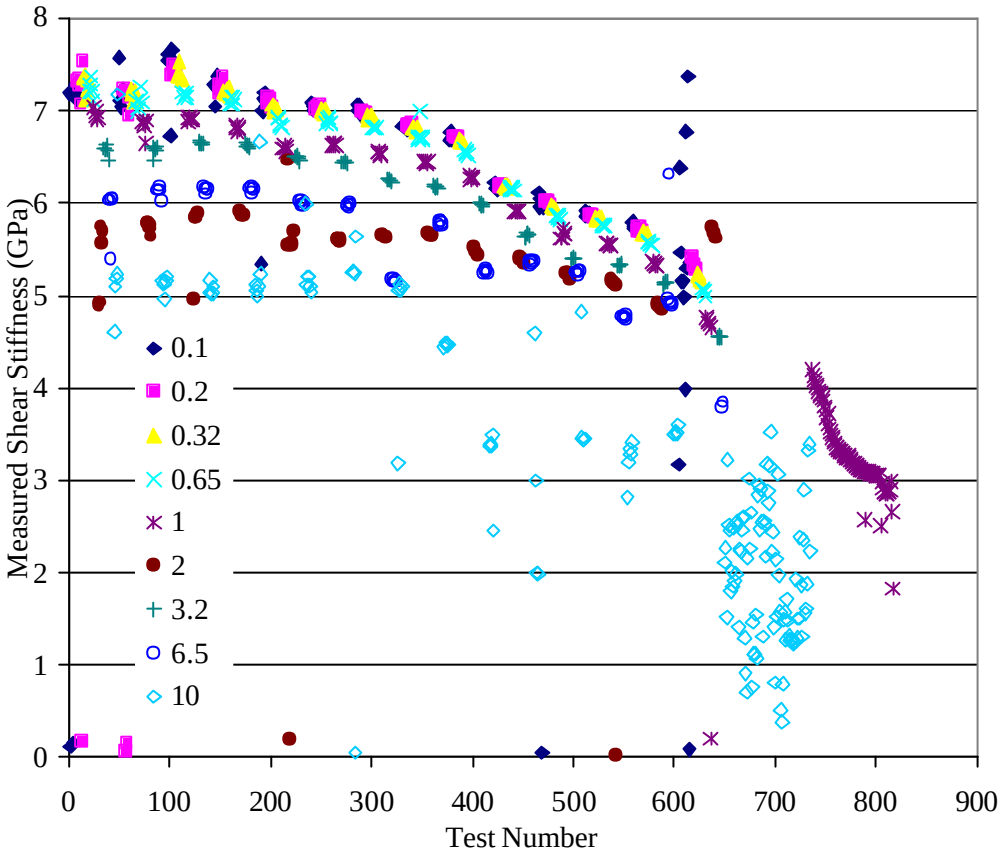

FIGURE 32 PANEL AP:10 MEASURED SHEAR STIFFNESS

The duplicate sets of frequency sweeps at one-amplitude are shown in Figure 32. The bounding curve for the effective stiffness is evident for the range of the tests and a FFT analysis was not required for this set of results. The peak effective stiffness was 7.7 GPa.

5.3.7 COMMENTS

This observational data demonstrate on these panels the difference in the response of this masonry to a dynamic load when compared to the static load. These results confirm that the measured stiffness has frequency dependence. The confirming element in this analysis was the standard statistical method using the Fast Fourier transforms which is illustrated with the results from Panel AP: 6. There is no other satisfactory or physically sound explanation for this result.

5.4 ANALYSIS OF THE RESULTS

5.4.1 INTRODUCTION

This section presents the analysis of the critical data for the determination of the measured stiffness and the effective stiffness from the experimental program. The objective of the analysis was to estimate the results for the change in the effective stiffness during the test program. An outline of the pertinent findings is summarized for the eight masonry panels. The detailed results that form the core elements to this analysis are presented in Appendix A.[288] The analysis of the effective stiffness summarized in this section was used to determine the degradation of the damage parameter with strain.

5.4.2 MEASURED STIFFNESS

The theoretical relationship between the effective stiffness and the measured stiffness was presented in Appendix B.[289] A standard statistical analysis using Fast Fourier transforms has demonstrated that the change in the frequency present in the loading pattern is the sole contributor to the variation between the effective stiffness and the measured stiffness. These detailed results are presented in this chapter.

The relationship is:

(23) $$k^2(t) \; ^3 \; l^2(t)$$

The effective stiffness, $k^2(t)$, has been shown to have a theoretical error of less than one percent at 0.8 Hz for zero damping when compared to the measured stiffness, $l^2(t)$, and a practical static limit for non zero damping from these eight panels test results of 0.4 Hz. The limit has been identified with the symbol Υ. The functional use of the t dependent variable provided the method to establish the loading pattern that systematically investigated the changes in the measured stiffnesses defining equation:

(24) $$l^2 = f_b(E, e, \dot{e}, f)$$

The experimental data typically shown in Figure 32 support the observations that the measured stiffness was bounded by the elastic modulus, E, as an upper limit, the change in measured stiffness was strongly dependent on the f, particularly for values greater than 1 Hz even for low levels of strain and strain rate. The measured stiffness decreased

[288] Refer pg. 177.
[289] Refer pg. 227.

for increased strain, but for strain rate or the change in strain the observational data suggests only a weak effect, if any effect exists at all. These results can be stated as:

(25) $$l^2 = f_b([E > k^2],[e : l^2 = g_1 e],[\dot{e} : l^2 = g_2 \dot{e}],[f : l = g_3 f])$$

Where g_2 can be estimated from the observation for zero phase lag that the strain and the strain rate during each test are:

(26) $$e = \frac{A}{\mathrm{D}}(\sin wt)$$

(27) $$\dot{e} = \frac{A}{\mathrm{D}} w(\cos wt)$$

The damage parameter, D, was determined numerically using the principal characteristics of equation (25) that of using the low frequency tests and hence low strain rate tests to estimate the change in the effective stiffness where we have shown that:

(28) $$k^2 = f_a([E = k_{\max}{}^2 : e < e_{yield}],[e < e_{yield} : l^2 = g_1 e],[\dot{e} : l^2 = g_2 \dot{e}],[\lim_{f \to 0} k \equiv l])$$

The encapsulation of the damage parameter proceeds directly from the relationships established in equation (28). This function merely provides a shorthand notation to encapsulate the varying values of the independent variables and provides specific equations to estimate the effective stiffness with strain.

5.4.3 DAMAGE PARAMETER

The damage parameter, D, has been estimated using the form set out in equation (28) and using equation (7)[290]. The limit as the frequency approaches zero has $k \cong l$ which was shown to have an effective upper frequency limit of $Y = 0.4$ for the eight panels. A typical set of results for Panel AP: 7 is presented in Table 34. The results with the standard deviation are presented for the mean values for the effective stiffness for the tests with a frequency less than $Y = 0.4$. The damage parameter was estimated from these results using equation (13).[291]

[290] Refer pg. 72.
[291] Refer pg. 83.

TABLE 34 TYPICAL DAMAGE PARAMETERIZATION RESULTS

Strain (με)	Effective Shear Stiffness (GPa)	Standard Deviation in Effective Shear Stiffness (GPa)	Damage Parameter D
30	8.466	0.261	0.00
60	7.172	0.269	0.15
75	6.694	0.056	0.21
100	6.237	0.088	0.26
150	4.929	0.250	0.42
200	4.064	0.325	0.52
400	2.83	NA[292]	0.67

A summary of the calculated results for the damage parameter for the eight panels is presented in Figure 33.

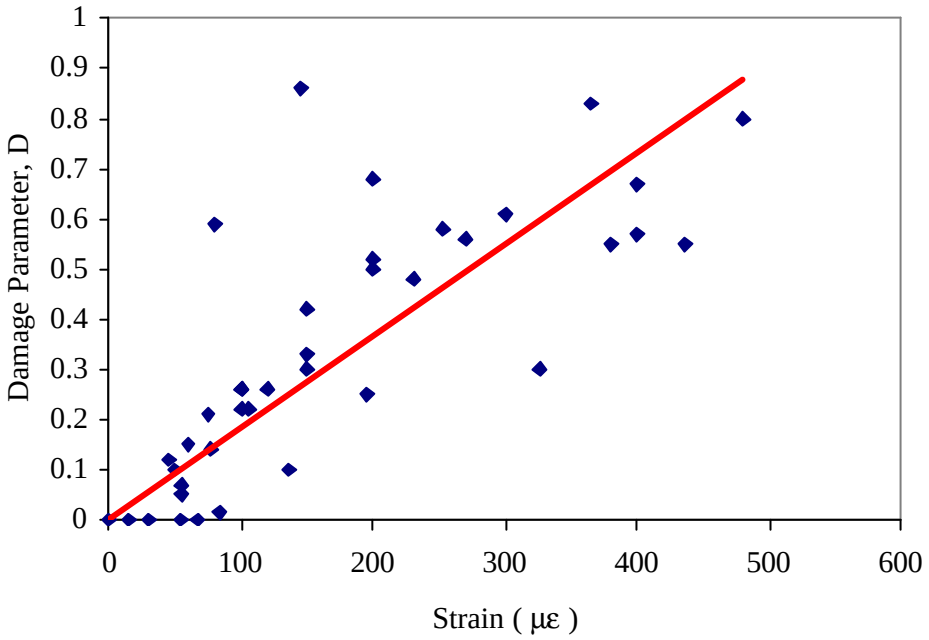

FIGURE 33 DAMAGE PARAMETER RESULTS SUMMARY

The trend line has the form:

(29) $$D = 0.0018e$$

Where the strain was measured as με. The results are shown for each panel in Figure 34.

[292] Insufficient tests were available to compute a statistically significant value.

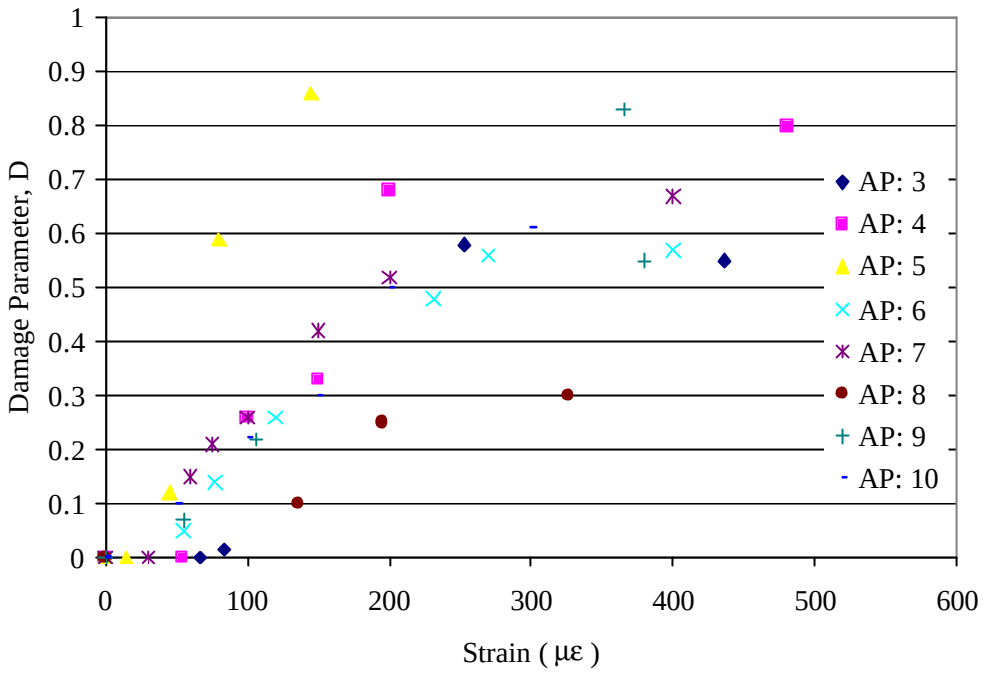

FIGURE 34 DAMAGE PARAMETER RESULTS FOR EACH PANEL

The encapsulation of the damage parameter from this information as a design function is presented in Chapter 6.

Two interesting sets of results are for Panel AP: 5 and Panel AP: 8. Panel AP: 5 failed in a static test rather than a dynamic tests as for the other panels. This panel constructed on day 331 had a high value for the shear stiffness. This type of variation is common in masonry, but is not considered typical for design purposes. The results are interesting but not considered to be statistically significant for these test purposes. Panel AP: 8 failed in a dynamic test with an amplitude of 6.3 mm and a frequency of 0.06 Hz. The stiffness declined from 7 to 5 GPa at the point of failure. The strain in this panel showed two significant jumps firstly to 200 με, again at a low frequency and then the final jump to 350 με. This panel was tested with a time of 90 seconds. These results show a panel degrading at a slower rate than the remaining panels and failing in a static test. These results are also considered atypical.

The remaining results show a clear trend in the data at 0 με, 200 με, and 400 με. The 200 με mark appears to point to the initiation of the development of the cracking in the panel. The 400 με mark represents failure of the panel with the creation of two manifolds. The theory of elasticity pertaining to a manifold fails at this point of cracking.

5.5 SUMMARY

The experimental test rig has been used to quantify the damage to a series of masonry test panels. This chapter has presented the statistical background for the test methods, details of the failure pattern, analysis of the results, statistical study results, and the damage parameterization.

The results show that even at reasonably low values of strain the masonry was degrading. The results for the measured stiffness were analysed using a linear regression and discrete fast Fourier transform technique. The results show that the discontinuities in the stiffness visible in the measured stiffness results were related in a one to one correspondence to the applied loading pattern. The results confirmed the stiffness theory presented in Appendix B. The effective stiffness can be recovered from the measured stiffness using a quasi-static frequency limit of 0.3 - 0.4 Hz.

The typical results of the linear regression analysis of the measured stiffness presented in Figure 71[293] demonstrate why the measured stiffness has the form shown in Figure 32.[294] The effective stiffness does not significantly degrade over a short period for low strain rate, but the energy of the forcing function was absorbed in the damping and the mass terms. This introduces a circular frequency into the stress and strain data that at higher frequencies limits the ability of the linear regression technique to recover the actual effective stiffness. This problem was caused by our test method. The results however are identical in concept to those of Baker. A higher apparent dynamic stiffness exists, which can be attributed to the stress wave loading postulated by some researchers or in essence we err in using the term dynamic stiffness therefore over simplifying the conceptual background to Newton's differential equation of motion. We suggest that Baker provided the first observation of the dynamic stiffness and correctly implied that it was strain rate dependent as shown in equation (28).[295]

The results indicate that a minimum value of 0.2 MPa as a characteristic strength was achievable with the bricks. There was no evidence to support a change in this value as the minimum adopted flexural strength value for AS 3700 *Masonry Structures*. The results do point to a problem with masonry that was poorly constructed, which in the case of this experimental work was quite clearly identified as having a characteristic flexural strength less than 0.2 MPa.

[293] Refer pg. 224.
[294] Refer pg. 132.
[295] Refer pg. 134.

Chapter 6 Progressive Degradation Study of Masonry Shear Walls

6.1 INTRODUCTION

This chapter presents the findings of the research on the progressive degradation of masonry shear walls. The progressive degradation has been investigated for the time dependent in plane loading of the shear walls. Post earthquake reconnaissance surveys have shown that masonry shear walls can degrade, crack, rock, slide, and collapse when these walls have been subjected to some forms of dynamic loading. The degradation of the shear walls reduces the stiffness of the masonry elements and affects the ability of the structure to withstand additional cyclic loading. This research has investigated the degradation of the masonry shear walls up to the point of cracking. The elements of rocking, sliding, and collapse are not part of the study. Dynamic loading arises from a variety of sources. The interest in this research lies in the seismic range of amplitudes and frequencies. This set of frequencies is typically within the range of 0 to 10 Hz. The amplitudes and frequencies have been varied systematically to investigate the properties of the degrading material as the amplitude increases and the frequencies follow a preset pattern. The experimental work was designed to use an in plane static non proportional compression stress and a harmonic shear stress which was applied to a panel of masonry constructed from pressed bricks and a [1:1:6] cement: lime: sand mortar.

This review presents a discussion of the progressive degradation of the masonry panels based on the data measured from the in plane testing of the panels and the analysis of the results. The broad aims of the research work and the derived principal objectives are reviewed in the section 6.6 which relates the discussion on the progressive degradation to the aims and objectives. The critical factors influencing the degradation of the stiffness are identified and discussed, and the practical relevance of the results are described using the FEMA 273 *NEHRP Guidelines for the Seismic Rehabilitation of Buildings* (1997) as a starting point.

6.2 PROBLEM AIMS AND METHODS

Masonry is a general brittle material that is poorly defined using plastic concepts. Ceramic materials, which include pressed masonry shear walls, have an observationally documented distinct static stiffness and distinct dynamic stiffness. The literature survey has shown that a number of alternative definitions and equations have been postulated

and experimentally encapsulated to account for the two observed material strengths. The two material strengths have been observed to be dependent on the frequency and the rate of loading. Irrespective of the observations, the properties of the materials such as masonry must be understood in terms of the fundamental principles of elasticity, dynamic motion and the field of damage mechanics. A low strain rate loading test on masonry that was monotonically increasing in force to failure shows a linear relationship between the stress tensor and the strain tensor (Nichols and Totoev, 1997a).

This research on the degradation of masonry shear walls was based on the assumptions of Hooke's law, using an orthotropic model. The orthotropic model, whilst being a continuum, provided a simple method to account for the differing Young's moduli that were established as normal and parallel to the bed joint. The model retained the shear modulus as a linear equation. The level of orthotropicity was mild and the results can be expressed as isotropic for design purposes.

Newton's second law established the defining differential equation of motion. The analysis focused on the change in the stiffness of the material as it was loading under varying harmonic conditions. Krajcinovic (1996) presented the theory of damage mechanics for a general brittle material. The damage parameter was introduced to provide an internal state variable that represented the accumulation of damage in the sample. The change in the effective stiffness against strain has traditionally been used as the determinant of the damage model.

The experimental study presented in this thesis undertook to establish an estimate of the damage parameter for a masonry shear wall that was subjected to harmonic loads. The broad research aims are:

I. To explain and confirm the various experimental observations of the effective and dynamic (or measured) stiffness.
II. To investigate the mathematics of the differential equation of motion of the system to satisfactorily explain the various observed stiffness operators.
III. To provide a set of numerical values for the damage parameterization that is related to the total strain in a specimen for the loading pattern.

The principal objectives are documented in 0. The experimental determination of the damage parameter was the first stage of the research. The damage parameter curve is only a mathematical entity that has to be related to the design methods used in the real engineering world of economic, legal, and political constraints. The transition for the

effective stiffness measurements from a theoretical physics result to an engineering design curve has been presented in this chapter. The engineering curve can be used for the seismic design of masonry structures. The experimental methods are presented in Chapter 4. The results are presented in Chapter 5. This section provides a summary of the elements of the experimental methods, presents the results for the measured stiffness in terms of the mathematics presented in the previous section, and relates these results to the effective stiffness.

6.3 THE CONCEPT OF EFFECTIVE AND MEASURED STIFFNESS

Damage mechanics is used to study the process of the degradation of masonry. This study of the degrading stiffness properties of masonry panels subjected to harmonic loads was based on a primitive assumption that an elastic stiffness constant forms an upper bound to an equivalent effective stiffness and that the effective stiffness essentially monotonically decreases with loading (Krajcinovic, 1996). The fundamental definition of the stiffness, k^2, from the physical sciences has only the displacement term as a component. The effective stiffness, $k^2(t)$, in damage mechanics implicitly carries a time - strain component. The differential equation of motion based on the concept of an effective stiffness that varies with time is:

$$m\frac{d^2x(t)}{dt^2} + h\frac{dx(t)}{dt} + k^2(t)x(t) = F_0 + F_i(t) \tag{30}$$

The analysis completed by Benedetti and Pezzoli (1996) succinctly demonstrates the alternative definitions that can be provided for the effective stiffness. The Italian research is summarized in Appendix B and Chapter 2. The differential equation can be transformed using a change of axes to eliminate the constant force term, by assuming that the forcing function is strictly harmonic with a constant amplitude, and by making the assumption of zero damping. As a practical starting point, this reduces equation (30) to:

$$(k^2(t) - mw^2)x(t) = A\sin(wt) \tag{31}$$

A further simplification using equations (54) and (66)[296] reduces equation (31) to the form:

$$F_i(t) = l^2(t)x(t) \tag{32}$$

[296] These equations are not repeated here for simplicity. Refer pg. 240 for details of the equations.

Where $l^2(t)$ is defined as the measured stiffness that has the displacement, velocity, and acceleration as linearly independent components, and has the frequency term present in the forcing function. The inequality derived from equation (31) holds for the seismic range of frequencies:

(33) $$k^2(t) \neq l^2(t)$$

Equation (33) demonstrates that two operators are determinable from the defining differential equation. The two operators are nominally termed stiffness, however this is only a practical name for the $l^2(t)$ term and is provided purely to retain compliance with the existing engineering literature. Thus, the effective stiffness is represented by $k^2(t)$ and the measured stiffness is represented by $l^2(t)$ based on the assumptions used in the theoretical derivation presented in Appendix B.

The derivation of the effective stiffness and the measured stiffness had a number of theoretical constraints on the damping and the amplitude. The use of non zero damping does not change the form of equation (33) because of the limits to and the value for the damping terms are constrained by the principles of entropy and the phase lag. The increasing change in frequency will affect the size of the mass and damping terms proportionally greater than the effective stiffness terms. The practical result is that equation (33) is valid for all harmonic loading cases. The last theoretical aspect is that a Fourier decomposition of a cyclic wave pattern will derive harmonic wave patterns, thus equation (33) will hold for each Fourier wave and thus for the summation of the waves. There are limitations, but the restrictions to a seismic range of frequencies provide practical constraints that remain within the reasonable Fourier definition range.

The impact of the inequality shown in equation (33) is to introduce a piecewise continuous form to the measured stiffness which will not have a continuous first derivative. This matter is demonstrated with an abrupt step in the frequency at low loading levels. This is an essential feature of the measured stiffness, which is evident at a change in frequency. Hence this step, introduces as a minimum, a discontinuity in the first derivative. This step occurs without a break in the manifold, only requiring a change in the frequency of the testing. This result implies that the first derivative of the measured stiffness may not exist between all data points.

The definition of the effective stiffness is predicated on the mathematical concept of a manifold. The first derivative of the function is assumed to exist, as the function within

reasonable limits is smooth. The breaking of the manifold, which is evident with the cracking of the masonry panel, negates the boundary conditions required for the solution of the differential equation to be applicable. This breaking of the manifold provides the practical limit to the measurement of the effective stiffness. It also demonstrates that the measured stiffness is not a true effective stiffness. The problem of crack sliding under these broken manifold conditions has been outlined in Krajcinovic (1996, 374 - 379). This aspect was not investigated in this research.

The measured stiffness has been shown to approach the effective stiffness as the frequency of the loading function approaches zero. This theoretical limit was estimated assuming zero damping and a 1 % systematic error as being acceptable between the measured stiffness and the effective stiffness. The theoretical limit for the cut off for a quasi-static frequency was established as 0.8 Hz. A pragmatic frequency cut off limit based on damping evident in the test data is 0.3 to 0.4 Hz. This result was seen in the measured stiffness data shown in Figure 54.

6.4 SUMMARY OF THE STIFFNESS RESULTS

6.4.1 INTRODUCTION

This section presents details of the estimation of the effective stiffness and the damage parameterization based on these experimental results for the measured stiffness and from the mathematical analysis presented in Chapter 3 and Chapter 5. The engineering curve that will be used in seismic design can be derived from this effective stiffness and damage parameter data. The transition from orthotropic effective stiffness experimental data to an isotropic engineering design curve requires the application of engineering judgement. This judgement is applied when determining the appropriate model for encapsulating the change in the effective stiffness with increasing strain level.

6.4.2 MEASURED SHEAR STIFFNESS RESULTS

The critical results for the measured shear stiffness have been presented in Chapter 5. The measured shear stiffness has a frequency dependence that was shown with Fast Fourier transform for Panel AP: 6 and analysis of the residuals for the linear regression to be directly related to the loading pattern. The measured stiffness results for single frequency testing on Panel AP: 3 are shown in Figure 35.

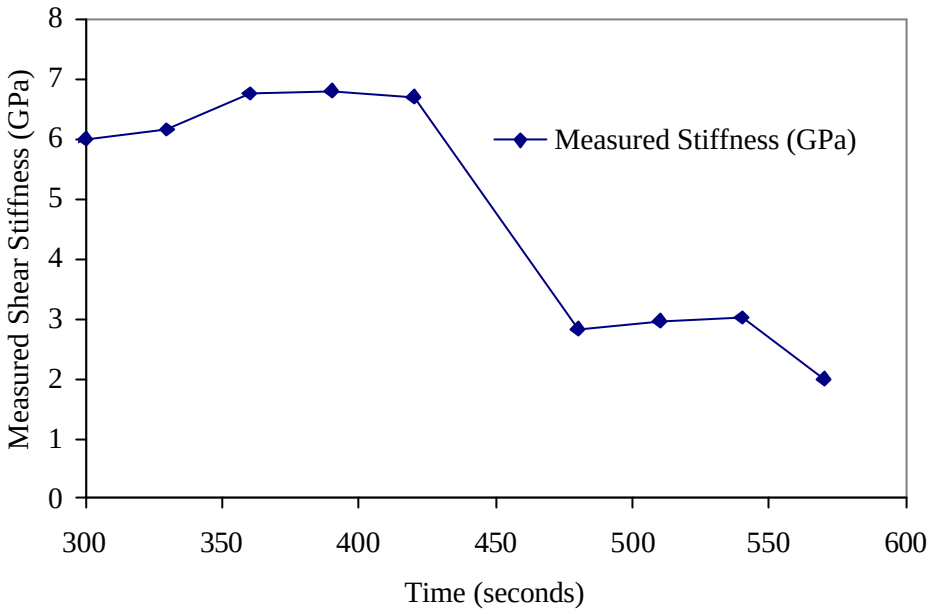

FIGURE 35 TYPICAL MEASURED SHEAR STIFFNESS RESULTS

6.4.3 EFFECTIVE SHEAR STIFFNESS RESULTS

These results for the eight panels are presented in Appendix A.[297] The effective shear stiffness was established from the measured stiffness data points using points with a frequency of forcing function that was less than 0.4 Hz. A typical set of results and the error in the results for panel AP: 7 is shown in Table 35.

TABLE 35 TYPICAL SET OF RESULTS EFFECTIVE SHEAR STIFFNESS

Strain (με)	Effective Shear Stiffness (GPa)	Standard Deviation in the Effective Shear Stiffness
30	8.466	0.261
60	7.172	0.269
75	6.694	0.056
100	6.237	0.088
150	4.929	0.250
200	4.064	0.325
400	2.83	NA[298]

The results show the degrading value of the effective stiffness with increasing strain levels.

[297] Refer pg. 177.
[298] Insufficient tests are available to compute a statistically significant value.

6.4.4 PSEUDO DYNAMIC TESTING

The use of a testing protocol that replicates the dynamic application of a force system applying the load at a quasi-static rate has been termed a pseudo dynamic test. The advantages of this type of test include the cost of the test, the number of specimens that can be repeated quickly, and the ability to compare results between different laboratories. The work of Paulson and Abrams (1990) was typical of this method. The static force system however, is not equivalent to an equivalent dynamic force, because of the application of the acceleration and the velocity terms with increased frequency of loading. The use of the energy equation is limited by the losses in the damping and the damage in the material. This is a problem with this test rig as it lacks stiffness in the surrounding frame.

Panel AP: 5 was tested in the equivalent of a pseudo dynamic test. The limited conclusion that can be drawn from this set of results and the observations on the low frequency tests is that the pseudo dynamic test creating a tensile failure provides an estimate of the degradation of the structure. There is insufficient information to confirm that the results for the damage parameter will be consistently lower than the typical dynamic test values seen for Panel AP: 5. This problem could be studied with a small dynamic test rig. The rig could use cored samples of masonry, such as Sugo (2000) used for his tests. The results for the measured stiffness as the frequency was systematically increased at constant amplitude demonstrated the difference between static and dynamic response of a ceramic masonry panel. This confirms previous experimental observations starting with Baker (1912) that the dynamic response is different from the static response.

6.4.5 COMMENTS

The effective stiffness data for the eight panels was determined from the measured stiffness data. The difference in response between a dynamic application of the load and a static load application has been shown with the test protocol to exist and be explainable in terms of Newtonian physics. The earlier observations for pseudo dynamic testing are confirmed.

6.5 DAMAGE PARAMETERIZATION

6.5.1 INTRODUCTION

The results of the damage parameterization can be used for engineering design purposes to quantify the change in the effective stiffness in masonry subjected to applied strains. This section presents the analysis and the results for the damage parameterization.

6.5.2 THE ELASTIC CONSTANTS

The basic theory of damage parameterization assumes that the elastic constants are intrinsic invariant numbers. The results for prism tests for Young's modulus are presented in Appendix G. The results for the determination of the Poisson's ratio for this style of brick are presented in Nichols and Totoev (1997a).

The shear modulus was estimated using the standard isotropic relation between the shear modulus and Young's modulus. The typical isotropic design values established for this pressed clay masonry from the prism results and the panel test results are shown in Table 36. The sources of the test data are provided with the results.

TABLE 36 TYPICAL ISOTROPIC ELASTIC CONSTANTS

Elastic Constant	Units	Range of numerical values from panel tests	Numerical values from prism tests	Reference for prism tests
Young's modulus	GPa	16 – 20	15.7 ± 3.2	Appendix G.4
Shear modulus	GPa	7 – 8	6.0 ± 1.5	$G = \frac{(1 - u)}{2} E$
Poisson's ratio		0.2 – 0.3	0.22 - 0.29	Nichols and Totoev (1997a)

The results for the elastic constants are considered to represent masonry of a similar standard of construction. These results demonstrate that the static test results can be used as a starting point for the determination of the degradation of the effective stiffness with strain or time of loading.

6.5.3 DAMAGE PARAMETERIZATION

Krajcinovic (1996, 457, equation 4.4.2) establishes the definition for the damage parameter. The parameter, D, is related to the effective shear stiffness, $\overline{E}$, by equation (34).

$$D = 1 - \frac{\overline{E}}{E}, \qquad 0 \le D \le 1 \tag{34}$$

The critical damage parameter, D_c, is defined at the break of the manifold structure. This point, D_c, represents the cracking of the masonry panel into two separate pieces. The damage parameterization results for the eight panels are shown in Figure 36.

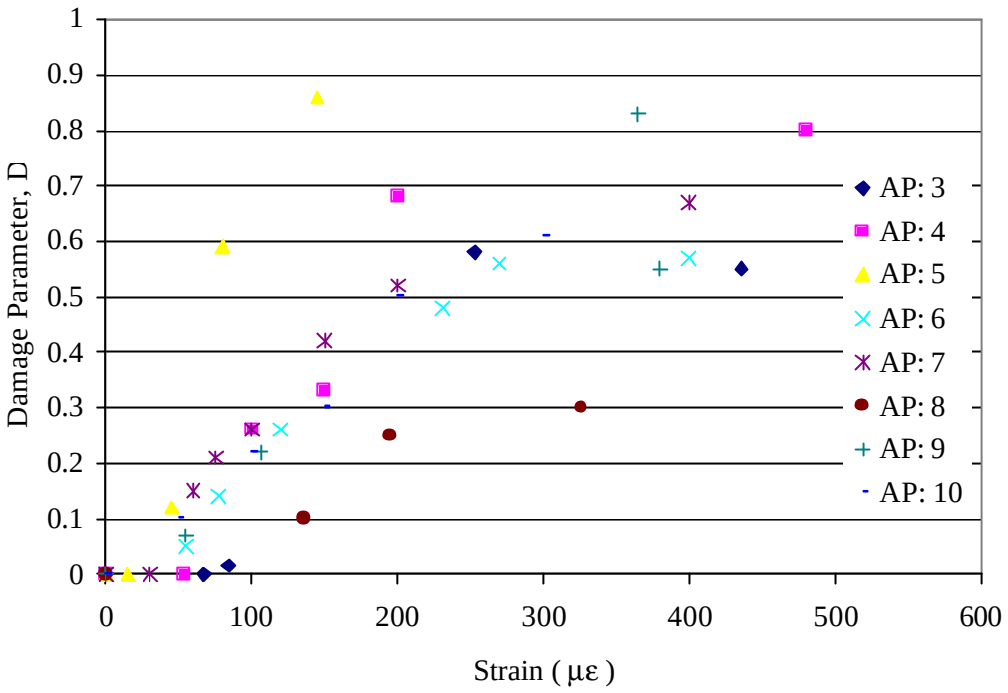

FIGURE 36 DAMAGE PARAMETERIZATION RESULTS FOR THE CLAY MASONRY PANELS

Comments were provided in section 5.4.3[299] on the two outlying curves for Panels AP: 5 and AP: 8 which failed in a static tests and a low frequency dynamic test, respectively. The trend in the data is evident in Figure 36. A linear regression analysis provided a straight line fit to the data. These results are shown on Figure 33.[300] The regression equation has an intercept of zero and a slope of 0.0018. The regression coefficient is 0.5787. This error level is acceptable given the scatter in the data points.

There is sufficient information in the results for the damage parameterization to provide a review of the alternative models that are available to encapsulate the data. The three models are all linear, with the first a standard regression, the second bi-linear, and the third tri-linear. The estimated critical points for the three models for the damage parameterization are presented in Table 37.

[299] Refer pg. 134.
[300] Refer pg. 135.

TABLE 37 TYPICAL MODEL VALUES FOR THE DAMAGE PARAMETER

Strain Level (με)	Linear Model	Bi-linear Model	Tri-linear Model
0	0.0	0.0	0.0
25	0.045	0.0	0.0
200	0.36	0.33	0.5
400	0.72	0.7	0.7

The essential differences in the models relate to the zero point and the value of the damage parameter at a strain level of 200 με. The linear model offers computational speed, whereas the bi-linear model underestimates the typical range of the damage parameter at 200 με. The 200 με level appears to be the critical level at which cracking is initiated in the manifold. The complete breaking of the manifold occurs at 400 με. The theory of a single manifold breaks down at 400 με. The tri-linear and linear models are shown in Figure 37. The additional damage parameter term, D_{ci}, has been introduced to identify the onset of cracking in the manifold.

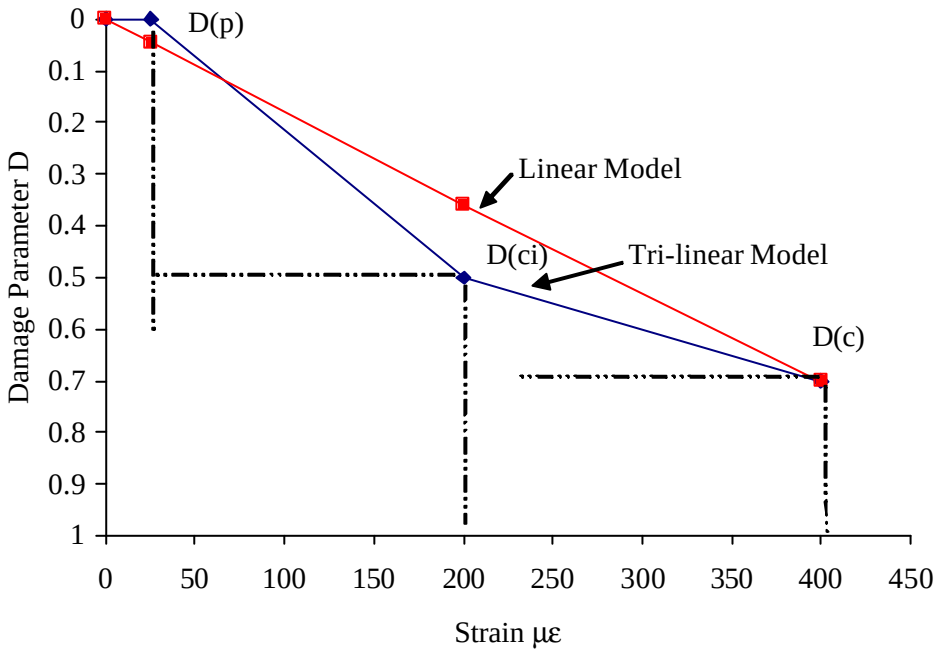

FIGURE 37 DAMAGE PARAMETERIZATION MODELS FOR PRESSED CLAY MASONRY

6.5.4 SUMMARY

This section of the research determined the damage parameterization for the pressed clay masonry panels. The results demonstrate the loss of stiffness in the masonry when it is subjected to increasing cyclic loading generating a slowly increasing peak tensile

principal stress. Three potential design curves have been established from the results. The linear curve is computationally faster to implement, but not as close to the mean results curve which is better represented by the tri-linear form. The tri-linear results are recommended values for design purposes.

6.6 REVIEW OF THE RESEARCH OUTCOMES

6.6.1 INTRODUCTION

The principal objectives of the study have been presented in 0. The key findings of the research have been presented in this chapter. These key findings relate to the determination of the progressive degradation of masonry shear walls subjected to harmonic loads. The central facit of the findings is presented in Figure 36.[301] This section provides a brief review of the principal objectives and relates these objectives to the research outcomes. The original research outcomes, which are relevant to the research objectives, were the experimental outcomes and the analytical outcomes.

6.6.2 EXPERIMENTAL OUTCOMES

The first objective was to investigate the dynamic properties of shear walls constructed from a single wythe of pressed clay masonry. The experimental study has addressed the properties of pressed masonry constructed in a 1.2 metre square panel. The dynamic properties were investigated within the seismic range of frequencies. The second objective was to determine the appropriate form for the development of a loading pattern to be used in the experimental work. This form of the loading pattern was established from a finite element analysis of two storey and seven storey masonry structures analysed using a range of earthquake traces. The forcing function pattern applied with the ITM to the masonry panels was based on the estimated loading at the shear wall element and not for the free field acceleration. The third objective was to design and construct a test rig to support the experimental work. The detailed design and procedures for the test rig and the program are presented in the appendices. The *major experimental objective* was to observe the change in properties of shear walls subjected to specific loading and boundary conditions. The measured stress field and strain field were determined and recorded for a series of masonry panels. The stress field was determined from the forcing function at the ITM. The strain field was determined across a uniformly strained section of the masonry panel. The loading pattern was systematically varied to investigate different aspects of the measured stiffness. The purpose was to provide sufficient data for

[301] Refer pg. 146.

the statistical analysis for the effective stiffness and to demonstrate that the hypotheses were supported by the experimental results. As for all Newtonian physics, the observation data supports the use of Hooke's law within the field of damage mechanics, however the normal limitations of the Newtonian physics of real materials apply to these results. Three hypotheses were proposed in Appendix B that relates the measured stiffness to the effective stiffness. The experimental data, the observed failure mechanism, and the analysis of the results confirm that the:

I. Three hypotheses are reasonable for pressed masonry.
II. Measured stiffness corresponds to the dynamic strength concepts presented in Chapter 2.
III. Effective stiffness can be established from the measured stiffness under some limiting conditions.
IV. Equation $k^2(t) \equiv l^2(t)$ holds for the seismic range of frequencies.
V. Measured stiffness has frequency dependence.
VI. Effective stiffness, $k^2(t)$, is a monotonically decreasing function dependent on the strain level and not the frequency of loading and constrained thermodynamically by $\dot{D} > 0$.

The results of the analysis of the measured stiffness are presented in Chapter 4 and Chapter 5.

6.6.3 ANALYTICAL OUTCOMES

The Fast Fourier transform method was used to investigate the measured stiffness of the masonry panels. The use of Fast Fourier transforms showed that the measured stiffness was controlled by the frequency element of the loading pattern. The FFT results identified the conditions of loading in terms of amplitude and frequency that yielded the experimentally observed static stiffness and the dynamic stiffness. The mathematical constraint was identified in Appendix B between the measured stiffness, $l^2(t)$, and the effective stiffness, $k^2(t)$, as:

$$k^2(t) \equiv l^2(t). \tag{35}$$

The effective stiffness could be recovered from the measured stiffness for some test conditions. The critical test condition to recover the effective stiffness was with a frequency of loading less than 0.3 to 0.4 Hz. This frequency, Υ, defines the effective

quasi-static limit of loading. The time domain degradation of the effective stiffness was determined from the measured stiffness and used to encapsulate the damage parameter and determine the critical damage level.

6.7 SPECIFIC APPLICATION OF THE RESULTS

6.7.1 INTRODUCTION

Masonry is a material with high compressive strength, but inferior tensile strength. These properties and the failure surface formed for pressed clay masonry were documented by Page (1979). The research on clay masonry panels subjected to a harmonic shear stress represents a direct extension of the work by Page and others in the last three decades. The properties of masonry at serviceability and strength limits have been investigated in a systematic manner for the static and the dynamic loading condition. Within this broad area of research interest, the critical aspects of the research can be discussed from both a current and a future perspective. These areas are divided into the general fields of research interest, analysis, and specific applications. This purpose is to identify the critical aspects and factors from this theoretical research and to discuss the use of the results in terms of existing and future engineering methods, standards, and problems, and to provide examples of the practical relevance of the results. A review of the standard properties of the pressed masonry, the use for the isotropic model and the structured continuum, the place of future damping research, the explanation for and uses of the measured stiffness, and crack analysis and propagation are discussed in this section. Section 6.8 uses the FEMA 273 (1997) manual to illustrate the application of the results presented in this section for the further development of standards and codes.

6.7.2 THE STANDARD PROPERTIES OF THE PRESSED CLAY MASONRY

Masonry as a research and a construction material has the problem of variability within what is nominally a common sample population. The best illustration of this problem from the research on the clay masonry was the statistically significant difference in prism strengths between the specimens constructed on day 245 and 246. The Student's t test results indicate that the two samples vary and that the variation is significant at the 5 percent confidence interval. The equivalent stress results for day 245 and 246 are a mean compressive stress of 25 ± 5 MPa and 13 ± 3 MPa respectively. The differences between the results for days 245 and 246 for prisms made from the one pallet of bricks and a standard mix are attributed to the prewetting of the bricks at the end of day 245, by the bricklayer. The purpose for the prewetting given by the bricklayer was to improve the bond on the high IRA bricks, which was measured by Sugo (2000) as 5.3 kg/min/m^2. The

second indicator test used for masonry quality control is the bond wrench test (AS 3700). The statistical results for the bond wrench data are presented for the prisms manufactured on the five construction days in Table 38.

TABLE 38 FLEXURAL STRENGTH STATISTICAL RESULTS

Description	Units	Day 245	Day 246	Day 329	Day 331	Day 77
Mean Flexural Strength:	MPa	0.85	0.29	0.37	0.62	0.42
Standard Deviation:	MPa	0.16	0.06	0.11	0.11	0.07
Coefficient of Variation:	%	19	20	29	18	16
Characteristic Strength Factor K:		0.83	0.82	0.75	0.84	0.85
Characteristic Flexural Strength:	MPa	0.51	0.16	0.17	0.44	0.20

A Student's t test showed that the bond strength results are statistically different at the 5 % significance level for day 245 and day 246 samples. The results highlight the issue of using a brick with a high IRA, the care needed in the production of the mortar, and care in the construction method. The weaker specimens constructed on day 246 and 329 typically failed during the placement before testing. A minimum required bond strength of 0.2 MPa as per AS 3700 is considered reasonable and is supported by this research. It is achievable with a moderate level of quality control, typically by batching the samples and testing the mason. Pressed clay is a general brittle material that will always suffer from the common sample problem. The results demonstrate that a pressed brick even with a high IRA can achieve a reasonable bond level. The practice of prewetting these types of bricks is not supported by the findings of this study. The dynamic test procedure provided an excellent repeatability on the measurement of the effective stiffness results for a single panel.

6.7.3 ISOTROPIC MODEL AND THE STRUCTURED CONTINUUM

The assumption of an orthotropic model for the experimental analysis of the data provides a level of complexity that is consistent with the highly structured and mildly orthotropic continuum of masonry. The complexity introduced in the Young's' moduli and Poisson's ratios was negated by the shear modulus remaining linear in the model. The mildly orthotropic model is simply too intractable and unsuitable for use in a design setting. An isotropic model was used for providing design data. These results for the elastic constants for the pressed clay masonry are presented in Table 36.[302] The error present in the masonry results for the panels such as the shear modulus is approximately ±25 %. This error is consistent with other recent masonry tests, and reflects the natural material

[302] Refer pg. 145.

variations and not the ability of the measurement equipment to take and record readings to the order of 2 %. The material has been analysed assuming a continuum with uniform strains developed in the central measurement section of the masonry. These results should be used with care with models that do not have this level of homogenization. The strain levels at the mortar strip were not measured in these experiments.

6.7.4 THE PLACE OF FUTURE DAMPING RESEARCH

A future research effort will focus on the analysis of the damping data within the current data files. The observation that the term, $h\frac{dx}{dt}$, has a frequency component in the velocity, and the simple observations of the steps in the measured stiffness at constant test regimes suggests that the damping term, h, has potential frequency dependence. A second area of future work will be to determine the bounds for the damping and whether a reduction in the effective stiffness affects the damping term. The feature of this research would be to provide explicit bounds for damping and to determine if there is a variation in the damping with strain level. No specific recommendations have been determined for the damping parameter from this current research.

6.7.5 CRACK ANALYSIS AND PROPAGATION

The last four decades has witnessed the development of the field of damage and fracture mechanics. These fields of research investigate the changing intrinsic properties of materials. This masonry research on masonry panels subjected to harmonic shear stress provides data for code development in both the finite and the boundary element fields. This damage parameter data provides information to allow the automatic calculation of the cracking behaviour and the adjustment of the topological features of models without human intervention. This represents a critical future feature in the use and development of these modelling techniques. The research has demonstrated for the pressed clay masonry that there is a variation in the damage parameter with strain. The levels are moot for research purposes; the critical aspect is that this data provides a direct functional link between the stress and strain for the damaged model of pressed masonry. This type of model provides the mathematical framework to encode the damage model into finite element models. The feature of this type of research is that the encoded material would allow an automatic crack propagation algorithm. Whilst this is a topologically difficult task, it would extend the work on boundary element crack propagation commenced by van Vroonhoven (1996). The proposed method would use a finite element or boundary element program to track the first principal tensile strain levels for each element. The tracking of the level of tensile strain would need to occur in the time domain assuming

that small enough time steps can be applied. The tensile strain levels are computed and the effective stiffness determined from an encapsulated version of Figure 37.[303] The areas of the mesh that have a reduced effective stiffness or that have theoretically cracked can be determined for the strain results. The elemental mesh for the damaged elements can then be subdivided using standard procedures (Abbo and Sloan, 1996; Muniruzzaman, 1997; Page, 1979; Sudhakar, Powell, Orr, and Wheaton, 1972; van Vroonhoven, 1996).

The feature of this work is that at some future time a FE or BE model of a building can be constructed subjected to known earthquakes, and the patterns of damage can be verified. This is of fundamental importance in determining the residual strength of buildings that will become of increasing importance as the risk levels are adjusted for earthquake losses in the twenty-first century. The difficulty from the point of view of the practicing structural engineer is the computational expense of this type of procedure unless it is available as a specific element in the finite or boundary element program. The calibration of this type of program is straightforward with the analysis of shear walls. The walls, if subjected to a slowing increasing in plane harmonic shear loading, will crack in the classic cross pattern observed in experimental research (Paulson, and Abrams, 1990). Other failure modes could be included in the analysis. As a final note, a linear variation assuming that D_p has a maximum value of zero would be reasonable as a first approximation, however a higher order model such as tri-linear will provide a sounder approximation for the damage parameter at the 200 με level. This method confirms the assumption made in the design of masonry structures that a reduction of the Young's modulus by at least one half occurs with loading (Kariotis, personal communication, June 1999).

6.8 APPLICATION TO STANDARDS AND CODES

6.8.1 INTRODUCTION

This section on the application to standard and codes shows how these experimental and analytical results may be used in the development of future standards and codes. This section takes a broad perspective to highlight the potential uses of this and any future research using FEMA 273 as a sample code.

The world has vast areas of masonry dwellings. This is not likely to change in the near future. Masonry buildings can range in age from the two millennium of the Scottish

[303] Refer pg. 147.

Broach to the recent subdivisions in the Newcastle region of Australia. The future of buildings within this broad range is interesting to consider. The short lifespan of timber and steel and concrete buildings in some regions must not illogically constrain the reality of the lifetime of masonry structures. Heyman (1996) discusses the life stages in detail. This is extended in the recent FEMA 273 manual (1997) to consider the design assumptions for a building. This set of assumptions can range from that of life safety to operational soundness after an environmental event. The research on shear wall degradation is tied to the design and performance of buildings under seismic loads. The application of the research findings from the preceding section is now placed in the context of use by practicing structural engineers and the masonry research community. The first area of practical engineering application and interest is in the level of strain damage and the problem of frequency matching of a loading to the natural frequencies of the building. This review area provides an extension of the theoretical application of the crack analysis and propagation methods to analysis of real world buildings. The second area is in the development of fragility curves for buildings. A fragility curve relates the probable damage in a structure to a given level of ground shaking. One use of fragility curves is to assess the losses after earthquake events and to determine the cost effective methods of mitigation before earthquake events. The development of fragility curves was based traditionally on the observation of building damage after previous earthquake events and from some simple methods of finite element analysis. This review will discuss the use of the damage parameter data in refining the existing fragility curves for masonry structures. The third area is in the development of the FEMA 273 manual (1997). This presentation forms a starting point for demonstrating the practical relevance of the results. FEMA 273 was selected, as it is important in the development of design standards for seismic design and retrofitting. This intermediate standard will evolve during the formal code process. The revisions to establish code constraints and deemed to comply rules will provide safeguards and limits to the engineering and general community.

6.8.2 STRAIN DAMAGE AND FREQUENCY MATCHING

Strain damage is relevant to assessment of damaged structures, particularly for seismic events where the natural frequency of the structure and ground block matches the seismic trace. Frequency matching is considered to present a significant problem that has been observed in earthquakes such as Mexico in 1985 discussed in Chapter 2. There is an age old observation with masonry related to the similar buildings standing side by side, one fails in the seismic event and the other appears to be unharmed. The repeated damage evident in ancient Mediterranean and Indian structures that fail in one place, the damage repaired, and then the failure was repeated in the same place in a second event represents

an analogous mode. The presumption that a seismic loading on a building can be reduced to an equivalent static load is an interesting assumption that unfortunately fails under some, but not all circumstances. The results with failure are often catastrophic and fatal to the residents.

This experimental study has investigated the effect of frequency on the change in the effective stiffness. There is no direct evidence that an increased frequency changes the effective stiffness. The effective stiffness is dependent only on the peak value of the first principal strain. However, the problem of frequency matching between the seismic trace and the building that results in a tuned building means that resonant peaks of strain will results in a rapid degrading of the effective stiffness. The detuned buildings with significantly lower strain levels are not damaged to the same extent. This is an indirect frequency impact that will become of increasing importance in retrofitting masonry structures and in attempting to deliberately detune new structures to the surrounding ground. The damage parameter determined for the pressed clay masonry can be used in an analysis that explicitly considers the impact of tuning of the structure. The development of synthetic traces that can test buildings close to their natural frequency is an area of future research potential. The effective stiffness results can be applied directly with this type of analysis. The philosophical design issues of using synthetic traces and the level of sophistication required in the use of finite element analysis means that the application of this technique will remain in the laboratory for the moment, except for a few specialized engineering design groups. The observations were made by Jacob's (1997) that multiple traces should be used to investigate a range of solutions and the designer seeks an appropriate solution given the building constraints.

The economical design, retrofit, and construction require provision of pragmatic design details that improve the seismic behaviour of masonry buildings. This research provides a component by allowing for the estimation of realistic force levels and being able ultimately to determine a cracking pattern for a building. Normal delay must of course be allowed for in the implementation in this process.

6.8.3 DAMAGE PARAMETER AND FRAGILITY CURVES

Fragility curves attempt to quantify the probability that a structure or group of structures will be damaged in an earthquake event of given magnitude and location. The development of the damage parameter provides an additional means of quantifying the degradation of shear walls and determining the impact on the overall structural capacity. The application of the damage mechanic in the development of theoretical fragility curves

provides the next evolution relating the modelled structures to the reality of fragility curve development after an earthquake. This is an important step in developing fragility curves for areas such as New Madrid that have been seismically quiet for long periods. Determining the building components that cause high damage level or fatalities is critical.

6.8.4 APPLICATION TO THE FEMA 273 MANUAL

FEMA 273 (1997) provides an estimate of the Young's modulus as a multiple of the characteristic compressive strength or by using a standard stress strain plot to estimate the secant modulus. The linear method of analysis used in the initial development of masonry codes has broadened to the use of yield line type theories (AS 3700) and the development of non linear force displacement curves based on the results of racking tests (FEMA, 1997). An assumption that the Young's modulus reduces by one half in the long term is used in some analysis situations (Kariotis, 1999, personal communication). The cracking in unreinforced masonry structures is observed to continue to grow in the months after an earthquake attributed to the effective stiffness declining with applied strain and further cracking of a structure (Nichols, 1999). The resolution of these issues with a consistent method of explaining the variations in the effective stiffness of masonry shear walls is critical to explaining the measured deformations in buildings and to determining the residual capacity of the structure. It is also critical in estimating the deformations in new structures and to estimating the likely extent of cracking and the rate of propagation of the cracking. The specific changes that can be made in the FEMA 273 manual relate to a refined estimate for the non linear force displacement curve up to the point of cracking, rocking and sliding. The study of the elements of cracking, rocking and sliding could be done with the test rig for some limited circumstances. The preferred method is to use a shear wall experimental procedure as set out in Macchi's alternatives.

6.9 SUMMARY

This chapter presents the results of the progressive study of the degradation of masonry shear walls that are subjected to harmonic shear loads. The results show that the effective stiffness degrades with increasing strain. The damage parameter, D_{ci}, for the onset of cracking, has been identified as having a value of approximately 0.5 at 200 $\mu\varepsilon$. The failure of the manifold at the damage parameter, D_c, occurs at approximately 400 $\mu\varepsilon$ with a value of 0.7.

Chapter 7 Conclusions

7.1 SYNOPSIS

This dissertation presents the experimental and analytical work; and the results and conclusions for this study of the progressive degradation of masonry shear walls subjected to harmonic shear loading. Masonry shear walls form an essential element to many building types. Masonry, as a structured continuum, has a high compressive strength and an inferior tensile strength. It is classified as a general brittle material. Shear walls that are subjected to tensile stresses that exceed the elastic capacity of the masonry can degrade, crack, rock, and slide. The tensile stress regime in buildings that causes strain damage and a reduction of the effective stiffness is typically generated by environmental loads such as seismic events.

The purpose of the research was to investigate the properties of the masonry shear walls as they degrade in a known stress field, specifically investigating the properties of pressed clay masonry panels up to the point of cracking. The shear walls were subjected to a nonproportional uniform biaxial compressive stress field and a harmonic shear stress field. The masonry panels were single wythes of 110 mm pressed clay bricks with a principal dimension of 1.2 m. The harmonic shear force had a peak value of 320 kN with a peak displacement of 12.5 mm.

This chapter presents the background and introduction to the study, outlines a summary of the results, analysis and the applications of the research findings, and presents a section on the future directions for research into the dynamic properties of masonry shear walls.

A literature review presented in Chapter 2 outlines the existing knowledge on the static and dynamic response from experimental studies of shear walls and buildings. The literature review established the constraining information and previous studies in the areas of an historical perspective, masonry practice, seismicity, masonry buildings, damage mechanics, and fracture mechanics. Experimental observation has shown a consistent difference in the static and dynamic strength of ceramics including masonry. Baker (1912) probably reported the first observation of the increased strength for the dynamic loading mechanism. This observation related to the dynamic loading of mortar samples in tension. The difference between the static and dynamic response characteristics of masonry shear walls was clearly shown by Paulson and Abrams (1990). Freund (1990) provides the mechanical explanation for the two responses based on the difference in the rate of stress wave loading.

Macchi (1982) documents the four methods available to test masonry shear walls. The four test procedures are shown on Figure 11.[304] The fourth procedure of using a masonry panel subjected to uniform bi-axial compression and harmonic shear was selected as appropriate for this research study. The test rig was designed to apply a slowly increasing shear strain to the clay brick wythe. The strain regime drives the first principal stress from compression into tension. The change in effective stiffness can be measured during each test cycle of 30 seconds to permit a numerical analysis of the change in the damage parameter, D, with strain.

In Chapter 3, the degradation of masonry was considered in terms of the previous experimental work that included observational data on analytical aspects of the dynamic properties of masonry and other materials. This information, coupled with the data from the literature review, provided the conceptual engineering background for the problem definition and the solution method. The problem definition was to investigate the dynamic properties of masonry shear walls and to explain the results in terms of the theories of mechanics and damage mechanics. The solution method established the basic form for the experimental and analytical research work. The solution method required the development of a loading pattern.

The loading pattern developed from consideration of previous patterns and an FEM analysis of two masonry structures, a 2 storey Italian house and a 7 storey Perth apartment block. Well-known earthquake traces were used in the FEM analysis considering both intraplate and interplate events. The developed pattern was based on an incrementally increasing strain, with a 90 block set of 30 sec. tests at each amplitude point. A typical 90 block set had a frequency range of single tests from 0.06 to 10 Hz in 15 block sets.

In Chapter 4, the experimental study was presented in terms of the selection and construction of the masonry panels, the design of the experimental equipment and methodology. A pressed clay masonry brick of Sydney, Australia origin was used with a [1C: 1L: 6S] mortar to construct the 1.2 metre test panels. The test rig is shown assembled in Figure 85.[305] The test rig design, hydraulic and electronic systems are detailed in the appendices. Central to the development of the experimental methodology

[304] Refer pg. 90.
[305] Refer pg. 264.

and the subsequent analysis of the results was the review of the mechanics of stiffness presented in Appendix B.[306]

It was postulated that there are two distinct mathematical entities representing the static and dynamic stiffness. The first entity is the effective stiffness, k^2, deemed the mathematical functional representation of the stiffness defined explicitly by the displacement term of the differential equation of motion for a harmonic function. This functional representation has no frequency dependence (Kaplan and Lewis, 1971, 554; Krajcinovic, 1996). The second entity is the measured stiffness, l^2, that is defined to be the experimentally determined stiffness that is obtained by dividing the stress field results by the strain field results for each recorded time step (Paulson and Abrams, 1990). The loading pattern and the experimental methodology were designed to systematically explore the statistical and physical properties of the effective and the measured stiffness. The mathematical analysis had concluded that a relationship existed between the effective and the measured stiffness where:

(36) $$k^2(t) \; ^3 \; l^2(t)$$

The fundamental primitive[307] for the field of damage mechanics is that the elastic constants are invariant maximums. There is then simple calculus of functions that will permit the recovery of the effective stiffness and the elastic constants from the measured stiffness under certain test conditions for equation (36). A critical objective was to establish these test conditions. The final result was that at a frequency of testing of less than 0.4 Hz the measured stiffness provided a sound approximation to the effective stiffness and at strains significantly less than the yield point the effective stiffness provides a lower bound estimate to the elastic constants.

In Chapter 5, the results for the testing of the masonry panels were presented in terms of the measured stiffness data from the two critical panels AP: 3 and AP: 6. The first panel, AP: 3, clearly demonstrated the degradation of the measured stiffness with time of loading and increasing strain rate. This panel was effectively tested at a constant frequency of 1 Hz. This result was shown in Figure 41.[308] The second panel, AP: 6,

[306] Refer pg. 227.
[307] A primitive represents a starting point or a known fact for a theory. One of the primitives of Newtonian physics is the observation that mass is invariant with time. This primitive does not exist in non-Newtonian physics. The primitives limit the scope of any theory.
[308] Refer pg. 183.

clearly confirmed the fundamental relationship between the effective stiffness, $k^2(t)$, and the measured stiffness, $l^2(t)$, presented in equation (36).

The first step in this demonstration was to confirm the frequency dependence for the measured stiffness that was clearly shown in Figure 54.[309] The parabolic equation between the frequency, f, (Hz) and the measured stiffness, $l^2(t)$, was established as:

(37) $$l^2(t) = 8.4 - 1.5 f + 0.086 f^2$$

The result applies to the particular loading pattern for this test set.

The three hypotheses, which are presented in Appendix B for the relationship between the effective stiffness and the measured stiffness, were confirmed for this pressed clay masonry panels that are a general brittle material. The first hypothesis was that the effective stiffness could be determined from the measured stiffness for some test conditions. This hypothesis was proven. The second hypothesis was that the dynamic stiffness did not exist as a separate unique entity. The dynamic stiffness is a concept that simplifies the analysis and presentation of results for dynamic testing. The observation that ceramic materials respond with a greater stiffness to a high strain rate or equivalently high frequency of loading is result of the form of Newton's second law and the solution method adopted for the analysis of the results, and is not a separate entity *per se*. The experimental method used a harmonic loading that means that only two of the three variables are independent in the set of wave, amplitude, frequency and strain rate. The selection of the loading pattern determined the independent variables and hence constrained the third variable. The second hypothesis was proven. Richter (1958) commented on this point related to the interdependence of the variables. The testing was within the seismic range of frequencies suggested by Richter.

The effective stiffness, $k^2(t)$, has a continuous first derivative up until the point of cracking of the manifold that had been demonstrated for other general brittle materials (Vecchio and Collins, 1986; Krajcinovic, 1996). The effect of the relationship $k^2(t) \neq l^2(t)$ can now be clearly seen in the results for panel AP: 6 shown in Figure 27[310] and in the limit as the frequency, f, approaches zero, confirming the third hypothesis.

[309] Refer pg. 202.
[310] Refer pg. 39.

In Chapter 6, the damage parameterization was established for the pressed clay masonry panels. A review was provided for the research outcomes for the experimental and analytical work. The analysis and specific application of the results were presented and then extended to examples of applications for standards and codes. This work was based on the FEMA 273 manual (1997). The design curve for the damage parameter, D, established for pressed clay masonry is presented in Figure 38. The tri-linear model is recommended for design of masonry structures subjected to a seismic strain field.

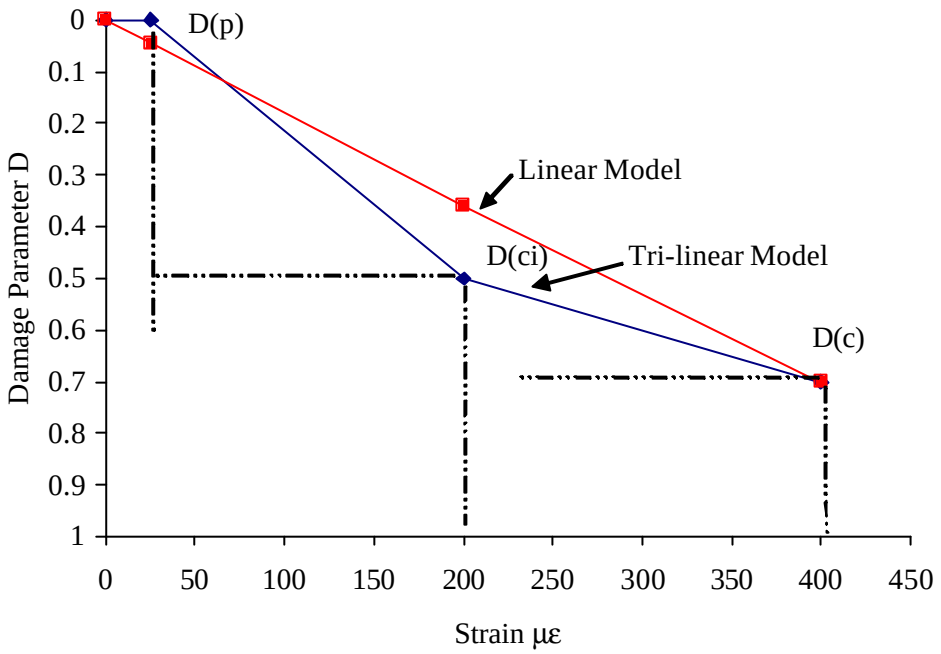

FIGURE 38 DAMAGE PARAMETER RESULTS FOR PRESSED CLAY MASONRY

The interesting observation from the experimental work was that visible cracking did not occur until a strain level of 200 με was reached. This point represents a drop in the effectives stiffness of 50 % of the elastic constants at the onset of cracking.

7.2 FINAL CONCLUSIONS

The principal conclusions are that:

I. The pressed clay masonry behaves as a general brittle material, with a damage parameter that has a critical value of approximately 0.5 at a first principal tensile strain of 200 με for the start of the cracking and a value of 0.7 at 400 με for the failure of the manifold.

II. The static elastic modulus of pressed clay masonry can be used to establish the starting point for the application of the damage parameter results established in this research.

III. The minimum characteristic strength for masonry applicable with these results is 0.2 MPa when tested in accordance with the procedures in AS 3700. The site experience shows that a bond strength less than this level provides an extremely weak masonry wall that thus fails to conform to reasonable site practice.

IV. The relationship between the effective stiffness and the measured stiffness $k^2(t) \neq l^2(t)$ and the relationship between the frequency of loading and the measured stiffness shown in equation $(37)^{311}$ demonstrate the effect of the damping and acceleration terms on the apparent strength or stiffness of a general brittle material as it is loaded at higher strain rates. This confirms the observation first made by Baker (1912) with tests on mortar samples.

V. An effective limit between quasi-static loading and dynamic loading rates can be established at a frequency Υ of 0.3 to 0.4 Hz. This applies to stroke amplitude less than 5 millimetres.

VI. For pressed masonry, a homogenized isotropic model provides a reasonable method for applying these results.

VII. Static and dynamic forces with the same peak amplitude are not equivalent loads and the principal of equivalent energy levels needs to be applied.

VIII. The results provide a source of data to develop fragility curves for masonry buildings and for considering the impact of frequency matching of buildings and seismic traces. This issue of frequency matching is a problem in larger seismic events such as the Nahanni event where the broad band of energy will still supply resonant frequencies as the building degrades and the natural frequency response changes.

IX. The use of a damage parameter method in place of the linear elastic assumptions used in codes such as the FEMA 273 manual (1997) is a reasonable design step. The analysis of simple structures usually does not warrant this level of complexity, but the introduction of the method into finite element codes for complex masonry structures is recommended.

X. Future research should investigate the damping characteristics of the panels from the data. The types of procedures developed for NLFIT by Kuczera

[311] Refer pg. 160.

(1994) would be a suitable method. The properties of extruded and repressed bricks can be investigated with the test rig.

7.3 SUMMARY

Masonry that is detailed for seismic loads and constructed to a reasonable level of quality control can withstand loads generated by seismic events (Melchers and Page, 1992; Tena-Colunga and Abrams 1992). This research work, which extends the static research of the last few decades (Page, 1979; Ganz, and Thurlimann, 1982), has concluded that the degrading properties of pressed clay masonry are consistent with the model for a general brittle material (Krajcinovic, 1996). The effective stiffness has been shown to reduce to half as the material was strained to 200 $\mu\varepsilon$, when visible cracking was evident in the pressed clay masonry panels. The experimental study used harmonic shear stresses in the normal seismic range. The strain criteria to account for the increasing damage level was found to be the first principal stress as it passed into a tensile range. The equivalence of a static and dynamic force requires consideration of the energy and momentum equations, rather than assumption that the peak amplitude of force provides an equivalent measure of damage. This finding provides an alternative formulation for the difference between the static and dynamic strengths to that provided by Freund (1990) who explained the phenomena in terms of the stress wave loading rate.

BIBLIOGRAPHY

Abbo, A.J., and Sloan, S.W., (1996), An automatic load stepping algorithm with error control, *International Journal for Numerical Methods in Engineering*, 39, 1737-1759.

Abe, K., and Yoshida, Y., (1992), Seismic response analysis of alluvial valley with dipping layers by a boundary element - finite element coupling method, *International Journal for Numerical Methods in Engineering*, 35, 1753-69.

Abercrombie, R.E., Agnew, D.C., and Wyatt, F.K., (1995), Testing a model of earthquake nucleation, *Bulletin of the Seismological Society of America*, 85, 6, 1873-8.

Abrams, D.P., (1997), Keynote address, *Earthquakes in Australian Cities*, Brisbane, IE (Australia), Paper 1.

Abrams, D.P., and Shinozuka, M., (1997), *Final Report Loss Assessment of Memphis Buildings*, Urbana: NCEER.

Abrams, D.P., Noland, J.L., and Atkinson, R.H., (1985), Response of clay unit masonry to repeated compressive force, *7th International Brick / Block Masonry Conference*, 17-20 Feb. 1985, Melbourne: UM, 1, 565-76.

Ali, S., (1987), Concentrated loads on solid masonry, Diss. 1143, U of Newcastle.

Angel, R., Abrams, D., Shapiro, D., Uzarski, J., and Webster, M., (1994), *Behavior of reinforced concrete frames with masonry infills*, Urbana: UIUC. 183.

Arnold, V.I., (1981), *Mathematical Methods of Classical Mechanics*, New York: Springer-Verlag, translated by K. Vogtmann and A. Weinstein (1981), 462.

AS 1141.11-1996/Amdt 1-1999, *Methods for sampling and testing aggregates - Particle size distribution by sieving*, Standards Australia: Sydney.

AS 1170.1-1989 (Amdt 1), Minimum design loads on structures (known as the SAA Loading Code) – Dead and live loads and load combinations, Standards Australia: Sydney.

AS 1170.2-1989 (Amdt 3), Minimum design loads on structures (known as the *SAA Loading Code*) - Wind loads, Standards Australia: Sydney.

AS 1170.4-1993/Amdt 1-1994, Minimum design loads on structures (known as the *SAA Loading Code*) - Earthquake loads, Standards Australia: Sydney.

AS 1226 (Set) *Methods of sampling and testing clay building bricks*, Standards Australia: Sydney.

AS 1250-1981/Amdt 2-1984, The use of steel in structures (known as the *SAA Steel Structures Code*) (incorporating Amdt 1), Standards Australia: Sydney (withdrawn).

AS 1672.1-1997, *Limes and limestones - Limes for building*, Standards Australia: Sydney.

AS 2758.1-1998, *Aggregates and rock for engineering purposes - Concrete aggregates*, Standards Australia: Sydney.

AS 3700-1998/Amdt 1-1999, *Masonry structures*, Standards Australia: Sydney.

AS 3972-1997, *Portland and blended cements*, Standards Australia: Sydney.

AS/NZS 4455:1997, *Masonry units and segmental pavers*, Standards Australia: Sydney.

Atkinson, G.M., and Boore, D.M., (1995), Ground motion relations for Eastern North America, *Bulletin of the Seismological Society of America*, 85, 1, 17-30.

Australian Building Code Board, (1996), *Building Code of Australia*, Canberra: CCH Australia, 2 vols. (Last amended May 5, 1999).

Baker, I.O., (1912), *Treatise on Masonry Construction*, New York: Wiley, 10th ed, 746.

Banerjee, P.K., and Butterfield, R., (1981), *Boundary Element methods in engineering science*, Maidenhead: McGraw Hill Book Co (UK) Limited.

Benedetti, D., (1997), Letter to the author, including Irpinia earthquake trace.

Benedetti, D., and Pezzoli, P., (1996) *Shaking table tests on masonry buildings - results and comments*, Milano: Politecnico di Milano.

Bent, A.L., (1994), The 1989 (M_s 6.3) Ungava, Quebec Earthquake: A complex Intraplate event, *BSSA*, 84, 4, 1075-88.

Binda, L., Gatti, G., Mangani, G., Poggi, C., and Sacchi Landriani, G., (1992), The collapse of the civic tower of Pavia - A survey of the materials and the structure, *Masonry International*, 6, 1, 11-20.

Bolotin, V.V., (1964), *The dynamic stability of elastic systems*, San Francisco: Holden-Day Inc, (translated by V.I. Weingarten, L.B. Greszczuk, K.N. Trirogoff and K.D. Gallegos).

Boore, D., (1997), Letter to the author.

Borowski, E.J., and Borwein, J.M., (1989), *Dictionary of Mathematics*, 2nd ed., Glasgow: HarperCollins Publishers.

Brigham, E.O., (1988), *The fast Fourier transform and its applications,* Englewood Cliffs: Prentice.

Brigham, E.O., (1974), *The Fast Fourier Transform,* Englewood Cliffs: Prentice. 252.

Chopra, A.K., (1995), *Dynamics of Structures Theory and Application to Earthquake Engineering,* NJ: Prentice Hall.

Clarke, S., and Engelbach, R., (1930), *Ancient Egyptian Masonry - the building craft,* Oxford: Oxford UP. 242.

Clarke, W.B., (1869), On the causes and phenomena of earthquakes, especially in relation to shocks felt in New South Wales and in other provinces of New South Wales, *Transactions of The Royal Society of New South Wales,* 2, 51-86.

Cornell, C.A., (1968), Engineering seismic risk analysis, *BSSA,* 58, 5, 1583-1606.

Cotton, L.A., (1921), The Kurrajong Earthquake of August 15, 1919. *Proceedings and Journal of the Royal Society of New South Wales,* 55, 83-104.

Cowan, H.J., (1977), A history of Masonry and Concrete Domes in Building Construction *Building and Environment,* 12, 1-24.

Crouch S.L., and Starfield A.M., (1983), *Boundary element methods in solid mechanics with applications in rock mechanics and geological engineering,* London: Allen.

Cruden, S., (1960), *The Scottish Castle,* Edinburgh, Nelson, xvi +272 and 48 plates.

Davidge, R.W., (1979), *Mechanical Behaviour of Ceramics,* Cambridge: Cambridge UP. 1st paperback ed. 163.

Denham, D., Weekes, J., and Krayshek, C., (1981), Earthquake evidence for compressive stress in the southeast Australian crust, *Journal of the Geological Society of Australia*, 28, 323-32.

Dhanasekar, M., (1985), The performance of brick masonry subjected to in-plane loading, Diss. 990, University of Newcastle.

Dick, I.D., (1964), Extreme value theory and earthquakes, *3rd ICEE,* NZ, 3**,** 45-53.

Ebel, J.E., and Kafka, A.L., (1999), A Monte Carlo Approach to Seismic Hazard Assessment, *BSSA,* 89, 4, 854-866.

EDR, (1996), *User manual for the PC30F and PC30G series boards,* South Africa: Eagle Appliances, 5th ed., March 31, 1996.

Epperson, G.S., and Abrams, D.P., (1989), *Non-destructive evaluation of masonry buildings,* Urbana: ATC. 208.

FEMA, (1997), *NEHRP Guidelines for the Seismic Rehabilitation of Buildings*, no. 273, Washington: FEMA.

Field, E.H., and Jacob, K.H., (1995), A comparison and test of various site response estimation techniques, including three that are not reference site dependent, *BSSA*. 85, 4, 1127-43.

Filonenko-Borodich, M., (c1958), *Theory of Elasticity*, Moscow: n. pub.

Francis, A.J., (1969), Structural brickwork design: basis of the code provisions *Symposium on the Australian Standard CA 47 1969 SAA Brickwork Code*, Perth: IE (Australia), Paper 2**,** 1 –29.

Frankel, A., Mueller, C., Barnhard, T., Perkins, D., Leyendecker, E.V., Dickman, N., Hanson, S., and Hopper, M., *Seismic-hazard Maps for the conterminous United States*, Denver: USGS, Open File Report 97-131-A.

Freund, L.B., (1990), *Dynamic Fracture Mechanics*, Cambridge: Cambridge UP. xvii + 563.

Ganz, H.R., and Thurlimann, B., (1984), *Tests on Masonry Bricks under Normal and Shear Forces*, Zurich: Swiss Federal Technical University: Institute for Structural Statics and Construction.

Ganz, H.R., and Thurlimann, B., (1982) *Tests on the strength of masonry walls under bi-axial load*, Zurich: Swiss Federal Technical University: Institute for Structural Statics and Construction. Report Y/OLS - 93/7.

Gaull, B.A., Michael-Leiba, M.O., and Rynn, J.M.W.,(1990), Probabilistic earthquake risk maps of Australia, *Australian Journal of Earth Sciences*, 37, 169-87.

Gebara, J.M., and Pan, A.D., (1994), Finite block analysis of masonry arches, *The Masonry Society Journal*, 13, 1, 55-65.

Goodbody, A.M., (1982), *Cartesian Tensors with applications to mechanics, fluid mechanics and elasticity*, Chichester, Ellis Horwood.

Gorenc, B.E, and Tinyou, R., (1984), *Steel Designers Handbook*, Sydney: New South Wales UP. 374.

Grady, D.E., and Kipp, M.E., (1985), Geometric statistics and dynamic fragmentation, *Journal of Applied Physics*, 58, 1210-22.

Griffith, M., [1997], Interview with the author and multiple earthquake traces.

Grimm, C.T., (1996), Masonry throughout History, *TMSJ*, 14, 5 - 9.

Groundtest Pty. Ltd., (1990), Results of Particle Size Distribution Test - Hunter Region, Graph. Newcastle.

Gubbins, D., (1992), *Seismology and Plate Tectonics*, Cambridge: CUP , 2nd ed. 339.

Gutenberg, B., and Richter, C.F., (1942), Earthquake Magnitude, Intensity, Energy and acceleration, *BSSA*, 32, 3, 163 - 191.

Gutenberg, B., and Richter, C.F., (1956), Earthquake Magnitude, Intensity, Energy and Acceleration, *BSSA*, 46, 105 - 143.

Gutenberg, B., and Richter, C.F., (1954), *Seismicity of the earth and related phenomena*, 2nd ed., Boston: Princeton UP.

G+D Computing (1993), *Strand 6 Reference Manual and User Guide*, Ultimo.

Hadjian, A.H., (1992), The Spitak, Armenia Earthquake - Why so much damage?, *10th WCEE*, 19 -24 July 1992, Madrid, 1, 5-10.

Halliday, D., and Resnick, R., (1971), *Fundamentals of Physics*, NY: Wiley.

Heidebrecht, A.C., (1995), Insights and challenges associated with determining seismic design forces in a loading code, *Bulletin of the New Zealand Society for Earthquake Engineering*, 28, 3, 224-46.

Hetenyi, M., (1950), *Handbook of experimental stress analysis*, NY: Wiley, (M. Hetenyi editor.) 1077

Heyman, J., (1995), *The Stone Skeleton*, Cambridge: Cambridge UP.

Heyman, J., (1998), *Structural Analysis A Historical Approach*, Cambridge: Cambridge University Press. xii+172.

Hill, R., (1949), *The Mathematical Theory of Plasticity*, Oxford: Clarendon.

The Holy Bible (King James Version), (1940), Cambridge: Cambridge UP.

Horton, S.P., Barstow, N., and Jacob, K., (1997), Simulation of earthquake ground motion in Memphis, Tennessee, *11th WCEE*, June 23-28, Acapulco: Elsevier. Pr. 1302.

Housner, G.W., (1947), Characteristics of strong motion earthquakes, *BSSA*, 37, 19 – 31.

Housner, G.W., (1955), Characteristics of strong motion earthquakes, *BSSA*, 45, 197–218.

Hutchinson, G., Wilson, J., Pham, L., Billings, I., Jury, R., and King, A., (1995), Developing a common Australasian earthquake loading standard, *Bulletin of the New Zealand Society for Earthquake Engineering*, 28, 4, 288-93.

Hughes, D.M., and Zsemby, S., (1980), A Method of Determining the Flexural Bond Strength of Brickwork at Right Angles to the Bond Joint, *2nd CMS,* Ottawa.

Imamura, A., (1937), *Theoretical and Applied Seismology*, Tokyo: Maruzen.

Instron Ltd., (1985), *Instron Instruction Manual for Electro-hydraulic actuator series 3375*, Wycombe: Instron, Manual No. M1-7-69-11, Issue A, Sept.

Instron Ltd., (1984), *Model 2165 Control console operating manual,* Wycombe: Instron, Manual No. M1-7-49-19, Issue A, March.

Instron Ltd., (1984), *Analogue Function Generator Instruction Manual*, Wycombe: Instron, Manual No. MSY 10527, Issue 3.

Ioakimidis, N.I., (1993), Locating a crack of arbitrary but known shape by the method of path independent integrals, *International Journal for Solids and Structures*, 30, 14, 1939-56.

ISO/FDIS (1999), Draft 9652-5 *Masonry – Vocabulary,* ISO, Geneva.

Jacobs, K., (1997), Letter to the author and Marked Tree, synthetic earthquake traces.

Johnston, A.C., and Kanter, L.R., (1990), Earthquakes in Stable Continental Crusts, *Scientific American,* 262**,** 3, 42-9.

Kachanov, M., (1996), On the relationship between fracturing of brittle micro-cracking solid and its effective elastic properties, *ASME-AMD,* Dallas Texas, The Winter Annual Meeting DB 3, 109, 11-5.

Kachanov, M., Tsukrov, I., and Shafiro, B., (1994), Effective Moduli of Solids with cavities of various shapes, *Micro-mechanics of Random Media,* M Ostojap-Starzewski and I Jasiuk Editors, ASME Book No AMR139, pp. S151-S174.

Kafka, A.L., and Levin, S.Z., (1999), Does The Spatial Distribution of Smaller Earthquakes delineate Areas where Larger Earthquakes are likely to occur?, *BSSA*, (Submitted).

Kaplan, W., and Lewis, D.J., (1971), *Calculus and Linear Algebra,* NY: Wiley.

Kariotis, J., (2000), Personal communication.

Kateiva, G., (1969), Structural brickwork design: Practice, *Symposium on the Australian Standard CA 47 1969 SAA Brickwork Code*, Perth: IE(Australia), Paper 3**,** 1 –29.

Kingery, W.D., Bowen, H.K., and Uhlmann, D.R., (1976), *Introduction to Ceramics*, 2nd ed., NY: Wiley, 1032.

Kleeman, P.W., and Page, A.W., (1990), The in-situ properties of packing material used in compression tests, *Masonry International*, 4, 2, 68-74.

Klopp, G.M., (1996), *Seismic design of unreinforced masonry structures*, Diss. UA.

Klopp, G.M., and Griffith, M.C., (1993), Dynamic characteristics of unreinforced masonry buildings. *Australian Civil Engineering Transactions*, 35, 1, 59 – 68.

Knutsson, H.H., (1993), The stress strain relationship for masonry, *MI*, 7, 1, 31-33.

Knutsson, H.H., and Nielsen, J., (1995), On the modulus of elasticity for masonry, *MI*, 9, 2, 57-6.

Kotò, B., (1893), On the causes of the great earthquake in Central Japan, 1891, *Journ. Coll. Science. Imp. Univ. Japan*, 5 ,4, 296-353.

Krajcinovic, D., (1996), *Damage Mechanics*, NY: Elsevier.

Krishnsamy, G., Rizzo, R.J., and Liu, Y., (1994), Boundary Integral Equations for thin bodies, *International Journal for Numerical Methods in Engineering*, 37, 107-121.

Kuczera, G., (1994), *NLFIT A Bayesian Non-linear Regression Program Suite, Version 1.00g*, Newcastle: UN.

Lafuente, M., Casatilla, E., and Genatios, C., (1996), Experiences on the seismic resistant behaviour of masonry wall structures, *7NAMC*, 2-5 June 96, Notre Dame, 2, 1121-9.

Lam, N.T.K., Wilson, J.L., and Hutchinson, G.L., (1995), The seismic resistance of unreinforced masonry cantilever walls in low seismicity areas, *Bulletin of The New Zealand Society For Earthquake Engineering*, 28**,** 3, 179-195.

Lee, W.H.K., Wu, F.T., and Jacobsen, C., (1976), Catalogue of Historical earthquakes in China compiled from recent Chinese publications, *BSSA*, 66, 6, 2003-16.

Lekhnitskii, S.G., (1963), *Theory of Elasticity of an anisotropic elastic body*, San Francisco: Holden-Day. (trans: P Fern).

Lemaitre, J., (1992), *A course on Damage Mechanics*, Berlin: Springer-Verlag.

Little, W., Fowler, H.W., Coulson, J., Onions, C.T., and Friedrichsen, G.W.S., (1973), *The Shorter Oxford English Dictionary on Historical Principles*, Oxford: Clarendon P.

Lizzi, F., (1981), *The restoration of static monuments*, Genoa: Sagep.

Lourenço, P.B., (1995), *Computational Strategies for Masonry Structures*, Diss. Delft UP.

Lourenço, P.B., and Rots, J.G., (1997), *On the use of homogenization techniques for the analysis of masonry structures,* Delft: n. Pub.

Macchi, G., (1982), Behaviour of masonry under cyclic: actions and Seismic design, *6th Brick Masonry Conference,* Rome: ANDIL, LI - LXXV.

Magenes, G., and Calvi, G.M., (1997), In-plane seismic response of brick masonry walls, *Earthquake Engineering and Structural Dynamics*, 26, 1091-1112.

Mann, W., König, G., and Ötes, A., (1988), Tests on masonry walls subjected to seismic forces, *8IB²MC*, 2, 764-773.

Marshak, S., and Paulsen, T., (1997), Structural Style, Regional Distribution, and Seismic implications of Mid-continent Fault-and Fold Zones, United States, *Seismological Research Letters*, 68, 4, 511-520.

Masiani, R., and Trovalusci, P., (1996), Cosserat and Cauchy Materials a continuum model of brick masonry, *Meccanica,* 31, 421-32.

Masiani, R., Rizzi, N., and Trovalusci, P., (1995), Masonry as structured continuum, *Meccanica,* 30, 673-83.

McCue, K., and Love, D., (1997), Microtremor survey of Adelaide, *Earthquakes in Australian Cities*, 19, 1-3.

McGuire, R.K., (1995), Probabilistic seismic hazard analysis, and design earthquakes: Closing the loop, *BSSA,* 85, 5, 1275-84.

McLachlan, N.W., (1951), *Theory of Vibrations,* NY: Dover.

McNeilly, T.H., (1969), Architects and the Code, *Symposium on the Australian Standard CA 47 1969 SAA Brickwork Code* Institution of Engineers, Perth, Paper 4, 1 - 15.

Megson, T.H.G, (1996), *Structural and Stress Analysis*, London: Arnold, xii+641.

Melchers, R.E., (1999), *Structural Reliability Analysis and Prediction*, Chichester: Wiley.

Melchers, R.E., and Page, A.W., (1992), The Newcastle Earthquake, *Building and Structures,* 94, 143-156.

Miller, I., and Freund, J.E., (1977), *Probability and statistics for engineers*, Englewood Cliffs, NJ: Prentice-Hall.

Milne, J., (1898), *Seismology*, 1st ed. London: Kegan Paul, Trench, Truber.

Moroni, M. O., Astroza, M., and Tavonatti, S., (1994), Non linear models for shear failure in confined masonry walls *TMSJ,* 13, 1, 72.

Mott, N.F., (1947), Fragmentation of Shell cases, *Proceedings of the Royal Society (London),* A300, 300-308.

Muniruzzaman, A.R.M., (1997), A study of the serviceability behaviour of masonry, Diss. 2005, UN.

Muniruzzaman, A.R.M., Page, A.W., and Kleeman, P.W., (1996), Serviceability Behaviour of Masonry Walls - A three-dimensional study *7NAMC,* Notre Dame, 1**,** 348-59.

Muniruzzaman, A.R.M., Page, A.W., and Kleeman, P.W., (1999), The Role of the Damp Proof Courses in the Serviceability Behaviour of Masonry Structures, *MI,* 13,1, 17-21.

Muniruzzaman, A.R.M., and Totoev, Y.Z., (1998), Generation of 3D mound shapes for the analytical study of masonry on reactive soils, *ACSE Transactions*, Canberra.

Musson, R.M.W., (1993), Comrie: a historical Scottish Earthquake Swarm and its place in the history of Seismology, *Terra Nova,* 5, 5, 477-80.

Nakamura, Y., (1989), A method for dynamic characteristics estimation of subsurface using microtremor on the ground surface, *Quarterly report of the Railway Technical Research Institute,* 30, 1, 25-32.

Nichols, J.M., (1999), The assessment and repair of certain structures after the Newcastle Earthquake, *Masonry International,* 13, 1, 11-12.

Nichols, J.M., and Totoev, Y, Z., (1999), Experimental Investigation of the Damage Mechanics of Masonry under Dynamic In-plane Loads, *North American Masonry Conference,* Austin Texas.

Nichols, J.M., and Totoev, Y, Z., (1998), Criteria for establishing a dynamic test loading pattern for Masonry, *Australasian Structural Engineering Conference,* Sept 30 – Oct 2 1998, Auckland, NZ, 2.

Nichols, J.M. and Totoev, Y.Z., (1997a), A comparative experimental study of the Modulus of Elasticity of Bricks and Masonry, *11thIB^{2}MC,* Shanghai.

Nichols, J.M., and Totoev, Y, Z., (1997b), Experimental determination of the dynamic Modulus of Elasticity of Masonry Units, *Proceedings of the 15th ACMSM - 97,* Melbourne.

Page, A.W., (1973), *Structural Brickwork, a Literature Review*, Newcastle: UN.

Page, A.W., (1979), The inplane deformation and failure of brickwork, Diss. 636, UN.

Page, A.W., (1992), The design, detailing and construction of masonry - the lessons from the Newcastle earthquake, *Australian Civil Engineering Transactions*, 34, 4, 343- 53.

Papa, E., and Nappi, A., (1995), A test rig for the application of bi-axial cyclic loads to structural models, *Building and Structures*, 28, 299-307.

Paulson, T.J., and Abrams, D.P., (1990), Correlation between static and dynamic response of model masonry structures, *Earthquake Spectra*, 6, 3, 573-91.

Press, W.H., Teukolsky, S.A., Vetterling, W.T., and Flannery, B.P., (1992), *Numerical Recipes in FORTRAN*, 2nd ed., Cambridge: Cambridge UP.

Reece, R., (1998), Filter Amplifier, *Plan*, Newcastle: UN.

Reece, R., (1997), Ring Displacement Transducer, *Plan*, Newcastle: UN.

Richter, C.F., (1958), *Elementary Seismology*, San Francisco: Freeman. viii+767.

Rosenblueth, E., (1960), The earthquake of 28 July 1957 in Mexico City, *Proceedings of the 2nd International Conference on Earthquake Engineering*, 1, 359-79.

Rutherford and Chekene, (1997), *Development of procedures to enhance the performance of rehabilitated URM buildings--Appendices*, California.

Segerlind, L. J., (1984), *Applied Finite Element Analysis*, NY: Wiley.

Shing, P.B., Manivannan, T., and Carter, E., (1990), Evaluation of reinforced masonry shear wall components by pseudo-dynamic testing, *4th National Conference On Earthquake Engineering*, Palm Springs California, 2, 829 - 838.

Shiono, K., (1995), Interpretation of published data of the 1976 Tangshan, China Earthquake for the determination of a fatality rate function, *Japan Society of Civil Engineers Structural Engineering / Earthquake Engineering*, 11, 4, 155s-163s.

Sinadinovski, C., (1997), Letter to the author and Newcastle earthquake, synthetic trace.

Sokolnikoff, I.S., and Sprecht., R.D., (1946), *Mathematical Theory of Elasticity*, NY: McGraw.

Spivak, B., (1965), *Calculus on Manifolds: A modern approach to classical theorems of advanced calculus*, NY: Benjamin.

Staley, H.R., (1940), A petrographic study of the Bond between Bricks and Mortar, *Transactions of the British Ceramic Society*, 39, 85-100.

Steinbrugge, K.V., and Moran, D.F., (1954), An engineering study of the southern California earthquake of July 21, 1952 and its aftershocks, *BSSA*, 44, 2B, 210-460.

Stevens, N.J., Uzumeri, S.M., and Collins, M.P., (1991), Reinforced Concrete subjected to Reversed Cyclic Shear-Experiments and Constitutive Model, *ACI Structural Journal*, 88, 2, 135-146.

Sudhakar, A., Powell, G.H., Orr, G., and Wheaton, R., (1972), Computer Program: Ularc: *Sample Elasto-Plastic Analysis Of Plane Frames*, Berkeley: UC.

Sugo, H.O., (2000), Strength and Microstructural Characteristics of Brick/mortar Bond, Diss. (unnumbered), UN.

Sugo, H.O., Page, A.W., and Lawrence, S.J., (1998), The influence of lime and methyl cellulose on the microstructure and bond strength of mortars in combination with calcium silicate units, *8th CMC*, May 31-June 3, 1998, Jasper, Canada, 1, 348-59.

Sugo, H.O., Page, A.W., and Lawrence, S.J., (1998), Influence of Age on bond strength in clay brickwork, *5th ANMS*, Gladstone: UN, 1-3 July, 1998, 1, 365-374.

Sugo, H.O., Page, A.W., and Lawrence, S.J., (1996), Influence of the Macro and Micro constituents of air entrained mortars on Masonry Bond Strength, *7th North American Masonry Conference*, Notre Dame, Indiana, 1**,** 230 - 241.

Sugo, H.O., Page, A.W., and Lawrence, S.J., (1998), The influence of lime and methyl cellulose on the microstructure and bond strength of mortars in combination with calcium silicate units, *8CMC*, May 31-June 3, 1998, Jasper, Canada, 348-359.

Sutherland, R.T., (1989), How much did workmanship affect the robustness and load bearing capacity of old masonry walls, *Proceedings of the British Masonry Society*, 3, 51-3.

Sykes, L.R., (1996), Intermediate and long term earthquake prediction, *Proceedings of the National Academy of Sciences of the USA*, 93, April, 3732-39.

Tena-Colunga, A., and Abrams, D.P., (1992), Response of unreinforced masonry building during the Loma Prieta earthquake, *10th WCEE*, Madrid, 19 -24 July 1992, 1, 79-84.

Tena-Colunga, A., and Abrams, D.P., (1996), Seismic behaviour of structures with flexible diaphragms, *ASCE Journal of Structural Engineering*, 122, 4, 439-45.

Tercelj, S., Sheppard, P., and Turnsek, V., (1969), The influence of frequency on the shear strength and ductility of masonry walls in dynamic loading tests, *Proceedings of the Fifth International Conference on Earthquake Engineering*, 3, 2292-9.

Tezcan, S.S., and Ipek, M., (1996), A reconnaissance report: 1995 Dinar, Turkey, earthquake, *Engineering Structures*, 18, 12, 906-16.

Timoshenko, S.P., and Goodier, J.N., (1970), *Theory of Elasticity*, NY: McGraw.

Tinker, A., (1997), WaveView *for DOS 1.26,* South Africa: Eagle Appliances, 5th ed., February 14, 1997.

Tomazevic, M., Klemenc, I., Petkovic, L., and Lutman, M., (1996), *Seismic Behaviour of confined masonry building: Part One: Shaking Table Tests of Model Buildings M1 and M2 Test Results,* A report to the Ministry of Science and Technology, Slovenia: National Building and Civil Engineering Institute ZAG, ZAG/PI-95/04.

Tomazevic, M., and Klemenc, I., (1997), *Seismic Behaviour of confined masonry buildings Part Two Shaking Table Tests of Model Buildings M1 and M2 Analysis of Test Result,* Slovenia:ZAG, ZAG/PI-95/06.

Tomazevic, M., and Lutman, M., (1988), Seismic resistance of reinforced masonry walls, *9th World Conference on Earthquake Engineering*, 6, 97-102.

Tomazevic, M., Lutman, M., and Petkovic, L., (1996), Seismic behaviour of masonry walls experimental simulation, *ASCE Journal of Structural Engineering*, 122, 9, 1040-7.

Tomazevic, M., and Lutman, M., (1996), Seismic behaviour of masonry walls: modelling of Hysteretic rules, *ASCE Journal of Structural Engineering*, 122**,** 9, 1048-54.

Tomazevic, M., and Modena, C., (1988), Design of reinforced masonry walls for seismic actions, *8IB²MC*, 2, 800-810.

Totoev, Y. Z., and Kleeman, P.W., (1998), An infiltration model to predict suction changes in the soil profile, *WRR*, 34, 7, 1617.

Totoev, Y.Z., and Nichols, J.M., (1998), Dynamic Testing of Masonry by the Longitudinal Vibration and Ultrasonic Pulse Velocity Method, *Proceedings of the 8th Canadian Masonry Conference,* Jasper.

Totoev, Y.Z., and Nichols, J.M., (1997) Further Dynamic Testing of Masonry by the Longitudinal Vibration and Ultrasonic Pulse Velocity Methods, *Proceedings of the 15th ACMSM - 97,* Melbourne.

Tsimas, S., and Raikos, K., (1995), Lime, an irreplaceable mortar constituent, *Zement-Kalk-Gips International,* 48, 6, 350-6.

Umemura, H., (1975), The development of dynamic design of buildings in Japan, 5th *ECEE,* Sept, 22-25, 1975, Istanbul, Turkey, 2, 122, 1-11.

USGS (1999), *Earthquake bulletins,* (owner-qedpost@NEIS.CR.USGS.GOV, now bigquake@gldmutt.cr.usgs.gov and qedpost@gldmutt.cr.usgs.gov), NEIS: Colorado.

van Vroonhoven, J., (1996), Dynamic Crack Propagation in Brittle Materials: Analyses based in Fracture and Damage Mechanics. Eindhoven: Philips Electronics N.V., iii+195.

Vecchio, F.J., and Collins, M.P., (1986), The modified compression-field theory for reinforced concrete elements subjected to shear, *ACI Structural Journal,* 83**,** 2, 219-31.

Vermeltfoort, A. Th., (1997), Properties of Some Clay Bricks under varying load conditions, *Masonry International,* 10, 3, 85-91.

Wolde-Tinsae, A.M., Atkinson, R.H., and Hamid, A.A., (1993), State of the Art: Modulus of Elasticity of Masonry, *6th NAMC,* Phil. PA., 6-9 June 1993, 1209-20.

World Conference on Earthquake Engineering, (1956), *Proceedings of the World Conference on Earthquake Engineering,* Berkeley: EERI, 1 volume.

Wysession, M.E., Wilson, J., Bartkó, L., and Sakata, R., (1995), Intraplate seismicity in the Atlantic Ocean Basin: A teleseismic catalog, *BSSA,* 85, 3, 755-774.

Appendix A Detailed Experimental Results

A.1 INTRODUCTION

This appendix presents the analysis of the results for the ten panels tested in the experimental study. The first two panels were used to verify the operation of the test rig. The set up for each subsequent panel, the specific details of the test protocol and the results from the analysis of the data files are presented in this appendix. The results are summarized and the overall conclusions drawn from this information are discussed for the ten panels. The structure of this appendix is:

I. A brief outline is provided for the statistical study. This section presents the nonlinear regression methods used in the analysis and a suggested method for future analysis that could be developed around a transformed stiffness. The mathematics of the transformed stiffness is briefly reviewed to highlight the problems and potential with this technique.
II. The measured stiffness and the derived results are presented for the experiments on the ten panels. The summary includes sufficient information for future use of the data stored on the CD's and the Fortran analysis programs by other researchers.
III. A brief summary is provided with the main summary presented in Chapter 5.

A.2 BACKGROUND FOR THE STATISTICAL STUDY

A.2.1 INTRODUCTION

This section summarizes the background statistical methods that were used to estimate the measured stiffness values for the experimental data points. The measured stiffness is established from the measurements of the stress field and the strain field. The statistical study used a simple systematic logic by varying the frequency and amplitude of loading to investigate the properties of the measured stiffness.

A.2.2 CURRENT NON LINEAR REGRESSION METHODS

The test rig was designed to apply a harmonic shear to the masonry panel as shown in Figure 11.[312] The shear modulus can be determined directly from the applied stress and strain using standard formula (Hetenyi, 1950) with the least error. The error is a minimum

[312] Refer pg. 90.

in shear because of the longer measurement lengths and the error in resolving the applied shear force for determining the other modulus. A determination of the remaining orthotropic elastic stiffness constants requires a nonlinear regression analysis (Kuczera, 1994). A typical technique in the nonlinear regression analysis is a hill climbing search. This orthotropic system of equations has known constraints. Thus, the problem can be solved for a given set of Poisson's ratios using a simpler computationally faster search technique (Nichols and Totoev, 1999) that is a slight variant on Kuczera's method (1994). This method places a grid over the solution space and then calculates all of the objective function values on the grid. The maxima can then be found for the objective function from a simple sort of the grid values. The objective function is the peak regression coefficient for the fit of the measured stiffness. This technique was used in this analysis.

A.2.3 FUTURE NON LINEAR REGRESSION TECHNIQUES

This technique will not work for further research work[313] proposed beyond this dissertation. Arnold (1981) explained that the theory of classical mechanics was based a series of experimental observations. These observations are only approximated by the theory of vibrations in Newtonian physics. The use of finer systematically controlled experiments will provide data that contradicts, requires clarification of, or amendment to the original theory. These experiments bring about a need for modification of the basic theory of a constant stiffness. The objective is to retain the simplicity and meaning of the original concepts whilst explaining and quantifying the extensions to the concepts from the field of damage mechanics. Forced harmonic oscillations can be approximated with the standard equation of motion that in its simplest form is:

(38) $$\ddot{x} = f(x) \qquad x \hat{I} \hat{A}$$

The extensions to the field of classical mechanics and damage mechanics to define an effective stiffness rather than a constant stiffness and a variable damping instead of a constant damping provide a plethora of alternative techniques to define the concepts. The simplest statement of these concepts is that of Krajcinovic (1996), who stated that the Young's modulus and the shear modulus are invariant intrinsic properties. There are numerous alternative methods of dealing with the measurement and definition of stiffness. However, the stiffness of direct interest in the study of the shear and Young's modulus is the entity that McLachlan (1951) defines as the idealized (or pure) mass and

[313] The computer programs contained in the CD have been written to generate the files required for this type of analysis. Sufficient work has been completed with NLFIT to demonstrate that the data is adequate for the purposes.

stiffness. He clearly demonstrates the alternative technique of defining an entity that has the appearance of the idealized stiffness, but that contains the damping term. This technique uses a translation of the form:

(39) $$x = e^{-kt}u$$

Which results in a pseudo-stiffness defined as:

(40) $$\ddot{u} = -a^2 u$$

The effective stiffness of Krajcinovic (1996) does not contain a damping term. The effective stiffness in the field of damage mechanics defined by McLachlan (1951) is the change in the pure stiffness with time. A future stage to the research work will investigate the change in the damping with the strain. This will require the sophistication of Kuczera's method, as the effect of the damping is determined from the data sets. The technique of using a transformed stiffness should be investigated with this work.

A.2.4 STATISTICAL TECHNIQUE

The testing of the masonry panels used a standard statistical technique. The procedure holds some variables constant and uses a systematic change in the domain of a single variable to produce a corresponding change in the range of the results. The frequency effect is evident in the results and Appendix B deals with the analysis method to confirm the cause for the change in measured stiffness. The purposes for the early tests up to Test AP: 6 were to:

I. Identify and determine the physical properties of the measured stiffness.
II. Relate this measured stiffness to the static and dynamic stiffness discussed in the literature (Paulson and Abrams, 1990).
III. Investigate the systematic variation of the frequency and amplitude on the measured modulus. This investigation used the concepts of a FFT coupled with linear regression to fit a combined linear equation and Fourier series to the data.
IV. Estimate the elastic stiffness constants at the start of the test of each masonry panel.
V. Confirm the definition for the effective stiffness from the start of testing to the breaking of the manifold. The broken manifold violates the assumptions required for measuring the change in the effective stiffness.

VI. Quantify the rate of degradation of the masonry shear walls as a function of the time of loading.

The purpose of the final tests from AP: 7 to AP: 10 were to:

VII. Further investigate the properties of the rate of degradation of the masonry shear walls as a function of the time of loading and frequency confirming the results established in panel AP: 6.

VIII. Confirm the assumptions that underpin the development of the definitions in the classical mechanics of stiffness presented in Appendix B.

IX. Further tests were at a single frequency to investigate the time dependent changes in damping in the final stage of damage to Panel AP: 10.

A.3 MEASURED STIFFNESS RESULTS FOR PANEL AP: 1

This test panel was used to check the rig. The test was successful. It demonstrated the minor modifications that were required to improve the clearances, and confirmed the use of plywood as a packing material instead of a rubberised belt material. No useful numerical results were obtained from the panel.

A.4 MEASURED STIFFNESS RESULTS FOR PANEL AP: 2

This test panel was used to check the operation of the linear velocity displacement transducers (LVDT) on the masonry panels and to confirm that the LVDTs would supply the output at the required rate. The panel was tested statically to confirm that the modifications made after testing Panel AP: 1 had provided adequate clearances for the dynamic tests. The LVDTs were attached to the panels using aluminium plates that were glued to the brick surface. The test was successful.

However, it demonstrated the problem of fixing the aluminium to the brick surface. An additional testing issue was the mass and size of the LVDTs, which was further complicated with the provision of the required lever arm for clearances. In addition, the aluminium plates separated during testing and the moment of inertia of the assemblies introduced further error with the vibration of the assemblages relative to the panels. A system of ring displacement transducers was developed because of these initial finding and these proved successful in overcoming the identified LVDT problems. Subsequent tests of the panels were dynamic tests. No useful numerical results were obtained from the panel.

A.5 MEASURED STIFFNESS RESULTS FOR PANEL AP: 3

A.5.1 INTRODUCTION

This test panel was used to confirm the existence of the change in the measured stiffness for a panel that was tested at varying amplitude with single test frequency. The LVDTs were used for this test, as the ring transducers (RDT) were still being constructed in the workshop.

A.5.2 TEST SET UP

The arrangement of the strain gauges is shown in Figure 39.

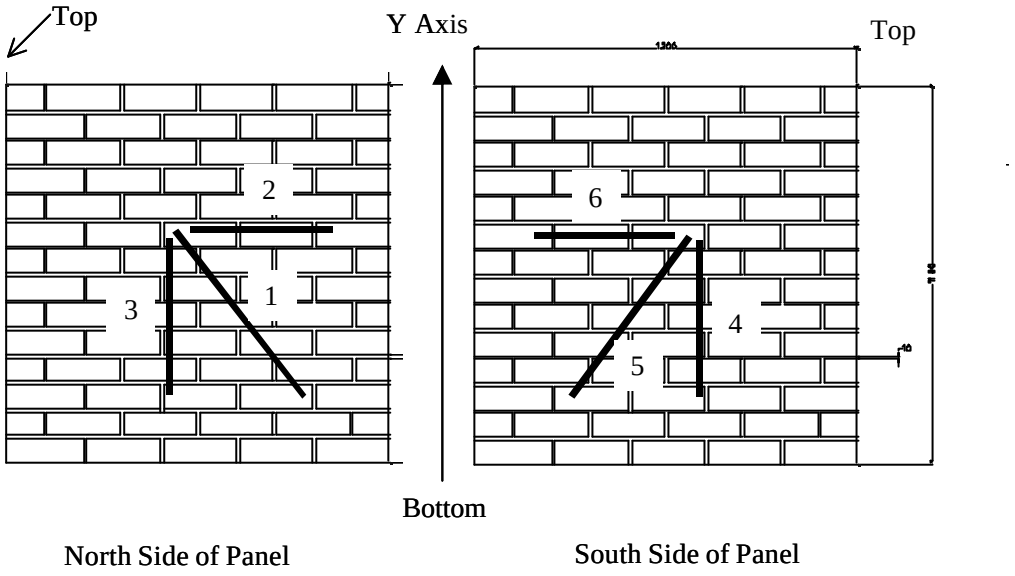

FIGURE 39 PANEL AP: 3 ARRANGEMENT OF STRAIN GAUGES

The type of strain gauge used for each of the six locations is tabulated in Table 39.

TABLE 39 PANEL AP: 3 GAUGE DETAILS

Location	LVDT Type used for Gauge	Length (mm)
1	0.5 mm	490
2		700
3		475
4	10.0 mm	445
5		648
6		490

The data channel numbers for the files generated during the experiments are presented in Table 40. The channel numbering system follows the conventional binary system of

commencing with zero. This system matches the numbering in the results files from the WaveView program output.

TABLE 40 PANEL AP:3 CHANNEL DETAILS

Channel	Unit	Calibration Details
0	ITM Load	1 V equals 100 kN
1	ITM Displacement	1 V equals 100 mm
2	LVDT 1 (0.5 mm)	2.5 V equals 0.5 mm
3	LVDT 2 (0.5 mm)	
4	LVDT 3 (0.5 mm)	
5	LVDT 4 (10 mm)	2.5 V equals 5 mm
6	LVDT 5 (10 mm)	
7	LVDT 6 (10 mm)	
8	Static Arm Pressure Y	5 V equals 68.9 MPa
9	Static Arm Pressure X	

A.5.3 LOADING PATTERN

The loading pattern is presented in terms of displacement at the ITM's ram and the forcing function frequency in Figure 40.

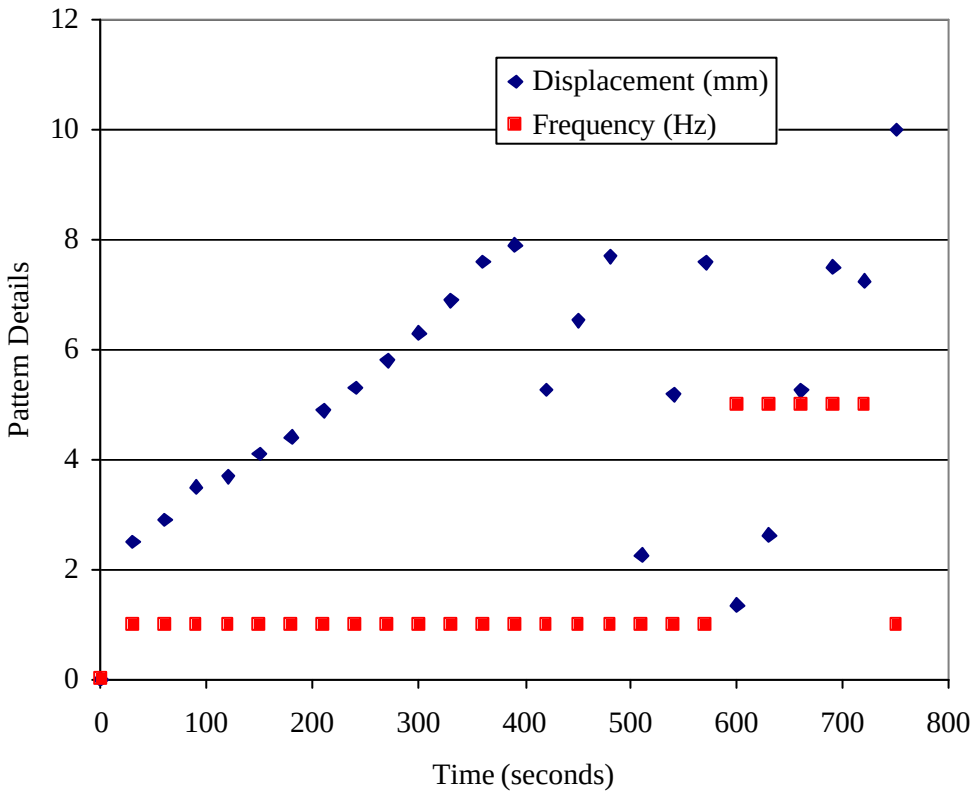

FIGURE 40 PANEL AP:3 LOADING PATTERN DETAILS

A.5.4 TEST METHOD

Panel AP: 3 was tested for 35 tests. Each test had a minimum duration of thirty seconds. The test frequency summary for panel AP: 3 is presented in Table 41.

TABLE 41 PANEL AP: 3 TEST FREQUENCY SUMMARY

Time of Loading (seconds)	Number of Tests	Frequency (Hz)
30	1	Ramp Up
540	27	1
150	5	5
30	1	1

This set of tests demonstrated the existence and form of the degrading effective stiffness. Subsequent testing showed that a frequency of 1 Hz was in the range of frequencies affected by the acceleration and damping terms, but the shape of the effective stiffness curve could be determined from this data.

A.5.5 TEST RESULTS

The mean of the measured stiffness results for panel AP: 3 is shown on Figure 41.

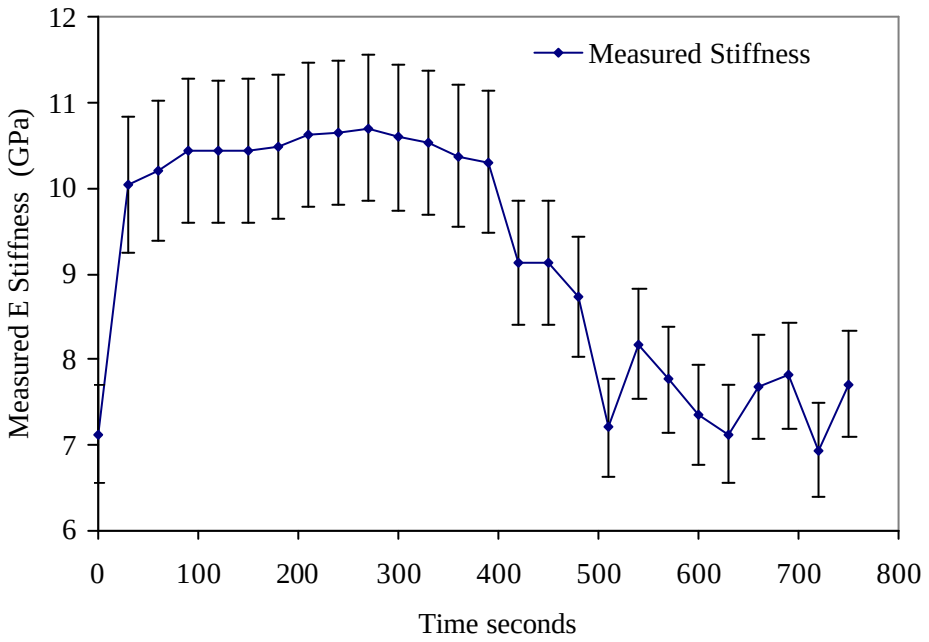

FIGURE 41 PANEL AP: 3 MEASURED STIFFNESS RESULTS

The results show a degradation of the measured stiffness with time of loading. This result provided sufficient statistical information to allow subsequent tests in 90 block steps to use a consistent variation in the frequency pattern whilst the amplitude was held constant for each 90 block test stage. The difficulty with these results was that this is the only panel tested from the panels constructed on day 246. The remainder were damaged before testing.

The mathematical theory postulated in Appendix B is based on the damage mechanics primitive of the invariant intrinsic shear and Young's modulus. The results for the Young's modulus for panel AP: 3 show an intrinsic invariant value of approximately 11 GPa and shear modulus of 7 GPa. This result is affected by the testing at a frequency of 1 Hz. However, the use of a low seismic range dynamic frequency allowed for confirmation of the basic tenet of the experimental work regarding the measurement of the damage parameter.

The estimated damage parameter at varying strain levels has been determined from the results for Panel AP: 3. These results are presented in Table 42.

TABLE 42 PANEL AP: 3 DAMAGE PARAMETER

Strain ($\mu\varepsilon$)	Damage Parameter
67	0
84	0.015
253	0.58
436	0.55

The results indicate that a failure has occurred in the effective shear stiffness at a strain level of approximately 250 $\mu\varepsilon$ and that the damage parameter has stepped from effectively 0 to 0.58. The extension to a strain level of 435 $\mu\varepsilon$ represents a rupture and probably the formation of a sliding mechanism.

A.5.6 DISCUSSION OF THE TEST RESULTS

The results from this panel demonstrate that the effective stiffness is degrading under these test conditions. The change is statistically significant. The results from this panel indicate that the test regime that should vary with frequency with the amplitude held constant. The pattern needs to permit the investigation of the peak rate of damage at a slower rate used for this panel. This change is necessary to document the change in the damage parameter during the failure process. This test results supports the hypothesis that the effective stiffness can be recovered from the measured stiffness.

A.6 MEASURED STIFFNESS RESULTS FOR PANEL AP: 4

A.6.1 INTRODUCTION

This test panel was used to investigate the results from a range of frequencies and amplitudes of loading. The first set of static ramp up tests was conducted using the LVDTs. The rings were introduced with the dynamic tests on the 23 December 1998, 0.5 mm LVDTs were used for panel AP: 4 on the southern side and the first set of ring displacement transducers (RDT) were used on the northern side. This procedure allowed the measurements from the two different displacement devices to be compared directly. This method confirmed that the RDTs provide an acceptable accuracy for the experimental work. This test of the loading protocol was designed to examine the steps in amplitude and range of frequencies that would be needed to provide sufficient statistical information to confirm the initial results from Panel AP: 3.

A.6.2 TEST SET UP STATIC TESTS

The arrangement of the strain gauges for the static tests on December 22, 1998 is shown in Figure 42.

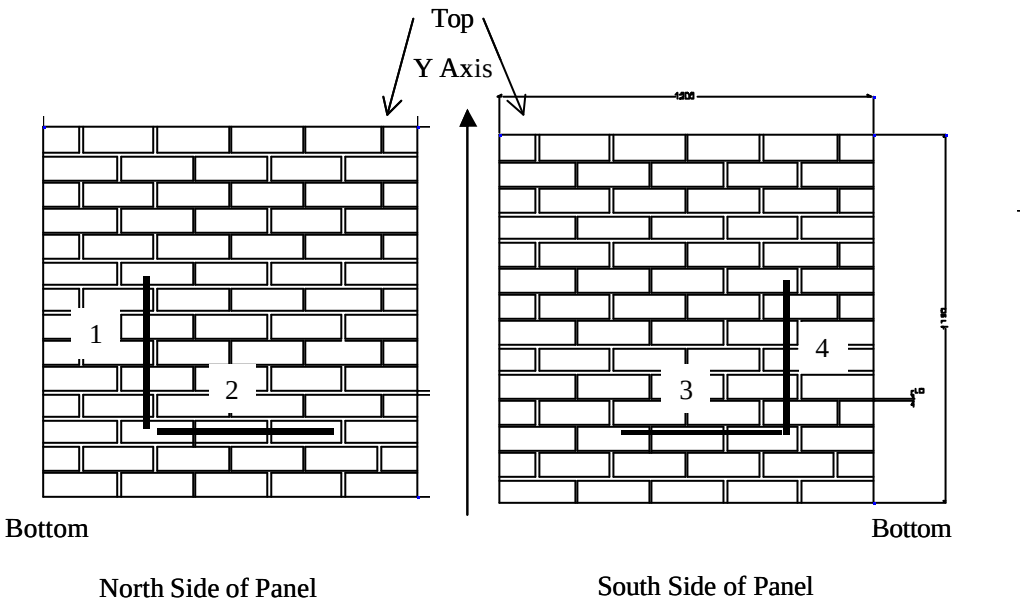

FIGURE 42 PANEL AP:4 ARRANGEMENT OF STRAIN GAUGE FOR THE STATIC TESTS

This set up applied to test number 1 - 9. The type of strain gauge for each of the four locations is tabulated in Table 43.

TABLE 43 PANEL AP:4 GAUGE DETAILS - STATIC TESTS

Location	LVDT Type used for Gauge	Length (mm)
1	0.5 mm	470
2		520
3		470
4	10.0 mm	520

The channel numbers for the generated data files are presented in Table 44.

TABLE 44 PANEL AP:4 CHANNEL DETAILS - STATIC TESTS

Channel	Unit	Calibration Details
0	LVDT 1 (0.5 mm)	2.5 V equals 0.5 mm
1	LVDT 2 (0.5 mm)	
2	LVDT 3 (0.5 mm)	
3	LVDT 4 (10 mm)	2.5 V equals 5 mm
4	Static Arm Pressure X	5 V equals 68.9 MPa
5	Static Arm Pressure Y	

A.6.3 TEST SET UP - FIRST DYNAMIC TESTS

The arrangement of the strain gauges for the dynamic tests on December 23, 1998 is shown in Figure 43.

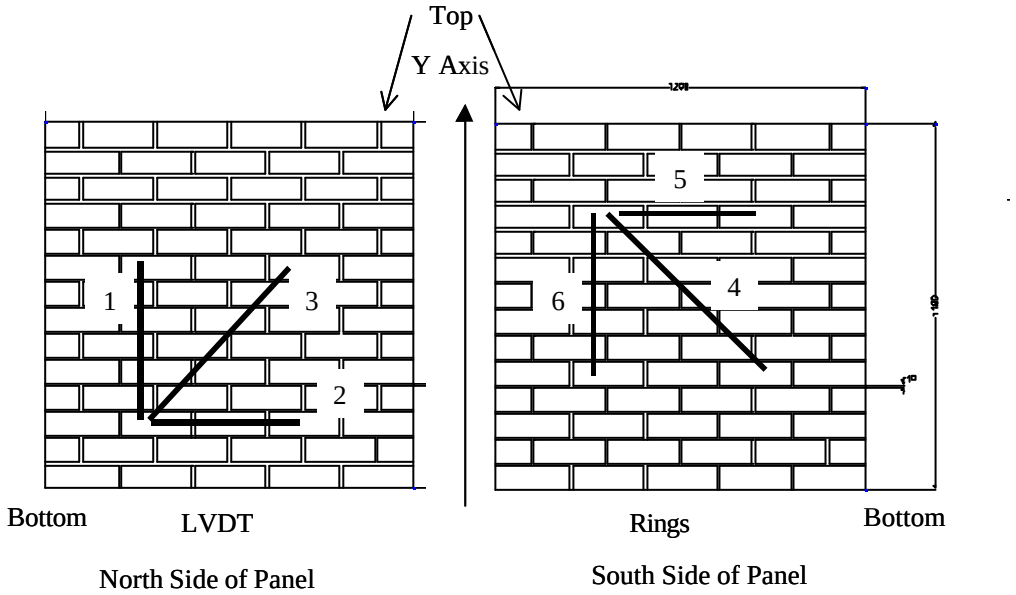

FIGURE 43 PANEL AP:4 STRAIN GAUGE ARRANGEMENTS - DYNAMIC TESTS

This set up applied to test number 1 - 29. The type of strain gauge for each of the six locations is tabulated in Table 45.

TABLE 45 PANEL AP:4 GAUGE DETAILS - FIRST SET OF DYNAMIC TESTS

Location	Type used for Gauge	Length (mm)
1	0.5 mm	470
2		700
3		530
4	RR 1	700
5		470
6		530

The channel numbers for the generated data files are presented in Table 46.

TABLE 46 PANEL AP:4 CHANNEL DETAILS - FIRST SET OF DYNAMIC TESTS

Channel	Unit	Calibration Details
0	LVDT 1 (0.5 mm)	2.5 V equals 0.5 mm
1	LVDT 2 (0.5 mm)	
2	LVDT 3 (0.5 mm)	
3	RR1 - 4	1 V equals 0.2 mm
4	RR1 - 5	
5	RR1 - 6	
6	Static Arm Pressure X	5 V equals 68.9 MPa
7	Static Arm Pressure Y	
8	ITM Load	1 V equals 100 kN
9	ITM Displacement	1 V equals 100 mm

A.6.4 TEST SET UP -SECOND DYNAMIC TESTS

The second set of dynamic tests was completed on January 7, 1999. The data channel numbers for the files generated for the experiments are presented in Table 47. The earlier configuration was maintained except that channels 4 and 5 have been inverted.

TABLE 47 PANEL AP:4 CHANNEL DETAILS - SECOND SET OF DYNAMIC TESTS

Channel	Unit	Calibration Details
0	LVDT 1 (0.5 mm)	2.5 V equals 0.5 mm
1	LVDT 2 (0.5 mm)	
2	LVDT 3 (0.5 mm)	
3	RR1 - 4	1 V equals 0.2 mm
4	RR1 - 6	
5	RR1 - 5	
6	Static Arm Pressure X	5 V equals 68.9 MPa
7	Static Arm Pressure Y	
8	ITM Load	1 V equals 100 kN
9	ITM Displacement	1 V equals 100 mm

A.6.5 LOADING PATTERN

The loading pattern evolved at this stage to a pattern that included a variation in the frequency and amplitude. A number of steps were tried in the prestressing force to judge the appropriate value for the remainder of the test panels. The details of the loading pattern used on panel AP: 4 is presented in Table 48 to Table 50. The tests numbered 132 to 154 were repeated three times each, and a sub number was used for each repeated 30 second test file except for test 136.

TABLE 48 PANEL AP: 4 TEST PROTOCOL

Number	File Name	Prestress (kN)	Frequency (Hz)	Stroke (mm)
1	245A001	Raise pressure Y	0	0.0
2	245A002	Reset gains		
3	245A010	70		
4	245011			
5	245A012		1	2.5
6	245A004			0.0
7	245A005			2.5
8	245A006			5.0
9	245A013	100		7.5
10	245A014			10.0
11	245A015			12.5
12	245A016			10.0
13	245A017	150		2.5
14	245A018			5.0
15	245A019			
16	245A020		5	2.5
17	245A021			5.0
18	245A030	100	1	0.0
19	245A031			2.5
20	245A032	100	1	5.0
21	2450321			
22	245A033			7.5
23	245A034			10.0
24	245A035			12.5
25	245A036	150		0.0
26	245A037			2.5
27	245A038			5.0
28	245A039			7.5
29	245A040			10.0
30	245A041			12.5

TABLE 49 PANEL AP:4 TEST PROTOCOL (CONTINUED)

Number	File Name	Prestress (kN)	Frequency (Hz)	Stroke (mm)
31	245A042	150	5	0.0
32	245A043			2.5
33	245A044			5.0
34	245A045			7.5
35	245A046			10.0
36	245A047			12.5
37	245A050			0.0
38	245A051			2.5
39	245A052			
40	245A053			
41	245A054			
42	245A055			5.0
43	245A056		5.5[314]	
44	245A057		5.5	
45	245A060		3.0	
46	245A061		1.0	
47	245A062			7.5
48	245A070		5.5	
49	245A071			
50	245A072			10.0
51	245A073			
52	245A074			
53	245A075			
54	245A076			12.0
55	245A077		4.5	
56	245A078			
57	245A079			
58	245A080			7.5
59	245A081			
60	245A082			
61	245A090	200		12.0
62	245A091			
63	245A092			
64	245A093			
65	245A094			
66	245A095			
67	245A096			
68	245A097			7.5
69	245A098			
70	245A099			
71	245A101			10.0
72	245A102			

[314] It was at this point that the mode in the transverse direction was found at about 5 Hz.

TABLE 50 PANEL AP: 4 TEST PROTOCOL (CONTINUED)

Number	File Name	Prestress (kN)	Frequency (Hz)	Stroke (mm)
73	245A130	100	1	0.0
77	245A131			2.5
80	245A132			5.0
83	245A133			7.5
86	245A134			10.0
89	245A135			12.5
92	245A136	150	4.5	0.0
93	245A137			2.5
96	245A138			5.0
99	245A139			7.5
102	245A140			10.0
105	245A141			12.5
108	245A142			0.0
111	245A143			2.5
114	245A144			5.0
117	245A145			7.5
120	245A146			10.0
123	245A147			12.5
126	245A150		4.5, 3.0, 3.5	2.5
129	245A151		4.5	5.0
132	245A152			7.5
135	245A153			10.0
141 - 146	245A154			
142	Comment	Broke the panel.		
150 - 160	Misc Test	Generally Ramp up tests to test Young's Modulus		

A.6.6 TEST METHOD

Panel AP: 4 was tested for 150 tests. Each test had a minimum duration of thirty seconds. A 30 second test provided time for the ITM's ram to return to the start of a cycle, except at the lowest frequency where a minimum 50 second recording period provided a minimum of 30 seconds of test data. This cyclic feature was due to the internal clock on the ITM and could not be adjusted manually.

A.6.7 TEST RESULTS

The protocol for the loading shown in Tables 51 to 53 generated a cyclic component. The measured shear stiffness results for the mean readings between the two sides of AP: 4 is shown on Figure 44. The integer file numbers have been retained on this graph to permit a direct comparison to the details in the preceding tables.

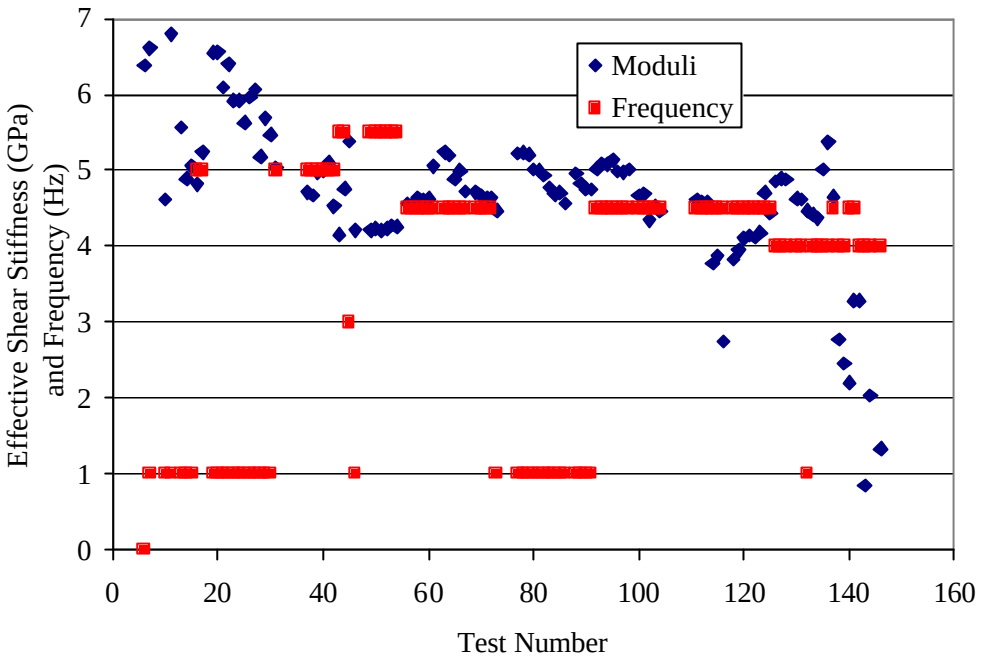

FIGURE 44 PANEL AP:4 MEASURED SHEAR STIFFNESS

It is evident from results for the measured shear stiffness when compared to the variation in the frequency of the loading pattern shown on Figure 44 that there is a cyclic pattern to the plotted points for the measured shear stiffness. The use of a standard linear regression analysis provided a plot of the residuals that confirm this postulated point (Figure 45).

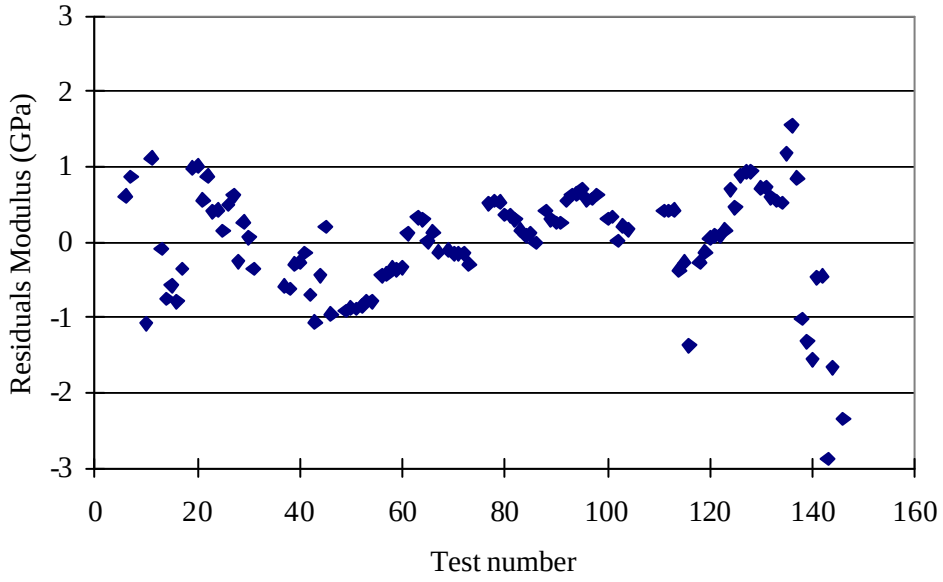

FIGURE 45 PANEL AP:4 MEASURED STIFFNESS RESIDUALS

The cyclic pattern was evident in Figure 45 and provided the confirmation that the loading pattern requires further investigation to demonstrate the relationship between the measured stiffness and the frequency pattern. To demonstrate this relationship the loading pattern was revised in the testing of the next panel. The measured shear stiffness results shown in Figure 44 were used to establish the damage parameter results (Figure 46).

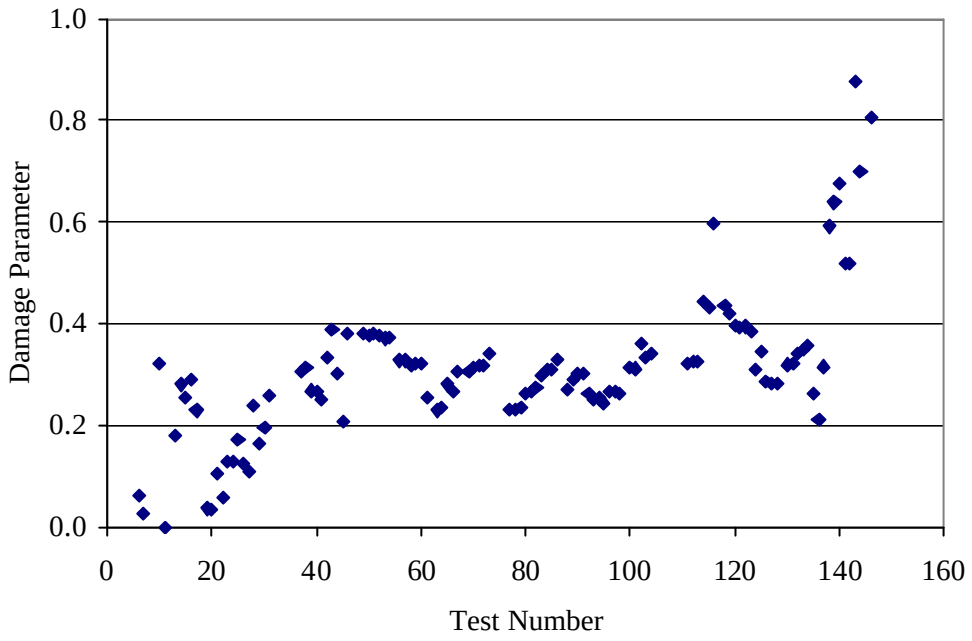

FIGURE 46 PANEL AP:4 DAMAGE PARAMETER

These results again reflect the cyclic pattern in the frequency of the loading protocol. The results for the damage parameter for a series of strain levels are presented in Table 51.

TABLE 51 PANEL AP:4 DAMAGE PARAMETER

Strain (με)	Damage Parameter	Comment
54	0	Peak Shear Stiffness
100	0.26	
150	0.33	
200	0.68	Rapid escalation in damage
480	0.80	Two manifolds

The measured shear stiffness continued to exhibit a slight rise at the start of testing. This phenomenon is discussed in Chapter 5.

A.6.8 DISCUSSION OF THE TEST RESULTS

The results from this panel demonstrate that the measured shear stiffness was degrading under these test conditions. The change is statistically significant. The results from this panel pointed to a test regime that should have a systematic variation in the test frequency with the amplitude held constant and incremented in small steps. This method retains a constant strain over sufficient replicates and then provides only minor increments in the strain between frequency blocks to permit a FFT analysis of the residuals from a linear regression analysis of the measured shear stiffness. The pattern again needs to approach the peak rate of damage in a slower mode than the rate used for this panel to observe the damage accumulation in the domain of 200 to 400 με.

A.7 MEASURED STIFFNESS RESULTS FOR PANEL AP: 5

A.7.1 INTRODUCTION

Panel AP: 5 was cracked in the second experiment with the application of the prestress load.

A.7.2 TEST METHOD

The locations for the gauges are shown on Figure 47.

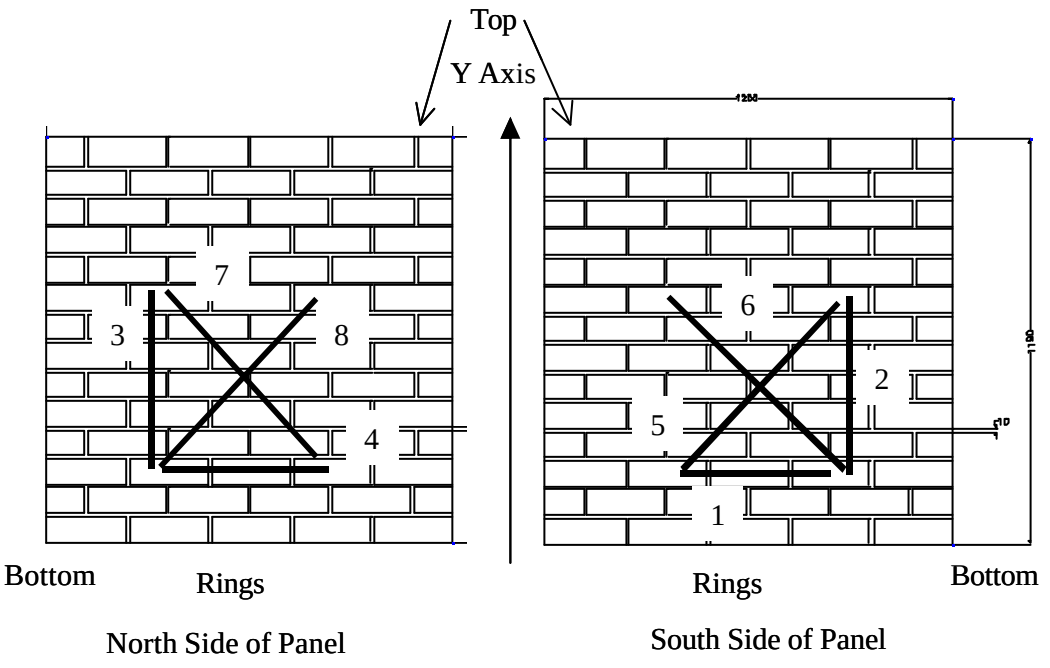

FIGURE 47 PANEL AP: 5 GAUGE LOCATIONS

This panel was tested as a single shear stress test to failure at 300 kN. No dynamic experiments were undertaken with this panel. The second set of rings, which are designated type RR 2 were used for the first time in this set of experiments. The thicker type RR 2 rings were used to measure the change in displacement on the diagonal. The ramp up time for the application of the shear force was about 30 seconds. The test is considered quasi-static as it was manually controlled to the point of failure. The data channel numbers for the files generated for the experiments are presented in Table 52.

TABLE 52 PANEL AP: 5 CHANNEL DETAILS

Channel	Unit	Calibration Details
0	RR1 - 1	1 V equals 0.2 mm
1	RR1 - 2	
2	RR1 - 3	
3	RR1 - 4	
4	RR2 – 5	
5	RR2 – 6	
6	RR2 – 7	
7	RR2 - 8	
8	Static Arm Pressure X	5 V equals 68.9 MPa
9	Static Arm Pressure Y	
10	ITM Displacement	1 V equals 100 kN
11	ITM Load	1 V equals 100 mm

A.7.3 TEST RESULTS

The analysis of the data file for the experiment provided the measured shear stress and the measured shear strains. A plot of these points is shown in Figure 48.

The results confirm the assumption of the continuous smooth concave form of the change in the effective shear strength that was postulated with the data from the Canadian reinforced concrete shear experiments and the work on Salem limestone. The effective shear stiffness was determined for increments of the strain from the data for Panel AP: 5 using standard linear regression techniques. The peak effective shear stiffness was 22.5 ± 1 GPa.

The results are consistent with the findings in compression for Salem Limestone shown in Figure 7[315]. The strain levels for the masonry illustrate the relative paucity of tensile strength of the material when compared to the higher strain levels achieved in a limestone subjected to a compression load pattern. This panel had a flexural strength of 0.62 ± 0.11

[315] Refer pg. 73.

MPa. The results for the effective shear stiffness were significantly higher than the other panels. These results are usual for pressed masonry. They merely serve to illustrate the vagaries of construction even for the ideal circumstances found in a laboratory setting.

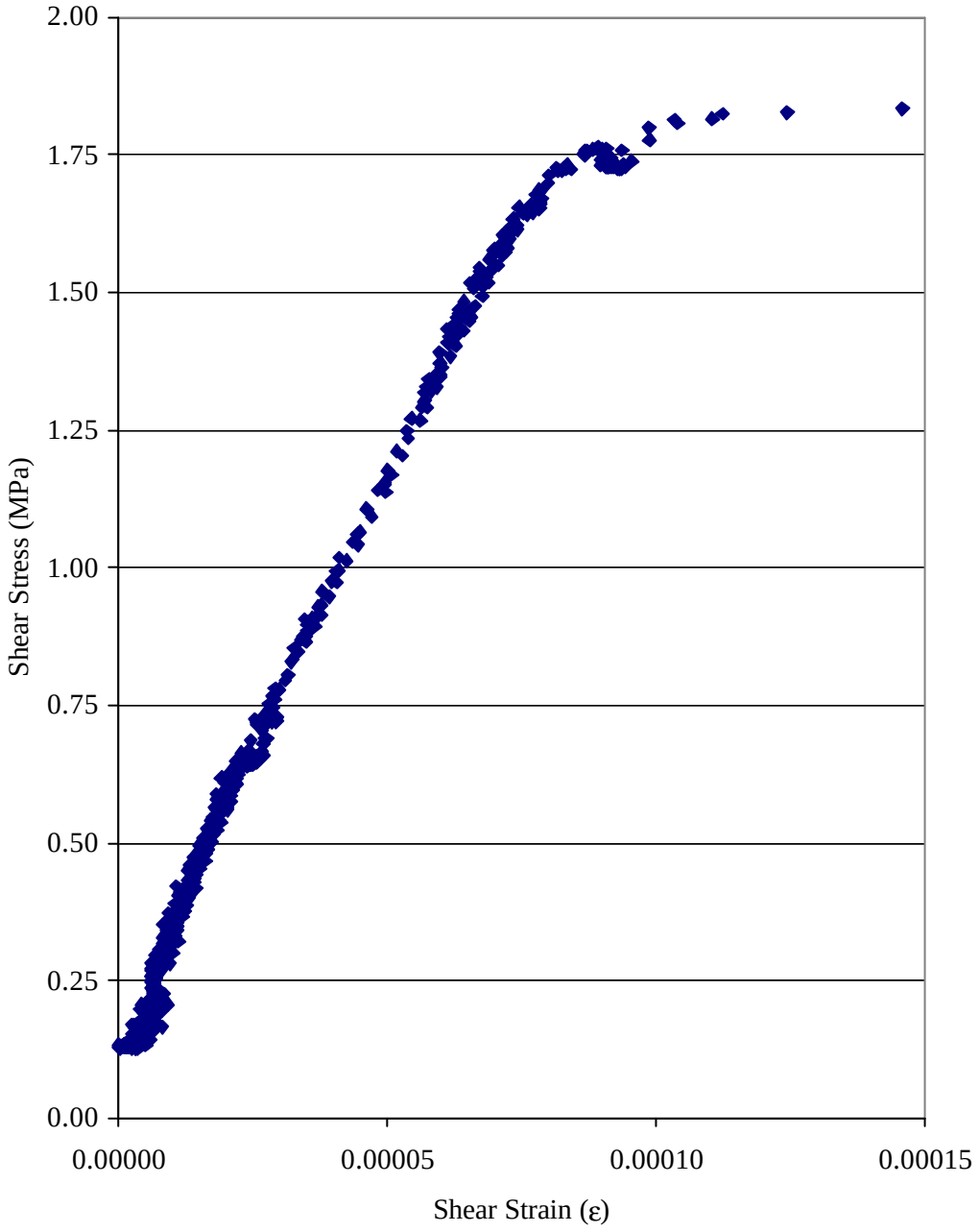

FIGURE 48 PANEL AP:5 SHEAR STRESS WITH RESPECT TO SHEAR STRAIN

The ratio of the damage parameter at various strain levels is plotted in Figure 49.

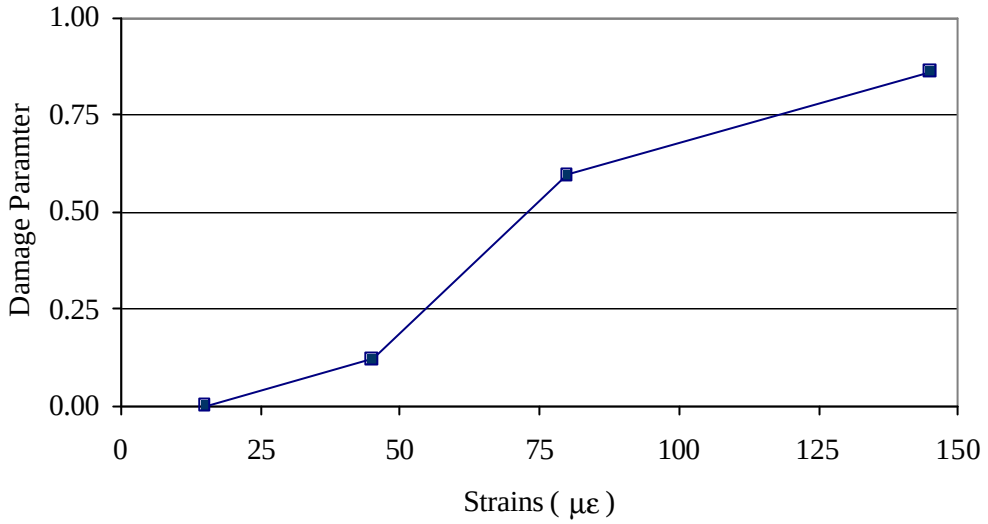

FIGURE 49 PANEL AP:5 DAMAGE PARAMETER

The results for the damage parameter for a series of strain levels are shown in Table 53.

TABLE 53 PANEL AP:5 DAMAGE PARAMETER

Strain (με)	Damage Parameter
15	0.00
45	0.12
80	0.59
145	0.86

A.7.4 DISCUSSION OF THE RESULTS

Panel AP: 5 was not intended to be tested in a single tensile test. However, the results from this test provided further confirmation of the underlying assumptions for the analysis. The change in effective shear stiffness is a concave descending continuous function to the point of failure. The testing of subsequent panels was thus designed to investigate and confirm the cause of the observed frequency effect on the measured stiffness results and to confirm the postulate that the effective stiffness does not have a frequency effect and can be recovered from the measured shear stiffness under some set of circumstances. The results from this panel provided insight into the further development of a cyclic loading pattern of increasing frequency with an increase in amplitude after a full test cycle of frequencies from the quasi-static to the dynamic level.

A.8 MEASURED STIFFNESS RESULTS FOR PANEL AP: 6

A.8.1 INTRODUCTION

This section presents the results for Panel AP: 6. This is one of the critical panels and the analysis included a FFT analysis of the residuals for a linear regression analysis of the measured shear stiffness.

A.8.2 TEST PURPOSES

This panel was loaded with a systematic pattern designed to determine and demonstrate the relationship between the effective stiffness and the measured stiffness. It was designed to demonstrate that the measured stiffness is a piecewise continuous curve controlled by the frequency of the loading function. The prestress load was set to 150 kN, which is half the peak load recorded for Panel AP: 5 in a straight shear test. This prestress level was maintained for all subsequent tests on the remaining panels. This investigation uses the concepts of a FFT coupled with linear regression to fit a combined linear equation and Fourier series to the data, estimate the elastic stiffness constants, and determine the effective shear stiffness for the panel from the measured shear stiffness.

A.8.3 TEST METHOD

The locations for the gauges are shown on Figure 50.

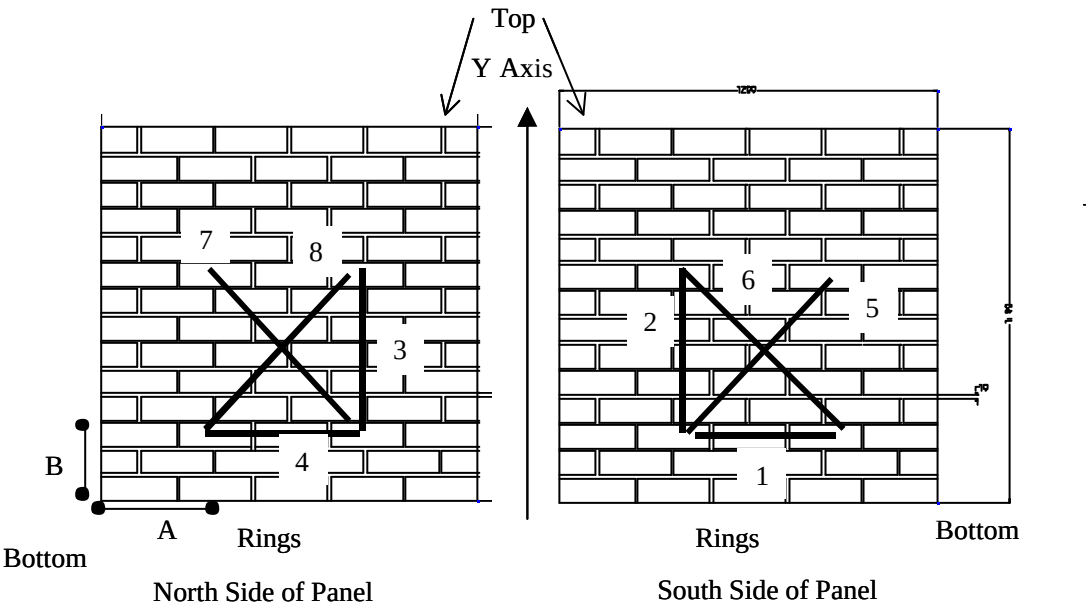

FIGURE 50 PANEL AP: 6 GAUGE LOCATIONS

The type of strain gauge for each of the eight locations is presented in Table 54.

TABLE 54 PANEL AP: 6 GAUGE DETAILS FOR THE DYNAMIC TESTS

Location or offset	Type used for gauge	Length (mm)
1	RR 1	480
2		524
3		524
4		480
5	RR 2	711
6		
7		
8		
A	North	350
B		380
A	South	310
B		300

The data channel numbers for the files generated for the experiments are presented in Table 55.

TABLE 55 PANEL AP: 6 CHANNEL DETAILS

Channel	Unit	Calibration Details
0	1	1 V equals 0.2 mm (Coded into the Fortran Programs)
1	2	
2	3	
3	4	
4	5	
5	6	
6	7	
7	Failed	
8	ITM Load	1 V equals 100 kN
9	ITM Displacement	1 V equals 100 mm
10	Static Arm Pressure X	5 V equals 68.9 MPa
11	Static Arm Pressure Y	
12	8	Replaced 7

A.8.4 TEST PROTOCOL

Panel AP: 6 was tested for 640 tests with the minimum duration of thirty seconds for each test. The earlier note on the lower frequency requiring a longer recording time applies to all subsequent tests at low frequency. The test frequency summary for panel AP: 6 is presented in Table 56. This frequency pattern was repeated in a 90 block pattern with an increase of amplitude after each block of 90 tests.

TABLE 56 PANEL AP: 6 TEST FREQUENCY SEQUENCE

Test Number- Sequence Begins	Test Number - Sequence End	Frequency (Hz)
1	15	0.06
16	30	0.1
31	45	0.3
46	60	1
61	75	5
76	90	10

The amplitude pattern[316] for Panel AP: 6 is presented in Table 57. Each unit of amplitude is 2.54 mm. The change in the frequency of the testing near to the point of failure was to avoid a static failure in the manifold.

TABLE 57 PANEL AP: 6 HARMONIC AMPLITUDES

Start Number	End Number	Amplitude Units	Frequency Changed
1	90	1	
91	180	1.5	
181	270	2.0	
271	360	2.5	
361	450	3.0	
451	540	3.5	
541	555	4.0	0.1
556	570		10.0
571	585		5.0
586	600		1.0
601	615	4.5	5.0
616	630		1.0
631	640	5.0	

A.8.5 TEST RESULTS

The panel was tested for 640 tests before failure occurred due to a tensile split on the first principal plane. The mean measured stiffness results between the two sides of AP: 6 is shown on Figure 27.[317] Each block of 90 tests represents one amplitude point in Figure 27. The next block of 90 tests represents an incremental increase in the amplitude as set out in Table 57. The two sets of measured shear stiffness results for panel AP: 3 and AP: 6 show the same relationship between the measured and the effective stiffness. The two graphs represent differing loading patterns that affect the plotted points for each

[316] Specific comments on these tests and any problems are contained in a comments file on the CD.
[317] Refer pg. 124.

30 second test of the measured shear stiffness. The upper bound to the measured stiffness results for Panel AP: 6 is approximately 8.7 GPa. The piecewise continuous measured stiffness curve is evident in each of the 90 block groups. The measured stiffness decreases as the frequency of the loading function increases. This result is evident in the decrease in the plotted results between Series 1 and Series 6 for each block of 90 results.

The usual increase in the upper bound during the initial low amplitude loading is again observed in the panel results. This is attributed to strain rate sensitivity with minor settling in of the test rig and the relative stiffness of the test rig to the panel. The results can be directly compared to the results for panel AP: 3 for the tests at a constant frequency. A fitted curve through the data points for a frequency of 0.06, 0.1 and 0.3 Hz, yields the change in the measured shear stiffness at low frequency as the amplitude is systematically increased. These results show the same functional form of a continuous function as was observed in the results for panel AP: 3 and for Panel AP: 5.

The peak strain for each test is shown in Figure 51.

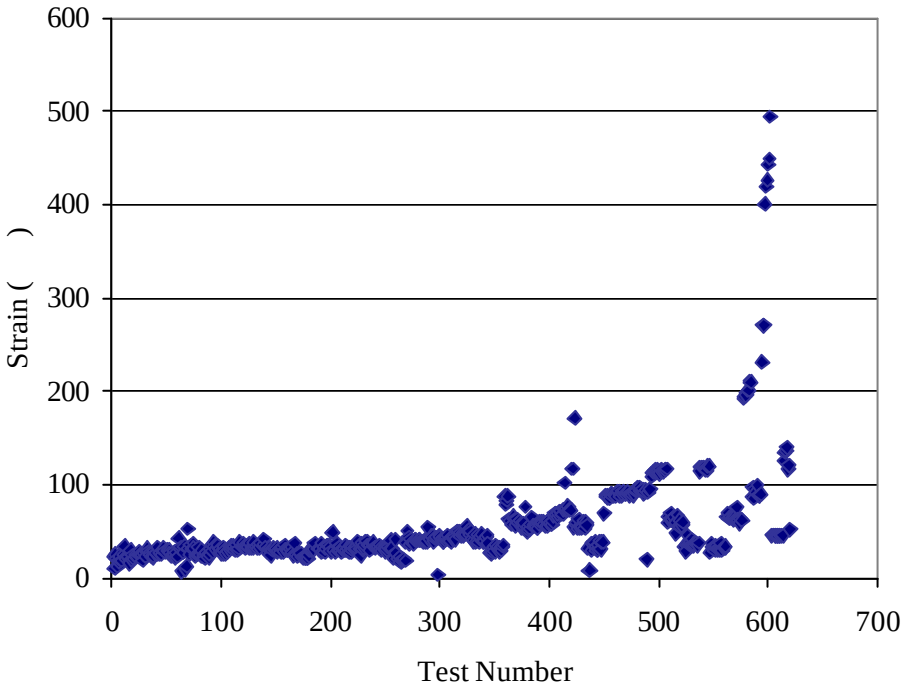

FIGURE 51 PANEL AP:6 PEAK SHEAR STRAINS FOR EACH TEST

The plot of the measured shear stiffness with respect to the peak shear strain for each test is shown in Figure 52.

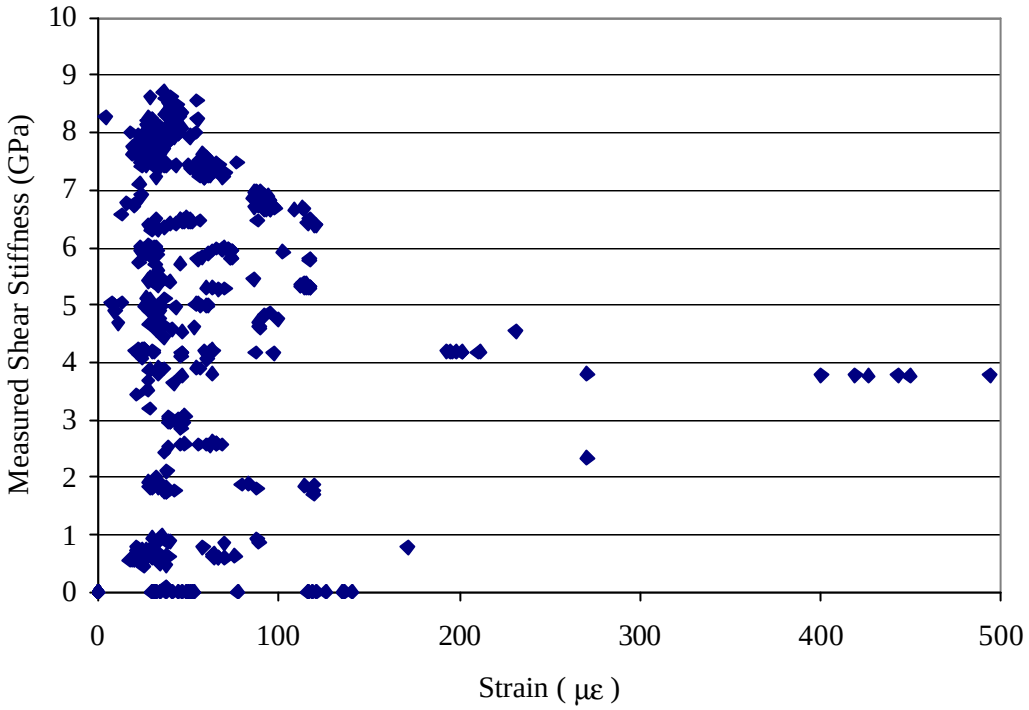

FIGURE 52 PANEL AP:6 MEASURED SHEAR STIFFNESS WITH RESPECT TO PEAK STRAINS

A plot of the damage parameter with respect to strain is shown in Figure 53.

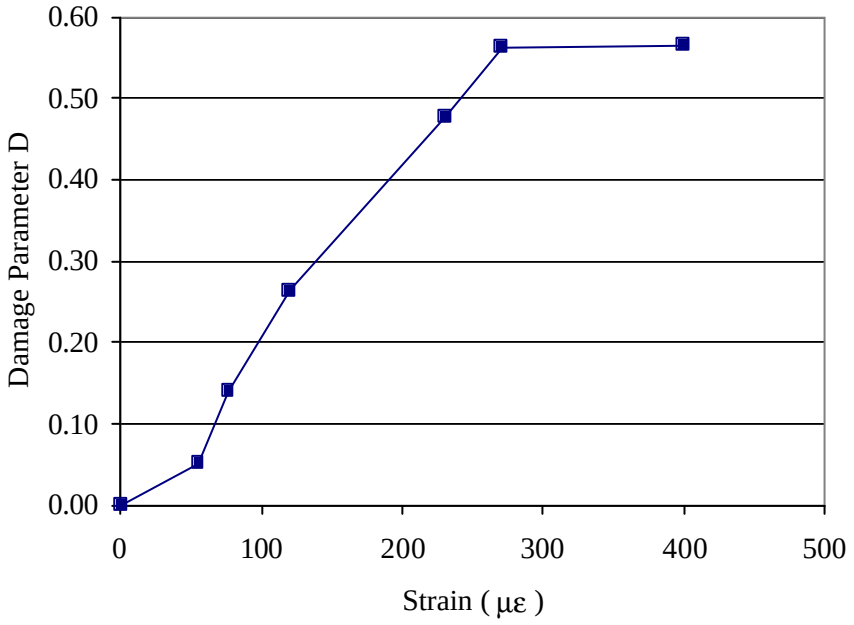

FIGURE 53 PANEL AP:6 DAMAGE PARAMETER

The damage parameterization details are presented in Table 58.

TABLE 58 PANEL AP:6 DAMAGE PARAMETER

Strain (με)	Damage Parameter
0	0.00
55	0.05
77	0.14
120	0.26
231	0.48
270	0.56
400	0.57

A.8.6 A TEST SET OF RESULTS AT A SINGLE AMPLITUDE

The results shown in Figure 27 represent the full set of 640 tests. At an initial viewing the interpretation of the information contained in the graph is obscured because of the systematic variation in the frequency at each amplitude point. The measured shear stiffness for single amplitude for tests numbered 271 to 361 is shown in Figure 54. Each point is the mean of fifteen measurements.

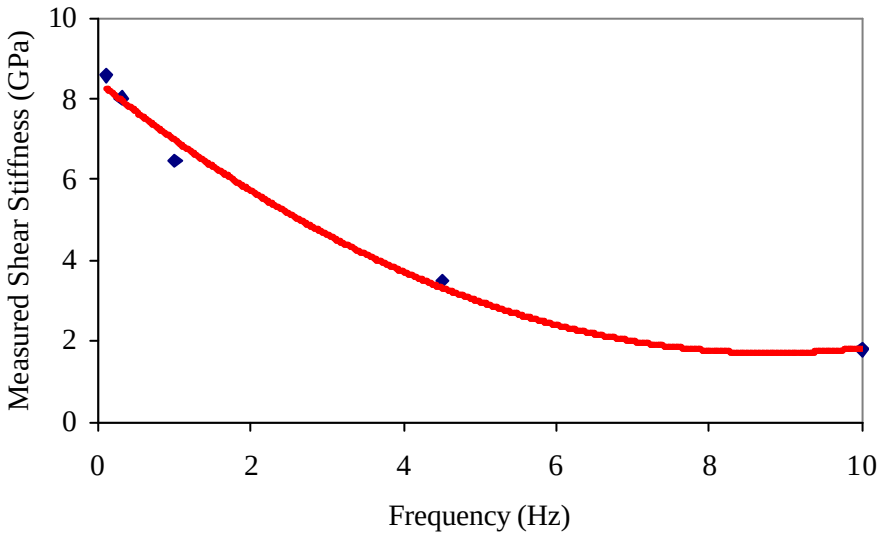

FIGURE 54 PANEL AP:6 SINGLE AMPLITUDE TESTS

The critical element of this plot is the observation that the mean effective shear stiffness from test numbers 270 and test number 361 can be determined from Figure 27. These tests represent the first test in each amplitude block at a frequency of 0.06 Hz that

is a quasi-static loading rate for each 90 block set. The results have an effective shear stiffness, $k^2(t)$, of about 8.4 at test 271 and about 7.5 at test 361. The conclusion is that the effective stiffness is degrading in this series of tests from 271 to 361. There is, however, no indication of a break in the manifold. The results plotted in Figure 54 show the relationship between the measured shear stiffness, $l^2(t)$, and the frequency, f, that is:

(41) $$l^2(t) = 8.4 - 1.5f + 0.086f^2$$

The fitted equation has a regression co efficient, R^2, of 0.988. The frequency term clearly dominates the shape of the measured shear stiffness from test point 270 to 360. The minimum shear stiffness occurs at 9 Hz. This is a reasonable estimate given the sparsity of the points to define the parabola. This pattern is repeated in each of the 90 block test points for constant amplitude. The results of the plot shown in Figure 54 can be compared to the results shown in Figure 41 for Panel AP: 3.[318] The typical results shown by panel AP: 3 were for a constant frequency of one Hz. These results for panel AP: 3 for comparable test points match the observed loss of the effective stiffness, $k^2(t)$, of about 8.4 at test 270 and of about 7.5 at test 361 for panel AP: 6. This result is entirely consistent with the results for Panel AP: 4 and the principle of a smooth change in the effective stiffness demonstrated in Panel AP: 5. The results for the measured shear stiffness shown in Figure 54 are clearly dominated by the frequency of the loading pattern. The comments that can be made from this graph and equation (41) are presented in Table 59.

TABLE 59 PANEL AP: 6 FREQUENCY EFFECTS COMMENTS

Number	Comments
1	The effective stiffness has an upper limit of 8.4 at the start of testing for this amplitude.
2	The frequency term f that represents the velocity or damping component dominates the frequency term f^2 that represents the acceleration component in the frequency range of 0.3 to 6 Hz. The parabola minimum is 9 Hz.
3	A non-linear NLFIT analysis is required to recover the damping characteristics. This level of research is beyond the scope of this study.
4	It is considered likely that the damping, whilst constrained within the usual limit range, is not likely to be constant across the series of tests. This observation would match the jumps evident in the measured stiffness between individual tests.
5	The pragmatic limit for quasistatic testing is 0.3 to 0.4 Hz.
6	The parabola minimum is about 9 Hz.

[318] Refer pg. 183.

A.8.7 DISCUSSION OF THE TEST RESULTS

Two methods have been used to interpret these results for this critical panel, AP: 6. The first method uses a pure mathematics approach of considering the form of the functions and the associated constraints from the linearly independent terms in the basic differential equation of motion. This approach provides a satisfactory explanation for the degrading stiffness results. The change in the measured stiffness is evident at approximately 0.3 to 1 Hz in Figure 27. The test results for panel AP: 6 confirm the results for the panel AP: 3 in terms of the shape of the measured stiffness results at constant frequency and increasing amplitude. The results demonstrate the pattern for the measured shear stiffness under a specific loading regime. In this case, the loading regime used a constant amplitude increase of 1.27 mm with a set of frequencies ranging from 0.06 to 10 Hz tested at each amplitude point. The results clearly demonstrate the impact of the frequency on the measured stiffness properties. This confirms the observations by previous masonry researchers on the change in stiffness between a static and dynamic loading case.

The data points can be used in the statistical study to determine the factors in the loading pattern causing the changes in the measured shear stiffness. These results can be used to establish that:

I. These results do not contradict the hypothesis that the effective stiffness can be derived from the measured stiffness.
II. The effective stiffness is a continuous and smooth curve, which for all practical purpose, is monotonically concave downwards.

The second method used a Fast Fourier transform analysis of the data to establish a linear trendline in the data and investigate the cyclic nature of the residuals for the fitted line. The results show that there are two independent processes controlling the measured stiffness. These are the increase in amplitude that is causing damage to the panel and the change in frequency that is causing the mass and damping terms to increase in value relative to the stiffness term. This results in the classic form for the measured stiffness shown in Figure 27. These measured shear stiffness results were analysed using Fast Fourier Transforms to determine the properties of the effective stiffness. The relationship between the effective stiffness and the measured stiffness established in Appendix B was shown to be applicable to these results. In summary, a transformation operation has been shown to exist between the residual input data and output data for the test panels. The operation and its known pattern clearly define the measured stiffness.

A.9 MEASURED STIFFNESS RESULTS FOR PANEL AP: 7

A.9.1 INTRODUCTION

This section presents the results for Panel AP: 7. The test purposes and protocol for this panel generally matches that of Panel AP: 6. This panel was initially tested for 79 tests, which proved to be unusable as the rig would not balance and then the shear yoke rods fractured due to fatigue loading. The rig was repaired and balanced and testing continued with the file set 245E. The first file set 245D was retained with the other input files.

A.9.2 TEST METHOD

The locations for the gauges are shown on Figure 55.

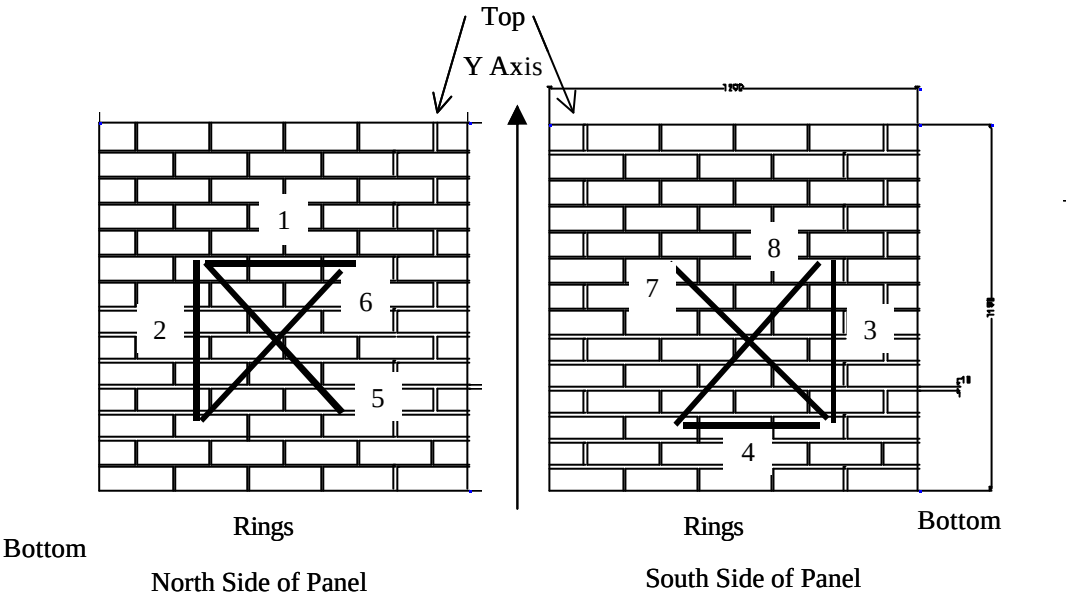

FIGURE 55 PANEL AP: 7 GAUGE LOCATIONS

The type of strain gauge for each of the eight locations is tabulated in Table 60.

TABLE 60 PANEL AP: 7 DYNAMIC TESTS - GAUGE DETAILS

Location or offset	Type used for gauge	Length (mm)
1	RR 1	480
2		524
3		
4		480
5, 6, 7, 8	RR 2	711

This panel was the first in which the holes for the bolts that held the rings in place were drilled through the bricks to provide matching strain data sets. The channel details for the recording of the data files for Panel AP: 7 are presented in Table 61.

TABLE 61 PANEL AP: 7 CHANNEL DETAILS

Channel	Unit	Calibration Details
0	1	1 V equals 0.2 mm (Coded into the Fortran Program.)
1	2	
2	3	
3	4	
4	5	
5	6	
6	7	
7	Failed	Not used
8	ITM Load	1 V equals 100 kN
9	ITM Displacement	1 V equals 100 mm
10	Static Arm Pressure Y	5 V equals 68.9 MPa
11	Static Arm Pressure X	
12	8	Replaced 7

A.9.3 TEST PROTOCOL

Panel AP: 7 was tested for approximately 700 tests, with the minimum test duration of thirty seconds. The test frequency summary for panel AP: 7 was essentially the same as for AP: 6. The test frequency pattern is shown in Table 62.

TABLE 62 PANEL AP: 7 TEST FREQUENCIES

Test Number - Sequence Begins	Test Number - Sequence End	Frequency (Hz)
1	15	0.06
16	30	0.1
31	45	0.3
46	60	1
61	75	5
76	90	10

The amplitude of the loading is presented in Table 63.

TABLE 63 PANEL AP: 7 NOMINAL TEST AMPLITUDES

Test Number Start	Test Number End	Amplitude Units	Nominal Amplitude (mm)
1	90	1	2.5
91	180	1.5	3.8
181	270	2	5.0
271	360	3	7.6
361	450	3.5	8.9
451	540	4	10.1
540	605	5	12.5

A.9.4 TEST RESULTS

The results for the measured shear stiffness for each 30 second test are shown on Figure 56. The legend shows the nominal frequency of each test point.

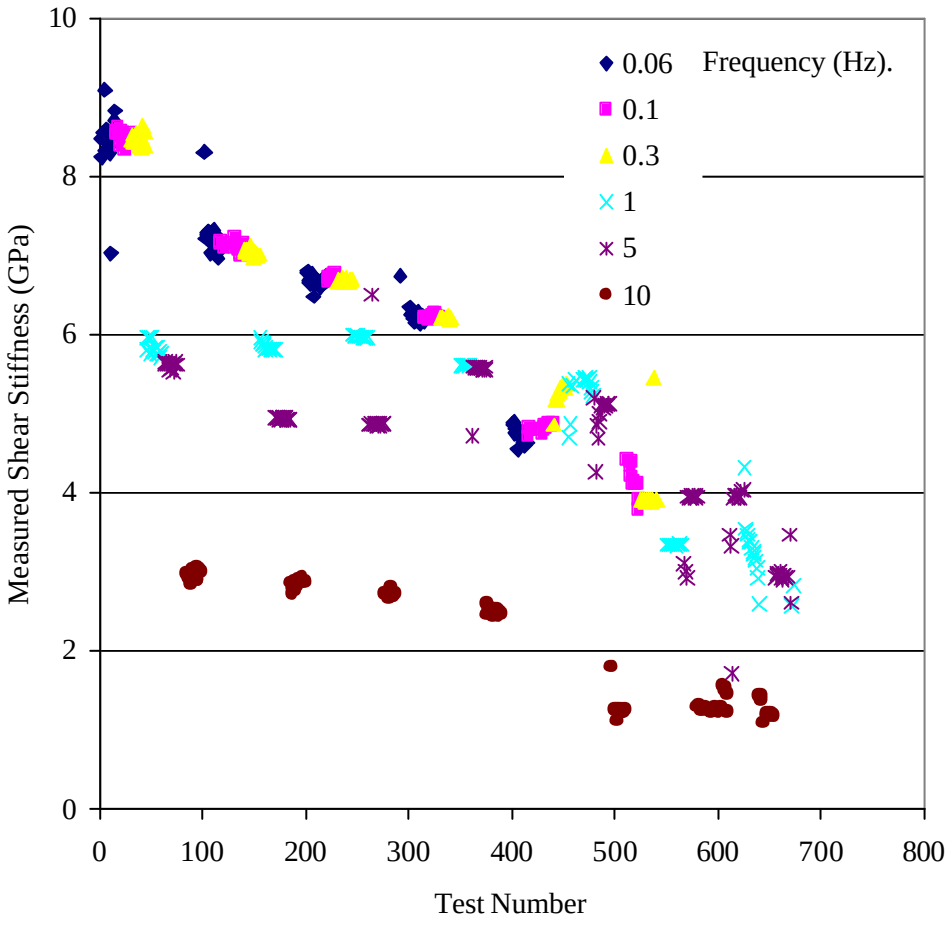

FIGURE 56 PANEL AP: 7 MEASURED SHEAR STIFFNESS

The last test cycles does not include the lower frequency tests to avoid premature failure the sample with a static test. The cyclic pattern in the results is again evident. This issue was discussed in relation to Panel AP: 6. The steeper gradient in the bounding curve that defines the effective stiffness is attributed to the revised pattern for the amplitude increases. The interesting feature is the test results for the one and five Hz frequencies at the low amplitudes of loading. This type of feature requires further research using NLFIT to investigate the functional form of the damping component. It is not considered significant for this study.

The bounding features of the effective stiffness is distinct at the low test frequencies and follows the traditional pattern for a brittle material's effective stiffness with increased levels of strain. The plot of the measured shear stiffness against the strain is shown in Figure 57.

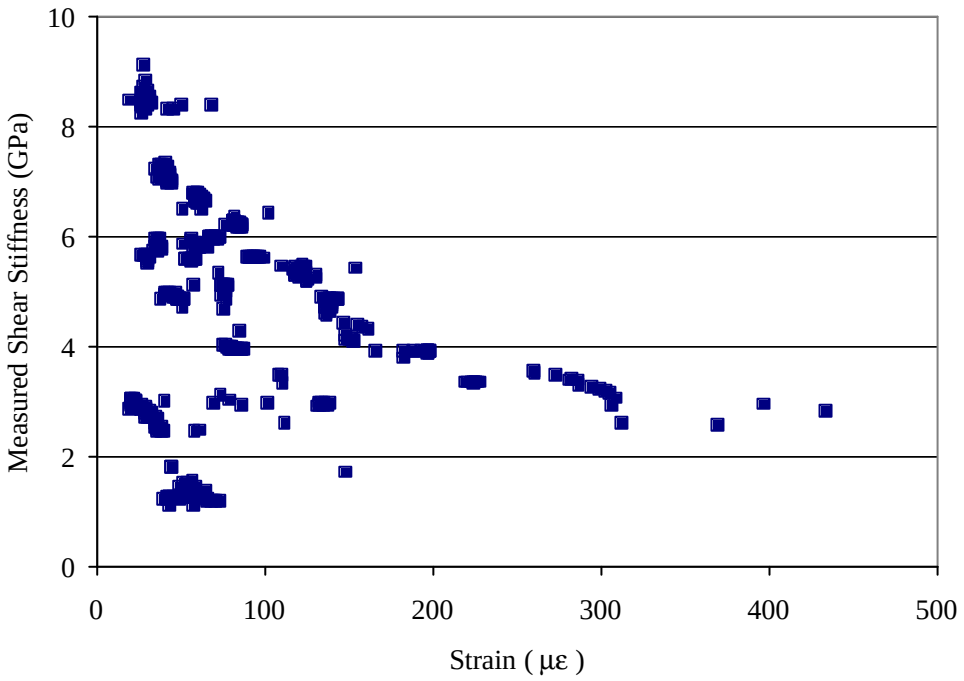

FIGURE 57 PANEL AP: 7 MEASURED SHEAR STIFFNESS

The area below the bounding curve in Figure 57 reflects the mathematically admissible solutions to the differential equation of motion. The bounding curve was recovered, the damage parameter determined and the results are in Figure 58.

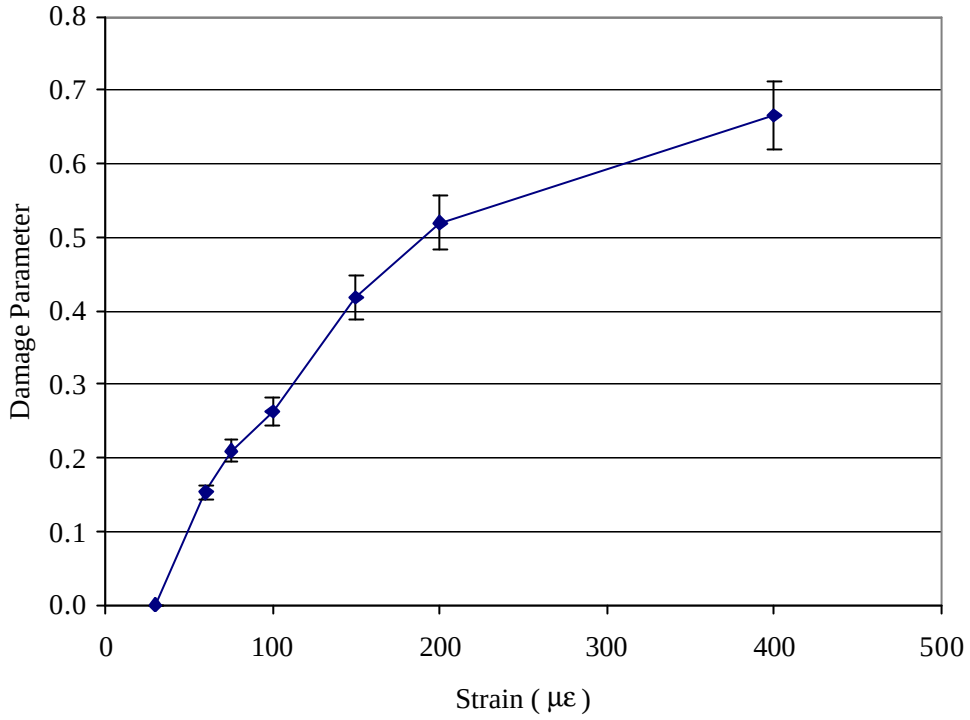

FIGURE 58 PANEL AP:7 DAMAGE PARAMETER

A.9.5 DISCUSSION OF THE TEST RESULTS

The results show two independent processes control the measured stiffness. These are the increase in amplitude that is causing damage to the panel and the change in frequency that is causing the mass and damping terms to increase in value relative to the stiffness term. This is the same observation that was made for the previous panel.

A.10 MEASURED STIFFNESS RESULTS FOR PANEL AP:8

A.10.1 INTRODUCTION

This experiment series was different to the two proceeding tests with a change in the test protocol to three tests of ninety seconds duration. The upper yoke rods broke due to fatigue loading during the initial test period. The Y16 mm rods were replaced with Y20 mm all threaded rods. This increased the stiffness of the shear yoke, which has been discussed in relation to the shape of the measured stiffness at low strain rates.

The basic pattern of the test amplitudes and frequencies was retained from that presented for Panel AP: 6 and Panel AP: 7, with a change to a 90 second period after the thirtieth test.

A.10.2 TEST METHOD

The locations for the gauges are shown on Figure 59.

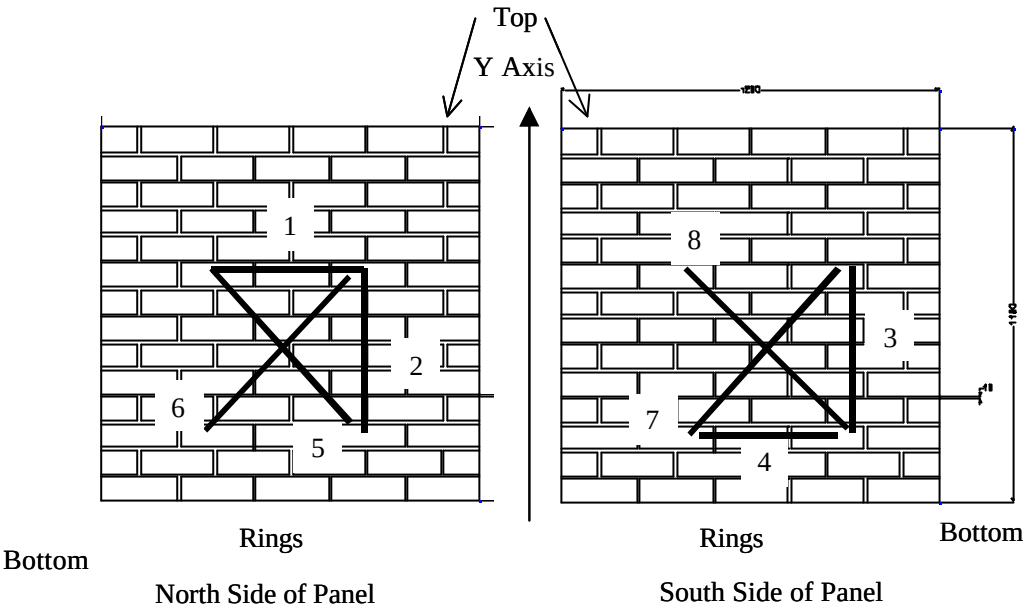

FIGURE 59 PANEL AP:8 GAUGE LOCATIONS

The type of strain gauge for each of the eight locations is tabulated in Table 64.

TABLE 64 PANEL AP:8 GAUGE DETAILS FOR THE DYNAMIC TESTS

Location or offset	Type used for gauge	Length (mm)
1	RR 1	480
2		524
3		
4		480
5	RR 2	711
6		
7		
8		

The data channel numbers for the files generated for the experiments are presented in Table 65.

TABLE 65 PANEL AP:8 CHANNEL DETAILS

Channel	Unit	Calibration Details
0	1	1 V equals 0.2 mm (Hard coded into the Fortran programs.)
1	2	
2	3	
3	4	
4	5	
5	6	
6	7	
7	Failed	
8	ITM Load	1 V equals 100 kN
9	ITM Displacement	1 V equals 100 mm
10	Static Arm Pressure X	5 V equals 68.9 MPa
11	Static Arm Pressure Y	
12	8	Replaced 7

A.10.3 TEST PROTOCOL

Panel AP: 8 was tested for 96 tests of minimum test duration of thirty or ninety seconds. The test frequency summary for panel AP: 8 is presented in Table 66.

TABLE 66 PANEL AP:8 FREQUENCY AMPLITUDE TEST DETAILS

Amplitude mm	Amplitude Units	Frequency					
		0.06	0.10	0.3	1.0	5.0	10.0
2.5	1.0	1-15	16-30	31-33	34-36	38-40	41-43
3.8	1.5	44-46	47-49	50-52	53-55	56-58	59-61
5.0	2.0	66-70	71-75	76-80	81-85	86-90	91-95
6.3	2.5	96					

A.10.4 TEST RESULTS

The results for the measured shear stiffness for each test are shown in Figure 60.

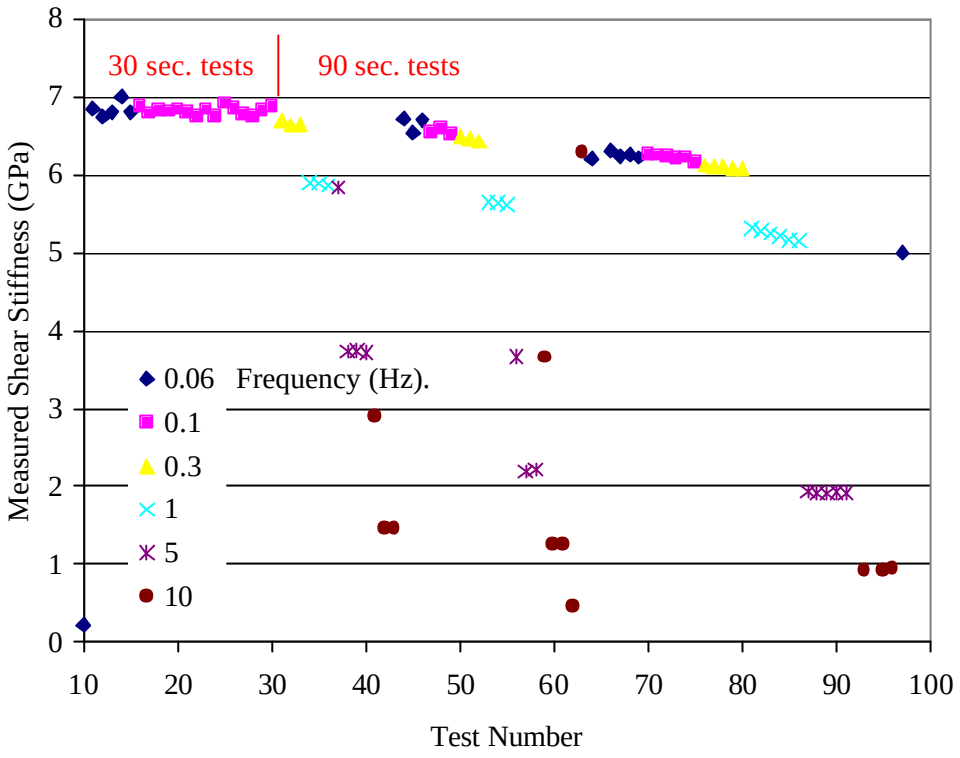

FIGURE 60 PANEL AP:8 MEASURED SHEAR STIFFNESS

The measured shear stiffness against the strain level is plotted in Figure 61.

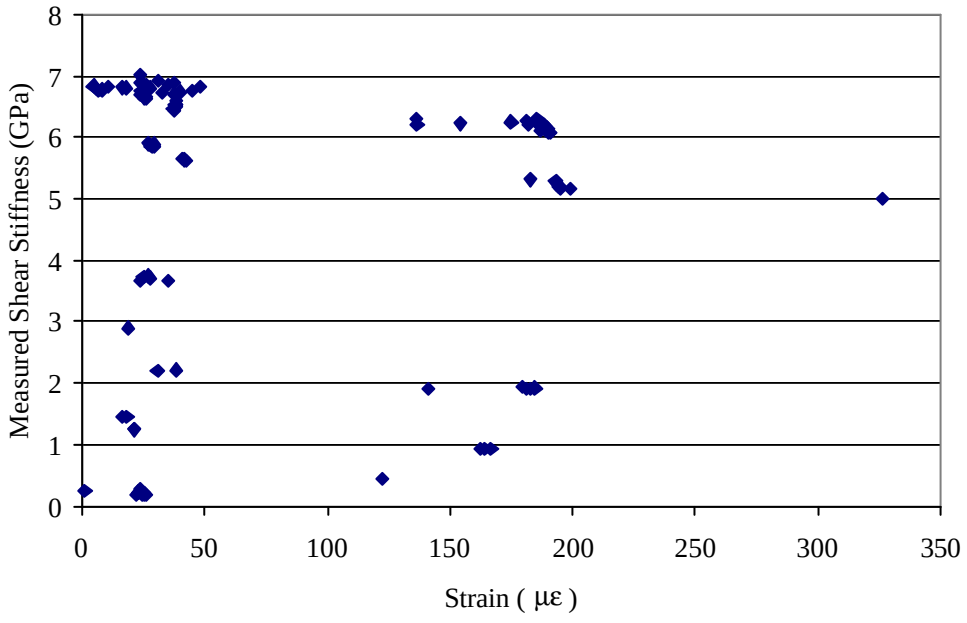

FIGURE 61 PANEL AP:8 MEASURED SHEAR STIFFNESS

The test panel was damaged in two tests with a frequency of 0.06 Hz. The panel reached a peak load of approximately 191 kN at test 66. The jump in the strains at this test and the test at failure are significant. The value for the shear stiffness during the last test was estimated as the panel failed at the beginning of the test. The strains used for calculating the tangent stiffness were adjusted for this plot to allow for the two significant steps.

The damage parameterization details for the effective stiffness are presented in Table 67.

TABLE 67 PANEL AP: 8 DAMAGE PARAMETER

Strain (με)	Damage Parameter D
23	0.00
136	0.10
195	0.25
326	0.30

A.10.5 DISCUSSION OF THE TEST RESULTS

This panel illustrates the intrinsic variability in the strength of masonry panels. The peak load of 191 kN during the test process has caused a step in the strains in the panel that can be attributed to failure on the weakest plane during the slow tests. This mechanism is identified in other experiments as the static failure mechanism. The degradation of the masonry continues to accumulate up to the point of failure. The material exhibits the behaviour of a brittle material with inferior tensile strength. The test pattern changes were a mistake in hindsight as was the rapid increase in the amplitude. The results showed that the loading pattern required revision to provide additional detail during the test process.

A.11 MEASURED STIFFNESS RESULTS FOR PANEL AP: 9

A.11.1 INTRODUCTION

This section presents the results for Panel AP: 9. This panel was loaded with a systematic pattern that further investigated the degradation of the panel at constant amplitude levels. The prestress load was set to 150 kN, which is half the peak load recorded for Panel AP: 5 in a straight shear test. The method repeated the frequency block before increasing the amplitude. The change was designed to provide a frequency set having equal energy levels avoiding the frequency 0.06 Hz, which required long test times for a complete cycle.

A.11.2 TEST METHOD

The locations for the gauges are shown on Figure 62. The failure plane for this panel is shown on the figure. This failure plane formed at the greatest distance from the central area of the panel out of all failures observed during this test program.

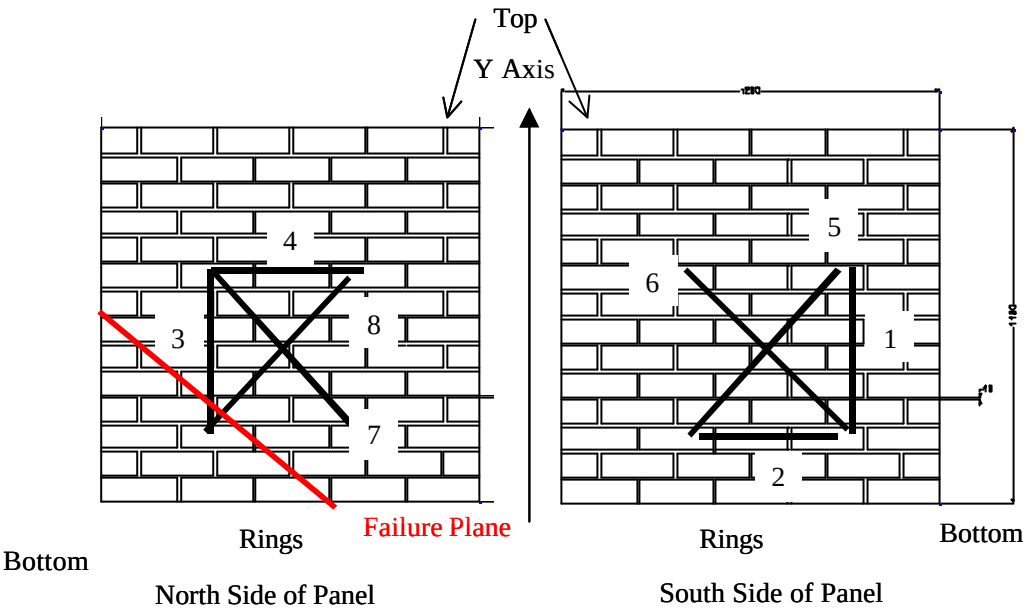

FIGURE 62 PANEL AP:9 GAUGE LOCATIONS

The type of strain gauge for each of the eight locations is tabulated in Table 68.

TABLE 68 PANEL AP:9 DYNAMIC TESTS - GAUGE DETAILS

Location or offset	Type used for gauge	Length (mm)
1	RR 1	524
2		480
3		524
4		480
5	RR 2	711
6		
7		
8		

The data channel numbers for the files generated for the experiments are presented in Table 69.

TABLE 69 PANEL AP: 9 CHANNEL DETAILS

Channel	Unit	Calibration Details
0	1	1 V equals 0.2 mm (Hard coded into the Fortran programs.)
1	2	
2	3	
3	4	
4	5	
5	6	
6	7	
7	Failed	
8	ITM Load	1 V equals 100 kN
9	ITM Displacement	1 V equals 100 mm
10	Static Arm Pressure X	5 V equals 68.9 MPa
11	Static Arm Pressure Y	
12	8	Replaced 7

A.11.3 TEST PROTOCOL

Panel AP: 9 was tested for 50 tests. The test pattern is presented in Table 70. The amplitude was provided in the output files. The amplitude was constant throughout the tests.

TABLE 70 PANEL AP: 9 TEST PATTERNS

Frequency (Hz)	Setting on ITM (Hz)	Amplitude (mm)	Replicates	Test Numbers	Comment
0.1	0.09	2.2	5	5	1A and B Ramp up
0.2	0.18			10	
0.32	0.29			15	
0.65	0.61			20	
1	0.9			25	
2	1.8			30	1 extra test
3.1				35	
6.5				40	41A back to 150kN
10				45	
0.1				50	Failure

A.11.4 TEST RESULTS

The results for the measured shear stiffness for each test are shown in Figure 63.

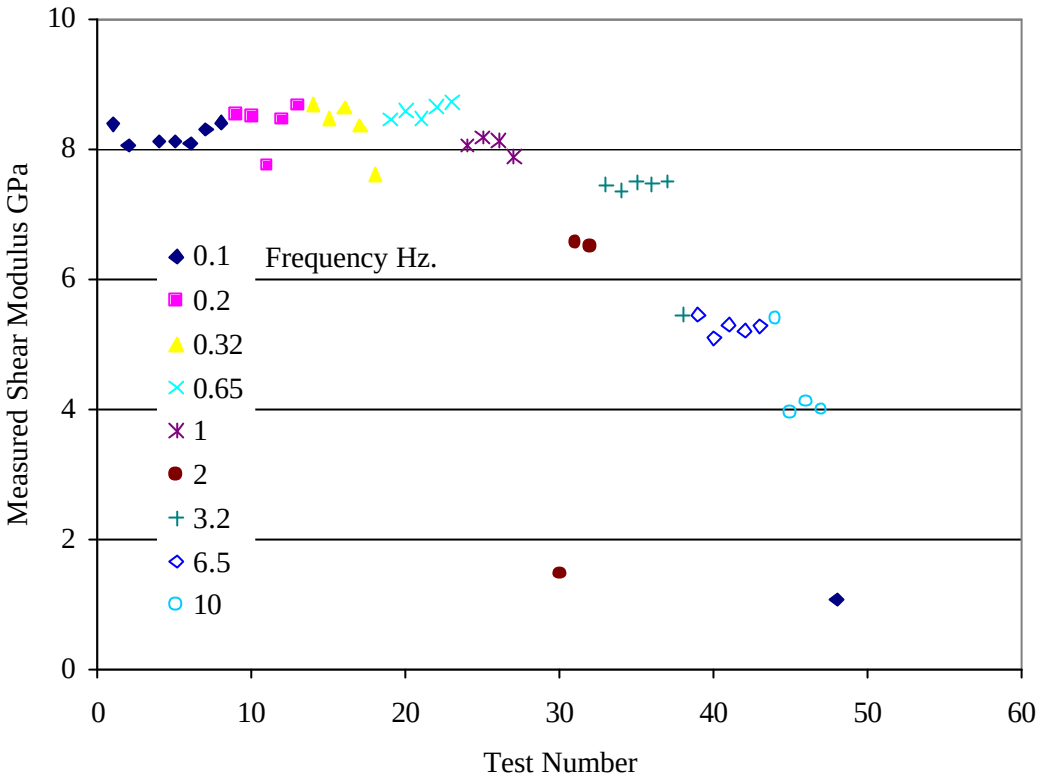

FIGURE 63 PANEL AP:9 MEASURED SHEAR STIFFNESS

The damage parameterization is presented in Table 71.

TABLE 71 PANEL AP:9 DAMAGE PARAMETER

Strains (με)	Damage Parameter
0	0
55	0.07
105	0.11
365	0.83
381	0.55

.

A.11.5 DISCUSSION OF THE TEST RESULTS

The test results for this panel confirmed the applicability of the revised frequency pattern. The failure plane was a small plane near the base of the panelthat failed at an early test. This strain point is considered to be on a weak plane of this panel. The last few tests at 0.1 Hz demonstrated that the panel had been damaged during the cyclic loading and that the effective stiffness had degraded. The strain data was adjusted for the specific jumps.

A.12 MEASURED STIFFNESS RESULTS FOR PANEL AP: 10

A.12.1 INTRODUCTION

This section presents the results for Panel AP: 10. The static pressure on the Y axis was raised to 2.7 MPa to avoid premature failure.

A.12.2 TEST METHOD

The locations for the gauges are shown on Figure 64.

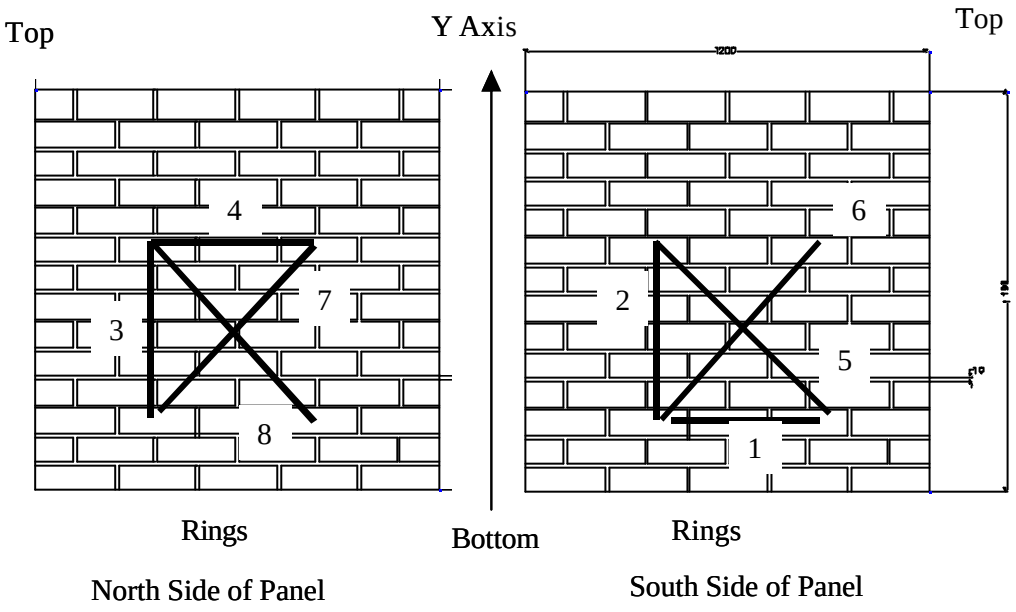

FIGURE 64 PANEL AP: 10 GAUGE LOCATIONS

The type of strain gauge for each of the eight locations is tabulated in Table 72.

TABLE 72 PANEL AP: 10 DYNAMIC TESTS - GAUGE DETAILS

Location or offset	Type used for gauge	Length (mm)
1	RR 1	480
2		524
3		
4		480
5	RR 2	711
6		
7		
8		

The data channel numbers for the files generated for the experiments are presented in Table 73.

TABLE 73 PANEL AP: 10 CHANNEL DETAILS

Channel	Unit	Calibration Details
0	1	1 V equals 0.2 mm (Hard coded into the Fortran programs.)
1	2	
2	3	
3	4	
4	5	
5	6	
6	7	
7	Failed	
8	ITM Load	1 V equals 100 kN
9	ITM Displacement	1 V equals 100 mm
10	Static Arm Pressure X	5 V equals 68.9 MPa
11	Static Arm Pressure Y	
12	8	Replaced 7

A.12.3 TEST PROTOCOL

Panel AP: 10 was tested using the frequency pattern established for Panel AP: 9. This pattern uses a revised set of frequencies that are approximately equally spaced in energy terms and the frequency block was repeated at each amplitude level twice. The amplitude details are provided in Table 74. The testing from test 623 to 801 was designed to provide large blocks of data at a constant amplitude and frequency.

TABLE 74 PANEL AP: 10 AMPLITUDE PATTERN

Test Number Start	Test Number End	Amplitude (mm)	Frequency Block repeat
1	90	1.27	Twice
91	180	2.54	
181	270	3.81	
271	360	5.08	
361	450	6.35	
451	540	7.62	
541	622	8.89	
622	710	4.0	10 Hz
710	780	12.2	1 Hz
781	791	16.0	
792	801	18.0	

A.12.4 TEST RESULTS

The results for the measured shear stiffness for each test are shown in Figure 65.

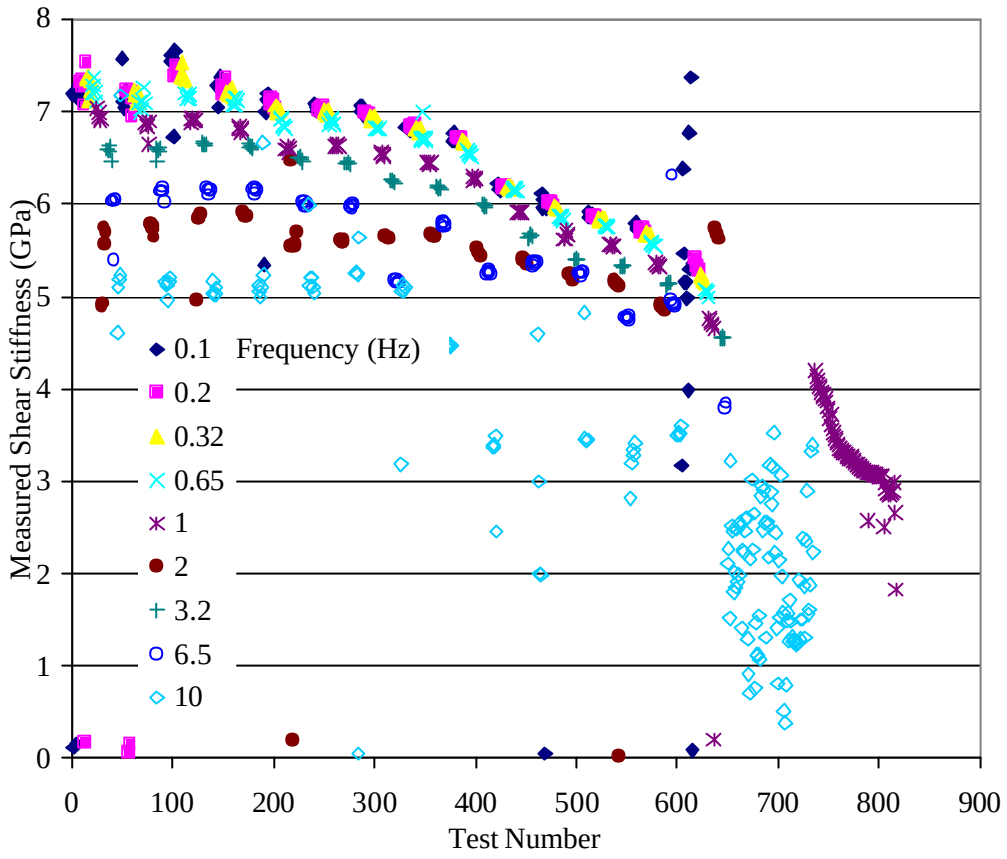

FIGURE 65 PANEL AP:10 MEASURED SHEAR STIFFNESS

The measured shear modulus against the shear strain is plotted in Figure 66.

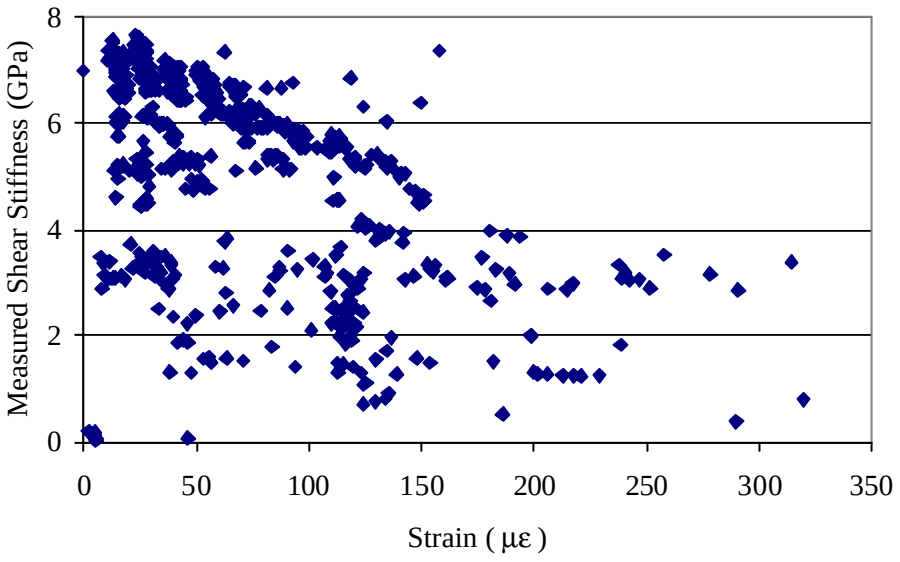

FIGURE 66 PANEL AP:10 MEASURED SHEAR MODULUS

The boundary lines that delineate the feasible solution spaces for the measured shear stiffness are self evident in the last two figures. These limits represent the effective stiffness at the time of the test. The damage parameter estimates for the panel are shown in Figure 67.

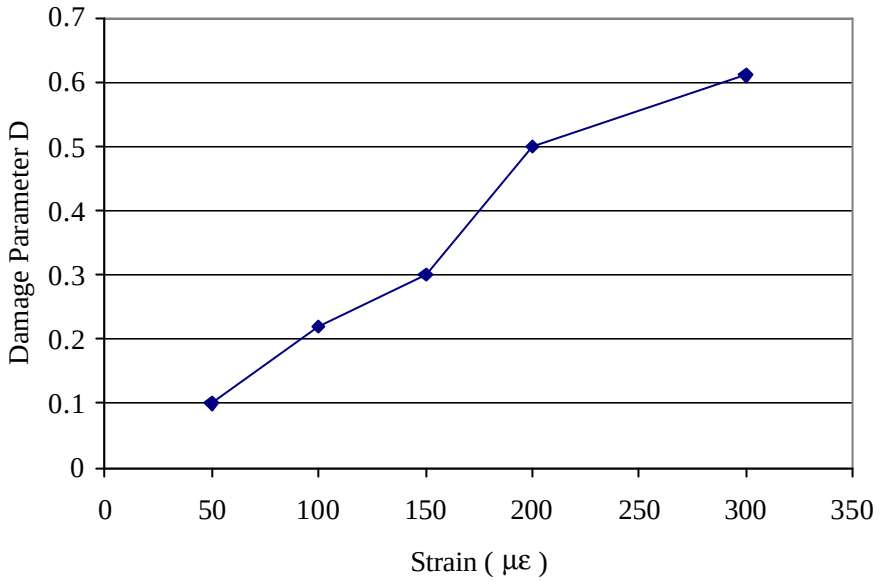

FIGURE 67 PANEL AP:10 DAMAGE PARAMETER

The estimated values for the damage parameter at a series of strains are shown in Table 75.

TABLE 75 PANEL AP:10 DAMAGE PARAMETER

Shear Strain (με)	Damage Parameter D
50	0.1
100	0.22
150	0.3
200	0.5
300	0.61

A.12.5 DISCUSSION OF THE TEST RESULTS

This set of results illustrates the direct relationship between the effective stiffness and the measured stiffness. The results are consistent with the previous panel results. The repeated pattern of the frequencies is visible in each amplitude block in Figure 65. The increasing rate of damage at higher amplitudes, and hence strain rates, is evident.

A.13 SUMMARY

The existing observational data supports the conclusions that a ceramic material responds differently to static and a dynamic loading of equivalent force levels. The statistical experimental method used the approach of holding one variable constant and systematically varying another variable. This standard method has gathered sufficient statistical information to provide:

I. Confirmation of the differences between the effective and the measured stiffness. These differences confirm the existing observational data related to the terms static stiffness and dynamic stiffness.
II. An estimate of the numerical values for the effective shear stiffness as a function of the loading, which leads directly to the maximum strains at specific test points.

A.14 SHEAR WALL REGRESSION RESULTS

A.14.1 INTRODUCTION

The regression analysis provided information on the statistical properties of the data sets. This appendix presents typical static and dynamic linear regression results for the measured stiffness. The results are provided for panel AP: 4 as a static test and for panel AP: 6 as a dynamic test. The panel AP: 6 test had a 1 Hz forcing function and the test was mid range in the group of tests. The purpose of providing the results is to confirm that the normal probability assumption made for the linear regression analysis was reasonable.

A.14.2 PANEL AP: 4 REGRESSION RESULTS

A typical statistical analysis for the Young's modulus is presented for a pristine sample stage of panel AP: 4. The details of the results are presented in Table 76.

TABLE 76 PANEL AP: 4 YOUNG'S MODULUS ESTIMATE

Description	Result
Panel Number	AP: 4
Test Number	002
Test type	Quasi-static ramp up of the prestress shear
Face	North
Direction of measurement	X
Young's modulus	24.7 ± 0.4 GPa

The statistical package used for this linear regression plot provides results for the normal probability plot and the residuals plot for the data. The linear regression of the Young's modulus data points for panel AP: 4 is shown in Figure 68.

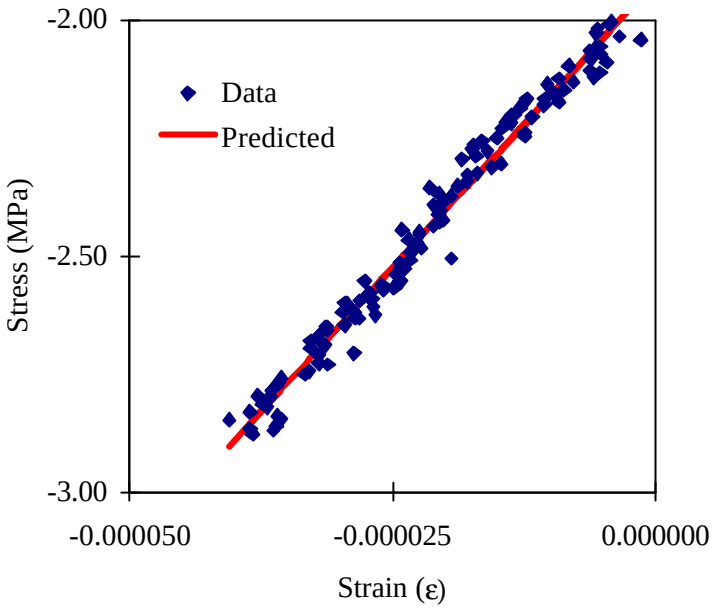

FIGURE 68 PANEL AP: 4 YOUNG'S MODULUS

The tabulated results from the regression analysis of panel AP: 4 test 002, which is shown in Figure 68, are presented in Table 77 and Table 78.

TABLE 77 PANEL AP: 4 LINEAR REGRESSION PARAMETERS

	Coefficients	Standard Error	t Statistic
Intercept	-1.91E+06	5.91E+03	-322
Slope	2.47E+10	2.39E+08	103

TABLE 78 PANEL AP: 4 LINEAR REGRESSION STATISTICAL PARAMETERS

Statistical Parameter	Value
Multiple R	0.993
R Square	0.986
Adjusted R Square	0.986
Observations	150

These results indicate that the material is reasonably elastic and is loaded well below the yield point. The purpose of the normal probability plot and the residuals plot is to present a data set of the difference between the linear fitted line and the raw data points. These plots provide a visual check of the validity of the underlying statistical assumptions.

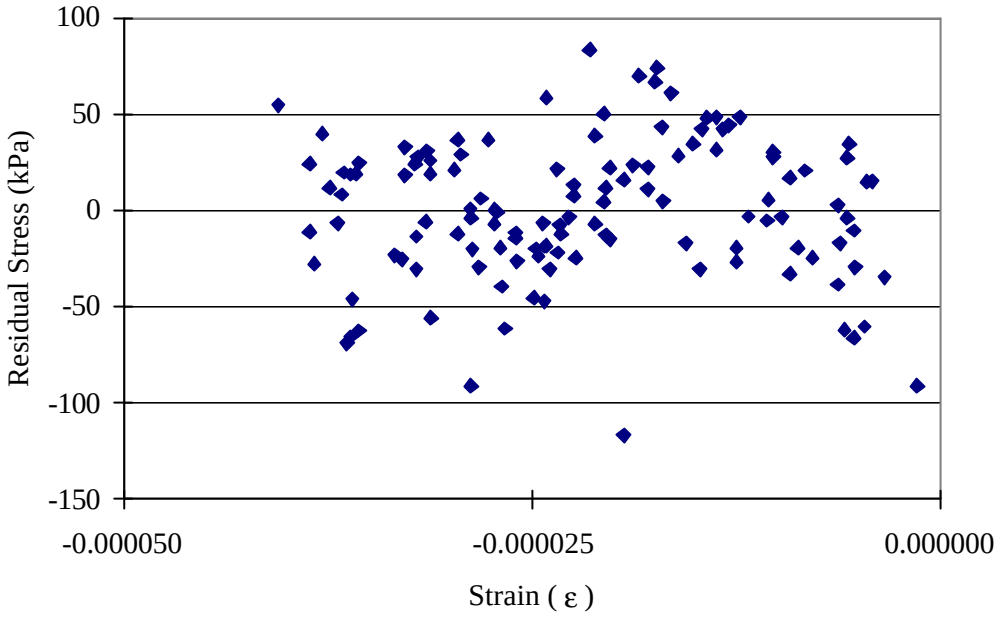

FIGURE 69 PANEL AP:4 TEST 2 - NORMAL PROBABILITY PLOT

The distribution of the residuals of the linear regression analysis for the test number 2 on panel AP: 4 is shown in Figure 70.

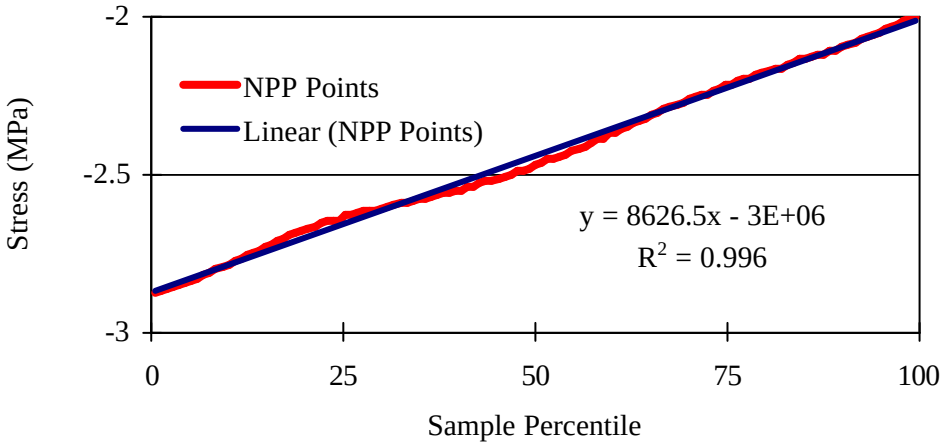

FIGURE 70 PANEL AP:4 TEST 2 - RESIDUAL PLOT

This result has a linear regression coefficient of 0.996. This result implies that that the data is normally distributed and that the assumptions underlying the linear analysis are reasonable.

A.14.3 PANEL AP: 6 REGRESSION RESULTS

A typical regression curve has been selected for panel AP: 6. This data was from an experiment at mid range in the total tests. It was test number 322 run at a frequency of 1 Hz. The results are presented in Figure 71.

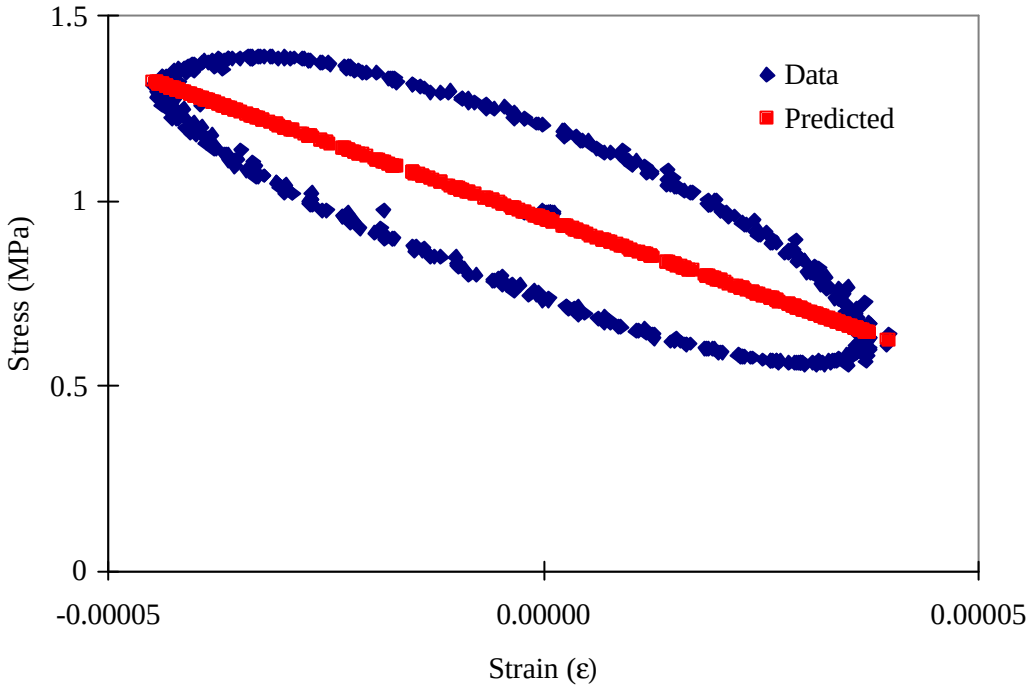

FIGURE 71 PANEL AP: 6 MEASURED SHEAR STIFFNESS LINEAR REGRESSION

The results for the linear regression are presented in Table 79.

TABLE 79 PANEL AP: 6 LINEAR REGRESSION FOR A 1 HZ TEST

	Coefficients	Standard Error	t Statistic
Intercept	952000	7200	132
Slope	8.27E+09	2.58E+08	32

The results for the linear regression analysis are presented in Table 80.

TABLE 80 PANEL AP: 6 LINEAR REGRESSION PARAMETERS

Statistical Parameter	Value
R Square	0.667
Observations	514

A summary of the statistics from the test 322 on panel AP: 6 is presented in Table 81.

TABLE 81 PANEL AP: 6 STIFFNESS RESULTS FOR TEST 322

Description	Result
Panel Number	AP: 6
Test Number	322
Test type	1 Hz
Face	Mean result
Direction of measurement	Vertical
Measured shear stiffness ± standard error	8.3 ± 0.3 GPa

The results for the normal probability plot for a 1 Hz test are shown in Figure 72.

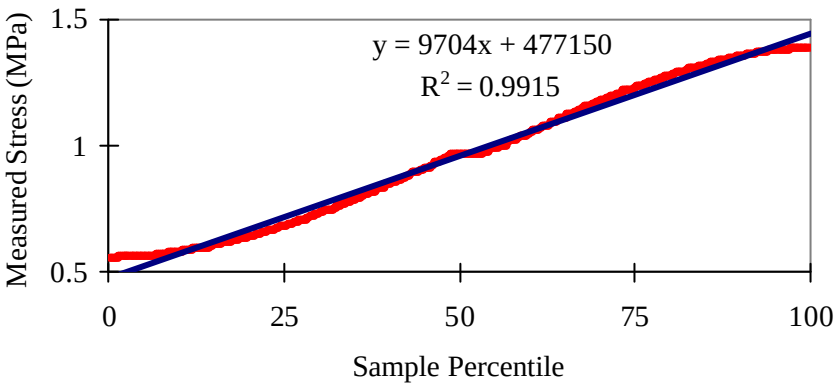

FIGURE 72 PANEL AP: 6 NORMAL PROBABILITY PLOT - 1 HZ TEST

These results show a cyclic pattern consistent with observations on Figure 71 for the linear fit. The results are consistent with the observations and comments given by Benedetti and Pezzoli (1996), which are graphically illustrated in Figure 5.[319] The results show the impact of the acceleration term that contains an w^2 component. A moderately elliptical shape was evident in Figure 71. A test frequency of 1 Hz is reasonably close to the quasi-static limits of 0.3 to 0.4 Hz. This result was evident in the regression coefficient of 0.99.

[319] Refer pg. 68.

The results for the residuals plot for the linear regression analysis of the measured stiffness for panel AP: 6 are shown in Figure 73. These results demonstrate the acceleration component.[320]

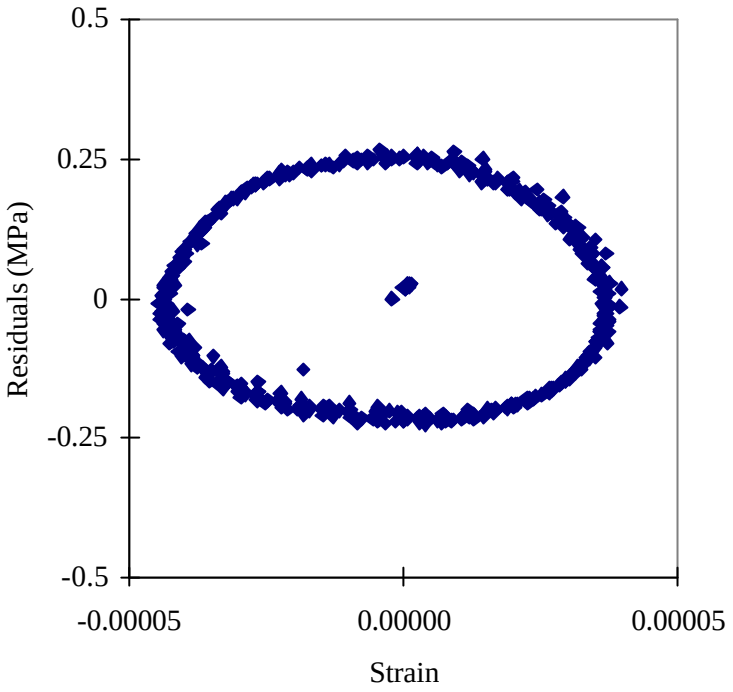

FIGURE 73 PANEL AP:6 RESIDUALS PLOT FOR THE LINEAR REGRESSION ANALYSIS

A.14.4 COMMENTS

In comparing the results shown in Figure 68 to those results shown in Figure 71, the affect of the frequency term is evident. The result of the increasing frequency is that energy is absorbed in the acceleration and damping terms. These cause an apparent reduction in the quantum of the forcing function. This reduction in the quantum of the forcing function results in a decrease of the average measured stiffness as the frequency increases.

The assumption of Gaussian distribution is reasonable for the estimation of the effective stiffness from measured stiffness tests at low frequency. The higher frequency test clearly includes a systematic error induced by the harmonic forcing function and the frequency of the test.

[320] The frequency is evident and matches the results expected from the work of Benedetti and Pezzoli (1996).

Appendix B The Mechanics of Stiffness

B.1 INTRODUCTION

The study of a degrading manifold structure requires mathematics from the fields of elasticity, harmonic motion, damage mechanics, and fracture mechanics of continuums. The mathematical techniques that are used in this appendix include Fast Fourier transforms, non-linear regression, and a small number of standard statistical methods (Kaplan and Lewis, 1971; Halliday and Resnick, 1971; Chopra, 1995; Lekhnitskii, 1963; Krajcinovic, 1996; Brigham, 1988; Kuczera, 1971). Two distinct mathematical entities are studied in this review of the theory of stiffness. The first entity is the effective stiffness that is deemed the mathematical functional representation of the stiffness defined explicitly by the displacement term of the differential equation of motion for a harmonic function. This functional representation has no frequency dependence (Kaplan and Lewis, 1971, 554; Krajcinovic, 1996). The second entity is the measured stiffness that is defined to be the experimentally determined stiffness obtained by dividing the stress field results by the strain field results for each recorded time step (Paulson and Abrams, 1990). The term stiffness is applied to both mathematical operators. The effective stiffness conforms to the physical sciences implicit definition of stiffness without a frequency component. The term $k^2(t)$ is used to define the effective stiffness, while $l^2(t)$ is termed the measured stiffness and is adopted to be consistent with the conventional engineering definitions of stiffness. The measured stiffness term is an operator, which includes a stiffness component.

This appendix defines the theoretical development for each stiffness operator and derives the mathematical theory that accounts for the properties of each operator and the relationship between the two entities. This theory relates the two defined stiffness operators to the observed static stiffness and dynamic stiffness detailed in Chapter 2. The effective stiffness is foremost a design parameter, except in tightly controlled and monitored experiments that use extremely stiff rigs, the effective stiffness is not directly measurable, but is represented as a limit of a function (Sugo, pers. comm., 1998; Bolotin, 1964, 31; Chopra, 1995, 9, equation 1.3.1; Krajcinovic, 1996; Kaplan and Lewis, 1971, 100). The elastic stiffness constants are the upper bound for the stiffness functions (Krajcinovic, 1996). The time and strain dependent properties of the effective stiffness function are of direct interest in the study of degrading structures. The appendix addresses the theory of elasticity in which the necessary mathematical primitive (Borowski and Borwein, 1989) of an invariant intrinsic set of moduli is shown to be acceptable from

previous experimental shear observations. The model type is reviewed and selected. The measured shear stiffness results for the first panel tested dynamically are presented and discussed. A relationship is derived between the effective stiffness and the measured stiffness using a limiting set of conditions. The stiffness definitions are explored to determine the physical meaning of each of the two stiffness operators within the mathematics of a harmonic forcing function. Finally, the static frequency limit is defined from the theoretical analysis and the experimental results.

B.2 THEORY OF ELASTICITY

B.2.1 INTRODUCTION

The theory of elasticity is based on the concept of a continuum, which in mathematical terms is called a manifold (Masiani, Rizzi and Trovalusci, 1995). The concept of a manifold leads directly to the field of boundary elements and the discrete structured continuums of the finite elements (Crouch and Starfield, 1983; Segerlind, 1983; Page, 1979). The interaction between distinct manifolds is an interesting phenomenon. It is extensively studied in masonry in the field of serviceability of masonry walls and geotechnical engineering in the study of in situ properties of soil materials (Muniruzzaman, Page and Kleeman, 1996; Abbo and Sloan, 1996). These studies of fine materials and cracked masonry are beyond the scope of this research work. The research is limited to a continuum, even if the problem is one of a discrete structured continuum rather than a Cauchy continuum (Page, 1979; Masiani, Rizzi and Trovalusci, 1995). The properties of interest for a manifold are based on Theorem 1:

Theorem 1: If M is a compact orientated k dimensional manifold with boundary and ϕ is a (k-1) form on M, then

(42) $$\int_M df = \int_{dM} f$$

Comment: The theorem attributed to Green is a special case of Stokes' Theorem for a two-dimensional manifold with boundary (Spivak, 1965,124). There exists the condition for crack growth for a manifold with an expanding surface. The principal difficulty in studying this problem is the mathematics of the creation of two manifolds both compact from a single compact manifold. This is the mathematics of crack growth, which may imply a change in the measured stiffness and the thermodynamic properties used as part of the study of the damage parameterization. This theorem highlights the problem of the change in surface affecting the internal properties of the material and implies a level of

sophistication with the physical measurements, which is simply beyond the current scope of masonry research for samples of the size investigated in this research work.

This study of crack growth into the manifold is a future area of research work. This proposed research could use small tensile samples tested in a dynamic rig requiring the mathematical sophistication implied by the requirements of this theorem and allowing for the fundamentals of thermodynamics (Sugo, 2000, pers. comm., 1999; Ioakimidis, 1993; Krajcinovic, 1996).

B.2.2 CONTINUUM MECHANICS

A magnified section of brick showing the grain structure is presented in Figure 74.

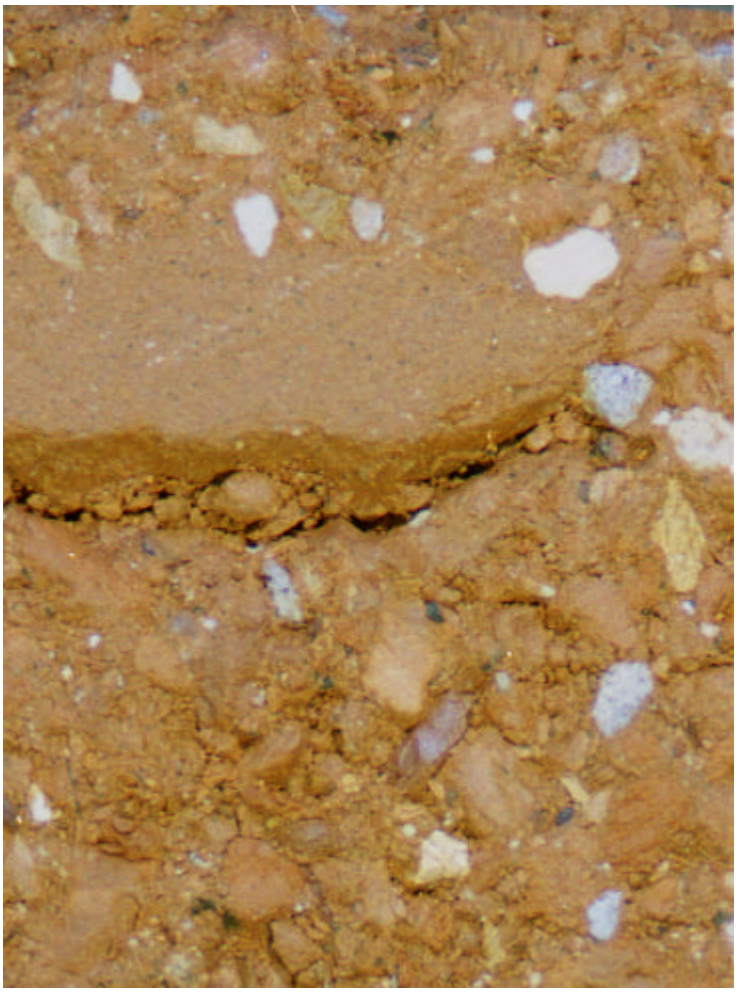

FIGURE 74 BRICK GRAIN STRUCTURE

Elastic analysis of materials assumes a continuum. The assumptions required to establish any theory constrain its applicability. This type of material is represented as a continuum within each discrete element of the structured continuum. The use of average strain and

stress fields in such a material provides a potential for a scatter in the results, particularly between distinct samples. The typical error level in masonry experiments is ±25 %. This level of error can be attributed to the natural variation in the material properties within a single group of bricks. This constraint is a fundamental issue in the field of masonry experimentation

B.2.3 EXPERIMENTAL RESULTS FOR THE MEASURED SHEAR STIFFNESS

A typical set of results for Panel AP: 6 is presented in Table 82.

TABLE 82 PANEL AP: 6 MEASURED SHEAR STIFFNESS

Measured Shear Stiffness (GPa)	Value ± Error	% Error
XY Southern Side	8.4 ± 0.2	5
XY Northern Side	4.1 ± 0.16	8
YX Southern Side	7.4 ± 0.1	3
YX Northern Side	6.3 ± 0.1	4
Mean Value	6.5 ± 1.6	24

This test[321] was conducted at a frequency of 1 Hz and a displacement of 6.35 mm. It was a mid range test in the 640 tests. The measurements from a single 30 second test show a high repeatability of the basic measurements of displacement across the shear wall element. A simple error analysis demonstrates the problem associated with assuming an isotropic material for the analysis of the results. The error in 5 V was ±2.4 mV. The calibration of the gauge introduces a systematic error into the calculation of the measured stiffness, but it does not contribute to the random error in a particular set of 30 second tests. The peak voltage of ±5 V provides a minimum error of about five parts per million. The ITM output provides an error of about 1 % from the ITM's electronics, and the 2.4 mV per reading was the absolute limit on the WaveView card. A calculation using accepted error theory provides an error of 2 % in the calculation of the random error for the effective shear stiffness. The systematic errors introduced by the constants used in the equations are not considered in this analysis as in the error analysis the interest was in relative values not absolute values. Student's t test results (Miller and Freund, 1977) supported the hypothesis that at the 5 % confidence level that the four values for the stiffness in Table 82 are statistically different. It is reasonable to conclude that the mean value is an acceptable engineering design value. However, it is not a sound representation of the data set of effective stiffness for the test results for the purposes of this research.

[321] This test was given a laboratory designation of 245B322.

The ability to measure the stiffness with finer and finer accuracy means that there are difficulties with the mathematical theory of isotropicity. To resolve the issue in this case the assumption is made that the material was orthotropic increasing the level of complexity of the analysis. The shear stiffness, which is still linear in this model, can be measured with the least error, but it will still suffer from the problem that the mean error of the averaged readings is not statistically related to the error in each individual reading.

B.2.4 THEORY OF AN ORTHOTROPIC ELASTIC MATERIAL

Lekhnitskii, (1963) provides a sound formulation of the theory of an orthotropic elastic material. The elastic constants for an orthotropic material are the two Young's moduli, the Poisson's ratios, and the shear modulus. The shear modulus is linear in one equation, while the other four constants are non linear in three equations.

These equations are presented as follows:

(43) $$e_{xx} = \frac{1}{E_{xx}} t_{xx} - \frac{u_{yx}}{E_{yy}} t_{yy}$$

(44) $$e_{yy} = -\frac{u_{xy}}{E_{xx}} t_{xx} + \frac{1}{E_{yy}} t_{yy}$$

(45) $$e_{xy} = \frac{1}{2G_{xy}} t_{xy}$$

(46) $$u_{yx} E_{xx} = u_{xy} E_{yy}$$

It is a primitive of the theory of damage mechanics that Young's modulus is an intrinsic invariant property and that the effective stiffness is a distinct measure quite separate to this intrinsic property (Krajcinovic , 1996). The mathematical statement that this primitive of damage mechanics makes is presented formally as:

Primitive 1: The effective stiffness, $G(t)$, has an invariant maximum value, K_0, that obeys the relationship $K_0 > G(t)$.

Supporting statement: The experimental work that supports this primitive is shown in Figure 8.[322] This is shown on the tangent stiffness on their Graph 4(a). The slope of the effective stiffness, $G(t)$, at the point 0.004 and 0.008 demonstrates that the function $G(t)$ is a concave function and equally demonstrates that it is a downward concave

[322] Refer pg. 76.

function. This property is also evident in the work on Salem limestone (Krajcinovic, 1996). This problem is reduced to one of what is the maximum of this type of function in a closed domain. Kaplan and Lewis (1971, 136) present the relevant proof.

B.3 MEASURED SHEAR STIFFNESS

B.3.1 INTRODUCTION

The experimental observation documented in the literature is that there are two distinct stiffness responses for a ceramic. These are a static stiffness and a dynamic stiffness discussed in section 2.2.3. This observation suggests that the problems are in determining what is the physical meaning and what is the mathematical theory that explains it.

B.3.2 HYPOTHESES

This problem can be stated succinctly as three hypotheses. The first hypothesis looks to establish the formal relationship between the effective stiffness and the measured stiffness. The second hypothesis proposes that the dynamic stiffness is not a separate phenomenon and directly implies that it can be quantified using existing techniques. The purpose of this appendix is to use the results from the analysis to show that the stated hypotheses are acceptable for masonry.

The hypotheses are:

Hypothesis 1: The effective stiffness can be derived from the measured stiffness data under some set of test conditions.

Proof: These conditions are derived and the hypothesis is tested on the data from the panel experiments.

Hypothesis 2: For this mathematical derivation of the stiffness, the dynamic stiffness *per se* does not exist as a separate phenomenon.

Comment: This hypothesis requires that this dynamic stiffness can be explained by current dynamic theory and by consideration of the measurement issues related to each of the experimental results. In the case of the results measured by Paulson and Abrams (1990), is the fundamental primitive related to the loading patterns too simplistic an assumption or is something interfering with the measurements?

This appendix presents the mathematics of a simple harmonic oscillator and extends the theory with strict limitations to a time varying constants model. These limitations are provided to keep the mathematics tractable and within the bounds of the meaning and error limits of the experimental measurements. The definition of the effective shear stiffness is then discussed. This section explains the preference for using this parameter for the encapsulation of the damage parameter. It forms one of the direct components of the stiffness of the test rig and shear wall elements. The initial results from panel AP: 3 are discussed to illustrate the properties that have been measured in the experiments (Nichols and Totoev, 1999). These are provided to illustrate the effect that batch testing has on the measured stiffness when compared to the continuous results obtained using the recent Canadian reinforced concrete tests of Stevens *et al.* (1991). This difference in the results of the experiments is used subsequently to investigate the properties of the mathematical explanation of the observed dynamic stiffness. The properties of the effective stiffness are then related to this dynamic stiffness concept based on the results from the experimental data.

B.3.3 MATHEMATICS OF A SIMPLE HARMONIC OSCILLATOR

The mathematics of a simple harmonic oscillator is dependent upon the mass, stiffness, and damping terms. The classical engineering form for the equations is presented in Chopra (1995, 15-27), which is identical in mathematical terms to the formulation in Kaplan and Lewis (1971).

The implicit assumption in each of these texts is that the system is based on the theory of linear elasticity. This mathematics is extended with a set of reasonable assumptions to present an alternative formulation using time dependent quantities. It is assumed that these quantities vary at slow enough rates that the derivatives of the functions can be ignored in the analysis.[323]

The conceptual difficulty in the mathematics is the damping term that is expressed as a function of the velocity term. This representation adds significantly to the complexity of the harmonic analysis and may disguise the straightforward explanation of the observed dynamic stiffness. The experimental rig is designed to be closer to its mathematical representation than the average structure. It is designed to have a low damping factor, so that discarding that term in the calculus is acceptable as a first assumption. The simplest representation of the simple harmonic system is thus of the form shown in Figure 75.

[323] This point on the rate of change of the derivates being negligible is important in the analysis and is the assumption that provides a tractable solution.

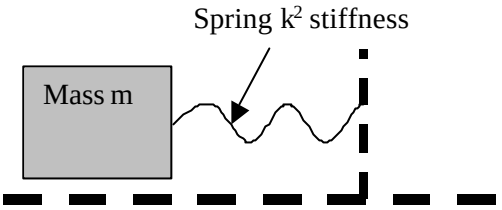

FIGURE 75 SIMPLE HARMONIC SYSTEM

In this system, which has no damping component or forcing component, the simple equation of motion based on Newton's second law (Kaplan and Lewis, 1971, 554) is:

(47) $$ma + k^2 x = 0$$

This generates a simple harmonic motion with a natural frequency of:

(48) $$w^2 = k^2 / m$$

This physical representation provides the limiting points to the problems encountered in seismic analysis. The simple substitution of $G = k^2$ provides an engineered solution.

The solution to the differential equation (47) is of the form:

(49) $$x = A\sin(wt + g)$$

The functional representation of the equation $x = A\sin(wt + g)$ implies directly that all of the terms represent constants. This assumption is not acceptable in a degrading system. The assumptions made for the analysis of the results and the developments of the mathematical fragment for understanding a degrading system are listed in Table 83.

TABLE 83 ASSUMPTIONS FOR THE STIFFNESS DERIVATION

Number	Assumption
1	The stiffness is defined as a slowly varying, concave down, continuous function. The function is represented by the term $k^2(t)$.
2	The mass is constant, which on the surface is a trivial restriction, but in a real masonry situation the spalling of masonry can be significant. This analysis assumes no spalling.
3	The forcing frequency remains constant throughout the 30 second test.
4	The element being damaged in a measurable sense is the masonry element.
5	The strain field and the stress field in the central region are uniform and the principal axes remain coincident.
6	Deformations are infinitesimal.
7	The material is orthotropic.

B.3.4 Shear Modulus

The shear modulus is determined experimentally in accordance with the standard equations for a strain rosette in Megson (1996, 402). In this experimental procedure, the significant changes are in the shear stress and shear strain. The shear modulus is linear in the orthotropic model and has the greatest change in length and the least percentage error in the measurement. The encapsulation of the damage parameter is best represented using the effective shear stiffness.

B.3.5 Experimental Results

The first panel that was dynamically tested in the rig was Panel AP: 3. This panel was tested at a frequency of 1 Hz for the bulk of the experimental work. The last few tests were at a frequency of 5 Hz. The measured shear stiffness results for panel AP: 3 are presented in Figure 76.

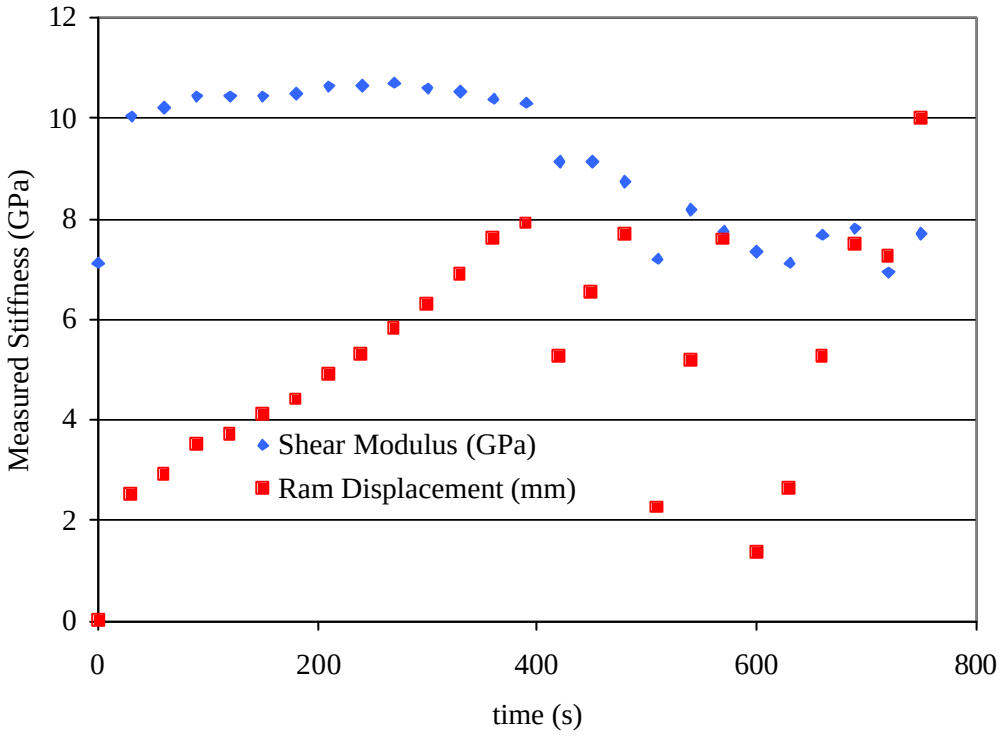

Figure 76 Panel AP: 3 Measured Shear Stiffness

These results do not contradict the first primitive[324] postulated by Krajcinovic (1996). There are a number of interesting features to be considered to determine whether they are significant or just part of the side effects from the set up of the test rig. The measured stiffness has a slight rise in the initial tests as the ram displacement is increased. This feature was commonly observed and was considered a seating of the shear yoke and the compression frame. It was not a significant material observation. The strain levels are not observed to follow the same pattern. The last few tests demonstrated that the frequency could be used to vary the results for the measured stiffness. This was at the point of failure and so the results pointed to the revisions in the loading pattern for subsequent tests, but were not in themselves considered significant. The difference between Stevens *et al*. (1991) and this test program is the continuous recording of data in the former experiments and the sequence of tests in this work.[325] The data from these earlier reinforced concrete experiments is useful in the derivation of the mathematics because of the continuity of the recording of the stiffness function.

The results demonstrate the degradation of the measured shear stiffness with the time of loading at a constant frequency level. Data were available to calculate the damage parameter. The critical damage parameter, D_c, for these tests was approximately 0.62 at a frequency of 1 Hz. The next step was to establish the method to obtain the effective shear stiffness from the measured shear stiffness data.

B.4 Relationship of Effective to Measured Stiffness

B.4.1 Introduction

This section of the appendix investigates the relationship between the two defined stiffness operators.

B.4.2 Damping Term

The damping term is defined to be a function of the velocity. If the resonant frequency is not approached too closely, then the damping term can be ignored in the first level of simplification. This assumption means that a simple function relates the acceleration to the displacement, which provides a method to establish the simplest meaning for the measured stiffness where the damping was low or negligible. After the relaxation of this

[324] Refer pg. 231.

[325] It is important to understand the difference. The earlier tests on the reinforced concrete was for a structure subject to a continuous loading, whilst our tests are for structures subject to short duration harmonic loads that were within the seismic range.

assumption for the damping, it was then possible to use nonlinear analysis to investigate the effective stiffness given a non-zero damping regime. The test rig's fundamental modes are about 4.5 to 5 Hz. Care was taken during the experimental work to avoid this region of the frequency domain.

B.4.3 METHODOLOGY

The development of the theory was undertaken in several stages. The calculus was designed to outline the distinct properties of the two stiffness operators. The operator $k^2(t)$ was deemed to represent the effective stiffness, which in the limit represents the relevant elastic stiffness constant. The procedure to develop the theory was to:

I. Examine the characteristics of the measured stiffness and then to determine its relationship to the effective stiffness.
II. Hypothesize that the effective stiffness acts as a bound to the measured stiffness.[326] This was formally stated as the first hypothesis.
III. Determine the functions that describe the limits for the measured stiffness. This function numerically approximates the effective stiffness.
IV. Determine a reasonable design limit for the lower bound to the frequency limit for the dynamic failure mechanism.

These limits and relations provide the information required to determine the encapsulation of the damage parameter in the time domain from the measured stiffness data for each set of experiments. This leads to the third hypothesis that relates the measured stiffness, $l^2(t)$, to the effective stiffness, $k^2(t)$, and establishes how the effective stiffness is derived from the measured stiffness data.

Hypothesis 3: An operator defined by the function $l^2(t)$ can be established that is equivalent in the limit as the frequency of loading approaches zero to the static Hooke's law. This $l^2(t)$ function has a defined frequency component whilst still satisfying the differential equation of motion.

Comment: The fundamental experimental observation was that there is a distinct difference in the static and the dynamic response. This hypothesis provides a method to

[326] This hypothesis is based on the use of the first primitive [pg. 231] to establish the first part of the hypothesis in which the elastic constants bound the effective stiffness.

investigate this difference and relate the difference to Newton's laws. The hypotheses form the main problem statement addressed in the appendix.

B.5 PROBLEM SOLUTION

B.5.1 INTRODUCTION

The method to demonstrate that the data is a reasonable fit to the hypotheses is outlined in this section of the appendix.

B.5.2 A SPRING SYSTEM

The mathematics of a spring coupled with a mass system is well known. Kaplan and Lewis (1970, 554) provide an elegant solution to the standard problem. The difficulty with the test rig system is that it is conceptually satisfying to model the system as a spring, mass, and dampener, but ignoring the damping permits a simple analysis system that does not use a transformation of variables that was the alternative approach. The simple engineering system is shown in Figure 77. This system can be treated as a mass on a spring responding to the forcing function. The transient solutions will die off rapidly and the steady state solution dominates the stress field and strain field results.

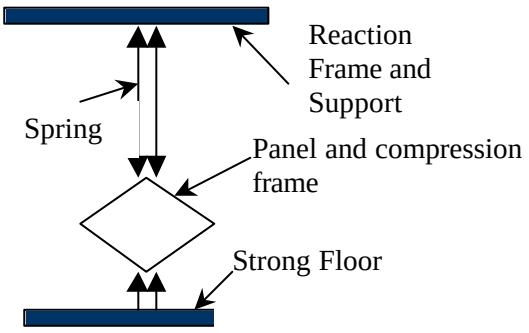

FIGURE 77 SIMPLE MATHEMATICAL MODEL

This simple mathematical assumption hides the reality that the mechanical system has a distributed mass and a rotational inertia.[327] However, a simple model is used in this section of the appendix to demonstrate the mathematical issues and analysis of results arising from a dynamic system that consists of a large concentrated mass vibrating on thin

[327] We are forced into the conclusion that a finite element model of the system will ultimately be required to fully answer all of the questions we have not yet asked. Such a step can not be taken until the properties of the various materials are documented and there are results to calibrate the model. This is a future research area.

rods. The equation for the simplistic model shown in Figure 77, which is based on Newton's second law, is presented in equation (50):

(50) $$\sum Forces = mass \times acceleration$$

B.5.3 SOLUTION TO THE DIFFERENTIAL EQUATION OF MOTION

A one-dimensional representation of this dynamic system[328] is presented in equation (51).

(51) $$m\frac{d^2x(t)}{dt^2} + h\frac{dx(t)}{dt} + k^2(t)x(t) = F_0 + F(t)$$

This equation has a mean load function, F_0, which ensured that the rig was retained in tension under the cyclic loading and takes the weight of the compression mechanism and shear wall element normally held by chains. The level of mean load adopted with the final loading pattern was 150 kN. The mean load was deleted from the analysis by using a translation of axes for the starting x coordinate. This technique eliminates the mean load term by measuring the displacements from the mean load position (Chopra, 1995, 19). The implicit assumption in the formulation of the differential equation of motion in both Kaplan and Lewis (1971) and Chopra (1995) was that:

(52) $$x \Rightarrow x(t)$$

The previous commentary on the assumption of constant mass again applies to this analysis. The use of the damping coefficient, h, matches the usual definition in the physical sciences. At low frequencies and acceleration, the equation of motion reduces approximately to the standard Hooke's law shown in equation (53):

(53) $$F(t) = k^2(t)x(t)$$

The form of the forcing function is a harmonic wave that is represented as:

(54) $$F(t) = A\sin(wt)$$

The ITM was designed to reduce the effects of transients. Whilst in a small number of tests transients were observed, they were generally damped out by the end of the first cycle. Transient solutions were not observed at low frequency loading. The steady state solution to equation (51) with the forcing function taken from equation (54) is shown in equation (55):

[328] Where the implicit assumption is that the mass and damping are constant.

(55) $$x(t) = [a(t)\cos(wt)] + [b(t)\sin(wt)]$$

The solution is a lagged sine wave. The cosine function is equivalent to a lag constant within the sine function. The measured stiffness for the same system can be expressed as:

(56) $$F(t) = l^2(t)x(t) \qquad for \quad w > 0$$

The ITM controller gives us the choice of three types of functions: a square wave, a harmonic wave or a triangular wave. The first and last are simply Fourier series harmonic waves. The single frequency harmonic wave was used for these experiments. This point is discussed in detail in Appendix D. Three equations can be used to simplify the presentation of the results for the differential equation. These equations are:

(57) $$[W(t)]^{-1} = [k^2(t) - mw^2]^2 + [hw]^2$$

(58) $$a(t) = -W(t)Ahw$$

(59) $$b(t) = A[k^2(t) - mw^2]W(t)$$

These equations demonstrate the interrelationship of the damping, mass, and stiffness matrices.[329] Chopra (1995) presents an equivalent derivation[330] in traditional engineering terms. Differentiation of equation (55) yielded equation (60),[331] with the assumption that $\dot{a}(t)$ and $\dot{b}(t)$ can be ignored for this simple analysis:[332]

(60) $$\dot{x} = w([b(t)\cos(wt)] - [a(t)\sin(wt)])$$

Differentiation of equation (60) yields equation (61) with the assumptions of constant coefficients:

(61) $$\ddot{x} = -w^2([b(t)\sin(wt)] + [a(t)\cos(wt)])$$

This can be expressed as equation (62):

(62) $$\ddot{x} + w^2x(t) = 0$$

[329] The problem of tuning a radio receiver presents a classic example of the mathematics of this type of differential equation.

[330] Chopra, A.K., (1995), *Dynamics of Structures Theory and Application to Earthquake Engineering*, (NJ: Prentice Hall), 68.The simpler pure mathematics derivation is used in this appendix.

[331] We use the dotted derivative to indicate differentiation.

[332] From a pure math viewpoint, this gross simplification is only slightly valid away from a resonant point where there is a significant velocity component. However, it is worth the simplification to separately understand the importance of the mass and damping effects in these experiments. Short 30 second bursts were used in the testing so that the evolution of the a(t) set of functions could be treated as piecewise continuous functions. For the 30 second test each a(t) function was considered a constant number, even though it could vary between tests.

This is the well known vibratory equation with the stiffness and mass central to the analysis and the damping ignored. This equation provides the theoretical form for the relationship between the acceleration and the displacement. It demonstrates the inverse nature of the relationship and the rapid amplification of the acceleration with frequency, and the physical limitation of finding a physically feasible solution (Chopra, 1995, 74, Figure 3.2.6; Halliday and Resnick, 1971, 231, Figure 13-7). Equation (62) can be substituted into equation (51) to yield equation (63):

(63) $$k^2(t)x(t) - mw^2x(t) = A\sin(wt)$$

Equation (63) can be simplified to equation (64).

(64) $$(k^2(t) - mw^2)x(t) = A\sin(wt)$$

Further simplification[333] using equations (54) and (66) results in:

(65) $$F(t) = l^2(t)x(t)$$

(66) $$l^2(t) = k^2(t) - mw^2$$

It is a simple step then to the inequality that:

(67) $$k^2(t) \geq l^2(t)$$

This result is based on the equality of equation (66) and the observation that the frequency and mass are always positive. The effective stiffness and the actual point data defined by $\overline{G}(t)$ are related by the equation (68):

(68) $$k^2(t) \geq \overline{G}(t)$$

Mathematically the relationship is not to be extended to assume a non zero damping. The inequality in the equation (67) takes care of the damping from a consideration of the thermodynamics of the failure of a masonry panel. In summary, equation (67) is the fundamental equation that explains the observed differences between a static experimental situation and a dynamic experimental situation.

[333] The conceptual leap can be made that the forcing function can be other than a harmonic function

B.5.4 THE ISSUE OF TIME AS A VARIABLE

Time in the experiments is not the defining independent variable for the measurement of the degrading effective stiffness. The independent variables are frequency, the strain rate, and the strain. The Young's modulus is an independent constant that sets the starting point for the two stiffness entities. The measured stiffness and the effective stiffness are defined with time as $l^2(t)$ and $k^2(t)$. Two functions were established to represent the effective stiffness and the measured stiffness with respect to the strain and other independent variables:

(69) $$k^2 = f_a(E, e, \dot{e}, f)$$

(70) $$l^2 = f_b(E, e, \dot{e}, f)$$

The form of f_a and f_b will be determined from increase in the strain in the loading pattern that provides the link to the time based definitions.

B.5.5 DISCUSSION

The definition for k^2 provided implicitly by Kaplan and Lewis (1971) has been extended with equation (69) to represent a limit of a function as the strain rate approaches zero, which implies zero frequency and returns the mathematical fragment to Hooke's law. The mathematics that establishes a set of equations and relationships that satisfy the three hypotheses has been developed from a review of the Newtonian physics. The iterative experimental process provides the data to confirm the assumptions and the hypotheses and reach conclusions on the relationships. The primitives are again the limitation.

B.6 A CONCEPT OF A QUASI-STATIC LOADING RATE

B.6.1 INTRODUCTION

The concept of a frequency, defined as Y, that is an upper bound to the range of quasi-static frequencies can be determined from equation (67). The frequency is estimated assuming an acceptable error on the measurement of the effective stiffness. The limits for Y are estimated in this section of the appendix. The procedure investigates the measured stiffness results for Panel AP: 6 to establish an limit for the quasi-static frequency, determines the quasi-static loading rates used in previous experiments and undertakes a review of the limits solution equation assuming zero damping and an acceptable error level. This review provides an upper bound to the quasi-static frequency limit.

B.6.2 SHEAR RESULTS FOR PANEL AP: 6

A typical set of results at a displacement of 2.5 mm for AP: 6 is presented in Table 84. These results point to an experimental limit to the static frequency of approximately 0.3 Hz for this particular test set. A review of the various data sets suggests a workable limit of at least 0.4 Hz. These results include the mass and damping term.

TABLE 84 MEASURED SHEAR STIFFNESS FOR PANEL AP: 6 AT 2.5 MM DISPLACEMENT

Frequency (Hz)	Measured Shear Stiffness (GPa)
0.06	7.81
0.1	7.64
0.3	7.5
1	7.1
5	5.4
10	0.7

B.6.3 PREVIOUS EXPERIMENTAL RATES

The use of the term quasi-static implies a slow loading rate so that a representation of the static stiffness is obtained from the measurements. Tomazevic and Lutman (1996) provided a definition in their recent experiments that a rate of 0.033 mm/s was a suitable quasi-static loading rate. This is shown in Figure 16.[334] This loading rate at the ram implies a frequency of loading of 0.0025 Hz for a 2.5 mm loading cycle. The mass of the test object was 4 tonnes. The error, e, in the estimate of $k^2(t)$ using $l^2(t)$ was about 1 part in 100,000 for these sets of results. This acceptable error level was significantly less than the random errors in the measurements. Therefore, it is concluded that this rate is a quasi-static rate. However, the ITM will not effectively cycle at this rate.

B.6.4 ANALYSIS WITH ACCEPTABLE ERROR

The estimation of the change over frequency, Y , between what is considered static and what is dynamic is controlled by the equation (71):

(71) $$k^2(t) \; ^3 \; l^2(t)$$

This can be converted to a strict equality as:

(72) $$k^2(t) = l^2(t) + err(t)$$

[334] Refer pg. 99.

The typical error, d , that was considered acceptable for the measurement of the stiffness due to mass effects in these experiments is in the order of 1 part in 100. This assumption of an acceptable error of 1 percent implies directly that if:

(73) $$(0 < err(t) \pounds 0.01)$$

(74) $$(k^2(t) - l^2(t)) < err(t)$$

With some algebra from eqns (73) and (74) yields that the limit for dynamic frequency is:

(75) $$Y < 0.8$$

This acceptable limit for the error implies a static frequency limit of 0.8 Hz as an acceptable upper bound on the static frequency. This result is that at that frequency the acceleration term is still bounded by the error function in the measurements. The velocity component has been ignored in this section. The effective experimental limit is approximately half of the frequency shown in equation (75). The point of this analysis is not that it is possible to measure the stiffness with finer and finer accuracy with a slower loading rate, but that the inequality $k^2(t) \neq l^2(t)$ is always going to affect the results. That the effect at a static frequency limit of 0.8 Hz is less than the other errors and is acceptable from an engineering design perspective does not mitigate the fact that this systematic error is always present. It is thus difficult to directly measure the term $k^2(t)$ using a test in the seismic frequency range, without also directly measuring the acceleration or finding an alternative test method.

B.7 DISCUSSION

The experimental observation documented in the literature review is that there are two separate stiffness operators measurable in a ceramic material. These are the static stiffness and the dynamic stiffness. The observation from the research undertaken by others to this point must be that in the limit as the frequency approaches zero the dynamic stiffness approaches the static stiffness. The explanation offered is that the stress wave loading does not allow the weakest plane to be activated. This is one explanation for the mass term absorbing energy from the applied force, which is then not available to form new crack surfaces on any plane. This, in all probability, is the mechanism that slows the rate of development of the cracks as identified correctly by Paulson and Abrams (1990).

The purpose of this appendix is to investigate the mathematical relationship and physical meaning of the effective stiffness and the measured stiffness. The effective stiffness is

deemed the mathematical functional representation of the stiffness defined explicitly by the displacement term of the differential equation of motion for a standard harmonic function. This functional representation has no frequency dependence. The measured stiffness is defined to be the experimentally determined stiffness obtained by dividing the stress field results by the strain field results for each recorded time step. The measured stiffness is a mathematical operator that has linearly independent terms of displacement, velocity, and acceleration. The measured stiffness as a stiffness term is retained for historical reasons. The measured stiffness has been related to the effective stiffness with a simple analysis using a number of simplifying assumptions related to the damping. A functional form has been established for the measured stiffness. The measured stiffness has been shown to be a lower bound to the effective stiffness. The lower bound estimate for zero damping in a theoretical sense has an acceptable error up to a frequency limit of 0.8 Hz. In a practical engineering sense for non-zero damping the limit must be at approximately 0.3 to 0.4 Hz. This analysis has provided a reasonable bound between frequencies that can be considered static and those that are within the dynamic range where the error function defined in equation (72) is greater than the random measurement errors. The limit based on the results including a damping term suggests a realistic limit to any future static testing of 0.3 to 0.4 Hz.

The three hypotheses conform to the known experimental data and the applicable Newtonian physics. The results provide the solution that the effective stiffness is the upper bound to the measured data on the shear stress and shear strain. The first hypothesis is supported by the experimental data and the quasi-static limit of $Y < 0.4$ provides a reasonable bound between the quasi-static region and the dynamic region of the solution for the differential equation of motion. The second hypothesis is proven with the derivation of the measured stiffness shown to have three independent components. The dynamic stiffness is a result of the method of measuring the stress and the strains. The effective stiffness is a distinct part of the dynamic stiffness, but this operator also contains damping and acceleration terms. The term dynamic stiffness has taken a concept from statics to explain the solution to the fundamental equation of dynamics. This term dynamic stiffness is a misnomer albeit useful. The third hypothesis rearranges the dynamic equation of motion into a static form using a number of simplifying assumptions. The quadratic form of the operator $l^2(t)$ is shown in the experimental data. This operator lacks the smooth continuous form of the effective stiffness and is not a true static stiffness.

Appendix C Earthquake Trace Analysis

C.1 INTRODUCTION

The world experiences a few earthquakes each day of magnitude M5.5 or greater (USGS, 1999). These earthquakes provide one of the harsh environmental loads that affect masonry buildings. Several earthquake traces were used in an elastic finite element analysis of two masonry buildings. The finite element analysis formed the commencement point for the review of existing loading patterns and the development of the loading pattern standard used in the experimental work. This appendix presents a summary of the mathematics of Fast Fourier transforms related to the time and frequency domain and a brief review of the earthquakes that were considered as part of the development of the loading pattern.

The time and frequency domain traces for an acceleration component for the Nahanni earthquake of the 23rd December 1985 are presented in Section 4. This earthquake trace was used to illustrate the FFT procedures.

C.2 AN INTRODUCTION TO TRANSFORMS

The Fourier transform is a special case of the Laplace transform. The discrete Fourier transform is derived in detail in Brigham (1974, 99). Brigham outlines the development in the mid sixties by Cooley and Tukey of their FFT algorithm. The Fourier transform provides a linear one to one relationship between the time domain and the frequency domain. The two are equivalent representation of the same waveforms. A scale factor is introduced to maintain equivalence between the continuous and the discrete transforms. The FFT scale factors of interest are presented in Table 85.

TABLE 85 FFT SCALE FACTORS

Functional relationship	Scale Factor	Comment
e^{-t}	T	The period between data collection points in the time domain
Fourier Harmonic Relationship $\cos(2\pi f_o t)$	T/(NT)	N is the number of samples in a single period
Discrete FT of a band limited periodic waveform	Time Domain AT_o	
	Frequency Domain $AT_o/2T$	The scale factor is 2T where T is the rate of data collection in seconds. The factor of 2 is derived from the negative frequencies.

In the case of seismic traces, the three quantities of interest are the acceleration, velocity, and the displacement with the acceleration of primary importance. A typical example of the time trace is presented for the Nahanni earthquake at the location noted as Station 1. This M6.8 event occurred in the Northwest Territories. The time trace for one of the horizontal components is shown in Figure 78.

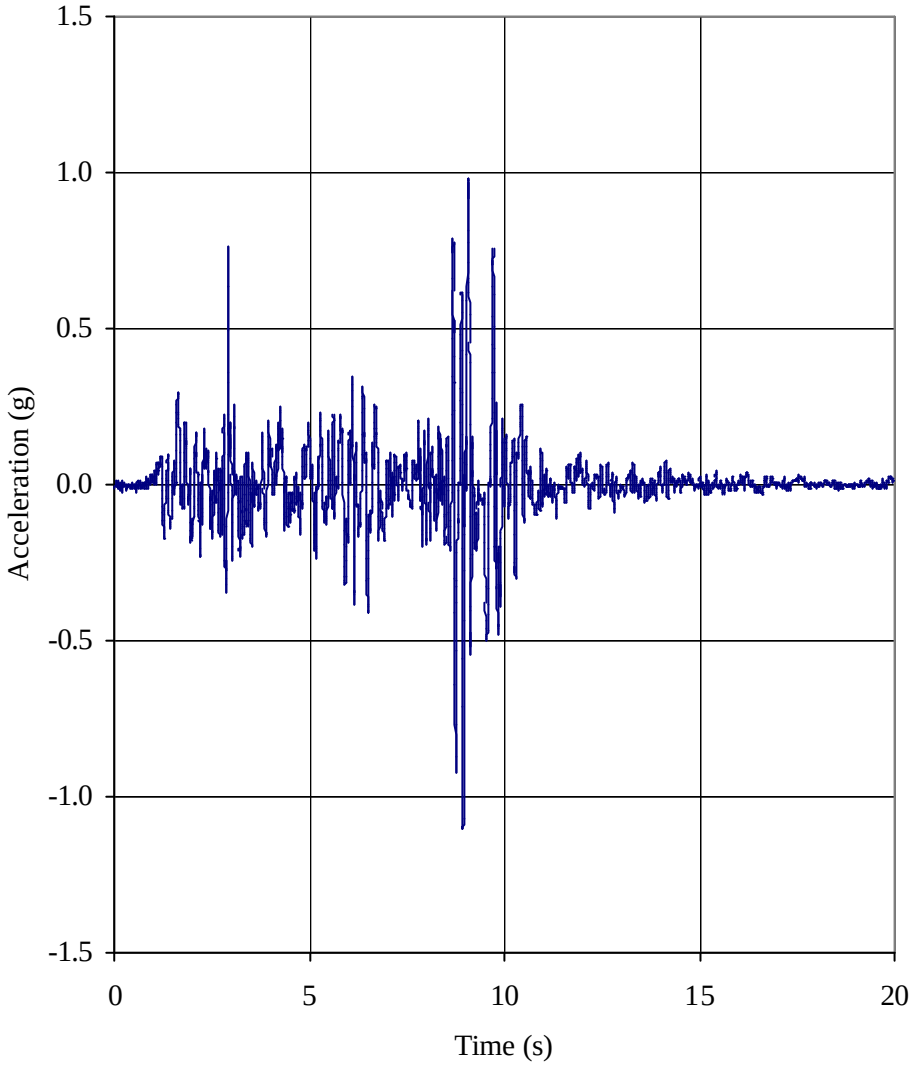

FIGURE 78 HORIZONTAL ACCELERATION TIME TRACE

Whilst the trace is instructive, it does little to provide guidance as to the frequency relationship for the earthquake trace. This is instructive when it is matched with building data and the modal frequencies. The same trace is transformed using the procedure from Numerical Recipes in Fortran[335] in a program named CONVERT.[336] The discrete Fourier

[335] Press *et al.*, (1994), *Numerical Recipes in Fortran* (Cambridge: Cambridge UP.), DFOUR Routine.

transform programs were validated using the exponential function routine and the square wave routine from Brigham (1988, Chapter 9). The results are truncated at the midpoint of the frequencies to avoid confusion with the negative frequencies. In terms of the discontinuity in the data, the midpoints between the upper and lower estimate of the function value were used in the analysis in accordance with normal practice. The resultant frequency domain trace for the time domain acceleration trace presented in Figure 78 is shown in Figure 79.

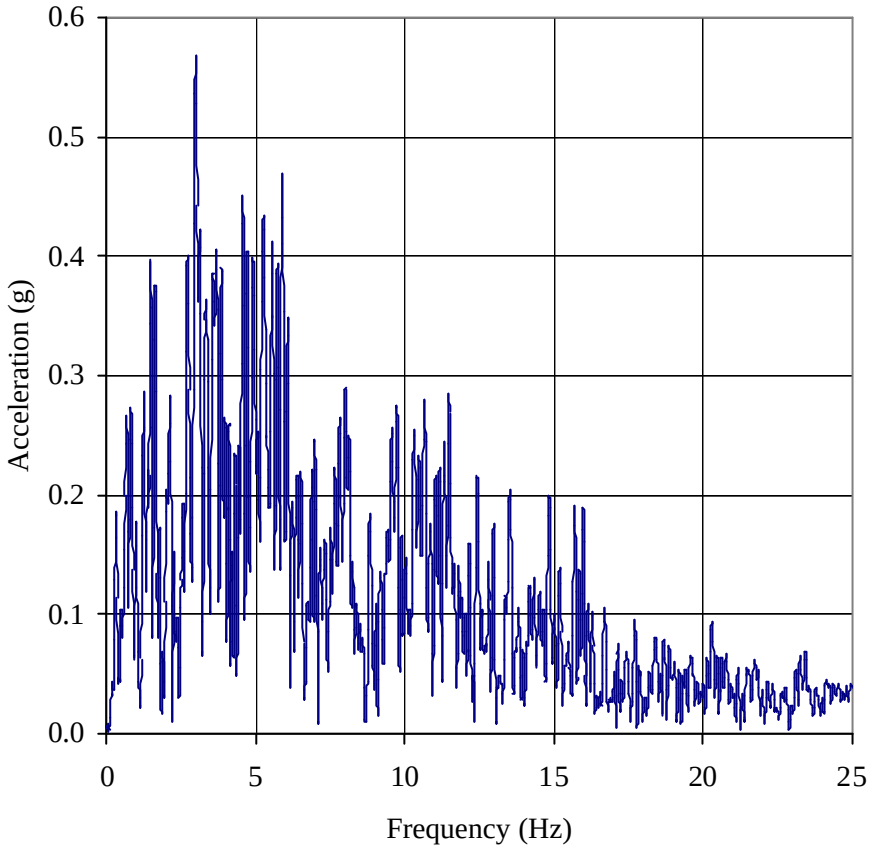

FIGURE 79 HORIZONTAL ACCELERATION DISCRETE FAST FOURIER RESULTS

C.3 EARTHQUAKES OF INTEREST

Seismologists have demonstrated that each earthquake has characteristic signatures in the time and frequency domains. The ground surrounding each epicentre is unique and acts as the primary filter to the ground movements caused by a particular earthquake.

[336] A copy of the program and the time traces used in the analysis are presented on the data CD.

Micro tremor measurements demonstrate the effect of foundation and ground conditions on the response of a building to minor dynamic loads. Buildings located in a random fashion across large areas of the world's surface act as the final filter to the earthquake strain energy. Thus, a series of events that starts slowly with strain build up ends briefly with stress release, and often with strain damage in buildings.

One of the current problems for science is the time scale difference between the geologic process of formation and the resultant strain release. The use of time series data on earthquake distribution suffers from a short database (Richter, 1958, 389). A fraction of a minute witnesses the release of the destructive power of an earthquake. All buildings within the seismic area are subjected to loading within a short time period. If this loading exceeds the design loading, or there has been poor quality of construction, then there is room for a substantial loss of life with the problem unlike cyclonic winds, that there is generally no warning period to evacuate (Tezcan and Ipek, 1996, 909).

The work of Atkinson and Boore (1995) for Eastern North America (ENA) provides one interesting seismic data set. The two specific events that were used in this work were at Saguenary, Quebec and Nahanni, Northwest Territories both located in Canada. The new ground motion relations provided by Atkinson and Boore cover the peak ground motions and response spectra for Eastern North America events in the range of M 4 to 5. Atkinson and Boore noted that this analysis is consistent with the data from the Nahanni and Saguenary earthquakes. The interest of this research lies in events beyond this size as competent design standards for even guild rules [provisions that are deemed to comply] should be capable of sustaining a M5 event without damage (Page, 1992). The Tangshan earthquake data (Shiono, 1995) suggests that masonry strength limits the ability of any masonry building to survive earthquakes of a maximum magnitude of approximately M8. These two limits provide a suitable range for considering earthquakes that will adversely affect masonry shear walls. The range of earthquakes is consistent with the USGS (1999) publishing criteria for all earthquakes, other than those in the continental US.

The response of Mexico City buildings to a single frequency highlights the problem of a tuned response. This problem points to the need to consider both the time and frequency domain in reviewing earthquake traces. Jacobs' (1997) comment was 'but there are few stable continental earthquakes with the proper M {Magnitude}, r {radius} and the right site conditions'. In addition, Boore (1997) commented 'that one is looking to use a set of earthquakes to minimize problems from holes in the frequency traces'.

Earthquake data from Japan, California, Europe, and Australia provides a range of events within the magnitude bounds of interest. Earthquake data was obtained from a number of sources—Griffith (1997), Jacobs (1997), Benedetti (1997), and Sinadinovski (1997).

These particular earthquakes are of interest to masonry researchers or have been in common use for a long period. The relevant information on the earthquake traces that were available for a number of locations and that were in areas likely to affect masonry structures are presented in Table 86.

TABLE 86 EARTHQUAKES, LOCATION, DATE, MAGNITUDE, AND DURATION

Earthquake Location	Recording Location	Date of the event	Magnitude	Duration
Marked Tree	Arkansas	Synthetic	7.25	40
Nahanni (1)	Station 1, Iverson, Canada	23 Dec 1985	6.8	12
Nahanni (2)	St 3, Battlement Creek, Canada	23 Dec 1985	6.8	20
Saguenary (1)	St 8, La Malbaie, Canada	25 Nov 1988	5.4	20
Saguenary (2)	St 16, Chicoutimi Nord PQ, Canada	25 Nov 1988	5.4	15
Irpinia	Calatrini, Italy	23 Nov 1980		70
Newcastle	Australia Synthetic	28 Dec 1989	5.5	6
Miramichi	Loggie Lodge, Canada	6 May 1982		1
Imperial Valley (1)	El Centro, USA	18 May 1940	7.1	30
Imperial Valley (2)	El Centro Peknold, USA	18 May 1940	7.1	28
Miyagi-Ken-Oki,	Sensai City, Japan	12 June 1978,		35
Parkfield	California	27 June 1966		20
San Francisco,	Cholame St, California	22 March 1957		10
Kern County	Taft High, California	21 July 1952	7.6	40

Time domain traces were obtained for one, two or three components of the various earthquakes. Results for the discrete FFT are determined for the amplitude (real), phase angle (complex), and magnitude (metric) for each of the earthquake time traces. The phase plots show a reasonably constant rate of rotation for the phase angle. This result is expected from the mathematics of DFFT. The time and frequency domain plots are reviewed against the frequency characteristics of each of the two buildings to select an appropriate set of earthquakes for the finite element analysis. The purpose of this method is to assist in the development of the loading pattern.

The earthquake recordings detailed in Table 86 have typical peak acceleration between 0.1 and 1.0 g's. Comments on each event and the associated FFT are presented in Table 87. These comments are broadly based on the useability of the events in a finite element analysis. They do not reflect any commentary on the earthquakes or any use in a general design setting.

TABLE 87 COMMENTARY ON THE TIME AND FFT TRACES FOR THE SELECTED EARTHQUAKES

Earthquake	Events used in Analysis	Comment on the Time and FFT Traces.
Marked Tree, Arkansas	Yes	Single trace, peaked in lower frequency at M7.25, considered an upper limit event of long duration, and acceleration of 0.5g. Typical synthetic event with little noise.
Nahanni Station 1	Yes	Three traces, a bit holey at 2,3,4 and 7 Hz above 0.1 g. Reasonable duration, but very high acceleration peaks (>1g in the time trace). This is an interesting event.
Nahanni Station 3	No	Duplicate event with a poorer, smoothed or attenuated signal.
Saguenary Station 8	Yes	Good design event, which is at the bottom end of the energy spectrum that is of interest in this study.
Saguenary Station 16	No	Duplicate event, again attenuated with distance.
Irpinia	Yes	Two traces, long duration and acceleration in range of masonry structures
Newcastle	No	Short, with holes in the frequency spectrum and synthetic.
Miramichi	No	Single trace; short duration event with a sharp attenuation.
Imperial Valley	Yes	A good design event.
Imperial Valley (2)	No	Duplicate.
Miyagi-Ken-Oki	No	Peaks at frequency of 1 Hz
Parkfield	No	Short and only two components
San Francisco	No	This event has holes in the frequency spectrum.
Kern County	Yes	A good design event.
SCT	No	This event has holes in the frequency spectrum.

C.4 NAHANNI EARTHQUAKE

The Nahanni event has a number of interesting features that are notably absent from most other strong motion traces. From a masonry research standpoint, this earthquake could be considered representative for ENA as a suitable abnormal event. This event has a broad energy spectrum to almost eight Hz. This covers the range of frequencies of interest to masonry designers. It has peaks within the region of 1 to 3 Hz, which are of direct interest in the design of large masonry structures. The event duration was reasonable for an intraplate event at about 10 seconds of destructive acceleration, and has few holes that extend below an acceleration level of 0.1 g. This earthquake was used as the illustrative loading for the Finite Element Model results presented in Appendix D.

Appendix D Test Loading Pattern

D.1 INTRODUCTION

A statistical determination of the degradation of the damage parameter for a ceramic material requires the development of a repeatable time varying load pattern. The pattern should resemble the essential characteristics of relevant earthquake loading on realistic masonry buildings, preferably from earthquakes recorded in both interplate and intraplate regions. The pattern should pass the criteria of similarity to existing patterns, whilst providing sufficient statistical information to allow the encapsulation of the internal damage parameter. This appendix presents the development of the analytical criteria for the first loading pattern. It provides a summary of the results from the first tests on a shear wall element. Finally, it provides a refined loading pattern that has a greater number of tests at each amplitude frequency point and a number of other minor changes. The revised pattern, developed because of the form of the early panel test results, meets the original criteria whilst increasing the available statistical information.

D.2 COMMENTS ON THE DEVELOPMENT OF THE LOADING PATTERN

D.2.1 INTRODUCTION

There are many loading patterns in use in engineering laboratories throughout the world. The characteristics of these loading patterns are diverse, yet it is difficult to compare one set of results to another. In this research work, the aims were:

I. To investigate and explain an experimentally observed dynamic stiffness.
II. To explain the observation of the accepted principles of harmonic motion in mathematical terms. This step provided the formal definitions for future analysis.
III. To measure the change in effective stiffness with time of loading and relate this to the strain levels.

The third aim is the primary objective of the thesis, whilst the first two aims are needed to understand the various stiffness observations in the experimental literature. The essential element being investigated in this work is the shear damage that occurs to masonry wythes of any masonry building. The key points about masonry buildings and this analysis are related to the frequencies of loading, the building slip joints, and the method of analysis.

D.2.2 FREQUENCIES

The normal frequency range that would be expected for masonry structures is 1 Hz for a tall structure and 3 to 8 Hz for a squat structure. The normal ranges of frequencies that have significant acceleration levels in an earthquake are limited to about 10 Hz.

D.2.3 BUILDING SLIP JOINTS

Masonry buildings are constructed with slip joints that are difficult to model. A simplification of the modelling is required for this type of joint, particularly for the concrete floor membranes that will not be as stiff as the Young's modulus of 20 to 25 GPa would suggest. The alternative flooring membrane used in masonry buildings is timber. This material has a lower Young's modulus. An average Young's modulus is used in the modelling to account for these varying materials and the joint slip.

D.2.4 ANALYSIS

Elastic analysis was assumed because the analysis and the testing required a starting point. The measurement of the damage parameter will occur as the amplitude of the load is increased for the loading pattern and it should increase linearly in the loading pattern.

D.3 DEVELOPMENT OF THE LOADING PATTERN

D.3.1 GENERAL

The degradation of the internal damage parameter for shear wall elements subjected to bi-axial non-proportional static compression, and time varying shear was investigated using the test rig. The development of a loading pattern was a crucial step in the development of the experimental protocol. Loading patterns used in a number of earlier masonry experiments modelled or copied recorded seismic events. A number of other tests used synthetic patterns and some tests used both types of patterns. These patterns provide a framework of principles or criteria for selecting a single pattern for this study. Results from tests using an initial pattern (Nichols and Totoev, 1998) demonstrated the degradation of the effective stiffness with time. However, the statistical analysis was unable to separate the effects of different variables with the brief number of tests at each amplitude frequency pair. The amendments to the loading pattern allowed for a greater collection of data for the statistical analysis, whilst remaining within the broad criteria developed in this appendix.

This appendix describes the changes to the pattern starting with the method, the analysis, the compromises, and the initial decisions on a pattern. Then, this appendix sets out the refinement of the pattern from the analysis of the results on the first few panels. The criterion for frequency suggested from the initial analysis consists of a pattern of several frequencies of broader range than initially used. The pattern applies each frequency for a fixed period, at constant amplitude and for a set number of tests. Quiescent periods occur between load applications, and differing frequencies will occur in sequence but not concurrently. The amplitude increases in steps with time, generally with a full range of frequencies tested for each of the amplitudes except for the final amplitudes at panel failure to avoid a static failure.

D.3.2 TWO MASONRY STRUCTURES

Masonry varies in size, complexity, and method of construction. A building that sits on a basement is likely to have less damage than an equivalent building without a basement (Rutherford and Chekene, 1997). The common elements in unreinforced masonry buildings are the shear walls that are usually rectilinear elements typically located in orthogonal directions.

Two building types in the domain of buildings are a 2 storey solid masonry structure and a 7 storey apartment block (Benedetti and Pezzoli, 1996; Page 1973). These buildings are suitable structures for use in a finite element analysis to determine the loading conditions on a masonry element as opposed to the use free field acceleration recorded for an earthquake. Benedetti and Pezzoli (1996) studied the dynamic response of a set of half scale 2 storey houses of typical Italian masonry and stone construction. This work was based on a standard ISMES house shown in Figure 80. This study used the Irpinia earthquake as the loading pattern for ISMES buildings. Each building was tested on a shaking table. Results were provided for a range of construction types. The Italian work had the aim of providing a design check on retrofitting protocols used in the seismic areas that contain these types of buildings. The accumulation of damage with time and the impact of retrofitting are evident in this study. Benedetti (1997) supplied details of the various measured moduli for the masonry.

Page (1973) provided details of a 7 storey masonry apartment building in Perth. This type of apartment was a common construction type in the regional Australian cities before the Newcastle earthquake. The building has been simplified for the analysis with overall dimensions of the building being 23 by 14 metres with a 170 mm reinforced concrete slab and 229 mm thick walls. A plan of the Perth apartment building is shown in Figure 81.

These two buildings provide a reasonable range of conditions for the study. In developing these models, the base conditions were assumed to consist of an independent block of high strength stone. The Perth building was modelled on a Salem stone (Krajcinovic, 1996) and the ISMES building on a weaker 20 GPa stone. These boundary conditions determined the natural frequencies of the models. These natural frequencies are within the range of interest for seismic modelling of masonry buildings of 1 to 10 Hz. The block size was set to a multiple of the building height to allow for ground block interaction. The graphical results presented in this paper are from the model based on the Perth building.

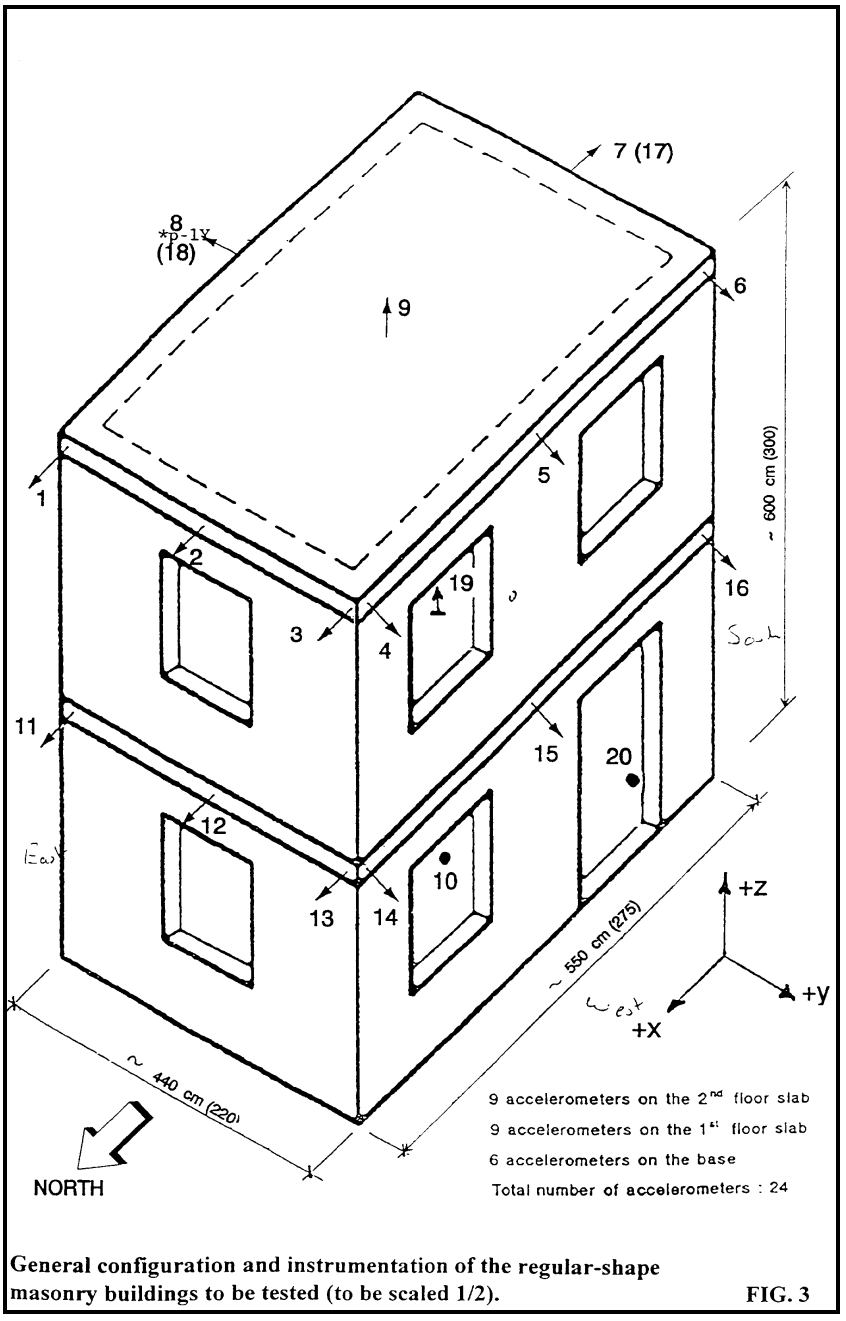

FIGURE 80 ISMES BUILDING

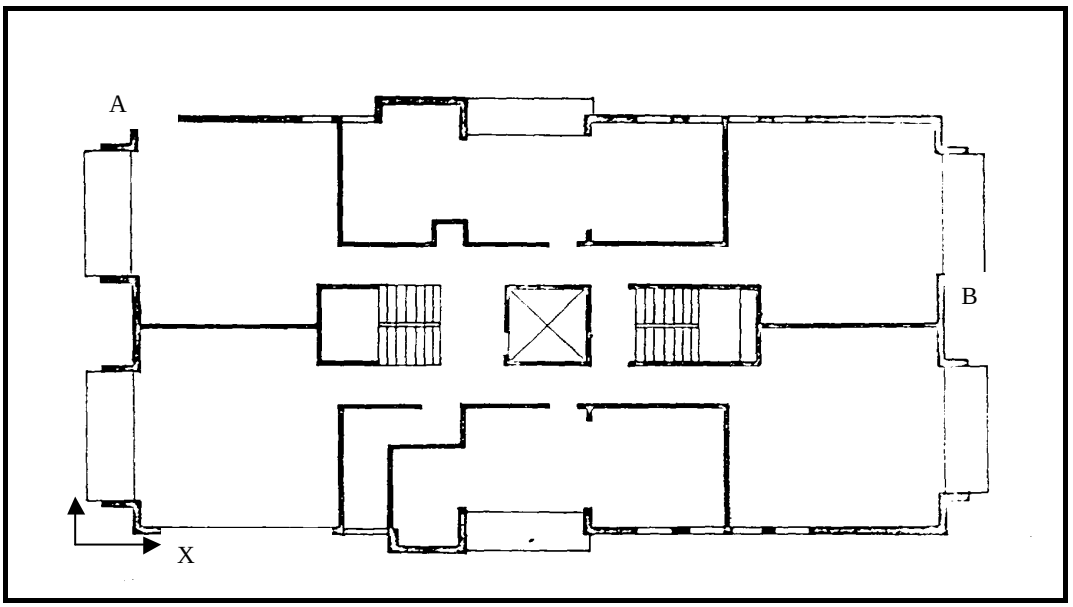

FIGURE 81 PERTH BUILDING (AFTER PAGE, 1973)

The model parameters adopted for the finite element analysis are presented in Table 88.

TABLE 88 INTRINSIC MATERIAL PROPERTY CONSTANTS

Material	Young's Modulus (GPa)	Poisson's Ratio
Mortar	1	0.35
Brick	20	0.15
Salem Stone	50	0.10
Stone	20	0.10
Floor Material	10	0.15

The floor material parameters are reasonable estimates given the slippage likely to occur on a 20-25 GPa concrete and the lower value required for timber. The walls of the ISMES building were chosen as 300 mm. The ISMES building was provided with a door of 1.2 m width on the ground floor and one window directly above in one model and the door and windows removed in the second model. The remaining windows provided in the tested ISMES buildings were not modelled in this analysis.

D.3.3 BUILDING FINITE ELEMENT MODELS

FEM analysis was completed using Strand 6.16 (G+D Computing, 1993). The linear transient dynamic solver used a Newmark-Beta method with full analysis, rather than modal superposition and damping of 1 %.[337] Each model was created with a single degree

[337] This was the default damping provided in the program. A higher value was not considered warranted for these types of tests.

of homogenization as perpends were not modelled. The buildings were simplified for the analysis and were modelled full size as a rectangular box arrangement. The finite element modelling of masonry structures approximates the structural action.

It is difficult to allow for the inferior tensile strength of masonry in an efficient manner in these types of models without recourse to topological tricks with the model connectivity. This step was not used in the modelling as the initial elastic points on the analysis spectrum were sought. The analysis was used to estimate nodal acceleration traces for a number of points in the buildings.

D.3.4 NATURAL FREQUENCIES

The results for the Perth and the ISMES model for the first three natural frequencies for the model are presented in Table 89**.**

TABLE 89 PERTH AND THE ISMES MODELS NATURAL FREQUENCIES

Natural Frequency	ISMES Model (Hz)	Perth Model (Hz)
X First	9.7	2.47
Y Second	11.5	2.97
Z Third	-	4.01

These natural frequencies have been deliberately given high values using the ground block in the finite element model. The frequencies in themselves are of no direct significance or meaning other than being dependent on the two plan dimensions of each building. The primary interest was in the response of the first two horizontal modes to the three components of the earthquake accelerations. The numbers are quoted to three significant figures purely for the point of demonstration. The model frequencies are approximations and the results should be viewed in light of the accuracy of the modelling.

The nodal time traces for acceleration were transformed using the Fast Fourier technique to estimate the response of the two buildings to each selected event (Brigham, 1974). These results were obtained to assist with the development of the loading pattern and should be viewed in that light.

A typical acceleration Fast Fourier transform for the Perth apartment building for the second mode is shown in Figure 82. This mode demonstrates the relative dominance of the modes in the mathematics of FEM.

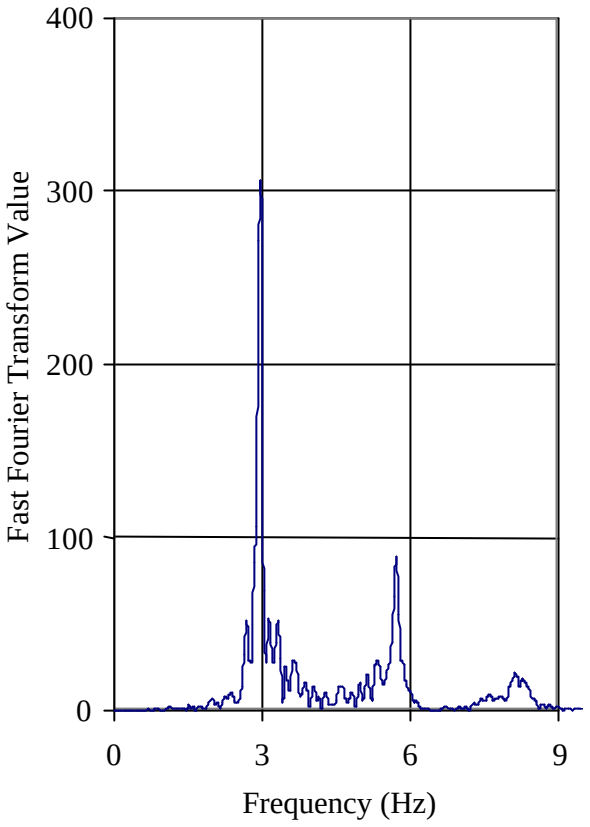

FIGURE 82 FAST FOURIER TRANSFORM FOR THE PERTH MODEL

The results are left as a metric[338] for comparison purposes, rather than being expressed as acceleration in terms of g. This graph shows the dominance of the second natural frequency for a particular shear wall node in a particular direction.

D.3.5 PATTERN PRINCIPLES

There are underlying principles that reflect the development of the loading patterns presented in the literature review. These principles provide a framework for the development of a single loading pattern to replace the four dynamic patterns used by Tomazevic and Lutman (1996). The four patterns consist of a monotonically increasing load, two cyclic patterns, and an earthquake pattern. The first of the true cyclic patterns, (B), uses a constant frequency with increasing amplitude steps. The second of the patterns, (C), is a beat pattern with a dynamic frequency of 1 Hz, and the final pattern is a specific earthquake. The first loading pattern is analogous to the quasi-static pattern that has been investigated by Page (1979), and Ganz and Thurlimann (1982, 1984). Without an FFT of the specific earthquake trace, it is difficult to assess the applicability of this

[338] The term metric is from the pure mathematics viewpoint of a measure.

earthquake event. The Yugoslavian event duration was 41 seconds. All earthquake traces used as actuator loads suffer from the problem of unique signature, quantification of the energy being applied, and the simple question of applicability to a generalized situation. The two cyclic patterns illustrate a number of features of sound pattern design. The first feature is increasing amplitude. The second feature is relatively constant frequency or mixture of frequencies.

In designing a pattern, there is an interest in mimicking a typical design earthquake scenario encountered by a range of masonry structures. Considering the analysis of the two buildings and using a number of earthquake traces, the engineering design features are that buildings can be subjected to multiple events that are separated in time by anything from seconds to decades. The damage suffered by masonry buildings accumulates with time. This damage with time is evident in structures subject to repeated events such as the recent Assisi swarm. Damage mechanics theory suggests an increasing destruction or damage to the material with applied energy. The application of an energy regime that is strictly quantifiable was of more than passing interest. Tomazevic and Klemenc (1997) have commented on this point.

The pattern should span the range of frequencies likely to be encountered by masonry buildings. The simplistic elastic analysis completed using Strand6 provides a reasonable guide to the likely range of events and building responses to particular earthquake events. It provides limiting criteria for the development of an actuator pattern for the experimental analysis of a shear wall element and this is not a free field acceleration trace.

The initial pattern design meeting the criteria is presented in Table 90.

TABLE 90 PATTERN DESIGN CRITERIA

Criteria	Comment
Type	Cyclic
Format	Repeatable at a frequency level
Frequency Lower Limit	0.06 Hz
Frequency Upper Limit	10 Hz
Amplitude	Increasing with time in a stepped pattern
Data	Able to monitor energy application
Quiescent Periods	Yes
Jerk	Limit
Beat Pattern	Not desirable
Load Application at Constant Amplitude	10 to 80 seconds

The lower limit to the frequency range of 0.06 Hz was set to be quasi-static and ensure that a full cycle occurred within the 30 second test period used in the experiments. The upper limit of 10 Hz was a realistic upper limit for earthquakes and the ITM.

D.3.6 THE PATTERNS

The basic principles of the loading pattern used for the experimental investigation of Panel AP: 6 are presented in Figure 83.

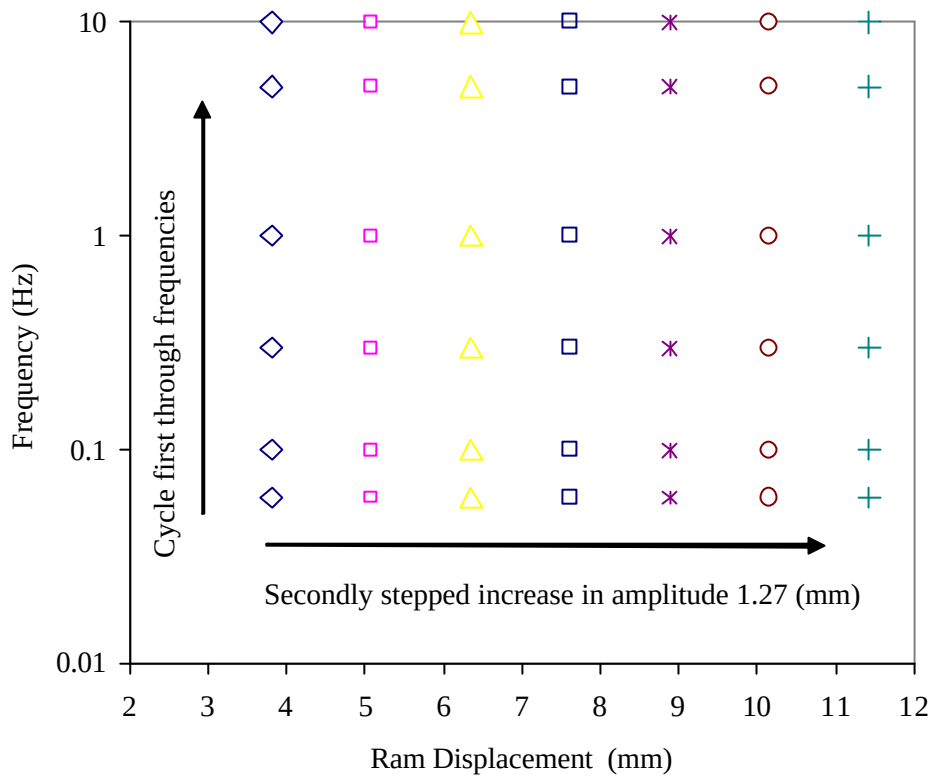

FIGURE 83 PANEL AP: 6 LOADING PATTERN.

The standard adopted for this set of tests used a 90 block pattern at each amplitude point.[339] Six frequencies, each with 15 replicates, are tested within each 90 block set. The amplitude point was increased by 1.27 mm and the frequency block repeated. The experimental results from this pattern shows that the measured stiffness, $l^2(t)$, has frequency dependence. The frequency and amplitude principles for this test series are presented in Figure 17[340] specifically dealing with Panel AP: 6. This figure presents the

[339] The Instron testing machines standard calibration for the dial gauge for the controller is in tenths of an inch. This accounts for the odd amplitudes.
[340] Refer pg. 101.

elements. It does not show the entire pattern; rather it schematically highlights the elements and the changes in frequency and amplitude in simple terms.

The changes that occurred to the pattern for Panels AP: 9 and AP: 10 were:

I. The spacing of the frequency was standardized to provide reasonably equal steps in the square of the frequency.
II. The pattern was amended to provide a block replicate, for each amplitude point. The full ranges of frequencies were twice repeated. This results in two blocks of 45 tests. The test number 1 to 5 and 41 to 45 match in amplitude and frequency.

The final loading pattern used for the panels is shown on Figure 84.

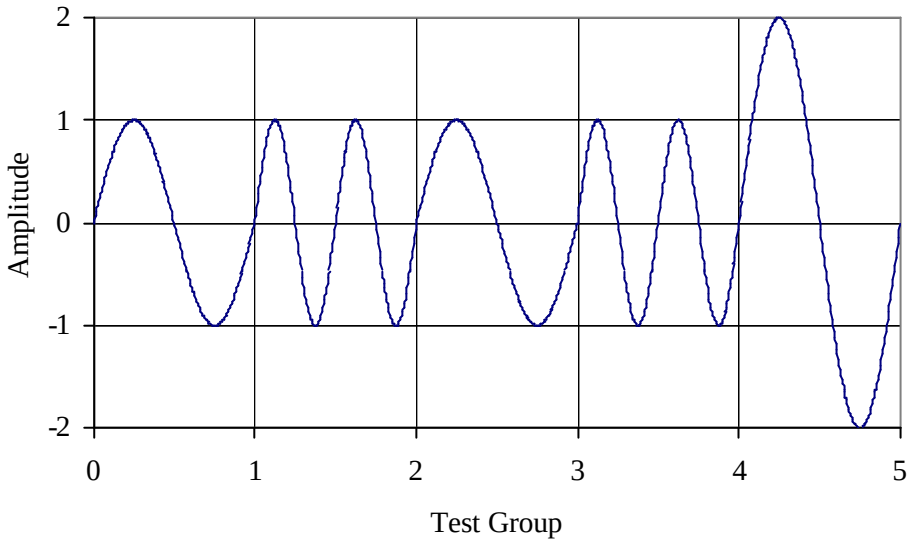

FIGURE 84 PANEL AP: 7 - 10 FINAL LOADING PATTERN

This simple sketch of the loading pattern demonstrates that:

I. The amplitude was applied after a prestress load was applied to the sample.
II. The amplitude was held constant for a number of tests, in this case schematically represented by a group.
III. The frequency was increased in set increments, represented by the change in test group 1 to 2.
IV. The pattern was repeated after 45 tests.

V. Test group 3 and 4 represent the repeated tests that are conceptually identical to the test group 1 and 2.

VI. Test group 5 represents the constant increment in the amplitude used for the next 90 tests. The 90 block test set then repeats the frequency pattern of the first 90 block test set.

D.3.7 DISCUSSION

An in plane dynamic shear analysis of masonry wythes requires the collection of sufficient data of a quality to permit a statistical analysis of the results. The testing regime had to be compromised due to the limited number of panels and the time needed to test each panel. The aim of this appendix is to outline the development and refinement of the loading pattern used in the experimental work. The first step presented the results of a FEM analytical analysis of two masonry buildings. This modelling provides data to review existing loading patterns. In particular, to review the patterns for their applicability in modelling the loads applied not in the free field situation, but at a shear wall element. Secondly, it shows development of a reasonable set of criterion arrived at for the loading patterns used in the experimental work. The analysis focused on the range of earthquakes that would cause the development and accumulation of damage in shear walls, being a range of M5.5 to M8. Within this range, a series of earthquakes were investigated using Fast Fourier transforms to confirm their applicability for use in a finite element analysis of two representative masonry buildings. The FEM analysis pointed to a shear wall loading dominated by a single frequency, rather than the multiple frequencies observed in free field acceleration traces. This result provided the first point in the development of the loading pattern. The variation in dominant frequencies was evident in the analysis. This result provided the second point that a range of frequencies needs to be investigated, in this case, in the general region of 0.1 to 10 Hz. The initial results pointed to amplitude dependence for the degradation of the effective stiffness.

The loading pattern used in the experimental work evolved over the test period as knowledge was gained on the impact of the different variables. As further experience is gained with the rig, it can be expected that the pattern will evolve further. The principal conclusion is that masonry shear walls can be experimentally loaded with a single frequency at one time and that this is consistent with the loading likely in a masonry structure. The frequencies have been varied systematically to determine the relative effect of each frequency.

Appendix E Equipment Details and Settings

E.1 INTRODUCTION

The design of the experimental equipment was based on the use of existing equipment at the university laboratory. This existing equipment includes:

I. A reinforced concrete strong floor.
II. A 4 metre high reaction frame.
III. A 250 kN ITM hydraulic ram supported by the reaction frame.
IV. A static Raripress hydraulic unit.
V. A set of eight 25 tonne hydraulic rams.
VI. Two electronic pressure gauges purchased for the experimental work.

Details of this equipment are presented in this appendix as a guide to the equipment and the set up for the experimental procedures.

E.2 REINFORCED CONCRETE STRONG FLOOR

The strong floor has a series of hold down points based on an 18 inch grid, equivalent to 457 mm. The strong floor was only capable of resisting a vertical applied loading. Applied shear loads were not permitted on the floor and a baseplate was required.

E.3 EXISTING REACTION FRAME

The University of Newcastle's Civil Engineering Laboratory has an existing reaction frame situated on the reinforced concrete strong floor. A photograph of the strong floor and the reaction frame is shown in Figure 85. The equipment that is present in the figure is:

I. The hydraulic and electronic equipment, seen in the central quadrant at the foot of the ladder.
II. A pallet of bricks, ready for the construction of the next set of panels visible immediately to the right of the test rig.
III. The bond wrench used in the laboratory is visible hanging on the reaction frame with masonry prisms ready for testing nearby the wheelbarrow.
IV. The element lifting device attached directly to a forklift is hard against the left hand side of the pallet of bricks.

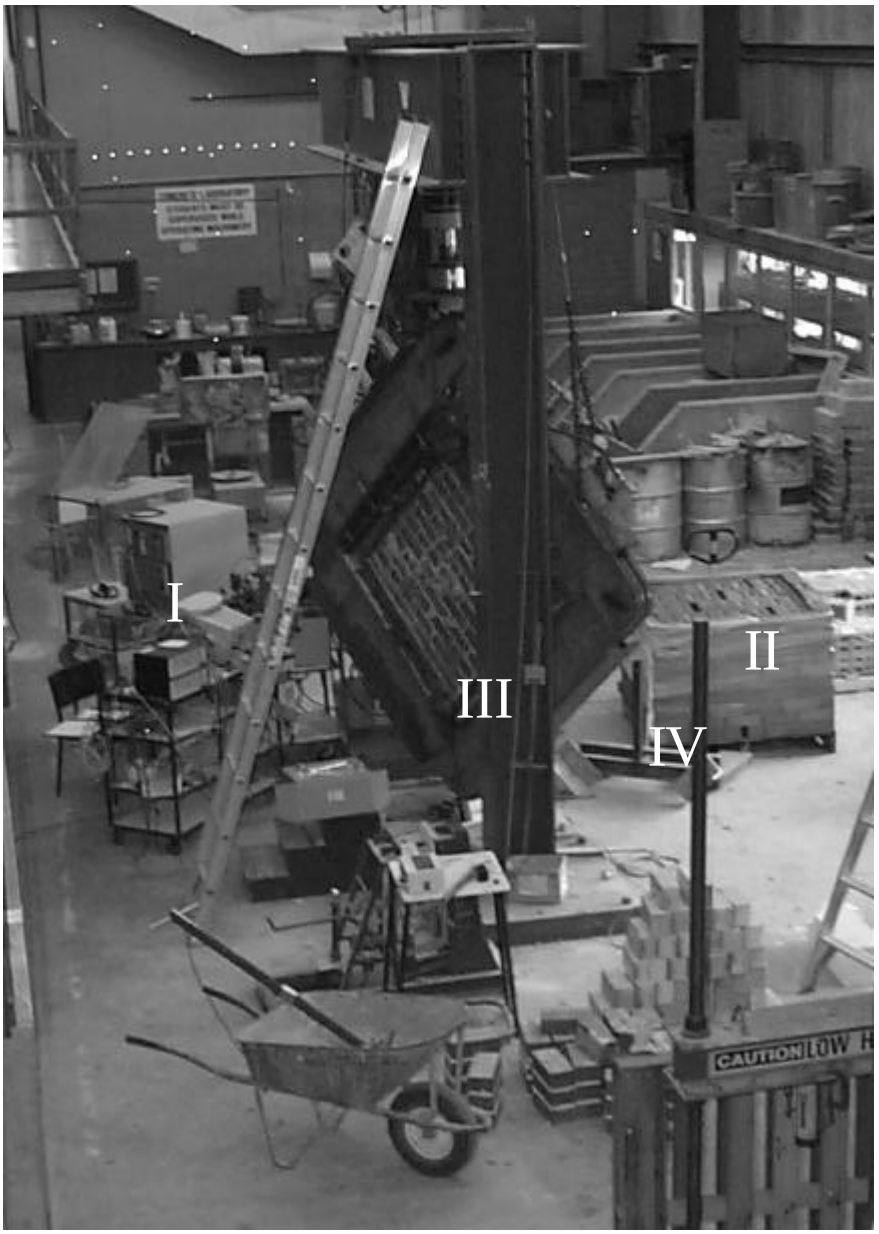

FIGURE 85 REACTION FRAME AND STRONG FLOOR WITH HANGING RIG

E.4 HYDRAULIC RAMS

The ram that supplied the static compressive force was a 25 tonne Enerpac ram with a stroke of 150 millimetres. Four rams were available to supply the compression force on each side of the panel. This set of rams provided 1000 kN of force in each direction. The spacing on the compressive arms was approximately 300 mm. Finite element modelling using a commercial elastic package and a quarter model of the shear wall element showed that the edge effects were mitigated within one brick width of the edge of the panel. The characteristics of the static pressure rams are presented in Table 91.

TABLE 91 DETAILS OF THE HYDRAULIC RAMS

Description	Unit	Quantity
Working Load	tonnes	23
Working Force	kN	233
Surface Area of the Ram	mm^2	33,200
Working Stress	MPa	70.1
Force Per Bank of Four	kN	932
Stroke of the Rams	mm	150

E.5 INSTRON TESTING MACHINE HYDRAULIC RAM

The ITM was technically considered capable of supplying a force of 250 kN, under a variety of load conditions. These load conditions consisted of force control, displacement control, and strain control. These experiments were undertaken using displacement control to permit the investigation of the degradation of the stiffness of the masonry panel with time. The pump set for the ITM had a capacity of 80 l/s. This pumping rate limited the combination of the force, stroke, and frequency. The maximum force available was 250 kN. This shear force applied to the shear wall element was approximately 15 % of the peak applied compressive force. The shear yoke arrangement was designed for the 250 kN force. The peak force measured was 320 kN. The ITM controller has a number of separate components that are discussed in this section. A photograph of the controller system is presented in Figure 86.

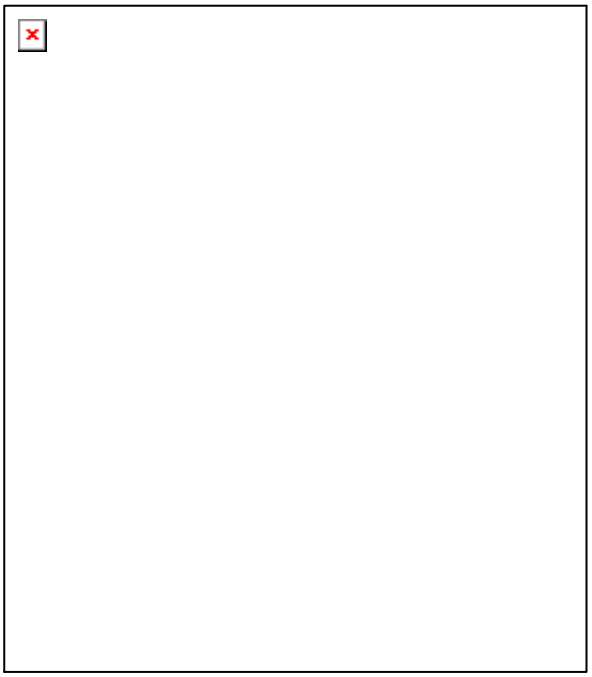

FIGURE 86 INSTRON TESTING MACHINE ELECTRONIC CONTROLLER

This system is a controlled manually in terms of the input function limits. The components of the system are a signal monitor used to output the displacement and the force at the ITM. Signal generator used to generate the harmonic signal controlling the ram displacement having a simple on off system and the displacement controller. The technical capability of the hydraulic ram is presented in the manual published by Instron Ltd. (1984a). The pumping unit rate limited the slew rate for the ram, providing the limitations on the operation of the system.

E.6 INSTRON TESTING MACHINE ELECTRONIC SYSTEM

E.6.1 INTRODUCTION

The details for the electronic system are published in the set of manual from Instron Ltd. (1984a, 1984b, 1985). This section of the appendix covers the operation of those components of the electronic system used in the experimental work.

E.6.2 SIGNAL MONITOR

The signal monitor was used to provide the analog signal for the displacement and the force at the ITM. The signal monitor switches and displays are shown in Figure 87.

There are two separate monitoring circuits. The two monitoring circuits in this experiment were used to monitor the displacement and the load at the ITM ram.

Each monitoring circuit has three components. A display light shows the position of the selector switches 1 and 2. Selector switch 1 and 2 that are toggled to change the display between load and displacement, and a read out display of the current settings by a set of three red lights indicating which of the control functions was operational on that particular circuit set.

E.6.3 SIGNAL FUNCTION GENERATOR

The signal function generator was used to generate the harmonic signal controlling the ram displacement. The ram displacement was maintained within preset limits as detailed subsequently in this dissertation. The function generator could not compensate for the slew rate of the ITM. The function generator, the on/off switches, and the displacement controller are shown in Figure 88. The three uppermost switches on the wave generator are used to select the type of function used in the experiments. The types of waves available are square wave, triangular wave, and sinusoidal wave. These experiments used a sinusoidal signal that was a steady state harmonic motion. The next five switches and

the dial gauge are used to select the frequency of the signal. This signal was calibrated using the data acquisitions Fast Fourier transform routine. The results were dependent on the use of the multiplier switches that were checked at every use.

The next switch provided the starting point and slope for the ITM ram. In the case of these experiments, it was selected as a rising wave. The aim of this system was to damp out the transient solutions to the forced motion. The second bottom switch is the start switch. The red light beside it indicated when the ram was travelling. There is an internal clock within the ITM controller. It was useful to increase the nominal recording time from the 30 seconds to allow a delay between the toggling of the start switch and the movement of the ram. The bottom switch is the reset switch. This signals the ram to stop when it has returned to the starting point in the displacement cycle.[341]

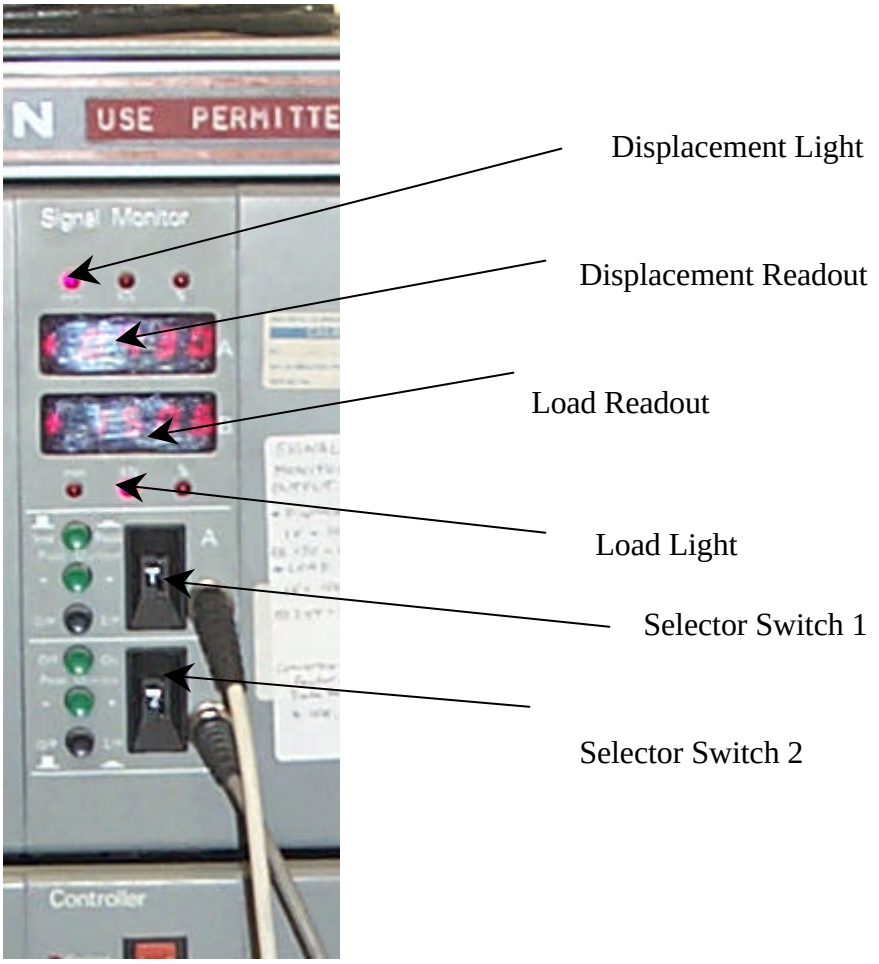

FIGURE 87 SIGNAL MONITOR

[341] It is important to note that this does not mean the same force level. Because, if the overall system stiffness is reduced, so will be the level of the pre-stress force. This should be watched and the pre-stress adjusted as required.

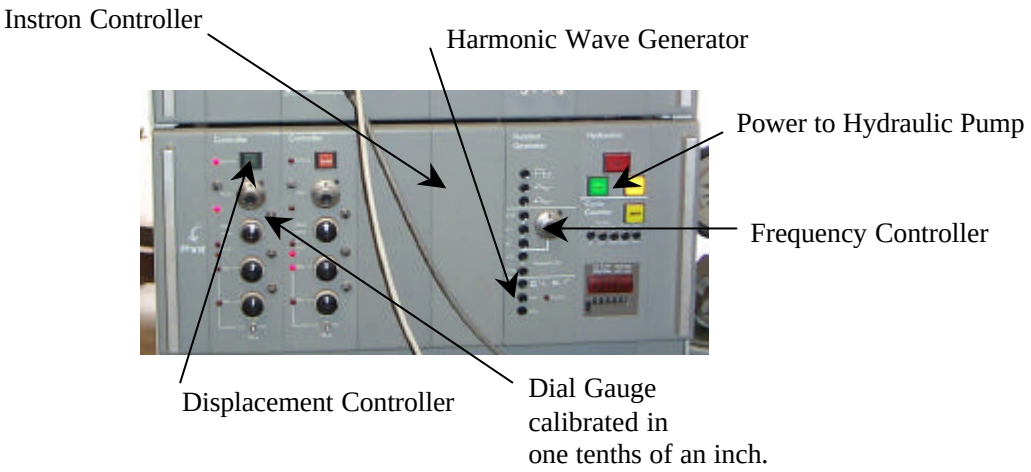

FIGURE 88 FUNCTION GENERATOR, ON/OFF SWITCHES, AND THE DISPLACEMENT CONTROLLER

The ITM ram and top of the rig are shown in Figure 89.

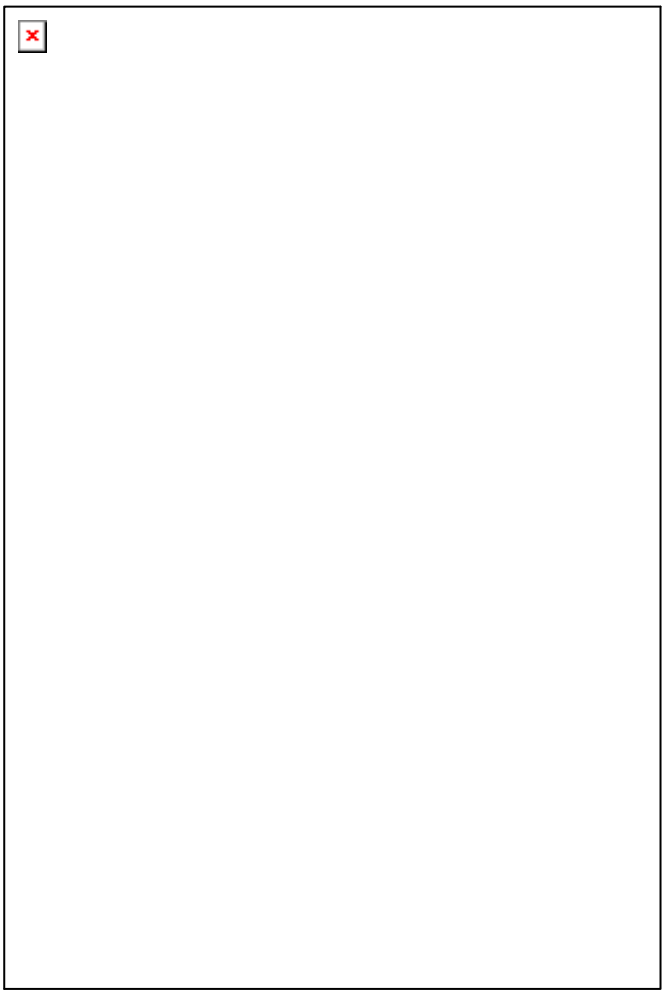

FIGURE 89 ITM RAM, COMPRESSION FRAME PEAK AND THE SHEAR YOKE

E.7 STATIC COMPRESSION PUMP SYSTEM

A Raripress pump supplied the hydraulic pressure to the test rig for the static rams. A photograph of the pumping unit with a detailed listing of the components is presented in Figure 90.

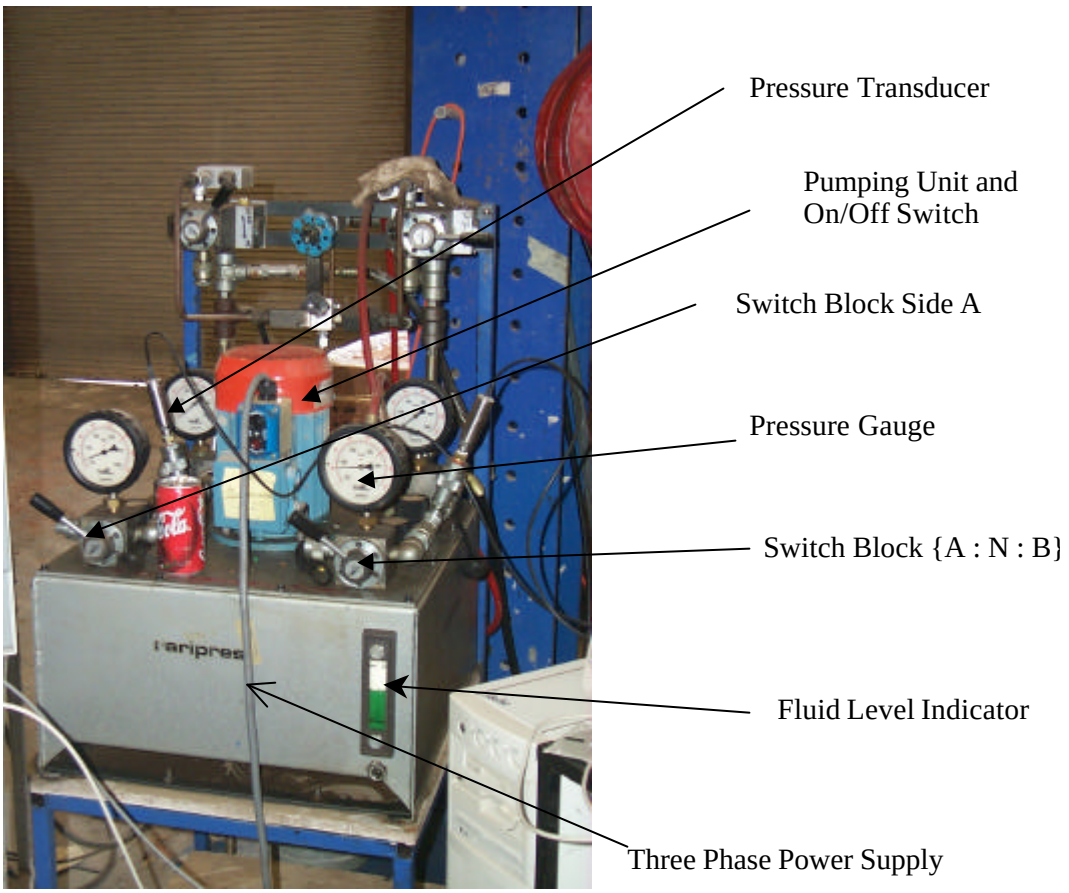

FIGURE 90 STATIC PRESSURE PUMPING UNIT

This unit was capable of supplying a pressure of 69 MPa. The unit has four separate pressure systems that can supply hydraulic pressure at four distinct values. The pumping unit has a set of dial pressure gauges. The details of these gauges are presented in Table 92.

TABLE 92 DIAL GAUGE DETAILS

Description	Unit	Amount
Gauge Maximum	psi	10,000
Gauge Divisions	psi	100

The gauges were used as a visual check on the pressure in the system. The two gauges in the front of the unit, as shown in Figure 90, were used for the two separate arms of the

compression frame. The pressure control valve was controlled with a dial and was used to set the pressure in each system. Care was taken with the operation of these dials, as they were sluggish to start with, and then pressure was applied quickly. The dial was immediately behind each switch block that controlled a particular pressure supply point.

The switch blocks were used to control the pressure in each pressure system. The control positions for the switches are presented in Table 93.

TABLE 93 SWITCH BLOCK DESCRIPTION

Switch Position	Comment
A	Pressure on
Neutral [Vertical]	Pressure held as is
B	Pressure off

The dial pressure gauges were used as a visual guide at start up, and then to check the pressures.

Appendix F The Masonry Panels

F.1 INTRODUCTION

The decision on the type and style of brick to use in the experimental work was a subjective decision. The selection criteria were based on the types of bricks and mortar that are likely to be subjected to intraplate earthquakes or that are likely to be used in repairs of such structures. This appendix:

I. Reviews the selection issues.
II. Provides details of the brick used in this research work.
III. Outlines the construction details for the panels.

F.2 SELECTION ISSUES FOR THE BRICKS

The type of bricks commonly used in construction of unreinforced masonry are calcium silicates units, pressed clay bricks with a frog, extruded clay bricks with and without a hole pattern, repressed extruded clay bricks, and concrete units. Initial testing (Nichols and Totoev, 1997b) concentrated on the properties of the brick units. This initial test program reviewed the units, which could be used in the final test program.

Market share comments and properties of interest on the types of brick available and used commonly in the Australian market are:

Extruded bricks — Comprise 60 % of the sales in the clay bricks market in Australia. This type of brick has a geometric anisotropy. This property makes it difficult to justify the testing of this type of brick over a brick with isotropic or mild orthotropic properties.

Pressed bricks — Comprise 40 % of the sales in the clay bricks market. A Boral Brooklyn pressed brick, which was tested until February 1997, showed secondary bending from the frog when compressed about the long axis. This could be attributed to the differential stiffness induced in the pressing of each brick. This brick was discontinued in manufacture before the final test program. Sugo (2000) has been studying a pressed clay brick from Austral and has documented the basic properties of this brick.

	This brick is attractive to investigate because of the existing information and because it only exhibits mild orthotropic properties when made into panels.
Calcium silicate	Small portion of the market.
Concrete	Small portion of the market, although their relatively uniform properties, like the calcium silicate units, make them attractive test bricks.
Re-pressed extruded bricks	Too hard to break in the rig.

F.3 HALF SCALE BRICKS

Page (1979, 1 - 7) used clay pavers at half size. The half size bricks are attractive from a handling issue and because of their relative isotropic nature. However, the extensive cutting and the soft hard side issue identified in this earlier research was of concern, as were the scale effects, although his work discounted this issue for the static investigation. Benedetti and Pezzoli (1996) used bricks that were half scale to model a number of southern European houses for testing on a shaking table. The issues of scale factors identified by this research group clearly highlight this scale issue as a problem. The secondary issue was the purchase of the half scale bricks.

F.4 FINAL SELECTION

The final criteria used for the brick selection for the shear wall elements were:

I. That the elastic properties not be highly anisotropic, as this was the first experimental work in this narrow field.
II. The bricks availability and applicability to the modern construction world.
III. Existing data available on the bricks of research quality.

The selected brick had a high initial rate of absorption, which caused problems in the manufacture of the panels. However, this brick unit had been extensively tested in the department over recent times, and it was thought likely to be only mildly orthotropic at the time of the panel construction.

The Austral chocolate mottled brown pressed brick was a reddish brown brick with reasonably high IRA. This brick was manufactured to the Australian Standard AS/NZS

4455:1997 Masonry Units and Segmental pavers. The bricks were delivered wrapped in plastic and stored in the laboratory weather shed before use.

F.5 PANEL CONSTRUCTION

The panels were constructed using the selected bricks and mortar, and each panel was laid by a local bricklayer who has previously constructed masonry for research work (Muniruzzam, 1997). The panels were constructed in three different months of 1998 and 1999. The panel designation was the Julian day of the year and the panel number constructed on the day expressed as an alpha character [i.e. panel 329D was made on day 329 of 1998 and it was the fourth panel made on the day]. Each panel was constructed from 70 standard Australian bricks of nominal dimension 225 by 110 by 75 millimetres. The shear wall elements were constructed with mortar 1:1:6 by volume of Portland cement, hydrated lime, and sand. The panel dimensions were maintained at 1200 ± 10 mm height and breadth dimension, and square. The number of panels constructed was greater than could be productively tested in this period. A number were damaged accidentally. The details of the laboratory designation, date of manufacture and testing, and thesis ID number for the panels discussed in this dissertation are presented in Table 94.

TABLE 94 PANEL IDENTIFICATION DETAILS

Laboratory Designation	Thesis Number	Number of Tests	Manufacture Date	Test Date	Last Test Date
210	AP: 1	1	210/98	August 98	
226	AP: 2	1	226/98	August 98	
246A	AP: 3	35	246/98	4 November 98	
245A	AP: 4	129	245/98	22 December 98	12 January 99
331A	AP: 5	1	331/98	23 February 99	1 March 99
245B	AP: 6	636	245/98	4 March 99	11 March 99
245D/E	AP: 7	700	245/98	18 March 99	25 March 99
245C	AP: 8	95	245/98	8 April 99	
331C	AP: 9	50	331/98	28 April 99	
329D	AP: 10	630	329/98	4 May 99	7 May 99

The panel dimensions for design purposes were 1200 mm in both of the principal axes. A 10 mm joint thickness was used and the joints were not tooled, but finished flush. This finish provided a uniform cross sectional area to the shear wall element.

Appendix G Standard Masonry Tests

G.1 INTRODUCTION

The standard test results based on the AS3700 standard are presented in this appendix for the different samples constructed on the five days. These tests are flexural strength of the prisms, compressive strength of the prisms, static modulus of elasticity, initial rate of absorption, and the mortar cube strength. The brick used in the experimental work was the Austral mottled chocolate. This brick was a pressed brick of Sydney origin. The mix design used was Portland cement: lime: sand in the ratio of 1:1:6. The weight design for this mix is presented in the Table 95.

TABLE 95 MIX DESIGN BY WEIGHT FOR BEACH AND RIVER SAND

Mix	Beach Sand by Weight (kg)	Ratio Beach Sand (kg)	Ratio Amatek River (kg)
Lime	0.98	4.7	5.3
Cement	2.3	11.2	10.3
Sand	17.2	84.0	84.3

The delivery of lime is the vexatious issue in the design of a mix. The test results are reported for the beach sand, which was the sand used in the experimental work. The determination of the static modulus of elasticity of the prisms used Amatek sand.

G.2 FLEXURAL STRENGTH

The statistical results for the bond wrench data are presented for the prisms manufactured on the five construction days in Table 96.

TABLE 96 FLEXURAL STRESS - STATISTICAL RESULTS

Description	Units	Day 245	Day 246	Day 329	Day 331	Day 77
Mean Flexural Strength	MPa	0.85	0.29	0.37	0.62	0.42
Standard Deviation	MPa	0.16	0.06	0.11	0.11	0.07
Coefficient of Variation	%	19	20	29	18	16
Characteristic Strength Factor K		0.83	0.82	0.75	0.84	0.85
Characteristic Flexural Strength	MPa	0.51	0.16	0.17	0.44	0.20

The university laboratory has a number of bond wrench apparatus. The machine used for these tests was the recent test machine developed at the CSIRO. The machine was designated No 4 in the laboratory. The difference in results between days 245 and 246 for the one pallet of bricks and a standard mix were attributed to the prewetting of the bricks

at the end of day 245. A Student's t Test showed that the results were statistically different at the 5 % significance level. The results highlight the issue of using a brick with a high IRA, prewetting of bricks, and the care required in the production of the mortar. The weaker specimens typically failed during the placement.

G.3 COMPRESSION TESTS OF PRISMS

The results for days 245 and 246 for the compression tests are presented in Table 97.

TABLE 97 COMPRESSION TEST RESULTS

Prism	Peak Load – Day 245 (kN)	Peak Load - Day 246 (kN)
1	441	291
2	637	306
3	700	269
4	754	418
5	641	346
Mean	630	330
Standard Deviation	±120	±60

The Student's t test results indicated that the two samples vary and that the variation is significant at the 5 % confidence interval. The equivalent stress results for day 245 was a mean compressive stress of 25 ± 5 MPa, and day 246 had a mean compressive stress of 13 ± 3 MPa.

G.4 STATIC MODULUS OF ELASTICITY

The elastic moduli results for the day 245 prisms are presented in Table 98.

TABLE 98 MODULUS OF ELASTICITY FOR THE MASONRY PRISMS

Prism	Side 1	Side 2
245a	15.5	21.7
245b	19.1	13.6
245c	16.3	12.9
245d	13.8	12.9
Mean for each column	16.2	15.3
Standard Deviation	± 2.2	± 4.3
Overall Mean and Standard Deviation	15.7 ± 3.2	

G.5 DIMENSION DATA

The data from the dimension tests in accordance with the AS 1226 are presented in Table 99. This method of testing does not provide a standard deviation to the results. The typical error in the measurements was 2 to 4 mm.

TABLE 99 DIMENSION DATA FOR THE MASONRY UNITS

	Overall Length for 20 bricks (mm)	Mean for One Brick (mm)	Nominal Dimensions (mm)
Length	4554	227.7	225
Breadth	2190	109.5	110
Depth	1511	75.5	75

G.6 INITIAL RATE OF ABSORPTION

This experiment is designed to allow for an assessment of the suction that the bricks exhibit in an oven dried state. An assessment of this allows for modifications to the laying technique such as prewetting of the bricks before construction of the masonry if the masonry units have a high IRA. A low IRA means that the bricks will not absorb moisture from the mortar. A high IRA means that the bricks will remove too much water from the mortar leaving a bony or dry mix. Sugo (2000) has tested the initial rate of the absorption of the bricks. He established a value of 5.3 kg/min/m^2. This value is high; however, prewetting the masonry units on Day 246 significantly reduced the bond strength and the flexural strength.

G.7 MORTAR COMPRESSIVE STRENGTH

The mortar was tested for compressive strength. The statistical mortar cube compressive stress results are presented in the Table 100.

TABLE 100 MORTAR CUBE STATISTICAL RESULTS

Description	Value	Unit
Dimension	70	mm
Area	4900	mm^2
Mean Stress	2.5	MPa
Standard Deviation	0.4	MPa

Appendix H Electronic Equipment

H.1 INTRODUCTION

The electronic equipment that was used in the experimental investigation is detailed in this appendix. The equipment comprises two separate systems that are:

The data acquisition system	A data collection board and software used with a PC (EDR, 1996; Tinker, 1996).
The filter amplifiers	Used to filter and amplify the displacement signals from the rings on the test rig and the other signals (Reece, 1998).

H.2 LIMITATIONS OF THE EQUIPMENT

The current equipment has the following limitations:

Number of channels	Sixteen channels for the data acquisition board.
Filter amplifiers	Eight channels to filter and amplify the signal. The eight channels were required for the four sets of ring transducers used on each of the two sides of the panel. This limitation affected the strain measurement system.
ITM controller analog data	Required two channels of the data acquisition board.
Static pressures	Required two channels of the data acquisition board.
Computer clock speed	The capacity of the data acquisition computer was stretched with a Fast Fourier transform analysis of the results.

An attempt was made to measure the displacement of the overall system using a potentiometer. This potentiometer was damaged due to the deflections of the rig. The measurement required a filter amplifier point, which affected the number of strain measurements. This potentiometer was only used for a few tests to provide data on the overall deflection of the system.

H.3 System Configuration

A photograph of the system configuration is presented in Figure 91.

FIGURE 91 CONFIGURATION OF THE INSTRUMENTATION

The screen, situated on the left in the photograph, shows the WaveView program output. The time domain output is shown in the upper portion of the screen and the frequency domain in the lower portion. The spike in the frequency domain is evident. The filter amplifiers are located centrally in the photograph. These filter amplifiers were used to filter the ITM's signal and the pressure transducer signals. The filter amplifiers for the transducer rings are shown on the right in the photograph.

H.4 Data Acquisition System

The computer system used an Intel 486 processor running with a DOS operating system. The data acquisition board was a PC30FG manufactured by EDR (1996). The software used to capture the data was WaveView, which was supplied with the board (Tinker, 1997). The data acquisition board had a fifty pin input type IDC-50. The WaveView program used a converter box to take the individual signals and convert them to the IDC 50 pin format required by the board. The relevant characteristics of the settings for the data acquisition board are presented in Table 101.

TABLE 101 DATA ACQUISITION BOARD SETTINGS

Description	Unit	Value
Card	Type	PC30FG
AD Range	V	± 5
AD Type		Single Ended
Fast Fourier Transform	Analyzed	Display
Interpolation	Graph	Linear

These typical settings were amended or altered as part of the testing. Any changes were noted on the experimental record sheets. The two common changes were to alter the voltage input range from ± 5 to ± 10. This was commonly required as the panel element failed. The second change was to change gains again as the panel element failed and the displacements significantly increased.

H.5 DATA ACQUISITION PROGRAM, SETTINGS, AND OUTPUT

The program provided a data acquisition capacity of 330 kHz. This section of the appendix outlines the features relevant to this series of experiments. Details of the operation of the program WaveView are published in the EDR board manual (EDR, 1996). The details provided in this section of the appendix relate to options available within the program. The typical settings are presented in Table 102.

TABLE 102 WAVEVIEW PROGRAM TYPICAL SETTINGS

Description	Unit	Value
Rings Type 1	Channels	4-6 and 12
Rings Type 2	Channels	0-3
Rings Type 1	Gain	10
Rings Type 2	Gain	10
ITM Load	Channel	8
ITM Load	Gain	1
ITM Displacement	Channel	9
ITM Displacement	Gain	1
Pressure A and B	Channel	10 and 11
Pressure A and B	Gain	1
Typical Test Period	Seconds	30-50
Typical Test Frequency at 0.6 Hz. Ram Frequency	Hz	200
Test Frequency Adjustment	Rate	Ratio of the frequencies with a limit of 2000 at 10 Hz ram speed.

Channel 7 was damaged during early testing.

A file naming system was adopted that was based on the laboratory designation for the panel, the test number, and an alpha character for special tests. A typical example is test result set 245D001A.TXT. This system is outlined in Table 103.

TABLE 103 FILE NAMING STANDARD

Component	Description
Date of Manufacture of the Panel	245
Panel No. on the Day of Manufacture	D
Test Number	001
Special Test	A, B etc.

This output initially was limited to the time domain data, however after January 10, 1999 tests the data files included the frequency domain data from the WaveView Program. The sample data is explained in Table 104.

TABLE 104 SAMPLE DATA OUTPUT EXPLANATION

Line Number	Purpose
1	Board Details
2	Number of total sample points and the sampling frequency across all channels
3	Voltage Input Range either ±5 or ±10 V
4	Number of channels and the channel Numbers sampled[342]
5	Date and time for first sample
6	Blank
7	Blank
8	Headings for the data
9	Typical data format: Count, time, and data

These results exclude the results from the Fast Fourier transform analysis. The Fast Fourier transform analysis was completed using an inversion algorithm that did not take the logarithm of the resultant. This method was preferred, as there is no distortion of the results on a logarithmic scale, which amplifies the effect of the noise in the signal and reduces the peaks. The Fourier transform data was used to track the degrading panel element. It was used to calibrate the frequencies on the ITM's dial gauge. The data has not been used for other purposes.

[342] In this case, Channel 7 was not recorded with this file due to damage from a prior voltage spike.

H.6 FILTER AMPLIFIERS

The filter amplifiers were constructed from a standard design developed by Reece (1998) at the University of Newcastle. The component details of the filter amplifiers are presented in Table 105.

TABLE 105 FILTER AMPLIFIERS DESCRIPTION

Component	Description
Offset Balance	Used to reset or alter the voltage output.
Gain	Used to select the desired gain. The gain of 0-500.
Voltage	The voltage source that excites the filter amplifier, set to 10 V.
Filter	A filter control switch.
Input Output Terminals	Two input types and one output type are supported.

The filter amplifiers were used to calibrate the ring transducers. Two screw settings on the rear plate control the offset and slope of the calibration. The procedure used was a standard linear fitting procedure.

H.7 SIGNAL FILTERS

The signal filters were used to reduce the noise on the signals from the ITM's controller and pressure gauges on the Raripress pumping unit. The settings used for these experiments are presented in Table 106.

TABLE 106 SIGNAL FILTER SETTING DETAILS

Component	Unit	Setting
Filter	Hz	2.6
Multiplier on Filter	Number	10

H.8 TRANSDUCERS

H.8.1 INTRODUCTION

Three types of transducer were used in this experimental work. A number of linear velocity displacement transducers (LVDT), eight ring transducers, and a potentiometer were used during the experimental study. This section of the appendix provides information on the standard LVDT devices and details the design of the ring transducers.

H.8.2 LINEAR VELOCITY DISPLACEMENT TRANSDUCER

Two LVDT types were used in this experimental work. The details of the LVDT types and the typical calibration constants used in the analysis are presented in Table 107.

TABLE 107 LVDT CALIBRATION DATA

Description	Serial Number	Calibration
RDP Electronics 0.5 mm	D5-620G8 676	1 V equals 0.2 mm
RDP Electronics 10 mm	D2-7200A 5848	0.0063147

The problem with the LVDT units is that they had a high mass and inertia. This made them relatively difficult to place and hold successfully on the bricks during dynamic experiments. The 0.5 mm LVDT units were used as a calibration check on the ring transducers during early tests on the panels. The 0.5 mm LVDT units were used to statically calibrate the rings and the associated filter amplifiers. A photograph of the calibration method is shown in Figure 92.

FIGURE 92 CALIBRATION OF THE RINGS

The procedure to test the equipment and crosscheck the operation of the ring transducers was first to test the first panel with 10 mm and 0.5 mm LVDT units to confirm the operation and check the results for the panel. This stage was completed on Panel AP: 3. The second stage was to use the 0.5 mm LVDT units to confirm the operation and calibration of the ring transducers to ensure that the rings were operating in accordance

with the design parameters. The final stage was to use ring transducers on both sides of the panel.

H.9 RING DISPLACEMENT TRANSDUCER

H.9.1 INTRODUCTION

The ring displacement transducers were developed in the laboratory of Newcastle University to provide a lightweight and robust method of measuring the movements on the shear wall element. A plan showing the original arrangement is shown on Drawing EF102 - 7.[343] The transducer displacement rings labelled RR Type 1 and RR Type 2 were used for the detail work on the sets of shear wall elements tested in 1999. A plan showing the set out of the rings is shown in Figure 93.

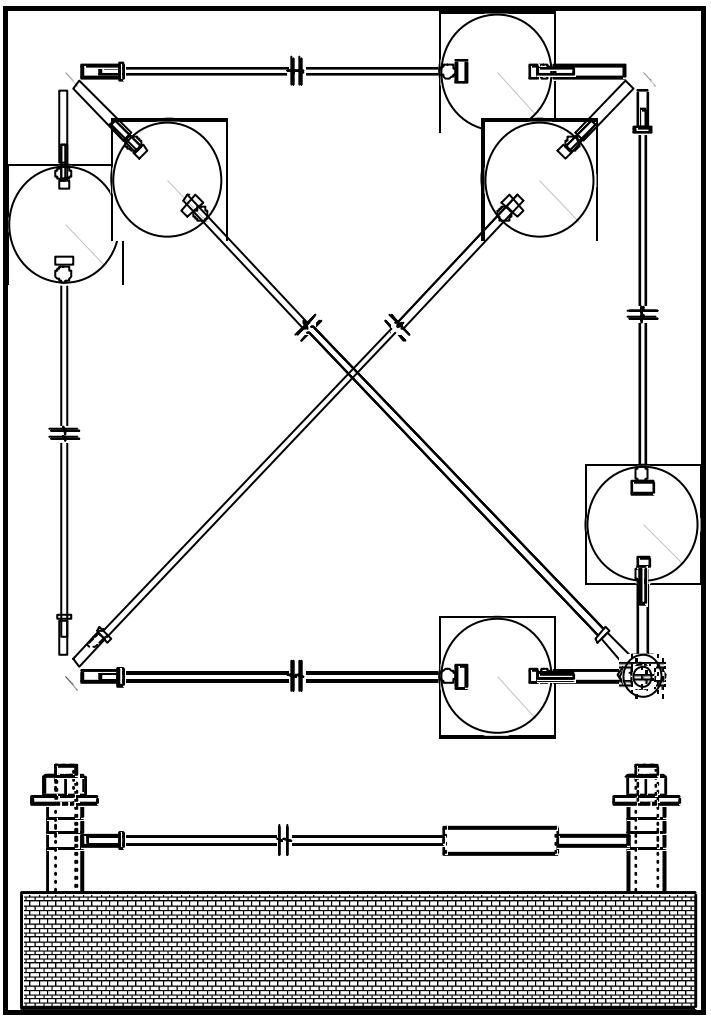

FIGURE 93 A PLAN OF THE RING TRANSDUCERS (AFTER REECE, 1997)

[343] Refer pg. 297.

A thicker walled type RR2 was used for the central measurements and a thinner walled type RR1 was used for the edge measurements. A photograph of the two different types of ring transducers is shown in Figure 94.

FIGURE 94 LOCATIONS OF THE RING TRANSDUCERS

H.9.2 RING DISPLACEMENT TRANSDUCER - DESIGN TYPE 1

The design details for Type 1 are presented in Table 108.

TABLE 108 RING DISPLACEMENT TRANSDUCER TYPE RR1 DETAILS

Description	Unit	Amount
Wall Thickness	mm	1
Height	mm	7.1
Diameter	mm	~32.5
Material	Type	Aluminium
Strain Gauges	Type	4 way Bridge
Calibration	Range	1 V equals 0.2 mm
Warm Up Time	Minutes	30

This set of ring transducers was labelled 1 to 4. The first and second transducers were always used on the same side with ring displacement transducers 5 and 6 of type RR2. The voltage could be read to 2.4 mV and a typical gain of 10 was used in the experiments. This provided a theoretical resolution of 4.8 μm.

H.9.3 RING DISPLACEMENT TRANSDUCER - DESIGN TYPE 2

The design details for Type 2 are presented in Table 109.

TABLE 109 RING DISPLACEMENT TRANSDUCER TYPE RR2 DETAILS

Description	Unit	Amount
Wall Thickness	mm	0.7
Height	mm	7.1
Diameter	mm	~32.5
Material	Type	Aluminium
Strain Gauges	Type	4 way Bridge
Calibration	Range	1 V equals 0.2 mm
Warm Up Time	Minutes	30

This set of ring transducers was labelled 5 to 8 and had a theoretical resolution the same as Type RR1.

H.9.4 A SAMPLE TEST RUN

A typical part of a recording sheet for a test is shown in Figure 95.

FIGURE 95 SAMPLE TEST PROGRAM

	Amplitude (mm)	Test Number					Comment
Frequency (Hz)	2.54						
0.1		451	452	453	454	455	
0.2		456	457	458	459	460	
0.32		461	462	463	464	465	

Appendix I Test Rig Design

I.1 Background to the Design

I.1.1 Introduction

The test rig design was based on the conceptual sketch by Macchi (1982). The rig comprised the compression frame and the shear yoke. Each is an independent member connected to the masonry panel. This appendix presents the design background, the design, and the design details. Comments are also provided on changes that occurred to the design of the rig during the construction or operational phases of the research work.

The loads from these rams and the ITM's ram are peak working loads. The use of a working stress standard provided a flexible design tool compared to a limit standard code. AS1250 - 1981[344] was used for the design of the compression reaction frame and the shear yoke.

I.1.2 Working Drawing List

The design drawings were used for the analysis and as a guide to production of the workshop drawings. The list of workshop drawings is presented in Table 110. The workshop drawings are included on the CD as AutoCAD R14 drawings.

Table 110 Workshop Drawing List

Drawing Number	Title
DD102-1	50 thick Floor Base-plate
DD102-2[345]	Plate Type Base 1
DD102-3	Beam Details Beams A and B
DD102-4	Beam Details Beams C and D
DD102-5	Plate Type A1 20 Thick
DD102-6	Plate Type A2 20 Thick
DD102-7	Plate Type B2 20 Thick
DD102-8	100 mm Pins and collars[346]
DD102-9	40 Thick Thrust Plate
DD102-10	Thrust Plate Stiffening Plates 20 thick
DD102-11	Instron and Base-plate Connectors
DD102-12	Rod Types 1,2 and 3

[344] AS 1250, (1981) *Steel Structures Code*, (Sydney: Standards Australia) *passim.*
[345] Not used in final configuration.
[346] The workshop team developed an alternative detail with plates and threads to hold the pins in place.

I.2 COMPRESSION FRAME DESIGN

I.2.1 INTRODUCTION

The compression frame is a simple four-pinned mechanism that is capable of applying a 1000 kN load on each of two arms using eight Enerpac rams. This section presents details of the thrust plate's design, beams design and the hydraulic ram spacing

I.2.2 THRUST PLATES

The eight thrust plates form part of the compressive reaction frame. The thrust plate is a 'mild steel welded tee' section. It was designed to uniformly spread the 25 tonne compressive load from each of the rams onto the faces of the shear wall element. The thrust plate was designed to be stiff. Deflections were limited in both principal directions with the stiff section properties. The detailed design of the thrust plate is shown on Drawing EF102-2. The workshop details are shown on Drawing DD102-9. Twelve mm threaded rod was used on each side of the thrust plate to provide alignment points into the main beam elements. These threaded rods used a nut to prevent the thrust plate from falling, which was a significant safety issue in the operation of the test rig.

I.2.3 DESIGN OF THE BEAMS

The beams were designed to act as pinned ended members. The pin is detailed elsewhere. The ram plates are located between the two back to back channels to load the beams on the external face. This means that a constant pressure is applied to each plate and that any differential movement is absorbed in beam bending. These beams were designed for the 25 tonne Enerpac rams. The criteria for the beam design are presented in Table 111.

TABLE 111 BEAM STRESS ANALYSES

Key Criteria		
Length between pinned joints	m	1.74
$Radius_x$	m	30.4
l/r_y	Ratio	60
Allowable stress	MPa[347]	165
Peak Stress Beam C	MPa	115 (ok)

A set of photographs of the thrust plates and the beams of the reaction frame are shown in Figure 96.

[347] AS 1250, (1981) *Steel Structures Code*, (Sydney: Standards Australia), Section 5.4.1(3).

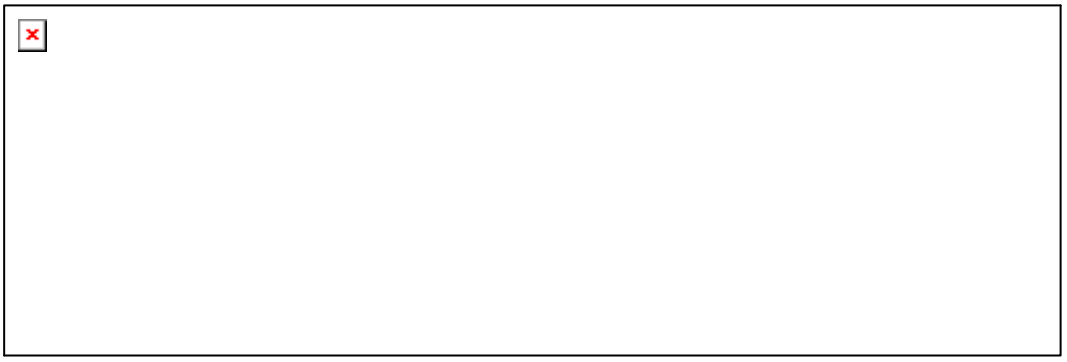

FIGURE 96 THRUST PLATES AND BEAMS

This figure shows the test rig being assembled for the first time. The guide bars can be seen attached to the fitted rams. The gap for the rams between the channels is visible in the two photographs.

I.2.4 HYDRAULIC RAM SPACING

The shear test rig developed by Stevens *et al.* (1991) had five rams per side and this rig was used to test reinforced concrete shear wall elements. Their rams had a spacing of 300mm within the frame. Vecchio and Collins (1986) used a similar rig to establish a modified compression field theory for reinforced concrete. The principles and measurement techniques were such that it was not possible to directly compare the Canadian concrete results to masonry. In this masonry testing, as in the previous Canadian reinforced concrete work, the design issue was to achieve a uniform compressive stress on the edge faces of the shear wall elements. A spacing of 300 mm was selected for the rams consistent with the Canadian experimental design. The design of the rig was based on the use of eight 25 tonne Enerpac rams. Four rams were used on each face. The total applied compressive load had a maximum value of 1000 kN per arm.

I.3 SHEAR YOKE DESIGN

I.3.1 INTRODUCTION

The second mechanism was a shear yoke. The shear yoke was designed to apply uniform shear on the four edge faces. The design is the interesting element of the whole mechanism because of its use of a bolted set of plates to supply the uniform shear. Plywood packing pieces and tension bolts supplied the friction required to develop the shearing stresses. The shear yoke was a thin rod and bar system designed to hold each panel and the compression frame in a central position relative to the ITM's centreline. This system was independent of the compression frame. The shear yoke was axi-

symmetric about the middle of the diamond shaped shear wall element. It was also mirrored on the two sides of the shear wall element.

I.3.2 DESIGN COMPONENTS

Two sets of components form the shear yoke mechanism. These components attach the shear yoke to the strong floor and the reaction frame and the secondary components transfer the applied uni-axial load to the shear wall element as an applied shear stress. The components are:

Floor base plate	A 50 mm thick plate used to anchor the system to the reinforced concrete strong floor. It consists of a mild steel base plate, which was designed quite deliberately to flex and ease out the perturbations in the loading from the ITM and any out of balance in the test rig. The base plate was anchored to the strong floor using six high tensile (HT) bolts.
ITM ram	The hydraulic ram used to impart the steady state harmonic load to the shear wall element. A 250 kN dynamic load cell was located on the base of the ram.
Shear yoke	The device mounted between the floor base plate and the ITM ram that translated the uni-axial load to a shear load. The shear yoke fitted between the ITM ram and the floor base plate in a 3 metre gap. This dimension provided one of the essential dimensions that set the limits on the size of the shear wall element.

The secondary components of the shear yoke spreader were four identical systems used to translate the uni-axial load into a shear stress. These four systems used a pinned joint and rods to translate the vertical stroke to a resolved shear along the edge of the shear wall element. These components are:

Connector plates	Two plates; one located on the ITM's ram attached to the load cell and the other attached to the floor base plate. These plates attach the clevis blocks to the reaction frame and floor.

Shear rods [primary] — Four 20 mm HT rods that have clevis blocks at each end. These were changed to 24 mm HT threaded rod as the initial rods fractured due to secondary bending and fatigue.

Pinned connector blocks — Three 20 mm HT bolts and two 25 mm connecting plates. These were designed to act as a pinned joint. They connect the single shear rods to the two secondary shear rods. These plates are illustrated in Figure 97. The tight tolerances (in some cases less than 5 mm) on the space between the clevis and the spreader plate bolts can be seen in the photograph.

Shear rods [secondary] — Four 16 mm HT rods that have clevis blocks at each end. These were changed to 20 mm HT threaded rod as the initial rods fractured due to secondary bending and fatigue

Clevis — Each clevis and rod set was designed to transmit one half of the force from the ITM load. The flaw in this reasoning was that when one breaks so does the other. However, the alternative of having a yoke system that was capable of carrying the force had problems with stiffness and assembly. Each clevis was made from a 40 mm square length of mild steel. A finite element analysis suggested that the grade of steel should have been higher. However, provided the rig was balanced the clevis blocks did not suffer from plastic deformation.

Shear loader plates — Each plate set was friction grip bolted to either side of the panel as a set of matched plates. Each plate was fitted with a plywood packing piece to provide a smooth stress distribution to the masonry. The bolt spacing was staggered to provide as uniform a shear distribution as could be achieved with this system.

A picture of this system is shown in Figure 97.

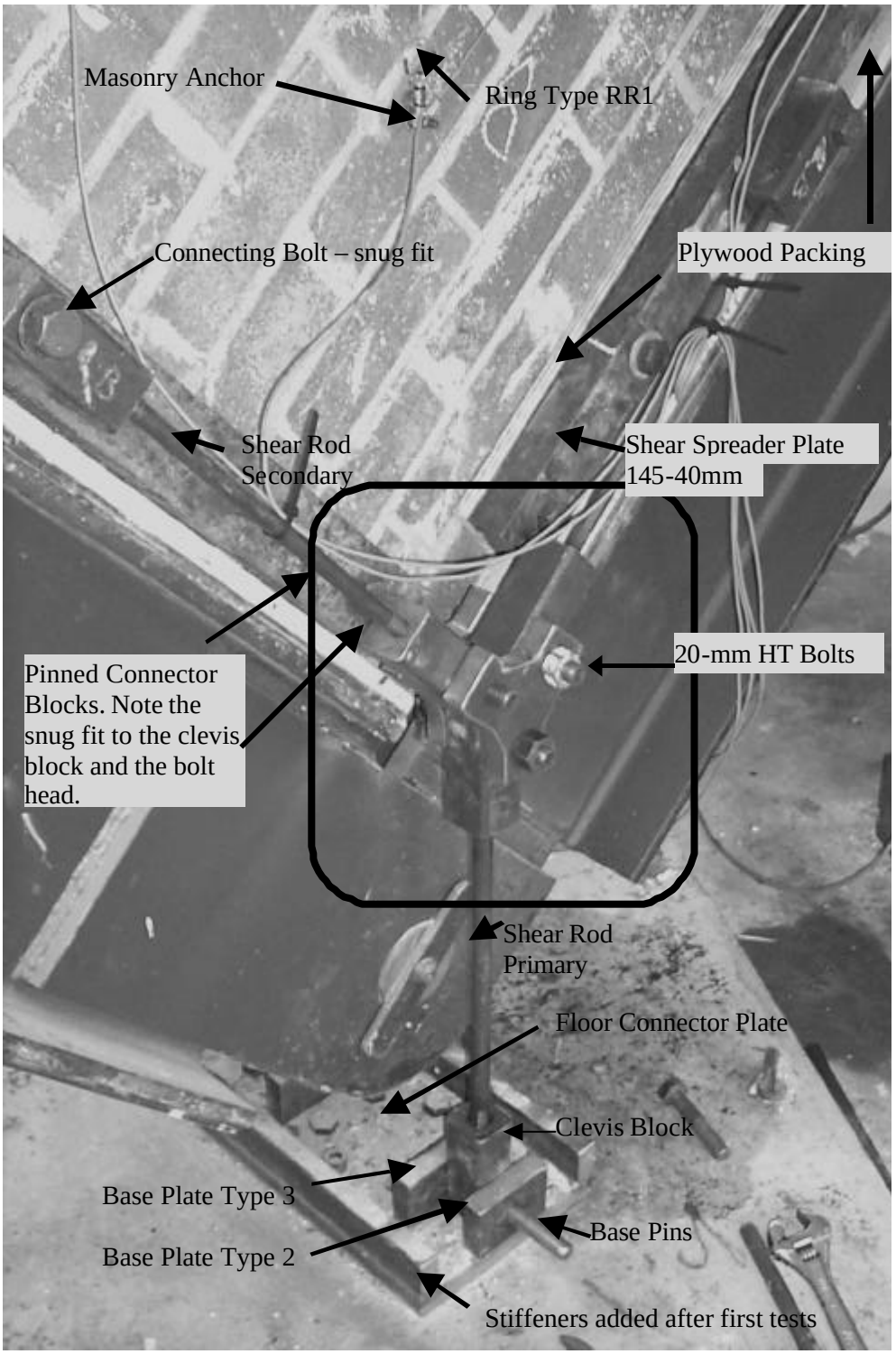

FIGURE 97 ANNOTATED PHOTOGRAPH OF THE SHEAR YOKE SYSTEM

I.3.3 FLOOR BASE PLATE DESIGN

A plate thickness range of 20 to 140 mm was analysed for load deflection. The essential results were the deflection, radius of curvature, and the peak stress. These results are presented in Table 112 for a range of plate sizes.

TABLE 112 BASEPLATE STRESS ANALYSES

Thickness (mm)	Stress XX (MPa)	Peak Deflection (mm)	Curvature (m)	Comment
140	7.3	0.05	2700	Too stiff
100	7.4	0.16	986	
60	11.7	0.76	213	
50	15.4	1.31[348]	123	Reasonable compromise

I.3.4 SHEAR SPREADER PLATE

The essential design issue was to achieve a uniform distribution of shear along the face of the panel. The components of the shear spreader plate are mild steel spreader plates that are stiff mild steel spreader plates 40 x 75 mm, 20 mm diameter connecting bolts being a snug tight grip bolt was used at the central point to apply the load whilst limiting the friction at this point. Four 20 mm diameter friction bolts were used per spreader plate pair spaced as shown on the drawings. Plywood sheet packing used beneath the plates. Plywood has a low Poisson's ratio,[349] which ensures that the friction grip was smoothly transferred to the masonry. It was to be expected that there will be some second order Poisson's effects from the difference in the Poisson's ratios between brick and plywood, but not as noticeable as steel and brick and not measurable. The shear loading yoke consists of 75 x 40 mm mild steel flat separated from the panel by 12.5 mm of plywood sheeting. The end bolts had a smaller area of steel to tighten up on than the mid point bolts. The bolts were tightened to the same torque. The second set of midpoint bolts had a substantially greater area of influence. The central bolt was left snug. A frictional coefficient was assumed for load transfer of 0.35.[350] This was used in the calculation of the applied normal force to the flats to transfer the shear into the masonry. There was no evidence in the boltholes after the tests that slippage had occurred between the plates and the masonry once the bolts were tightened. A comparison of the change in signals between the results for the vertical and horizontal rings suggests that the shear was being distributed tolerably uniformly for the experiments.

I.3.5 SHEAR RODS

The design for the yoke rod is presented in Table 113.

[348] The observed deflection on July 4, 1999 under 250 kN loading would have been in this order of magnitude.
[349] Kleeman, A.W., and Page (1990) measured the Poisson's ratio at less than the error in the measurements, whilst Lekhnitskii (1963, 62) gives values obtained in the aircraft industry as 0.071 and 0.036.
[350] Gorenc, R., and Tinyou, E.E., (1984), the value of 0.35 is taken from pg. 49.

TABLE 113 PRIMARY SHEAR RODS

Description	Unit	Amount
Load	kN	125
M20/8.8	Allowable load	89
M20/12.9	Allowable load	132
M24/8.8	Allowable load	130
Last two rods are acceptable. The use of M24 all threaded rod was preferred because of the rolled thread rather than the cut thread on the M20/12.9 that were specially made, and tend to fracture.		

The design for the secondary yoke rod is presented in Table 114.

TABLE 114 SECONDARY SHEAR ROD DESIGN

Description	Unit	Amount
load	kN	88
M16/8.8	Allowable load	57
M16/12.9	Allowable load	85
M20/8.8	Allowable load	89
Confirmation with manufacturer is needed as per Gorenc and Tinyou, (1984, 46), but last two rods are acceptable. The use of M20 threaded rod was preferred because of the rolled thread rather than the cut thread on the M16/12.9 that are specially made but are susceptible to fracture.		

I.4 DESIGN DRAWINGS

A list of the detailed design drawings is presented in Table 115.

TABLE 115 LIST OF DESIGN DRAWING FIGURES

Drawing Number	Figure
EF102 – 1	Figure 98 EF102 - 1 Masonry Test Panel Set Out Plan and General Notes
EF102 –2	Figure 99 EF102 - 2 Masonry Panel Frame and Thrust Block Detail
EF102 –3	Figure 100 EF102 - 3 Frame Beam Details and Ram Connections, Joint Details
EF102 –4	Figure 101 EF102 - 4 Frame Beam Details Beams C and D, Joint Details
EF102 –5	Figure 102 EF102 - 5 Footing and Peak Details, Pinned Joints
EF102 –6	Figure 103 EF102 - 6 Existing 610 UB Frame and Instron
EF102 –7	Figure 104 EF102 - 7 Electrical and Instrumentation Details Masonry Panels
EF102 –8	Figure 105 EF102 - 8 Shear Load Spreader and Yoke Detail, Pinned Joint

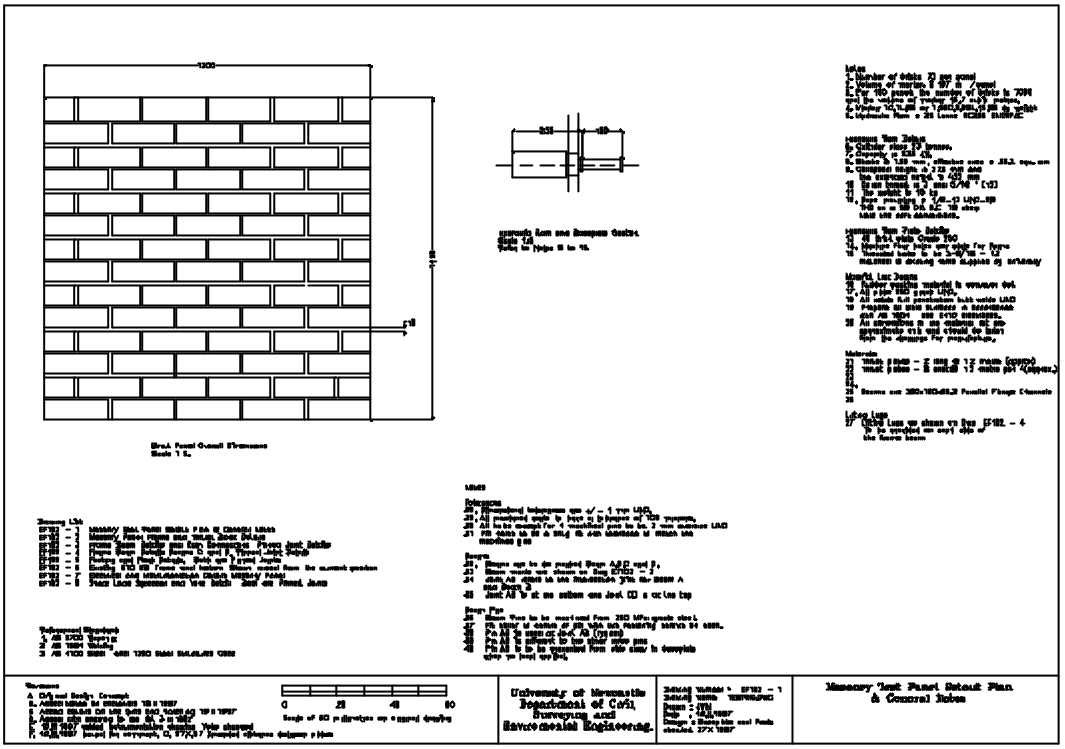

FIGURE 98 EF102 - 1 MASONRY TEST PANEL SET OUT PLAN AND GENERAL NOTES

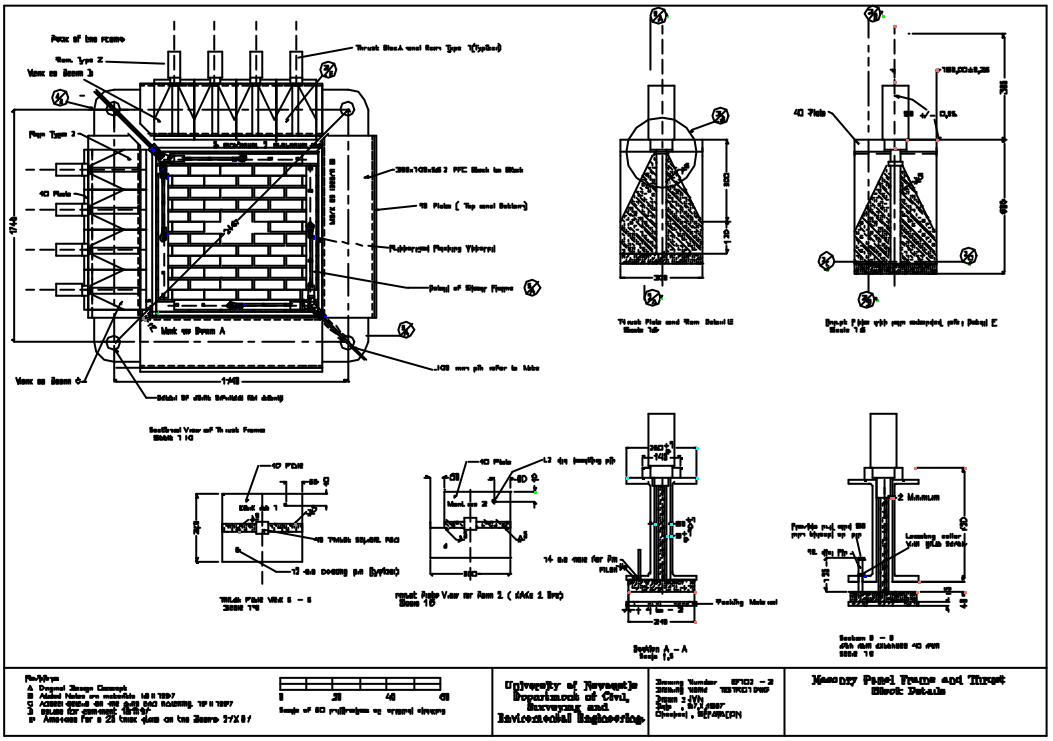

FIGURE 99 EF102 - 2 MASONRY PANEL FRAME AND THRUST BLOCK DETAIL

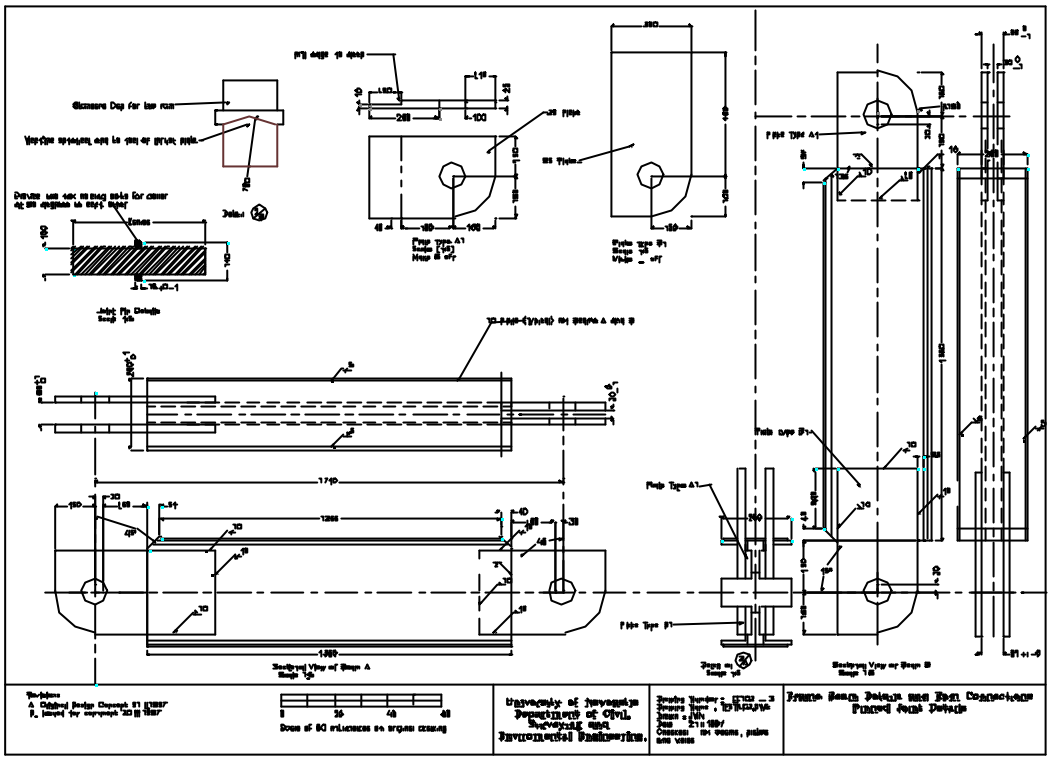

FIGURE 100 EF102 - 3 FRAME BEAM DETAILS AND RAM CONNECTIONS, JOINT DETAILS

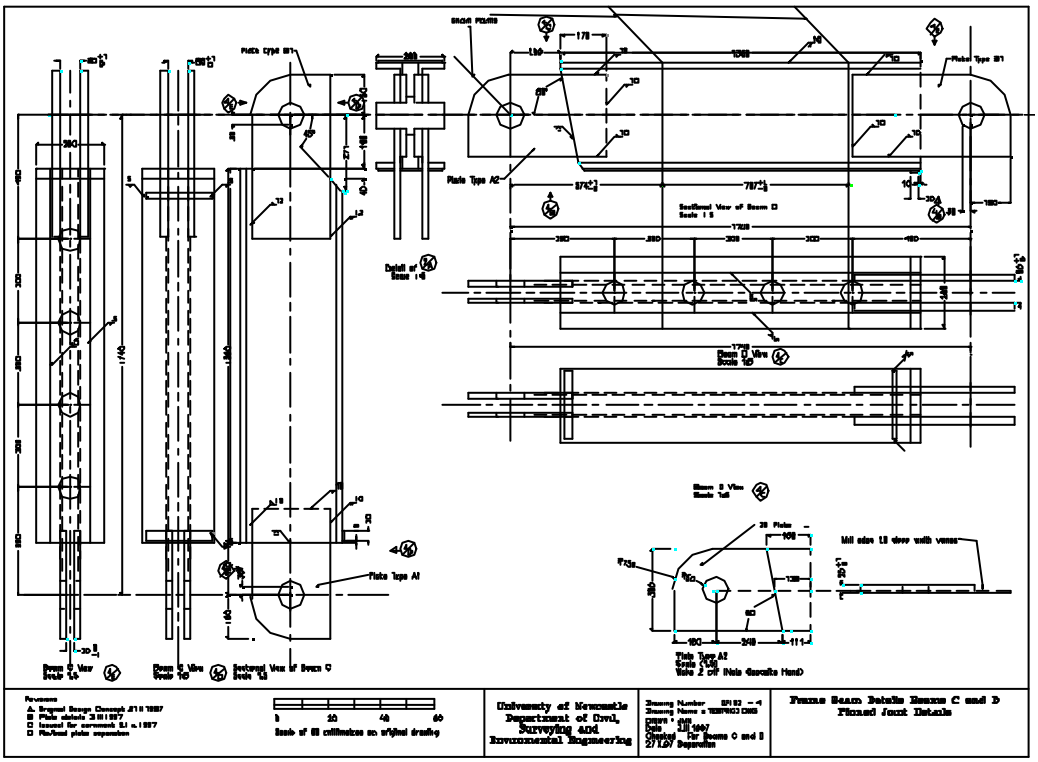

FIGURE 101 EF102 - 4 FRAME BEAM DETAILS BEAMS C AND D, JOINT DETAILS

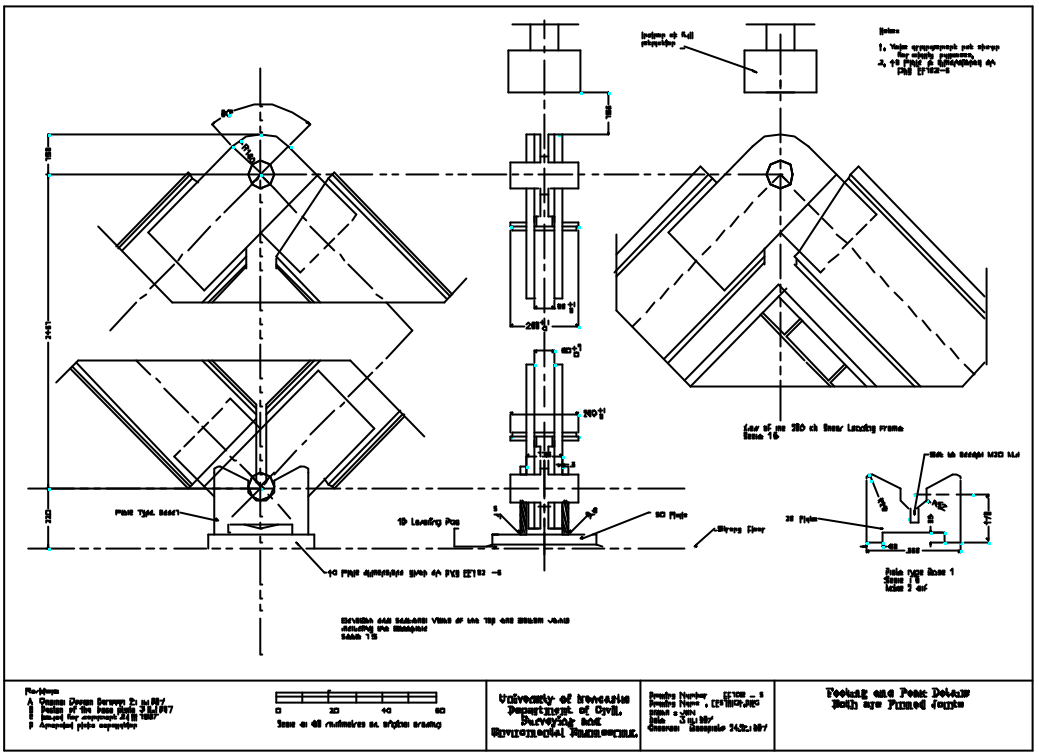

FIGURE 102 EF102 - 5 FOOTING AND PEAK DETAILS, PINNED JOINTS

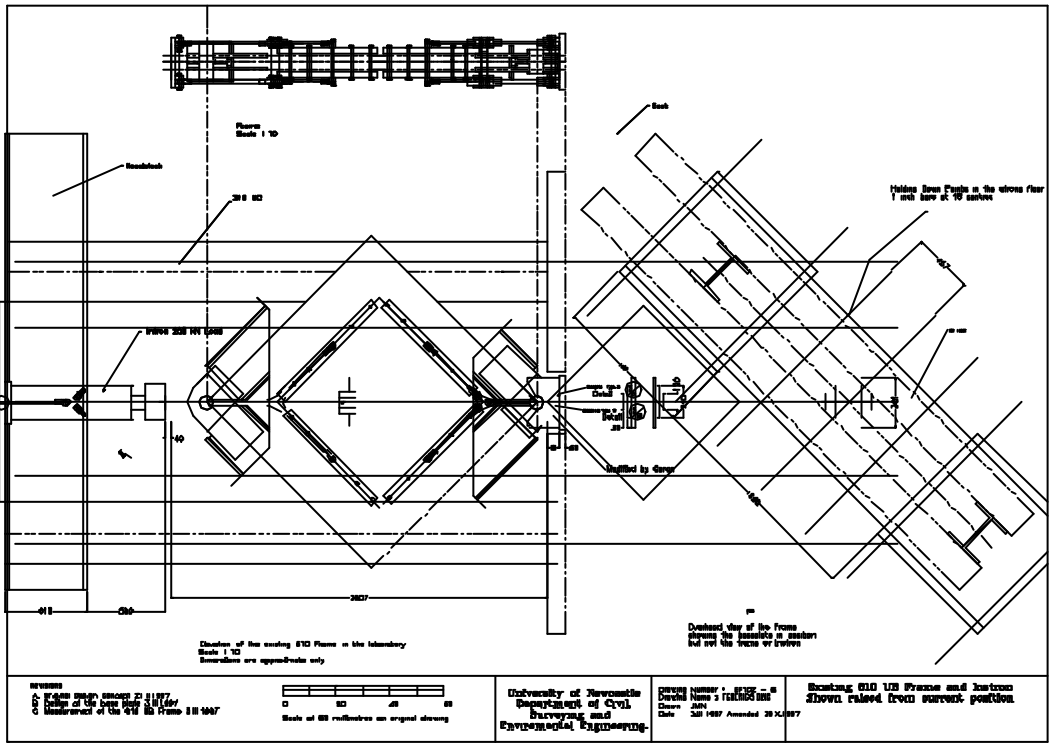

FIGURE 103 EF102 - 6 EXISTING 610 UB FRAME AND INSTRON

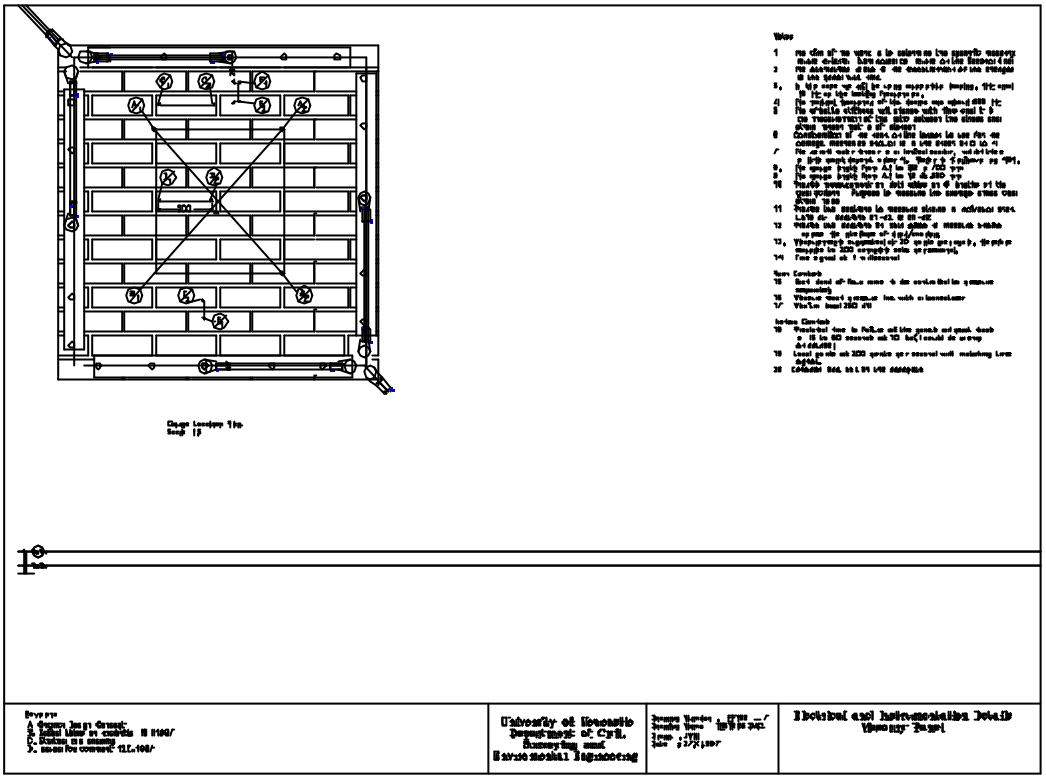

FIGURE 104 EF102 - 7 ELECTRICAL AND INSTRUMENTATION DETAILS MASONRY PANELS

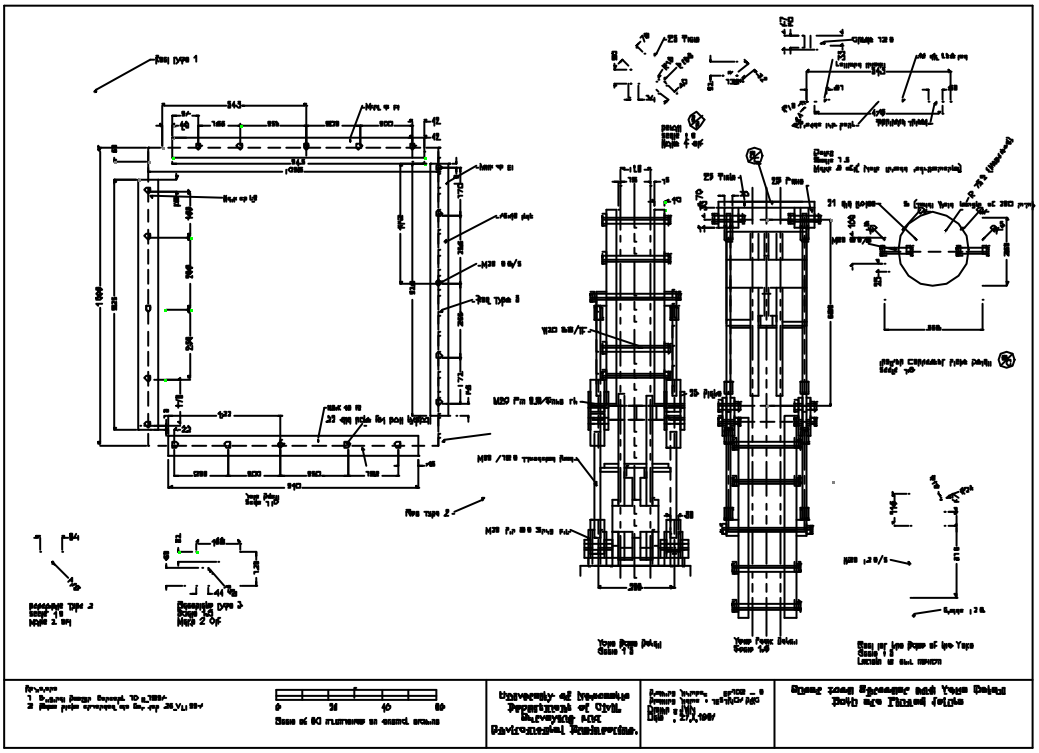

FIGURE 105 EF102 - 8 SHEAR LOAD SPREADER AND YOKE DETAIL, PINNED JOINTS